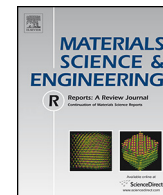




Contents lists available at ScienceDirect

# Materials Science and Engineering R

journal homepage: [www.elsevier.com/locate/mser](http://www.elsevier.com/locate/mser)



## Organic polymeric and small molecular electron acceptors for organic solar cells

Venkateswararao A.<sup>a</sup>, Shun-Wei Liu<sup>a,b,\*</sup>, Ken-Tsung Wong<sup>c,d,\*\*</sup>

<sup>a</sup> Department of Electronic Engineering, Ming Chi University of Technology, New Taipei City 24301, Taiwan

<sup>b</sup> Organic Electronics Research Center, Ming Chi University of Technology, New Taipei City 24301, Taiwan

<sup>c</sup> Department of Chemistry, National Taiwan University, Taipei 10617, Taiwan

<sup>d</sup> Institute of Atomic and Molecular Science, Academia Sinica, Taipei 10617, Taiwan

### ARTICLE INFO

#### Article history:

Received 10 January 2018

Received in revised form 23 January 2018

Accepted 25 January 2018

Available online xxx

#### Keywords:

Organic solar cell

Bulk heterojunction

Non-fullerene acceptor

Polymeric acceptor

Perylene diimide

Small molecule acceptor

Indacenodithiophene

### ABSTRACT

In organic solar cells (OSCs), the electron donor (D) and electron acceptor (A) blended active layer is the most crucial component for governing the power conversion efficiency (PCE). Various efficient donor materials with wide structural variations have been developed to couple with high-electron mobility fullerene-based acceptors, giving PCEs beyond 12%. However, fullerene-embedded OSCs encounter great challenges of low flexibility for structural modifications, poor absorption and blend morphological stability. The demand for alternative acceptors drives current OSC research towards non-fullerene acceptors (NFAs). Tailor-made NFAs of polymer or small molecule (SM) can typically exhibit tunable optical and electrochemical properties, high solubility, air stability, and favorable intermolecular interactions leading to compact packing and good nano-phase segregation in the active blend. In this review, we systematically depict the effects of molecular structures on the physical properties and device performances. The promising/most popular cores and general molecular design strategies of NFAs are outlined. The polymeric and SM NFAs were classified into several sub-groups based on their structural features, and in every sub-group, the structural evolution, current status, the champion case as well as the future challenges were highlighted and discussed. For polymeric NFAs, naphthalene diimide (NDI) and perylene diimide (PDI) are most promising and widely explored due to their easy synthesis, high electron affinity and mobility, leading to promising PCE when NDI and PDI units are conjugated with various electron-rich/deficient aromatics. Various electron-deficient core-based polymeric NFAs were also employed. Aromatic diimides (NDI and PDI) were also widely employed as the central core or terminal unit for SM NFAs. In particular, PDI was interested in electron deficient core, and their monomers, dimers, and trimers gave various degrees of success. PDI trimeric NFA showed superior PCE (~9.3%) because of its twisted 3D or fused geometry capable of interlocking the polymer donor allows optimum molecular packing, morphology and, therefore, efficient charge separation and transport. The excellent photochemical stability, strong absorption and synthetic flexibility of diketopyrrolopyrrole (DPP) produced promising SM NFAs. The rigid and co-planar indacenodithiophene (IDT) cores bearing various electron-deficient terminal groups were extensively explored, and the structural engineering on both the core and side chain groups together with post-treatments produced the highest PCE (~13.2%). These results conclude that NFAs possess the better possibility for tuning absorption profile, matched energy levels and optimal D/A nano-morphology for delivering promising PCEs. We highlighted the structure-property-performance relationships and future challenges, and hope this article can trigger new ideas for designing more promising NFAs.

© 2018 Elsevier B.V. All rights reserved.

\* Corresponding author at: Department of Chemistry, National Taiwan University, Taipei 10617, Taiwan.

\*\* Corresponding author at: Department of Electronic Engineering, Ming Chi University of Technology, New Taipei City 24301, Taiwan.

E-mail addresses: [swliu@mail.mcut.edu.tw](mailto:swliu@mail.mcut.edu.tw) (S.-W. Liu), [\(K.-T. Wong\).](mailto:kenwong@ntu.edu.tw)

## Contents

1. Introduction .....	00
2. Polymeric acceptors .....	00
2.1. Aromatic diimide-based polymers .....	00
2.1.1. Naphthalene diimide-based polymeric acceptors .....	00
2.1.2. Perylenediimide-based polymeric acceptors .....	00
2.2. Benzothiadiazole-based polymeric acceptors .....	00
2.3. Diketopyrrolopyrrole-based polymeric acceptors .....	00
2.4. Double B $\leftarrow$ N bridged bipyridyl-based polymeric acceptors .....	00
2.5. Miscellaneous polymeric acceptors .....	00
3. Small molecular acceptors .....	00
3.1. Co-planar aromatic hydrocarbons .....	00
3.1.1. Fluorene-based small molecular acceptors .....	00
3.1.2. Spirobifluorene-based small molecular acceptors .....	00
3.2. Co-planar aromatic heteroacenes .....	00
3.2.1. Indacenodithiophene-based small molecule acceptors .....	00
3.2.2. Carbazole-based small molecular acceptors .....	00
3.2.3. Dithieno-fused heterocycle-based small molecular acceptors .....	00
3.3. Aromatic (di)imides-based small molecular acceptors .....	00
3.3.1. Phthalimide-based small molecular acceptors .....	00
3.3.2. Naphthalene (di)imides-based small molecular acceptors .....	00
3.3.3. Perylene diimide-based small molecular acceptors .....	00
3.4. Diketopyrrolopyrrole-based small molecular acceptors .....	00
3.5. Isoindigo-based small molecular acceptors .....	00
3.6. Miscellaneous small molecular acceptors .....	00
4. Conclusions and Prospects .....	00
References .....	00

## 1. Introduction

Bulk heterojunction (BHJ) organic solar cells (OSCs) have attracted immense attention because they are potentially low-weight, cost-effective, semi-transparent, colorful, and flexible [1–3]. In OSCs, the electron donor and electron acceptor blended active layer is one of the most crucial component for governing the power conversion efficiency (PCE). Upon solar irradiation, the active layer absorbs sunlight, creates excitons (hole and electron pair weakly bound together) and diffuses at donor-acceptor interface into free hole and electron. Free charges are then transported, followed by collection at the oppositely charged anode and cathode, which generate the power by completing the electric circuit (Fig. 1). In 1986, Tang designed a bilayer OSC based on perylene tetracarboxylic derivative (PV) and copper phthalocyanine (CuPc) to achieve a PCE around 1% [4]. For the past two decades, various approaches have been developed for optimizing the active layer leading to a significant efficiency improvement [5–12]. Among them, the molecular design implementing various structural features onto respective constituents (donor or acceptor) generally plays the core role in this research field because the designated properties suitable for OSC applications can be feasibly and subtly tailored by chemical structures [10–12].

Several fullerene-based acceptors have been developed for OSCs, and their optimized devices showed high PCEs due to their several advantages, such as (i) high electron affinity, (ii) high electron mobility, (iii) electron transportation through its three-dimensional (3D) surface, (iv) multi-reversible reduction, and (v) ability to mix with donors and produce various mixed domains. Promising fullerene derivatives such as PC<sub>60</sub>BM, PC<sub>70</sub>BM and ICBA (Fig. 2) dominated other fullerene-based acceptors due to their high PCE till now [13]. However, they suffer from some significant drawbacks such as (i) high cost, (ii) limited absorption (UV region), which was the bottleneck for harvesting more photons from solar flux, (iii) difficult molecular designing towards red-shifted absorption, (iv) poor morphological stability due to aggregation tendency, which facilitates large size pure and mixed domains that

limit the exciton diffusion in an active blend. In the meantime, various efficient polymeric or small molecular (SM) donor materials with wide structural variations have been developed and coupled with high electron mobility fullerene-based acceptors to produce a PCE higher than 10% [11,12]. Nevertheless, OSCs employing conventional fullerene derivatives and the designated donor materials have reached the PCE plateau due to the difficulty in designing the molecules with spectral response covering the whole solar emission spectrum and simultaneously match to the energy levels of fullerenes. In addition, OSCs based on fullerene acceptors are generally suffering from the lower V<sub>OC</sub> as we expected from the energy difference between HOMO(D) and LUMO (A) due to poor interfacial charge-transfer states between the donor and the acceptor, high non-radiative recombination and non-geminate recombination [14,15]. To circumvent this limitation, OSC research is directed towards the development of new organic molecular acceptors, which are alternate to fullerene-based acceptors known as non-fullerene acceptors (NFAs).

NFAs potentially can retain the aforementioned advantages of fullerene-based acceptors along with additional benefits of (i) easy synthesis and purification process, (ii) tunable strong absorption with high molar extinction coefficients, (iii) efficient charge transfer with a low possibility of back electron transfer, (iv) higher solubility in common green solvents, (v) well mixing with donors and lead to compact packing and good nano-phase segregation in the active blend, and (vi) high morphological stability. In order to design the new NFAs, judicious selection of complementary donor was very important for a better spectral response of blend film covering the solar absorption region. Typically, donor and acceptor need a suitable energy levels alignment shown in Fig. 1b. The offset of highest occupied molecular orbital (HOMO) of donor and lowest unoccupied molecular orbital (LUMO) of acceptor directly governs the open circuit voltage (V<sub>OC</sub>) and, for effective charge transfer process ΔLUMO of donor and acceptor, should be in the range of 0.1 to 0.3 eV. Strategies to improve V<sub>OC</sub> can be made by raising the LUMO of acceptor and downshifting the donor HOMO with minimized

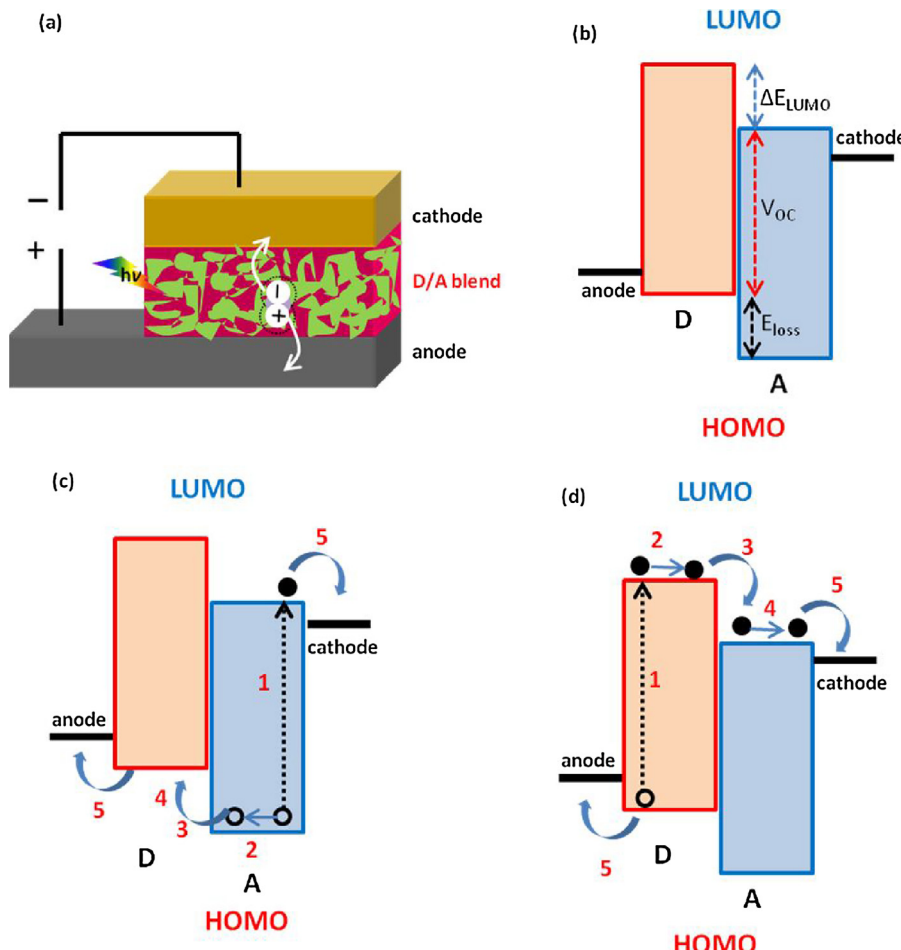


**Fig. 1.** (a) Typical BHJ OSC device configuration, (b) energetic of its components and excitation takes in (c) donor or (d) acceptor. Process involved: (1) photo excitation to generate exciton (2) diffusion of exciton (3) dissociation to exciton (4) transportation of hole or electron (5) collection of hole at anode or electron at cathode.

energy loss ( $E_{loss} = E_{BG} - V_{OC}$ ). When the device was irradiated with sunlight, unlike the fullerene acceptors, photoexcitation may more efficiently take place either in donor or acceptor and create exciton followed by diffusion, dissociation at donor-acceptor interface, and transport of electron towards the cathode (Fig. 1c) or hole towards the anode (Fig. 1d). Hence, NFAs might undergo both of these exciton processes, which were feasibly responsible for better device performance.

Importantly, NFAs should show suitable  $\pi-\pi$  intermolecular interactions for favorable donor/acceptor-separated nano-morphology with preferably “face-on” orientation crystallinity, which improves electron transport and then gives high short circuit

current density ( $J_{SC}$ ) and fill factor (FF) of the device. In case of polymeric NFAs, controlling molecular weight is also an essential factor in enhancing the crystallinity and “face-on” molecular orientation with respect to the donor-acceptor interface and electrodes [16,17]. Typically, increase in high molecular weight of the polymers improves the crystallinity by changing the “edge-on” orientation to “face-on” orientation, which drastically increases device  $J_{SC}$  as well as PCE. Aggregation of acceptors in the solid state is quite a serious problem, which can be manipulated by insertion of alkyl chains or integrate 3D geometrical designs that can also be beneficial for multi-directional charge transport like fullerenes. In addition, a careful molecular design on NFAs needs to balance

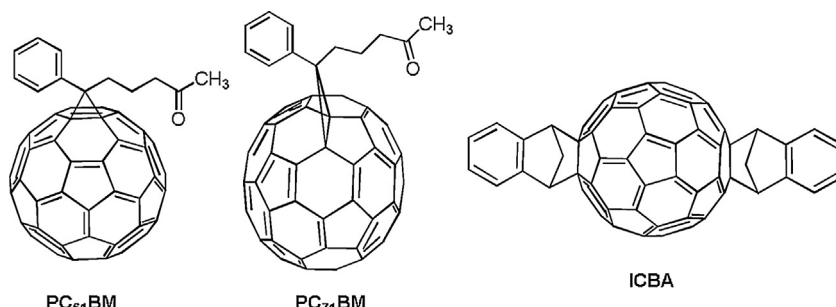


**Fig. 2.** Molecular structures of fullerene based acceptors.

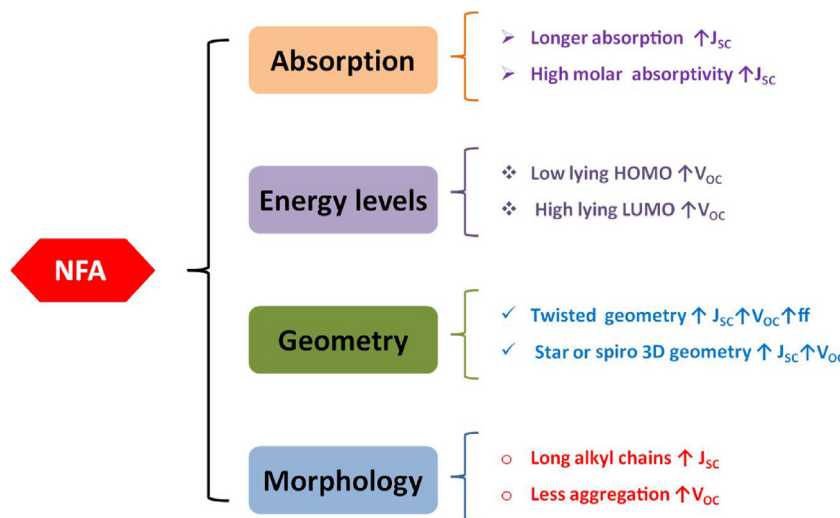


**Fig. 3.** Schematic representation: The effect of various factors on the performance of NFAs.

crystallinity and desirable morphologies, which enhance electron transportation and thus higher  $J_{SC}$  and PCE. Overall, the PCE of the NFAs-based OSCs mainly depend on the four parameters such as (i) absorption properties, (ii) frontier energy levels, (iii) molecular geometry, and (iv) blend film morphology. In these regards, the longer absorption wavelength and higher LUMO of NFAs enhance  $J_{SC}$  and  $V_{OC}$  of the corresponding devices, respectively. Introducing twisted or 3D geometry of NFAs via star-shaped or spiro configuration can effectively suppress aggregation and then form a better-blend morphology with nano-phase separation. Smooth-and uniform-blend morphology enhances charge transport and reduces geminate recombination resulting in an increase of  $J_{SC}$ ,  $V_{OC}$  and FF. The effect of all various parameters on the PCE of NFAs was shown in Fig. 3.

Since 1996, several varieties of wide, medium and narrow bandgap polymeric or SM donors have been developed to blend with NFAs for the construction of efficient OSCs. The chemical structures of donors used so far were shown in Figs. 4–8, which provide an idea for judicious selection of donor for matching the NFAs in terms of absorption and energy levels. They were mainly classified as (a) wide band gap polymer donors such as poly(3-hexylthiophene) (P3HT), polymers of thiophene derivatives and polyphenylenes (Fig. 4); (b) narrow band gap polymers composed of dithienobenzene (DBT) co-polymer with electron-deficient units, mainly benzotriazole (BTz) (Fig. 5), quinoxaline (Fig. 5), benzothiadiazole (BT) (Fig. 6), and diketopyrrolopyrrole (DPP)-based polymers (Fig. 7); (c) medium band gap carbazole- and fluorene-based polymers (Fig. 7); (d) narrow band gap SM donors (Fig. 8). Potential polymer donors such as P3HT, PTB7, PTB7-Th, PBDB-TF, PBDT-T and P3TEA were generally used to blend with polymeric or SM NFAs to produced highest PCE [18–23].

In order to develop efficient NFAs, the researchers need to acquire thorough knowledge of structure-property-performance relationship of all reported NFAs. This motivates us to summarize all reported organic polymeric and SM NFAs. The promising/most popular cores and general molecular design strategies of organic and polymeric NFAs were outlined in Fig. 9. Even though some focused reviews were published, so far, no one provided the complete collection of polymeric and SM NFAs. We need a deep and thorough correlation of structure-property-performance of both polymeric and SM NFAs to provide the future guidelines for better NFAs [24–29]. In this review, NFAs were basically classified into polymeric and SMs and they were subsequently divided into several sub-groups based on their structural features. In each

individual sub-group, the importance of the structural core unit, status, and the champion case was discussed. Finally, we concluded and highlighted that the promising class and then the future challenges and prospects of the NFAs to trigger more innovative ideas for better molecular designing of NFAs.

## 2. Polymeric acceptors

Generally, polymeric NFAs contain donor-acceptor architectures, which allow strong intramolecular charge transfer (ICT) for giving polymers with longer absorption maxima and high molar extinction coefficient, tunable optoelectronic energies, good solubility, better charge transport properties and flexible viscosity. Earlier, Heeger demonstrated a n-type cyano-substituted poly(phenylenevinylene) as NFAs for polymer OSCs in a blend with polymer donor [30]. Incorporation of various acceptors in polymer skeleton showed significant changes in absorption, energy levels and blend morphology. Also, they were widely investigated due to their easy synthetic protocols, excellent photophysical properties and ability to mix well with the donor in the active blend. In this article, NFAs were classified into several subgroups depending on the main electron-deficient building block involved in polymer.

### 2.1. Aromatic diimide-based polymers

In aromatic diimides, aromatic building blocks fused with cyclic diimide units gained an enormous response in the field of NFAs due to their strong absorption, high molar absorptivity, excellent photo and ambient stability, high electron affinities, good electron-transporting property. In addition, there are several available sites (imide N-position or various positions on aromatics) for further functionalization by either extending the conjugation or substitution with different  $\pi$ -conjugates. Depending on the nature of aromatic diimide unit used to construct NFAs, they displayed unique photophysical properties. In this line, they were classified into naphthalene diimide (NDI) and perylene diimide (PDI)-based polymeric NFAs. Nevertheless, NDI-based polymers exhibited a higher PCE over PDI-embedded derivatives due to their high electron mobility, good solubility and good intermixing with the donor in the active blend.

#### 2.1.1. Naphthalene diimide-based polymeric acceptors

In polymeric NFAs, NDI-based polymers have attracted significant research interest owing to its tunable absorption and energy

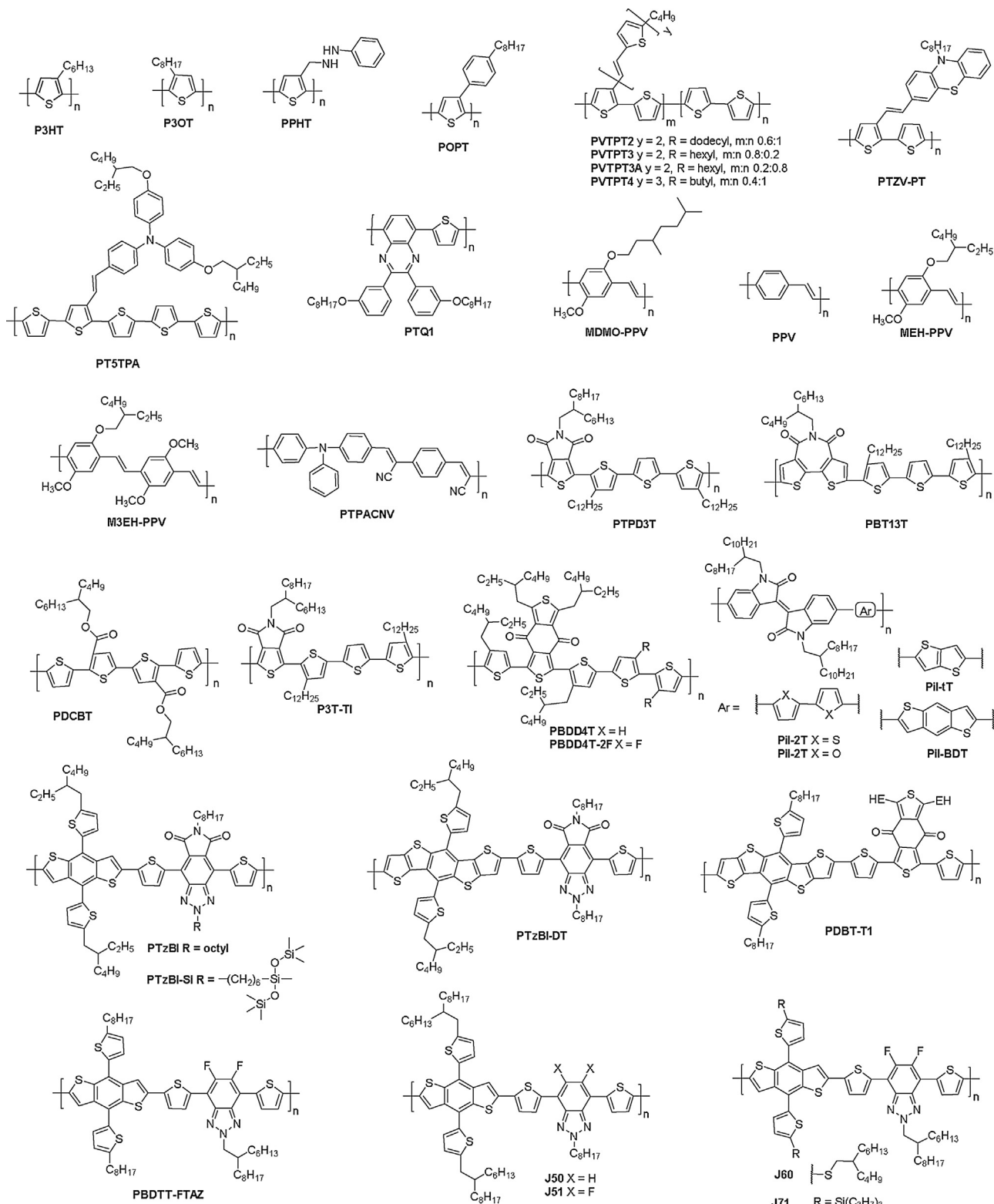
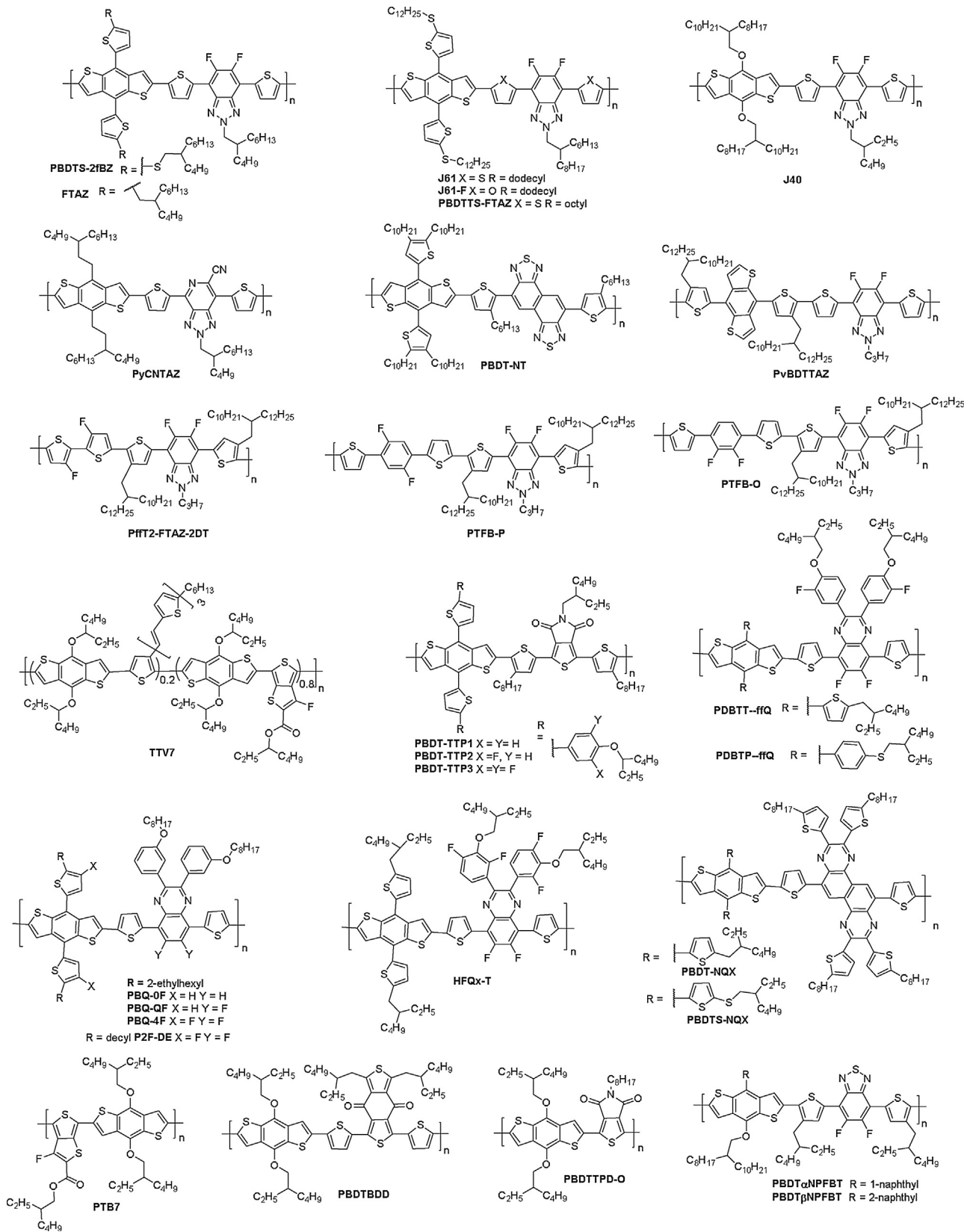


Fig. 4. Molecular structures of thiophene and dithienobenzene (DBT) based polymeric donors.

levels, high electron mobility, electron affinity, as well as excellent photochemical and thermal stability. NDI-based polymeric NFAs achieved highest PCE than other polymeric NFAs. Typically, various alkyl units were introduced at imide N-position for better solubility and extended conjugation via 2,6-positions to give linear polymers. In most of the reports, NDI was co-polymerized

either with oligothiophenes or fused electron rich/deficient heterocyclic units, and their general configurations are shown in Fig. 10 and their corresponding optical and device data are compiled in Table 1. The importance and effect of conjugated π-linker are systematically discussed and highlighted the structure-property relationship with photovoltaic parameters. Kim



**Fig. 5.** Molecular structures of dithienobenzene (DBT) based polymeric donors.

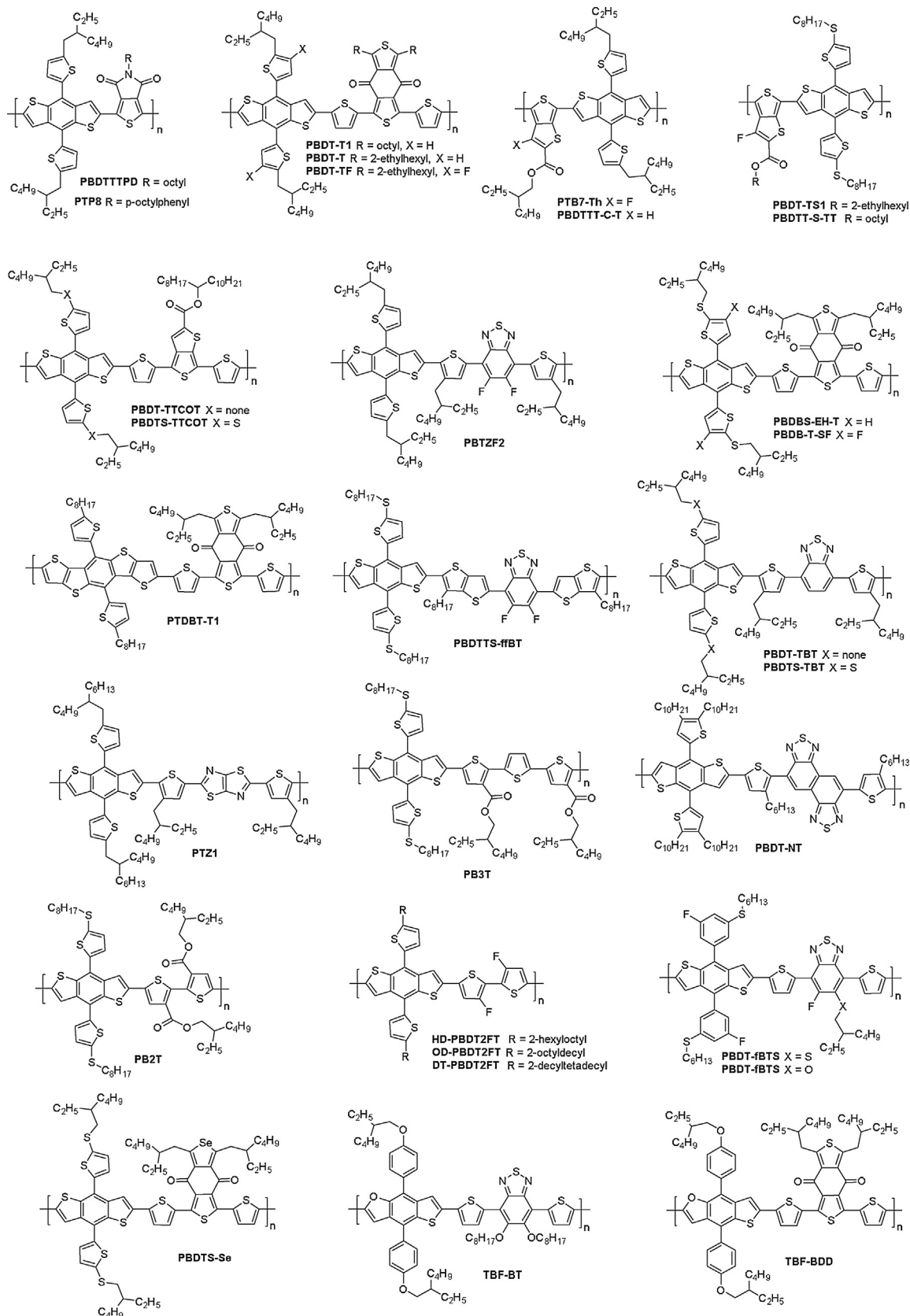


**Fig. 6.** Molecular structures of dithienobenzene (DBT) based polymeric donors.

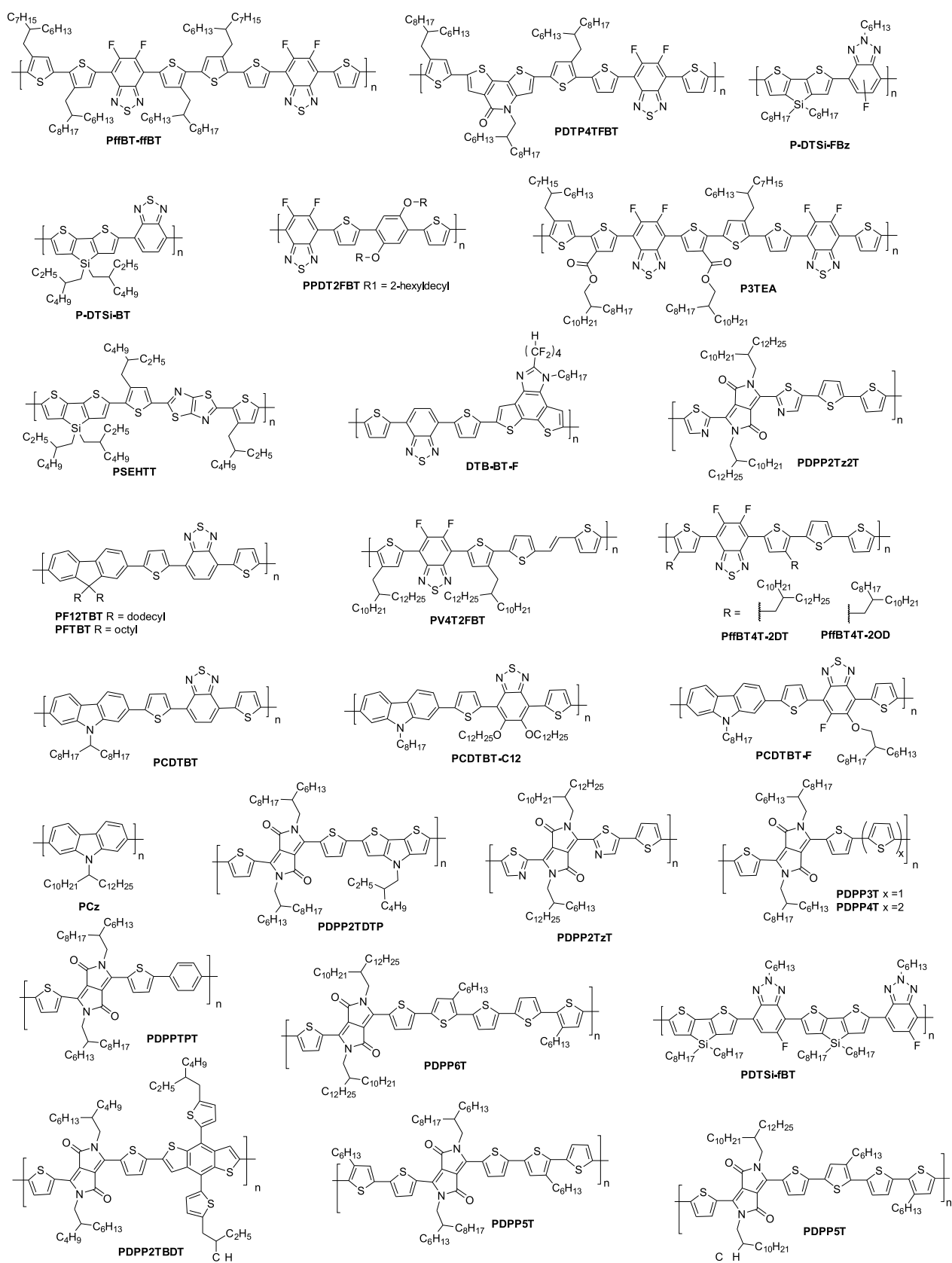


Fig. 7. Structures of benzothiadiazole (BT) and diketopyrrolopyrrole (DPP) based polymeric donors.

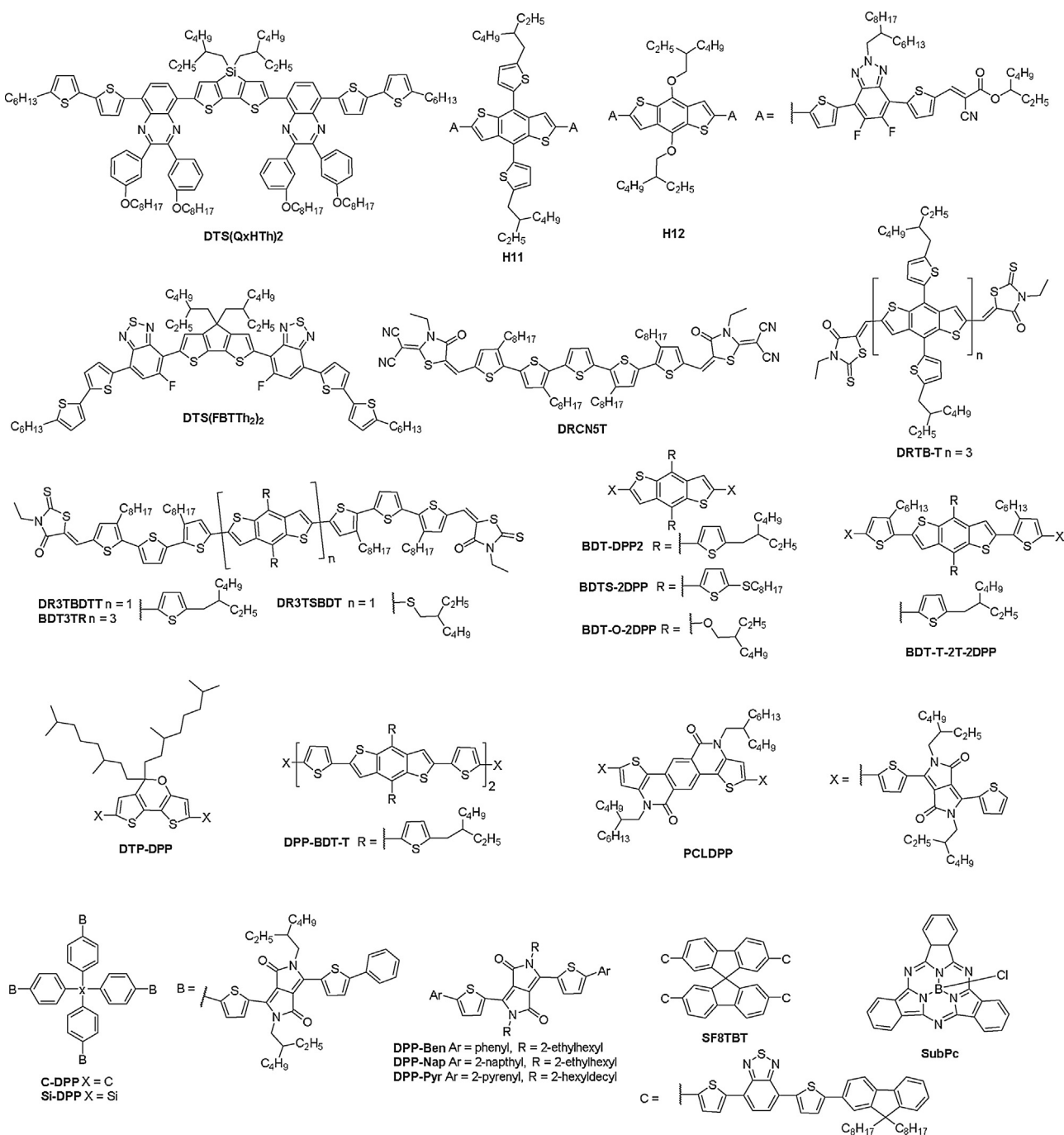


Fig. 8. Structures of small molecular donors.

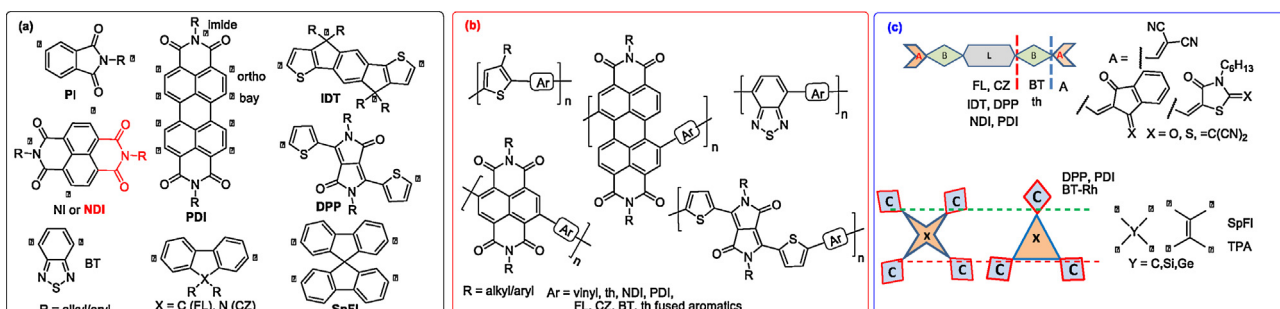
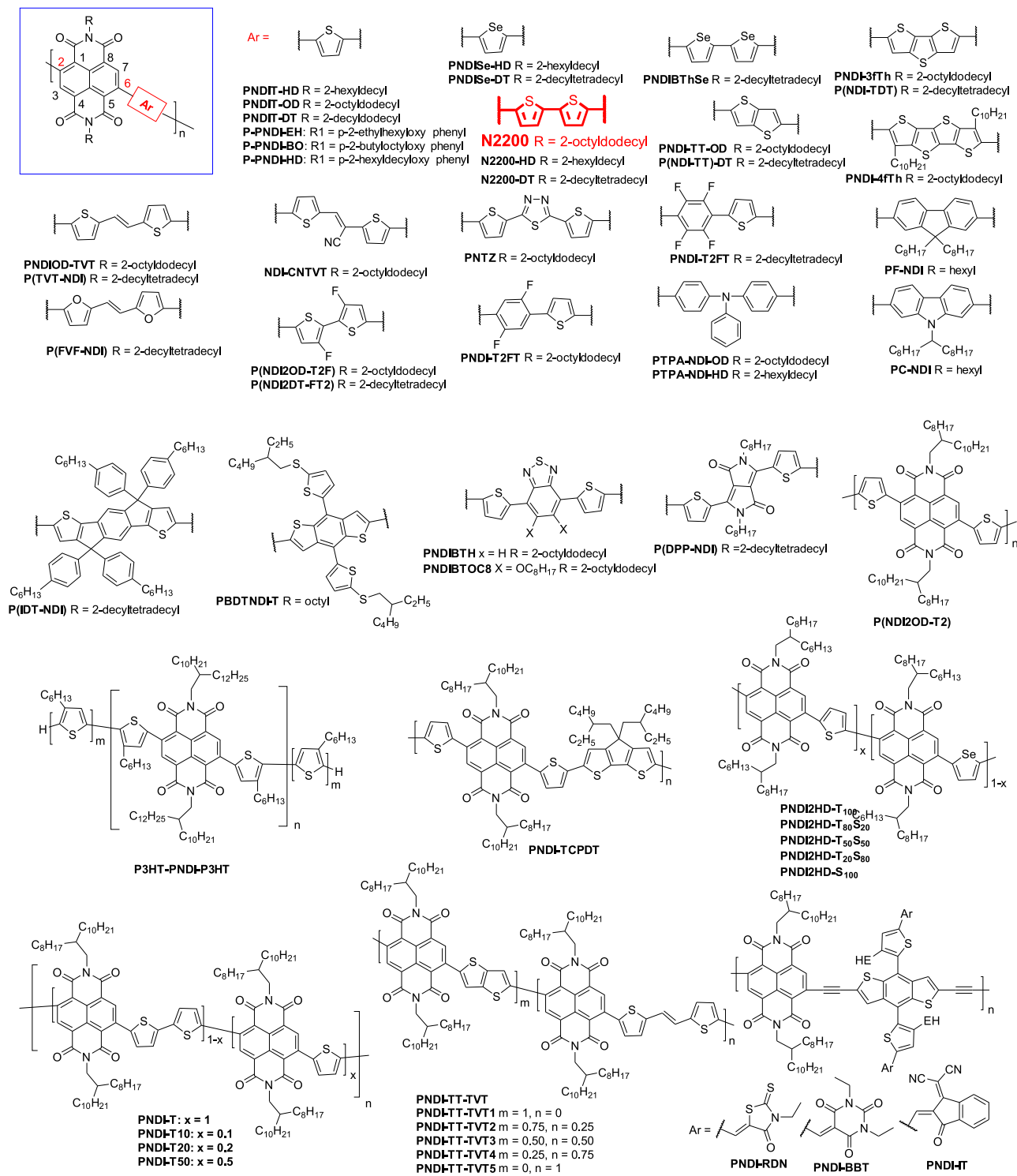


Fig. 9. (a) Promising/popular cores (- indicates possible points for extending conjugation) and general molecular design strategies for (b) polymer and (c) small molecules.



**Fig. 10.** General design and chemical structures of naphthalene diimide (NDI) based polymeric NFAs. [31–83].

et al. synthesized a polymeric NFA **PNDIT-HD** by combining NDI with thiophene and blending it with **PBDTTTPD** polymer donor; this blend exhibited superior PCE of 6.64% over the device based on PC<sub>60</sub>BM acceptor due to its high durability and flexibility [31]. Variation of alkyl chain length on NDI in **PNDIT-HD** greatly influences the phase separation and crystal orientation in active blend [32]. In addition, device fabrication using non-halogenated solvents also showed superior PCE over halogenated solvents due to balanced hole/electron mobility and favorable surface

morphology [33]. When π-linker changed from thiophene to selenophene (**PNDISe-HD**), PCE was further enhanced to 7.73% due to red-shifted absorption and thus a higher J<sub>SC</sub> of 18.80 mA cm<sup>-2</sup> [36]. Later, fluorinated polymer donor PBDT-TTP1-3 was used to optimize morphology with “face-on” oriented crystallites, which produced even higher V<sub>OC</sub> of 0.94 V and J<sub>SC</sub> of 12.22 mA cm<sup>-2</sup>, then a PCE of 7.13%. Co-polymer based on bithiophene and NDI results in a potential NFA **N2200**, which have been widely used together with several donors and showed better performance. The first time,

**Table 1**

Photo-physical and photovoltaic properties of naphthalene diimide (NDI) based polymeric NFAs.

NFA	$\lambda_{max}$ (nm)	HOMO (eV)	LUMO (eV)	Donor	$V_{OC}$ (mV)	$J_{SC}$ (mA Cm <sup>-2</sup> )	FF	PCE (%)	Refs.
<b>PNDIT-HD</b>	600	5.64	3.79	PBDTTTPD	1.06	11.22	0.56	6.64	[31]
				PTB7-Th	0.79	13.46	0.56	5.96	[32]
<b>PNDIT-OD</b>	550	5.65	3.80	PTB7-Th	0.80	11.97	0.53	5.05	[32]
				PTB7-Th	0.77	12.26	0.52	4.94	[33]
<b>PNDIT-DT</b>	550	5.64	3.81	PTB7-Th	0.81	7.81	0.52	3.25	[34]
<b>PPNDI-EH</b>	581	5.87	4.01	PTB7-Th	0.76	10.66	0.49	4.07	[35]
<b>PPNDI-BO</b>	580	5.87	4.00	PTB7-Th	0.77	11.15	0.49	4.25	[35]
<b>PPNDI-HD</b>	581	5.89	4.01	PTB7-Th	0.77	9.97	0.46	3.62	[35]
<b>PNDISe-HD</b>	605	6.00	3.84	PTB7-Th	0.81	18.80	0.51	7.73	[36]
				PBDT-Th-TP1	0.88	7.41	0.45	2.93	[37]
				PBDT-Th-TP2	0.94	12.22	0.62	7.13	[37]
				PBDT-Th-TP3	1.04	9.27	0.54	5.21	[37]
<b>PNDIT-DT</b>	542	5.77	4.00	PSEHTT	0.61	3.80	0.56	1.20	[38]
<b>PNDISe-OD</b>	556	5.70	4.00	PSEHTT	0.75	6.53	0.60	2.84	[38]
<b>PNDISe-HD</b>	556	5.65	4.00	PSEHTT	0.76	7.78	0.55	3.16	[38]
<b>N2200</b>	700	5.45	4.00	P3HT	0.52	1.41	0.29	0.21	[39]
				PTPD3T	0.87	6.75	0.55	3.22	[40]
				PTQ1	0.55	8.85	0.84	4.10	[41]
				P2F-DE	0.76	11.72	0.54	4.81	[42]
				PBDT-NT	0.77	11.30	0.53	4.70	[43]
				PBDTBDD	0.82	6.80	0.43	2.40	[44]
				PBDB-T	0.87	11.70	0.58	5.80	[44]
				J51	0.83	14.18	0.70	8.27	[45]
				J50	0.60	13.93	0.59	4.90	[45]
				PTB7	0.80	6.28	0.53	2.66	[46]
				PTB7	0.62	3.40	0.39	1.10	[47]
				PTB7-Th	0.79	13.00	0.56	5.73	[48]
				PTB7-Th	0.81	12.36	0.53	5.30	[49]
				PDP5T	0.68	5.20	0.48	1.70	[50]
				DPP-Pyr	0.78	4.45	0.59	2.05	[51]
				BDT-DPP2	0.82	7.60	0.60	3.74	[52]
				DTP-DPP	0.82	10.14	0.58	4.82	[53]
				C-DPP	0.87	8.59	0.62	4.64	[54]
				Si-DPP	0.86	8.14	0.54	4.02	[54]
				PTzBI	0.85	15.17	0.70	9.20	[55]
				PTzBI-Si	0.87	15.57	0.74	10.10	[56]
<b>N2200-HD</b>	690	5.40	3.95	PTB7-Th	0.81	14.08	0.54	6.14	[57]
				PTB7-Th	0.82	13.97	0.53	6.11	[49]
<b>N2200-2DT</b>	690			PTB7-Th	0.82	10.48	0.50	4.31	[49]
<b>PNDIBThSe</b>	700	5.95	3.94	P3HT	0.53	3.79	0.44	0.88	[58]
<b>PF-NDI</b>	513	5.93	3.61	P3HT	0.68	3.63	0.66	1.63	[59]
<b>PC-NDI</b>	530	5.71	3.68	TTV7	0.88	7.71	0.54	3.68	[60]
<b>PNDI-TT-OD</b>		5.59	3.94	PTB7-Th	0.57	3.56	0.39	0.79	[61]
<b>PNDI-TT-TVT</b>		5.34	3.88	PTB7-Th	0.79	12.66	0.49	4.86	[61]
<b>PNDIOD-TVT</b>	698	5.50	3.92	PTB7-Th	0.80	7.41	0.50	2.94	[61]
				PTB7-Th	0.84	11.40	0.43	4.25	[62]
<b>NDI-CNTVT</b>	604	5.97	3.94	PTB7-Th	0.69	8.39	0.48	2.76	[63]
<b>P(TVT-NDI)</b>	600	5.69	3.76	J51	0.81	13.10	0.61	6.43	[64]
<b>P(FVF-NDI)</b>	800	5.79	3.80	J51	0.83	13.09	0.48	5.21	[64]
<b>PNDI-TT-OD</b>	610	5.45	3.88	P3HT	0.51	0.46	0.39	0.11	[65]
<b>PNDI-3fTh</b>	645	5.31	3.91	P3HT	0.48	0.19	0.48	0.04	[65]
<b>PNDI-4fTh</b>	660	5.29	3.92	P3HT	0.47	0.57	0.55	0.13	[65]
<b>P(NDI-TT)-DT</b>	545	5.60	3.92	J51	0.74	11.02	0.45	3.70	[66]
<b>P(NDI-TDT)</b>	720	5.37	3.95	J51	0.69	11.91	0.62	5.10	[66]
<b>N2200</b>	704	5.49	4.05	PTB7-Th	0.79	11.92	0.56	5.28	[67]
<b>P(NDI2OD-FT2)</b>	630	5.50	3.91	PTB7-Th	0.81	13.53	0.62	6.71	[67]
<b>N2200</b>	627	5.75	3.78	PBDTTTPD	1.03	4.45	0.44	2.02	[68]
<b>P(NDI2OD-T2F)</b>	695	5.99	3.90	PBDTTTPD	1.00	11.68	0.52	6.09	[68]
<b>PNDI-T2FT</b>	600	5.64	3.90	PTB7-Th	0.78	4.80	0.34	1.30	[69]
<b>PNDITF4T</b>	590	6.10	3.87	PTB7-Th	0.78	11.70	0.52	4.60	[70]
<b>PNDI-T2FT2</b>	620	5.61	3.90	PTB7-Th	0.80	14.3	0.44	5.20	[69]
<b>PTPA-NDI-OD</b>	620	5.72	3.78	PTB7-Th	0.92	5.25	0.34	1.65	[71]
<b>PTPA-NDI-HD</b>	620	5.65	3.81	PTB7-Th	0.96	6.25	0.37	2.17	[71]
<b>PBDTNDI-T</b>	650	5.55	3.98	PBDTT-S-TT	0.86	5.62	0.59	2.88	[72]
<b>P(IDT-NDI)</b>	730	5.75	3.84	J50	0.78	9.68	0.55	4.12	[73]
				J51	0.93	9.55	0.60	5.33	[71]
				PTB7-Th	0.91	7.35	0.54	3.63	[73]
<b>PNDIBTH</b>	709	5.94	3.93	PBDTT-C-T	0.76	3.77	0.42	1.20	[74]
<b>PNDIBTOC8</b>	674	5.82	3.72	PBDTT-C-T	0.90	7.65	0.45	3.14	[74]
<b>P(DPP-NDI)</b>	841	5.30	3.99	PBDTT-C-T	0.58	1.16	0.44	0.30	[75]
<b>PNTZ</b>	565	5.70	4.02	PTB7-Th	0.71	13.26	0.46	4.35	[76]
<b>P(NDI2OD-T2)</b>	688	5.52	4.02	PTB7-Th	0.79	10.99	0.37	3.22	[62]
<b>P3HT-PNDI-P3HT</b>	546	5.60	4.22	P3HT	0.56	4.57	0.50	1.28	[77]
<b>PNDI-TCPDT</b>	723	5.35	4.15	P3HT	0.56	3.77	0.65	1.40	[78]
<b>PNDI-T10</b>	694	6.36	4.05	PTB7-Th	0.83	12.90	0.71	7.60	[79]
<b>PNDI-T20</b>	680	6.37	4.05	PTB7-Th	0.83	9.70	0.52	4.20	[79]

**Table 1** (Continued)

NFA	$\lambda_{\text{max}}$ (nm)	HOMO (eV)	LUMO (eV)	Donor	$V_{\text{OC}}$ (mV)	$J_{\text{SC}}$ (mA cm $^{-2}$ )	FF	PCE (%)	Refs.
<b>PNDI-T50</b>	644	6.38	4.00	PTB7-Th	0.83	5.80	0.48	2.30	[79]
<b>PNDI-T</b>	600	6.52	4.04	PBDTT-FTAZ	0.74	7.50	0.53	3.00	[80]
<b>PNDI-T10</b>	700	6.36	4.05	PBDTT-FTAZ	0.76	11.30	0.54	4.10	[80]
<b>PNDI-TT-TVT1</b>	615	5.59	3.94	PTB7-Th	0.57	3.56	0.39	0.79	[81]
<b>PNDI-TT-TVT2</b>	630	5.54	3.92	PTB7-Th	0.81	9.60	0.45	3.48	[81]
<b>PNDI-TT-TVT3</b>	645	5.50	3.92	PTB7-Th	0.80	10.86	0.43	3.65	[81]
<b>PNDI-TT-TVT4</b>	650	5.42	3.90	PTB7-Th	0.70	13.75	0.48	5.27	[81]
<b>PNDI-TT-TVT5</b>	675	5.34	3.88	PTB7-Th	0.80	7.41	0.49	2.94	[81]
<b>PNDI2HD-T100</b>	599	5.68	3.84	PTB7	0.79	6.64	0.48	2.50	[82]
<b>PNDI2HD-T80S20</b>	607	5.63	3.80	PTB7	0.79	7.02	0.49	2.73	[82]
<b>PNDI2HD-T50S50</b>	609	5.61	3.82	PTB7	0.76	7.41	0.49	2.87	[82]
<b>PNDI2HD-T20S80</b>	620	5.53	3.76	PTB7	0.79	7.88	0.51	3.21	[82]
<b>PNDI2HD-S100</b>	627	5.51	3.78	PTB7	0.79	8.99	0.51	3.60	[82]
<b>PNDI-RDN</b>	717	5.91	3.85	PTB7-Th	0.69	13.51	0.60	5.55	[83]
<b>PNDI-BBT</b>	774	5.89	3.97	PTB7-Th	0.56	14.85	0.48	3.96	[83]
<b>PNDI-IT</b>	745	5.90	3.97	PTB7-Th	0.56	15.66	0.59	5.13	[83]

Sirringhaus et al. used P3HT:**N2200** blend to construct OSCs but poor phase separation in active blend leads to poor PCE [39]. Marks et al. demonstrated that the high molecular weight of both donor and acceptor in the active blend improves crystallinity and phase separation and thus increase in  $J_{\text{SC}}$  [40].

Kim et al. found that the increasing number of average molecular weight of polymeric NFA remarkably shift lamellar crystallite textures from “edge-on” to “face-on” orientation, which was responsible for higher  $J_{\text{SC}}$  of 14.08 mA cm $^{-2}$  and then PCE of 6.14% [56]. Several donors were used to fabricate OSCs with **N2200**, giving promising results to establish a clear structure-property relation. To harvest more solar flux, **N2200** blended with complimentary absorbing low bandgap quinoxaline polymeric donors (PTQ1 and P2F-DE), while strong absorption and suitable energy levels of P2F-DE produced superior PCE (4.81%) over PTQ1 [41]. Similarly, low bandgap PBDT-NT donor gives the domain size in the range of 100 nm with “face-on” orientation that favors high  $J_{\text{SC}}$  (11.03 mA cm $^{-2}$ ) and PCE (4.70%) [43]. Hou et al. used PBDBTDD and PBDT-T donors to blend with **N2200** and found that PBDT-T showed high PCE of 5.8% due to favorable molecular interactions which allowed the formation of two dimensional (2D) nano-aggregates and decrease charge recombination and thus a high  $J_{\text{SC}}$  of 11.70 mA cm $^{-2}$  when compared to PBDBTDD [44]. Similarly, in the case of low bandgap fluorinated donors (J50 and J51), J51 displayed higher PCE of 8.27% due to the balanced hole and electron mobilities of nano-scale sized blend film [45]. Interestingly, PTB7-Th donor improves high charge-carrier generation and collection efficiencies (~80%) of the corresponding blend films, which were responsible for high  $J_{\text{SC}}$  (13.0 mA cm $^{-2}$ ) [48]. Also, side chain engineering on NDI with 2-hexyldecy chain **N2200-HD** showed noticeable crystalline changes which facilitate 3D charge transport that produces high  $J_{\text{SC}}$  of 13.97 mA cm $^{-2}$  and PCE of 6.11% [49]. Cao and workers optimized the fabrication of device by environmentally-friendly 2-methyl-tetrahydrofuran solvent based on **N2200** blended with PTzBI donor which results in high  $J_{\text{SC}}$  of 15.17 mA cm $^{-2}$  and remarkably high PCE of 9.16% attributed to enhanced exciton generation and dissociation and reduce bimolecular recombination [48]. Similarly, Ying et al. used the same solvent conditions and blended with a new siloxane-functionalized donor PTzBI-Si for **N2200**, achieved highest PCE up to 10.1%. It was attributed to the high crystallinity of blend film that improved charge carrier mobility and favors “face-on” orientation. [56]

NDI co-polymer with bi-selenophene  $\pi$ -linker (**PNDIBThSe**) showed blue shifted absorption and then lowers PCE (0.90%) when compared to **N2200** [58]. Tajima et al. incorporated a fluorene linker (**PF-NDI**) that showed a PCE of 1.63% blended with P3HT

[59]. When compared to **PF-NDI**, carbazole-conjugated polymeric NFA **PC-NDI** enhanced PCE to 3.68% due to its red-shifted absorption and leads to high  $J_{\text{SC}}$  (7.71 mA cm $^{-2}$ ) when TTV7 donor was blended (Table 1) [60]. Chen et al. reported PDI polymeric NFAs based on vinyl thiophene bridge (**PNDI-TT-TVT**) exhibited better PCE of 4.86% when it blended with PTB7-Th because of co-planar electron rich thienothiophene and vinyl-thiophene bridge showed red-shifted absorption and balance charge carrier mobility [61,62]. Incorporating vinyl-furan bridge **P(FVF-NDI)** showed drastic red-shifted absorption due to electron-rich co-planar linkage and produced a higher PCE of 5.21% than **P(TVT-NDI)** [64]. This result indicates that the electron-rich thiophene fused unit’s broadening spectral response is an essential key factor for OSC applications. In this context, incorporation of fused heterocyclic linkers resulted in a set of polymeric NFAs (**PNDI-TT-OD**, **PNDI-3fTh** and **PNDI-4fTh**), which blended against wide bandgap P3HT donor resulting poor photon to current conversion owing to the unfavorable energy levels [65]. Therefore, it is noteworthy to mention that frontier energy levels are very important along with a broad spectral response of NFAs. Since fluorine incorporation raises the LUMO level, improved crystallinity and phase separation in active blend and there by increases  $V_{\text{OC}}$  and PCE of the device. Jen et al. synthesized fluorine-substituted polymer **P(NDI2OD-T2F)** as NFA against PTB7-Th donor, and the corresponding blend showed enhanced crystallinity with preferentially “face-on” orientation resulting in higher  $J_{\text{SC}}$ ,  $V_{\text{OC}}$  and PCE (6.71%) than its parent NFA of **N2200** (5.28%) [67]. When it was blended with PBDTTTPD donor,  $V_{\text{OC}}$  enhanced to 1.00 V due to a favorable lower HOMO level (5.61 eV) of PBDTTTPD than HOMO of PTB7-Th (5.30 eV) [68]. These results motivated Ong et al. to incorporate disfluorobenzene linker (**PNDI-T2FT2**), which increases crystallinity and electron mobility and thus a high  $J_{\text{SC}}$  (14.30 mA cm $^{-2}$ ) and PCE of 5.20% [69].

The polymer of 2D conjugated DBT unit and NDI (**PBDTNDI-T**) exhibited a PCE of 2.88% blended with donor **PBDTT-S-TT** [72]. To further increase the absorption, IDT linker was incorporated to replace BDT linker of previous polymeric acceptor results a new NFA **P-IDT-NDI**, which was blended with medium bandgap donors (J50, J51 and PTB7-Th). Blend film based on J51 donor exhibited superior PCE (5.33%) attributed to its complimentary absorption and low HOMO level (5.26 eV) over other donors J50 (4.12%) and PTB7-Th (3.63%) [73]. Fu et al. synthesized **PNDIBTH** and **PNDIBTOC8** based on NDI conjugated with BT, and alkoxy substituted BT units for a broad spectral response [74]. Better solubility and high LUMO energy of **PNDIBTOC8** and dendrite-like phase separation of blend film produce higher  $V_{\text{OC}}$  of 0.90 V and PCE of 3.14% when compared with **PNDIBTH**. However, replacing

BT with DPP gave a new polymeric NFA **P-DPP-NDI**, which displayed a drastic red shift (140 nm), but its unmatched energy level produced poor PCE [75].

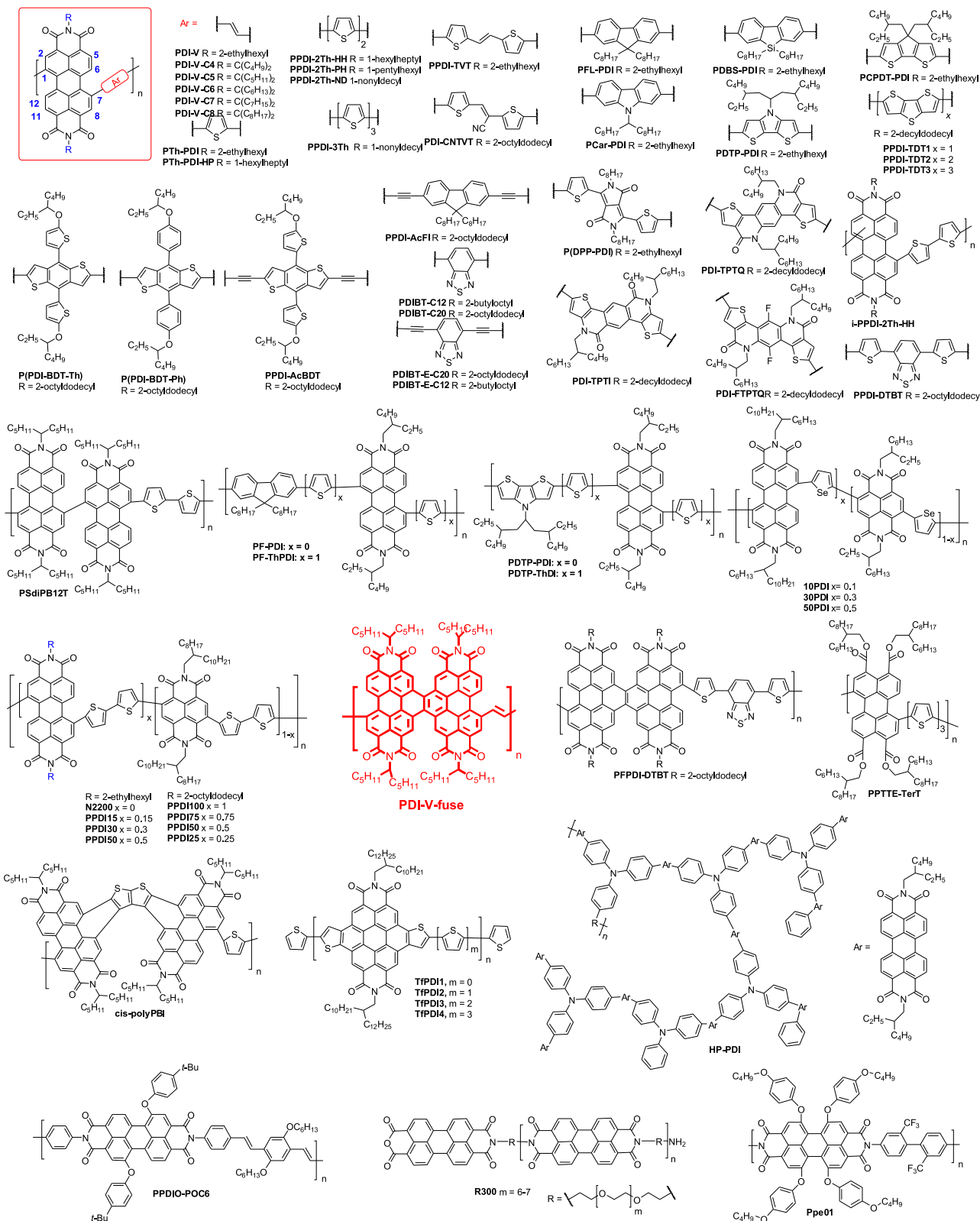
Li et al. made polymeric NFA **PNTZ** based on NDI and 1,3,4-thiadiazole showed complimentary absorption with the donor PTB7-Th in active layer, which results in a higher  $J_{SC}$  of  $13.26 \text{ mA cm}^{-2}$  and PCE of 4.60% (Table 1) [76]. Polymer containing thiophene on both sides of NDI (**P(NDI2OD-T2)**) showed red-shifted absorption and then high  $J_{SC}$  of  $10.99 \text{ mA cm}^{-2}$  when compared to one side thiophene-NDI polymer (**PNDIT-DT**) [62]. Nakabayashi synthesized block copolymers (**P3HT-PNBI-P3HT**) composed of P3HT and poly NDI segments displayed red-shifted absorption with tailing up to 950 nm [77]. Neher et al. synthesized a polymer of thiophene-NDI-cyclopentadithiophene named as **PNDI-TCPDT**, and it exhibited strong absorption than **N2200** polymeric NFA, but its low LUMO level produced a poor PCE (1.40%). For OPV, low FF was one of the main limiting factors, which can be improve by high electron mobility and favorable nano-phase morphology of active blend. In this context, Wang et al. made a series of polymers (**PNDI-T10**, **PNDI-T20** and **PNDI-T50**) by replacing a certain amount of bithiophene units in the **N2200** backbone by single thiophene units. These polymers are properly miscible with PTB7-Th donor and form nanostructure blend film with efficient exciton dissociation and charge transport [79]. In particular, **PNDI-T10** showed a superior PCE of 7.6% over its parent **N2200** acceptor under similar conditions due to enhanced device parameters ( $J_{SC}$  of  $12.90 \text{ mA cm}^{-2}$ ;  $V_{OC}$  of 0.83 V and FF of 0.71) [79]. When **PNDI-T10** blended with PBDTTS-FTAZ donor, a higher PCE of 6.60% was achieved due to the improved crystallinity of active blend [80]. Chen et al. synthesized **PNDI-TT-TVTS** which are composed of NDI units (m) and randomly distributed thienothiophene and thienylene-vinylene-thienylene units (n) in different ratios, and variation of this ratio changes the absorption, energy levels, charge transport, and morphology of the active blend [81]. Finally, **PNDI-TT-TVTS** (m:n = 0.25:0.75) achieved a higher PCE of 5.27% due to its blend which showed high balanced charge mobility when compared with other polymeric NFAs [81]. Recently, Ying et al. synthesized two dimensional cross conjugated polymeric NFAs (**PNDI-RDN**, **PNDI-BBT**, and **PNDI-IT**) bearing pendant acceptor groups such as rhodanine thiobarbituric acid, dicyanomethylene-3-indanone in the side chain, respectively, which effectively tuned the optical and energy levels. Among them, **PNDI-RDN** showed a better PCE of 5.55% as blended with PTB7-Th donor due to uplifted LUMO level and thus a high  $V_{OC}$  of 0.69 V [83]. Finally, NDI-based polymers containing oligothiophene-conjugated unit exhibited a broad spectral response, high electron affinity, good co-planarity and then good PCE. In particular, bithiophene linker-based polymer (**N2200**) exhibited a PCE as high as 10.1% as blended with PTzBI-Si donor. Also, fluorine incorporation into oligothiophene units and random copolymers with NDI as co-acceptor were promising candidates.

### 2.1.2. Perylenediimide-based polymeric acceptors

Research interest on PDI-based polymeric NFAs was continuously growing due to its easy functionalization at bay positions, and imide N-positions. Their planar structure offers favorable molecular  $\pi-\pi$  interactions, which grow micro-sized PDI crystal motifs suitable for charge transport leading to high electron mobility. General PDI-based polymeric NFAs were shown in Fig. 11, and optical and device parameters were summarized in Table 2. Various  $\pi$ -linkers conjugated with PDI at bay positions afford polymeric NFAs. In addition, incorporation of alkyl chains at imide N-positions of PDI can feasibly manipulate the solubility and aggregation behavior in thin film. The effect of  $\pi$ -linkers on photophysical and photovoltaic properties were systematically analyzed and correlated. For example, Hashimoto and co-workers

incorporated various  $\pi$ -linkers for making PDI polymer to optimize the film morphology and phase separation of active blend. The polymer **PDI-V** contains PDI conjugated with vinyl unit through bay positions (1 and 7), was blended with P3HT donor, produced a poor PCE (0.21%) due to weak absorption and high HOMO (P3HT:4.91 eV) of donor material [84]. To overcome these issues, Yan and co-workers blended **PDI-V** with PTB7-Th donor, which has a low HOMO of 5.39 eV, and complimentary absorption spectra, drastically enhanced  $J_{SC}$  and  $V_{OC}$  and then achieved a high PCE in the range of 5.97% to 7.40% [85]. Better co-planarity of vinyl unit with PDI is responsible for high electron mobility and then high  $J_{SC}$  and FF. Moreover, increasing side chain length improved the lamellar  $\pi-\pi$  spacing and crystallinity of active blend and hence brought about a moderate increase in FF of device [85,86]. When PDI-thiophene-conjugated polymers (**PTh-PDI** and **PTh-PDI-HP**) blended with different donors, **PTh-PDI-HP** achieved a high PCE of 3.48% in blend with isoindigo-based donor Pil-2T, which was attributed to high  $V_{OC}$  (1.01 V) and  $J_{SC}$  ( $6.91 \text{ mA cm}^{-2}$ ) [87]. Polymeric NFAs, **PPDI-2Th-ND** and **PPDI-3Th** composed of PDI and oligothiophene linkers exhibited a low PCE when blended with P3HT donor due to unmatched energy levels of both donor and acceptor in the active blend [88]. They blend with PTB7-Th donor improved PCE (2.50%) due to well-matched energy level and absorption spectra which lead to high  $V_{OC}$  (0.85 V) and  $J_{SC}$  ( $7.25 \text{ mA cm}^{-2}$ ), respectively [100]. Hashimoto and co-workers synthesized PDI-based polymeric NFAs containing  $\pi$ -linkers such as fluorene (**PFL-PDI**), carbazole (**PCar-PDI**), dibenzosilole (**PDBS-PDI**) and dithienopyrrole (**PDTP-PDI**) to fine-tune the absorption and energy levels. As the conjugate linker changes from fluorene to dithienopyrrole leads to red-shifted absorption and stabilized LUMO levels. When they blended with low HOMO (5.08 eV) polymer donor PVTPT3, high PCE values were obtained because relatively better phase separation of the active layer that gave high  $V_{OC}$  and  $J_{SC}$ . Among them, **PCar-PDI** exhibited a better PCE of 1.15% as blend with PVTPT3 donor [84]. Yang and co-workers made **PCPD-T-PDI** polymeric NFA based on cyclopentadithiophene conjugated with bay positions of PDI units. However, it showed poor PCE (0.43%) due to its un-favorable LUMO that reduced the photon conversion efficiency when blended with **P-DTSi-BT** [89]. Later, Marder and co-workers made a narrow bandgap polymer **PPDI-TDT1** with electron-rich dithienothiophene linker, leading to significantly red-shifted absorption as compared to those of previous linkers based NFAs (Table 2) [90,93]. Photovoltaic device based on **PPDI-TDT1** in combination with PVTPT2 donor showed better PCE of 1.50% due to its improved electron mobility [86]. Increasing the conjugation length of oligo(dithienothiophene) broadens the spectral response, and then high  $J_{SC}$  and PCE were obtained. Zhan and co-workers improved the PCE (3.45%) of **PPDI-TDT1** by choosing well-matched donor PBDTTT-C-T, which has high HOMO energy value [91].

Li and co-workers synthesized two PDI-based polymeric NFAs by combining PDI with thiophene and phenyl substituted DBT units. Blend film of PTB7-Th:**P(PDI-BDT-Ph)** gave good nano-fiber morphology and higher electron mobility and thus a higher PCE (4.31%) than **P(PDI-BDT-Ph)** [95]. Later, Cao and co-workers synthesized polymeric NFAs based on PDI linking with fluorene (**PPDI-ACFI**), and DBT (**PPDI-ACBDT**) through acetylene bond, giving PCE of 5.09% and 2.37%, respectively. It was attributed to the higher  $V_{OC}$  obtained from better charge carrier mobility of the active blend [96]. Yu and co-workers reported a series of polymeric NFAs (**PIP**, **PQP** and **PFP**) by incorporation of various aromatic amide units. When these NFAs blended with PTB7 and PTB7-Th donors, PTB7-Th:**PDI-TPT1** blend delivered a higher PCE of 3.52% because internal planarization of aromatic amide linker unit and better binding affinity with PTB7-Th donor favor “face-on” orientated crystallization in blend film [97]. Li and co-workers

**Fig. 11.** General design and chemical structures of perylene diimide (PDI) based polymeric NFAs [84–113].

made PDI-based polymers, composed of PDI and low bandgap chromophores, but led to low PCE due to poor photon to current conversion efficiency [98]. Low bandgap polymer **P(PDI-DPP)** blended with PBDTTT-C-T improved the PCE to 2.01% which was attributed to the relatively high electron mobility and preferable

micro-phase separation [75]. Pei and co-workers demonstrated that the regio-regular **PPDI-2Th-HH** improved charge collection efficiency and reduced recombination, which enhances FF when compared to irregular **i-PPDI-2Th-HH** [99]. Hashimoto and co-workers synthesized polymeric NFAs by incorporating fluorene

**Table 2**

Photo-physical and photovoltaic properties of perylene diimide (PDI) based polymeric NFAs.

NFA	$\lambda_{max}$ (nm)	HOMO (eV)	LUMO (eV)	Donor	$V_{oc}$ (mV)	$J_{sc}$ (mA Cm $^{-2}$ )	FF	PCE (%)	Refs.
<b>PDI-V</b>	597	5.83	4.05	P3HT	0.44	1.03	0.46	0.21	[84]
<b>PDI-V</b>				PVTPT3	0.58	2.23	0.38	0.48	[84]
<b>PDI-V-C4</b>	595	5.77	4.04	PTB7-Th	0.73	14.44	0.53	5.58	[85]
<b>PDI-V-C5</b>	595	5.76	4.04	PTB7-Th	0.73	14.88	0.55	5.97	[85]
<b>PDI-V-C6</b>	595	5.76	4.03	PTB7-Th	0.74	15.55	0.63	7.25	[85]
<b>PDI-V-C6</b>	600	5.77	4.03	PTB7-Th	0.74	15.80	0.63	7.30	[86]
<b>PDI-V-C7</b>	595	5.75	4.02	PTB7-Th	0.74	15.30	0.65	7.40	[85]
<b>PDI-V-C8</b>	595	5.77	4.04	PTB7-Th	0.74	14.83	0.63	6.91	[85]
<b>PTh-PDI</b>	559	5.84	3.94	P3HT	0.50	0.70	0.58	0.20	[84]
<b>PTh-PDI</b>				PVTPT3	0.62	3.24	0.49	0.97	[84]
<b>PTh-PDI-HP</b>	565	5.60	3.80	PiI-2T	1.01	6.91	0.50	3.48	[87]
<b>PTh-PDI-HP</b>	565	5.60	3.80	PiI-BDT	1.07	6.54	0.45	3.12	[87]
<b>PTh-PDI-HP</b>	565	5.60	3.80	PiI-2F	0.96	5.59	0.51	2.71	[87]
<b>PTh-PDI-HP</b>	565	5.60	3.80	PiI-tT	0.97	4.10	0.42	1.67	[87]
<b>PPDI-2Th-ND</b>	600	5.89	4.23	P3HT	0.54	0.32	0.40	2.33	[88]
<b>PPDI-3Th</b>	620	5.94	4.34	P3HT	0.56	2.81	0.51	0.80	[88]
<b>PFI-PDI</b>	570	5.93	3.61	P3HT	0.52	0.39	0.53	0.11	[84]
<b>PDBS-PDI</b>	551	6.01	3.71	P3HT	0.50	0.76	0.49	0.18	[84]
<b>PCar-PDI</b>	545	5.83	3.66	P3HT	0.58	0.91	0.55	0.29	[84]
<b>PDTp-PDI</b>	715	5.49	3.83	P3HT	0.46	0.76	0.50	0.17	[84]
<b>P-co-CDT</b>	690	5.22	4.02	P-DTSi-BT	0.68	1.40	0.38	0.43	[89]
<b>PPDI-TDT1</b>	619	5.90	3.90	PVTPT2	0.62	4.20	0.39	1.50	[90]
<b>PPDI-TDT2</b>	726	5.50	3.80	PBDTTT-C-T	0.75	8.55	0.52	3.45	[91]
<b>PPDI-TDT3</b>		5.40	4.00	PVTPT4	0.68	3.18	0.43	0.94	[92]
<b>PPDI-TVt</b>	626	5.70	3.67	PVTPT4	0.67	3.71	0.43	1.08	[92]
<b>PDI-CNTVT</b>	582	5.83	3.93	PBDTTT-C-T	0.76	2.80	0.40	0.81	[84]
<b>P(PDI-BDT-Th)</b>	554	5.50	3.89	PTB7-Th	0.66	7.32	0.36	1.74	[63]
<b>P(PDI-BDT-Ph)</b>	665	5.67	3.89	PTB7-Th	0.79	11.28	0.49	3.58	[95]
<b>PPDI-AcFl</b>	560	6.12	3.77	PBDB-T	0.85	9.60	0.63	5.09	[96]
<b>PPDI-AcBDT</b>	650	5.65	3.85	PBDB-T	0.76	6.09	0.52	2.37	[96]
<b>PDI-TPTQ</b>	494	5.97	3.97	PTB7	0.68	7.15	0.37	1.86	[97]
<b>PDI-TPTQ</b>				PTB7-Th	0.70	7.72	0.57	3.22	[97]
<b>PDI-TPT1</b>	622	5.73	4.04	PTB7	0.65	1.06	0.26	0.21	[97]
<b>PDIBT-C12</b>	491	5.64	3.93	PTB7-Th	0.69	4.94	0.39	1.43	[97]
<b>PDIBT -C20</b>	486	5.63	3.95	P3HT	0.68	4.13	0.34	0.97	[97]
<b>PDIBT-E-C12</b>	530	5.64	4.05	PTB7-Th	0.70	8.39	0.57	3.52	[97]
<b>PDIBT-E-C20</b>	640	5.63	4.03	P3HT	0.52	0.68	0.41	0.14	[95]
<b>P(PDI-DPP)</b>	700	5.42	4.07	PF12TBT	0.88	1.30	0.26	0.29	[98]
<b>i-PPDI-2Th-HH</b>	594	5.50	3.80	P3HT	0.23	3.90	0.50	0.45	[99]
<b>PPDI-2Th-HH</b>	594	5.50	3.80	P3HT	0.51	5.70	0.32	0.94	[99]
<b>PPDI-2Th-PD</b>	585	5.76	4.11	PTB7-Th	0.85	7.20	0.42	2.50	[100]
<b>PSdiPB12T</b>	580	5.77	4.07	PTB7-Th	0.75	11.20	0.54	4.50	[100]
<b>PF-PDI</b>	570	5.93	3.61	PVTPT3A	0.76	1.77	0.43	0.58	[111]
<b>PF-ThPDI</b>	626	5.80	3.69	PVTPT3A	0.64	0.73	0.29	0.13	[111]
<b>PDTp-PDI</b>	711	5.49	3.83	PVTPT3A	0.66	3.05	0.46	0.93	[111]
<b>PDTp-ThPDI</b>	748	5.27	4.00	PVTPT3A	0.60	0.68	0.31	0.13	[111]
<b>N2200</b>	645	5.42	3.90	PTB7	0.81	6.19	0.40	2.00	[112]
<b>PPDI15</b>	630	5.49	3.94	PTB7	0.79	8.96	0.41	2.91	[112]
<b>PPDI30</b>	618	5.51	3.94	PTB7-Th	0.79	10.65	0.49	4.13	[112]
<b>PPDI50</b>	605	5.60	4.00	PTB7	0.77	7.55	0.46	2.65	[112]
<b>PPDI100</b>	600	6.10	3.90	PTB7-Th	0.72	4.45	0.32	1.03	[103]
<b>PPDI75</b>	598	5.87	3.84	PTB7-Th	0.74	4.75	0.34	1.19	[103]
<b>PPDI50</b>	604	5.85	3.82	PTB7-Th	0.74	5.80	0.34	1.44	[103]
<b>PPDI25</b>	628	5.91	3.80	PTB7-Th	0.79	8.96	0.45	3.16	[103]
<b>N2200</b>	702	5.88	3.87	PTB7-Th	0.80	10.81	0.54	4.67	[103]
<b>PNDISe-HD</b>	622	5.95	3.84	PBDTTT-CT	0.81	4.16	0.40	1.36	[104]
<b>10PDI</b>	615	5.95	3.84	PBDTTT-CT	0.78	6.94	0.51	2.80	[104]
<b>30PDI</b>	578	5.95	3.89	PBDTTT-CT	0.79	18.55	0.45	6.29	[104]

**Table 2** (Continued)

NFA	$\lambda_{\text{max}}$ (nm)	HOMO (eV)	LUMO (eV)	Donor	$V_{\text{OC}}$ (mV)	$J_{\text{SC}}$ (mA cm $^{-2}$ )	FF	PCE (%)	Refs.
<b>5OPDI</b>	544	5.95	3.89	PBDTTT-CT	0.73	9.68	0.38	2.66	[104]
<b>TfpDI1</b>	574	6.04	3.54	PT5TPA	0.87	1.07	0.33	0.31	[105]
<b>TfpDI2</b>	630	5.87	3.51	PT5TPA	0.87	1.40	0.33	0.41	[105]
<b>TfpDI3</b>	654	5.70	3.51	PT5TPA	0.92	2.14	0.43	0.84	[105]
<b>PPTTE-TerT</b>	539	5.60	3.54	P3HT	0.83	2.74	0.34	0.76	[106]
<b>PDI-V-fuse</b>	547	4.03	5.94	PTB7-Th	0.74	17.07	0.67	8.59	[107]
<b>PDI-V-C5</b>	598	4.03	5.77	PTB7-Th	0.74	15.39	0.64	7.38	[107]
<b>PPDI-DTBT</b>	620	5.46	3.87	PTB7-Th	0.78	10.65	0.49	4.07	[108]
<b>PFPDI-DTBT</b>	520	5.75	4.04	PTB7-Th	0.76	14.13	0.58	6.23	[108]
<b>cis-PolyPBI</b>		5.82	3.79	PBDB-T	1.01	10.30	0.60	6.30	[109]
<b>R300</b>				P3HT	0.33	0.60	0.46	0.10	[110]
<b>SM-PDI</b>	528	5.74	3.85	PTB7-Th	0.73	0.70	0.29	0.15	[111]
<b>HP-PDI</b>	623	5.72	3.78	PTB7-Th	0.83	8.70	0.30	2.15	[111]
<b>PPDIO-POC6</b>	500	5.75	3.95	PPHT	0.60	2.98	0.39	2.32	[112]
<b>Ppe01</b>	602	5.84	3.96	P3HT	0.56	0.21	0.26	0.03	[113]

and N-alkyl dithienopyrrole linkers with PDI and thiophene-PDI units to fine-tune the absorption and energy levels [84].

Asha and co-workers successfully disrupted the  $\pi$ - $\pi$  stacking of the NDI-based polymeric NFAs by random/alternate incorporation of PDI as co-acceptor with NDI in **N2200**-based polymeric NFA. Random copolymers showed better compatibility with PTB7-Th donor and led to favorable nanoscale phase separation in the active blend. Finally, random copolymer (**PPDI30**), which contains 30% of the PDI unit, showed optimal crystallinity and compatibility, and then a higher PCE of 5.03% than other random copolymers contain various compositions of PDI. It is demonstrated that the random co-polymerization effectively controls the crystallinity and nano-phase phase separation of the active blend and governs PCE of the device [102]. Similarly, Jenekhe and co-workers incorporated PDI as a co-acceptor unit in different compositions with NDI acceptor unit in **PNDISe-HD** polymeric NFA. As **PNDISe-HD** blended with PBDTTT-CT donor, the crystallinity of blend varies with a gradual increase of PDI composition. Copolymer (**3OPDI**) with 30% of PDI unit showed a superior PCE of 6.29% better than other random copolymers and PC<sub>70</sub>BM, which was ascribed to the nano-phase separation with small-interconnected domains in active blend [104].

Zhao and co-workers demonstrated fused naphthodiperylene-tetraimide-vinylene polymer (**PDI-V-fuse**) made by fusing the vinyl unit with PDI as a successful NFA for OSCs when blended with PTB7-Th donor. The device employing **PDI-V-fuse** as acceptor exhibited a superior PCE of 8.59% higher than its parent **PDI-V-C5** (7.35%). The better efficiency was attributed to PTB7-Th:**PDI-V-fuse** blend which exhibited high hole and electron mobility resulting in high  $J_{\text{SC}}$  of 17.07 mA cm $^{-2}$  and high FF of 0.67 [107]. Later, Zhang et al. extended the conjugation of fused PDI with thiophene-BT-thiophene unit (**PFPDI-DTBT**) to enhance the absorption and raise LUMO level. Active blend PTB7-Th:**PFPDI-DTBT** exhibited a PCE of 4.07%, which was further improved (6.23%) after thermal annealing of blend film and additive treatment [108]. Later, Li and co-workers also used fused and twisted polymer (**cis-PolyPBI**) composed of binary PDI with thienothiophene (cis to PDI). The active blend with **PBDB-T** exhibits good electron transport ( $1.2 \times 10^{-2}$  cm $^2$  V $^{-1}$  s $^{-1}$ ) owing to its twisted conjugated backbone, which effectively prevents the aggregation and crystallization of PDI units, resulting in isotropic charge transport and favorable phase separation as evidenced by high  $V_{\text{OC}}$  of 1.01 V and  $J_{\text{SC}}$  of 10.30 mA cm $^{-2}$  and high PCE of 6.30% [109]. Also, few polymers based on PDI through imide linkage were reported and used as NFA in OSC applications. Alternating phenylenevinylene co-polymer with aryloxy substituted PDI unit, named as **PPDIO-POC6**, achieved a PCE of 1.67% when blended with PPHT donor. The PCE was enhanced to 2.32% due to more balanced charge transport of the active layer after thermal annealing of active blend [112]. Bo

and co-workers made hyper-branched 3D polymeric NFA (**HD-PDI**) and used to blend with PTB7-Th donor, which gave 14 times higher PCE (2.15%) than SM PDI acceptor because the 3D structure can effectively suppress the aggregation of PDI molecules and promote exciton separation and reduce charge recombination [111]. In case of PDI-based polymeric NFAs, as PDI units conjugated with electron-rich  $\pi$ -linkers typically led to strongly red-shifted absorption spectra, while PDI units conjugated with electron-deficient  $\pi$ -linkers reduced the bandgap as well as down shifted LUMO, and random copolymers with PDI units improve the charge transport of the device. Among PDI-based NFAs, fused PDI-alternated vinylene polymeric NFA **PDI-V-fuse** achieved the highest PCE (8.59%) due to better structural co-planarity that improves crystallinity and electron mobility.

## 2.2. Benzothiadiazole-based polymeric acceptors

Low bandgap BT building block was commonly used to synthesize linear conjugated donor-acceptor polymers through 4 and 7 positions. BT-based polymers have high electron affinity, low bandgap, and favorable  $\pi$ - $\pi$  intermolecular interactions thus ordered crystal packing. A few of BT-based polymeric NFAs as shown in Fig. 12 have been reported so far. Their corresponding photo-physical and photovoltaic properties were summarized in Table 3.

Earlier, McNeill and co-workers synthesized BT-based polymer **F8TBT**, which contains hexyl-substituted thiophene and fluorene linkers, showed broad absorption (300–700 nm). **F8TBT** used as NFA blended with P3HT exhibited a PCE of 1.8% [114]. Later, they improved the PCE by annealing device, which can increase phase separation of the blend along with ordering of the P3HT donor and good charge separation [115]. Benten and co-workers synthesized **PF12TBT** with variable molecular weights to study its effect on photovoltaic properties. While increasing the molecular weight of **PF12TBT** enhanced efficient charge generation and charge transportation as PCE was also increased from 1.9% to 2.7% [116]. Janssen and co-workers synthesized low bandgap polymers (**PTBT-BT**, **PTBTz-BT** and **PTBT-Q**) composed of alternate BT and different electron-deficient units such as BT, BTz and quinoxaline. Their active blend with P3HT showed a very poor PCE (~0.20%) due to low electron mobility hamper exciton dissociation, charge separation and collection [119]. Sirringaus and co-workers also synthesized novel high electron affinity conjugated copolymers based on alkyl BTz (**PBTz-BT**) and BT (**PBT-2BTz**). When they blend with P3HT, the device delivered high  $V_{\text{OC}}$  of 1.08 V and 1.23 V, respectively, but the inferior spectral response resulted in a very poor PCE [120].

Strong electron-deficient dithiazolyl-conjugated BT unit increased electron affinity and lowered the HOMO and LUMO as

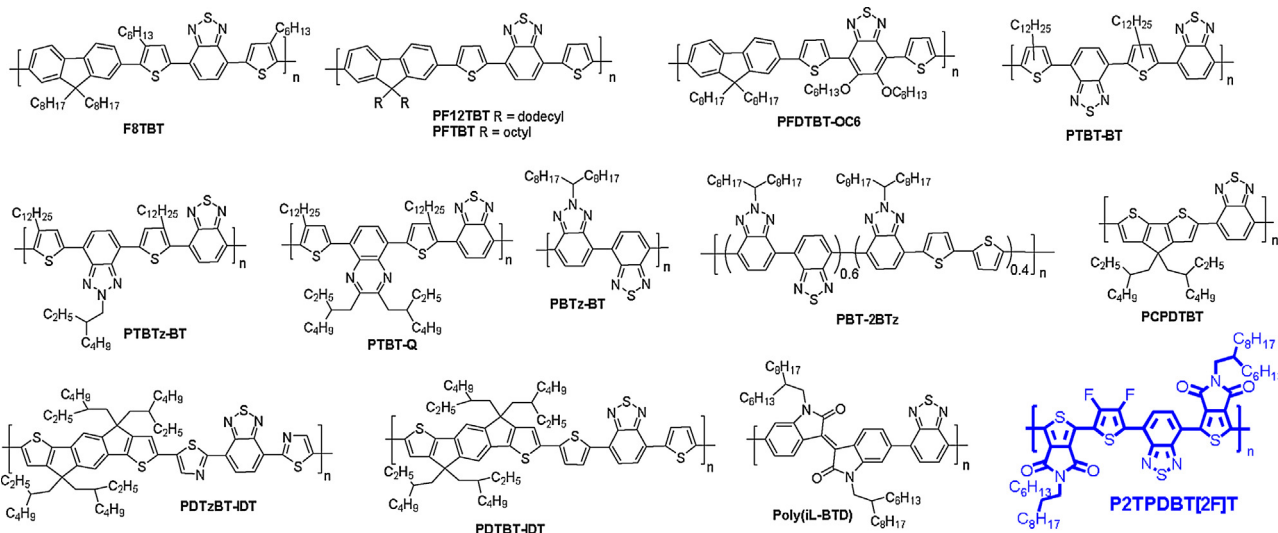


Fig. 12. Chemical structures of benzothiadiazole (BT) based polymeric NFAs [114–122].

Table 3

Photo-physical and photovoltaic properties of benzothiadiazole (BT) based polymeric NFAs.

NFA	$\lambda_{max}$ (nm)	HOMO (eV)	LUMO (eV)	Donor	$V_{OC}$ (mV)	$J_{SC}$ ( $mA\text{ cm}^{-2}$ )	FF	PCE (%)	Refs.
<b>F8TBT</b>	525	5.37	3.15	P3HT	1.15	3.60	0.34	1.20	[114,115]
<b>L-PF12TBT</b>	550	5.50	3.50	P3HT	1.22	3.80	0.41	1.90	[116]
<b>M-PF12TBT</b>	550	5.50	3.50	P3HT	1.24	3.30	0.50	2.04	[116]
<b>H-PF12TBT</b>	550	5.50	3.50	P3HT	1.26	3.88	0.55	2.70	[116]
<b>PFTBT</b>	530	5.20	3.20	P3HT	1.19	3.34	0.47	1.86	[117]
<b>PFDTBT-OC6</b>	526	5.30	3.22	P3HT	1.36	2.93	0.45	1.80	[118]
<b>PTBT-BT</b>	495	5.51	3.65	P3HT	0.99	0.65	0.35	0.23	[119]
<b>PTBTz-BT</b>	505	5.50	3.49	P3HT	1.10	0.58	0.28	0.18	[119]
<b>PTBT-Q</b>	500	5.46	3.52	P3HT	1.15	0.68	0.23	0.18	[119]
<b>PBTz-BT</b>	526	5.40	3.40	P3HT	1.08	0.82	0.35	0.31	[120]
<b>PBT-2BTz</b>	550	5.00	3.15	P3HT	1.23	0.95	0.23	0.24	[120]
<b>PDTzBT-IDT</b>	610	5.43	3.45	P3HT	1.00	2.60	0.45	1.18	[121]
<b>PDTBT-IDT</b>	595	5.28	3.21	P3HT	0.90	1.50	0.43	0.58	[121]
<b>P2TPDBT[2FJT]</b>	584	5.90	4.14	PBDT-TS1	1.00	11.00	0.44	4.80	[122]

compared with dithienyl-conjugated BT. Indacenodithiophene (IDT) polymers **PDTzBT-IDT** exhibited a high PCE of 1.18% due to high electron mobility when compared with **PDTBT-IDT** [121]. Therefore, electron mobility was the bottleneck for BT-based polymeric NFA even though they had strong absorption properties. In this line, Beaujuge and co-workers synthesized efficient polymeric NFA **P2TPDBT[2FJT]** which showed significant strong absorption (400–700 nm) and high electron mobility of  $6.1 \times 10^{-5} \text{ cm}^2 \text{ V}^{-1} \text{ s}^{-1}$ . Concurrently, all polymer solar cells based on PBDT-TS1:**P2TPDBT[2FJT]** blend exhibited superior PCE of 4.80% with high  $V_{OC}$  of 1.00 V and  $J_{SC}$  of  $11.00 \text{ mA cm}^{-2}$  [122]. Overall, BT-based polymeric NFAs containing electron deficient conjugate units suffer from poor absorption; exciton dissociation and charge transport properties and then gave inferior PCE, while the incorporation of electron-rich units in conjugation with BT showed a broad spectral response. In this class, **P2TPDBT[2FJT]** achieved a high PCE up to 4.80% when blended with **PBDT-TS1** donor due to high electron mobility and strong absorption in UV-Vis region.

### 2.3. Diketopyrrolopyrrole-based polymeric acceptors

The electron-deficient DPP unit was widely used to construct narrow bandgap donor-acceptor-type polymers by conjugating it with various  $\pi$ -linkers. Successfully, DPP-based polymers were used for various organic electronic applications due to their easily tunable strong NIR absorption, energy levels, and high electron

mobility ( $\sim 10 \text{ cm}^2 \text{ V}^{-1} \text{ s}^{-1}$ ). All the structures of DPP-based polymeric NFAs were presented in Fig. 13, and their photovoltaic properties were compiled in Table 4.

There were several reports on DPP-based polymers as a donor with impressive PCE up to 9% in combination with fullerene-based acceptors. However, the first time, Janssen et al. synthesized DPP-based polymeric NFAs composed of DPP conjugating with BT (**PPhDPP-BT**), fluorene (**PPhDPP-FL**) and thiophene (**PPhDPP-Th**). The incorporation of thiophene linker into DPP polymers increased donor-acceptor interactions and then drastic red-shifted absorption was observed. When they blend with P3HT, very poor PCE values were obtained due to low electron mobility and inefficient generation of long-lived free charge carriers [123]. Later, the same group used thiazole-DPP unit to make **PDPP2TzT2** polymer that showed high electron affinity and strong absorption ranging from 400 to 900 nm, thus, produced a PCE of 2.0% as blended with PDPP5T donor [124]. These promising absorption properties intrigued Li et al. to develop thiazole-DPP and DBT-based polymers (**PDPP2Tz-BDT**, **PDPP2Tz-TBDT** and **PDPP2Tz-STBDT**). However, the incorporation of bulky linkers decreased co-planarity and absorption maxima. The raised LUMO led to minimal energy loss as blended with PTB7-Th donor, giving OSC with moderate PCE (3.10%) [125]. Later, they made **PDPP2TzT2** random copolymers based on DPP conjugated with various ratios of DBT units. As the content of DBT derivative increased, the molecular weight and crystalline properties were also increased, leading to better PCEs

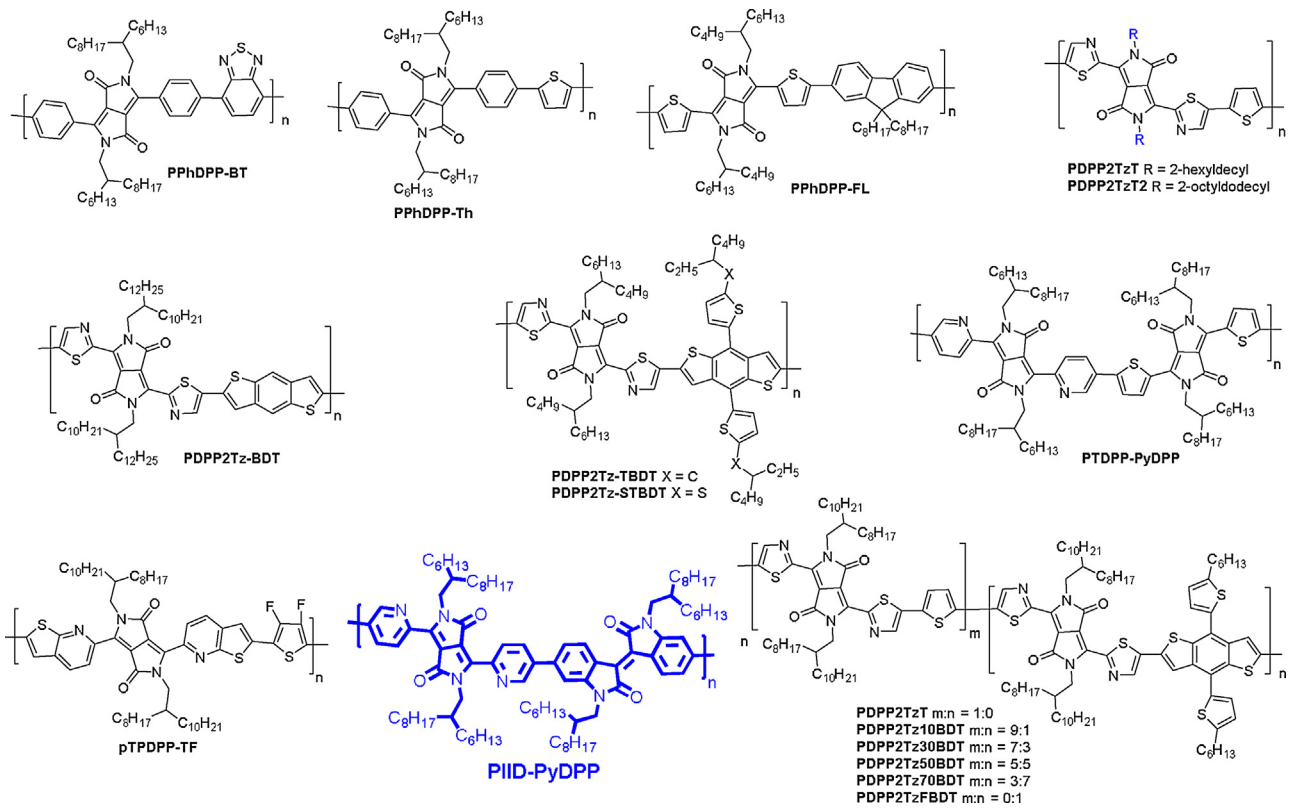


Fig. 13. Chemical structures of diketopyrrolopyrrole (DPP) based polymeric NFAs [123–128].

**Table 4**  
Photo-physical and photovoltaic properties of diketopyrrolopyrrole (DPP) based polymeric NFAs.

NFA	$\lambda_{max}$ (nm)	HOMO (eV)	LUMO (eV)	Donor	$V_{OC}$ (mV)	$J_{SC}$ ( $mA\text{ cm}^{-2}$ )	FF	PCE (%)	Refs.
<b>PPhDPP-BT</b>	520	5.66	3.61	P3HT	0.94	0.68	0.22	0.14	[123]
<b>PPhDPP-Th</b>	545	5.58	3.58	P3HT	0.90	0.44	0.27	0.11	[123]
<b>PPhDPP-FL</b>	650	5.43	3.71	P3HT	0.90	1.63	0.25	0.37	[123]
<b>PDPP2Tz-T</b>	760	5.63	4.00	PDPP5T	0.79	5.30	0.47	2.00	[124]
<b>PDPP2Tz2</b>	770	5.70	4.26	PTB7-Th	0.71	0.66	0.29	0.14	[125]
<b>PDPP2Tz-BDT</b>	754	5.71	4.18	PTB7-Th	0.95	3.20	0.36	1.10	[125]
<b>PDPP2Tz-TBDT</b>	745	5.69	4.16	PTB7-Th	0.99	6.40	0.37	2.40	[125]
<b>PDPP2Tz-STBDT</b>	720	5.67	4.09	PTB7-Th	0.94	7.50	0.45	3.10	[125]
<b>PDPP2Tz-T</b>	774	5.47	4.03	PDPP5T	0.81	7.10	0.49	2.90	[126]
<b>PDPP2Tz10BDT</b>	760	5.85	4.39	PDPP5T	0.79	5.70	0.49	2.40	[126]
<b>PDPP2Tz30BDT</b>	744	5.78	4.27	PDPP5T	0.75	4.10	0.46	1.70	[126]
<b>PDPP2Tz50BDT</b>	728	5.79	4.30	PDPP5T	0.75	1.60	0.43	0.68	[126]
<b>PDPP2Tz70BDT</b>	731	5.75	4.24	PDPP5T	0.76	1.80	0.42	0.54	[126]
<b>PDPP2TzBDT</b>	719	6.14	4.56	PDPP5T	0.67	7.40	0.41	2.10	[126]
<b>PIID-PyDPP</b>	667	6.19	3.98	PTB7-Th	1.02	6.10	0.39	2.30	[127]
<b>PIID-PyDPP</b>	667	6.19	3.98	PBDTTS-FTAZ	1.07	9.40	0.43	4.20	[127]
<b>pTPDPP-TF</b>	711	5.80	4.10	PTB7-Th	1.04	6.57	0.40	2.72	[128]

up to 2.10% [126]. Wang et al. synthesized two polymers **PTDPP-PyDPP** and **PIID-PyDPP** composed of pyridine/thiophene-flanked DPP and isoindigo units, respectively. They blended polymeric NFA **PIID-PyDPP** with two donors (PTB7-Th and PBDTTS-FTAZ), and out of these two donors, PBDTTS-FTAZ showed higher PCE of 4.20% due to its lower HOMO and better complementary absorption spectra with NFA (Table 4) [127]. Chen et al. reported planar NFA **pTPDPP-TF** based on thieno[2,3-*b*]pyridine diketopyrrolopyrrole and 3,4-difluorothiophene units, and exhibited a PCE of 2.72% in blend with PTB7-Th donor [128]. In short, DPP-based polymers typically exhibited a broad spectral response and favorable energy levels for uses in OSCs. In this regard, polymeric OSCs based on **PIID-PyDPP** as NFA and PBDTTS-FTAZ as donor gave the highest PCE of 4.20%.

Therefore, in order to achieve high PCEs, one needs to implement new molecular design on DPP-based polymers.

#### 2.4. Double B $\leftarrow$ N bridged bipyridyl-based polymeric acceptors

Recently, polymeric NFAs based on electron-deficient double B  $\leftarrow$  N bridged bipyridyl building block (BNBP) have attracted research interest for BHJ OSCs. This can be attributed to its fixed planar configuration, which facilitates  $\pi$ - $\pi$  molecular interactions in addition to high electron mobility, favorable energy levels, and strong absorbance in the visible region. Some BNBP-based polymers as shown in Fig. 14 were reported for NFAs application and their corresponding optical and device parameters are

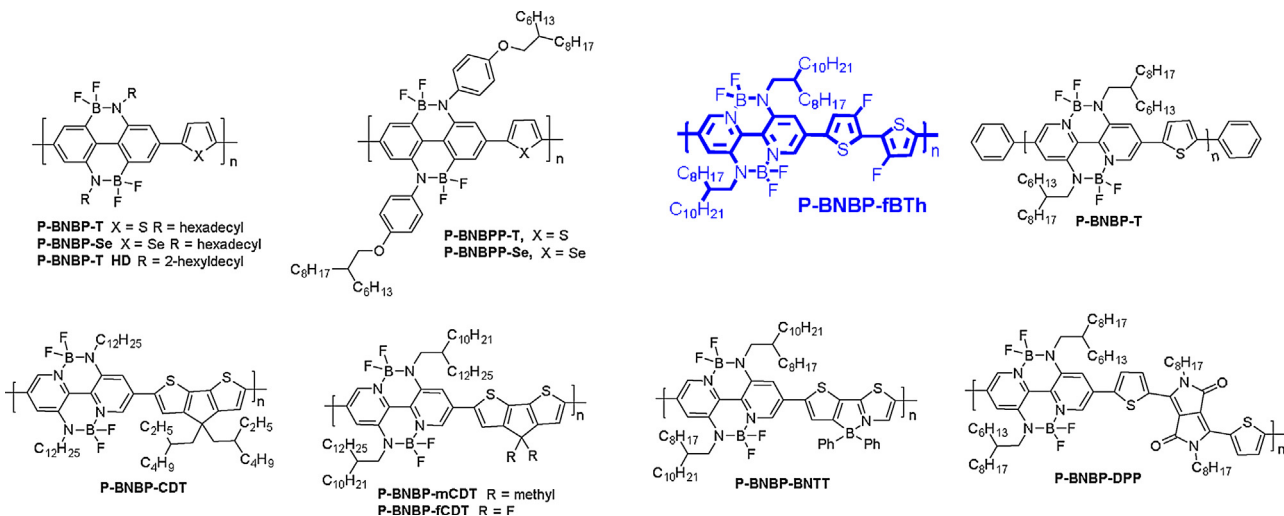


Fig. 14. Chemical structures of double B←N bridged bipyrindyl (BNBP) based polymeric NFAs [129–138].

**Table 5**

Photo-physical and photovoltaic properties of double B←N bridged bipyrindyl building (BNBP) based polymeric NFAs.

NFA	$\lambda_{max}$ (nm)	HOMO (eV)	LUMO (eV)	Donor	$V_{OC}$ (mV)	$J_{SC}$ ( $\text{mA cm}^{-2}$ )	FF	PCE (%)	Refs.
<b>P-BNBP-T</b>	593	5.77	3.50	PTB7-Th	1.12	5.24	0.39	2.27	[129]
<b>P-BNBP-Se</b>	600	5.84	3.66	PTB7-Th	1.03	10.02	0.42	4.26	[129]
<b>P-BNBPP-T</b>	581	5.74	3.72	PTB7-Th	1.11	7.58	0.45	3.77	[130]
<b>P-BNBPP-Se</b>	587	5.75	3.73	PTB7-Th	1.07	9.21	0.45	4.46	[130]
<b>P-BNBP-T HD</b>	580	5.80	3.50	PCDTBT	1.30	5.41	0.45	3.20	[131]
<b>P-BNBP-fBT</b>	622	5.87	3.62	PTB7-Th	1.07	12.69	0.47	6.26	[132]
<b>P-BNBP-T</b>	590	5.77	3.50	PTB7 p-DTS(FBTTh2)2	1.09	7.09	0.44	3.38	[133]
<b>P-BNBP-CDT</b>	628	5.64	3.45	P3HT	1.01	4.98	0.35	1.76	[135]
<b>P-BNBP-mCDT</b>	625	5.56	3.50	PTB7-Th	1.11	0.18	0.30	0.06	[136]
<b>P-BNBP-fCDT</b>	645	5.89	3.60	PTB7-Th	0.99	8.78	0.44	3.83	[136]
<b>P-BNBP-BNTT</b>	597	5.82	3.63	PTB7-Th	1.02	7.32	0.32	2.37	[137]
<b>P-BNBP-DPP</b>	761	5.32	3.57	PTB7	0.88	7.54	0.41	2.69	[138]

summarized in Table 5. Liu et al. have extensively studied the structure-property relationship of polymers (**P-BNBP-T** and **P-BNBP-Se**) based on BNBP and thiophene/selenophene units. The introduction of selenophene in **P-BNBP-Se** increased electron mobility for the corresponding blend film. As a result, OSCs based on PTB7-Th:**P-BNBP-Se** blend showed a PCE of 4.26% with higher  $J_{SC}$  ( $10.02 \text{ mA cm}^{-2}$ ) than **P-BNBP-T** [129]. Later, the same group judiciously selected PCDTBT as donor, which has a lower HOMO level to improve the  $V_{OC}$  as high as 1.30 V and produced a PCE of 3.20% [131]. Replacing the alkyl side chains of BNBP unit with alkoxyphenyl units lowered LUMO level and enhanced  $\pi-\pi$  stacking as well as electron mobilities as compared to those of its parent polymers [130]. Furthermore, they synthesized pseudo-straight configured **P-BNBP-fBT** polymer composed of conformational locked 3,3'-difluoro-2,2'-bithiophene and planar BNBP unit. The active blend PTB7-Th:**P-BNBP-fBT** showed “face-on” orientated nanophase morphology resulting in a high electron mobility of  $9.65 \times 10^{-4} \text{ cm}^2 \text{ V}^{-1} \text{ s}^{-1}$ , which increased  $J_{SC}$  of  $12.69 \text{ mA cm}^{-2}$  and  $V_{OC}$  of 1.07 V, and thus achieved a high PCE of 6.26% [132].

Low bandgap polymer (**P-BNBP-CDT**) composed of alternating BNBP and cyclopentadithiophene showed red-shifted absorption and uplifted LUMO level as compared to oligothiophene (**P-BNBP-T** and **P-BNBP-fBT**) and selenophene (**P-BNBP-Se**) based polymers. However, the optimized devices based on the blend film of P3HT:**P-BNBP-CDT** only produced a PCE of 1.76% [135]. Subsequently, the incorporation of fluorine atoms (**P-BNBP-fCDT**) showed drastic red-shifted absorption (645 nm) and enhanced electron mobility of  $3.46 \times 10^{-4} \text{ cm}^2 \text{ V}^{-1} \text{ s}^{-1}$ , which were responsible for higher PCE

of 3.83% [136]. Interestingly, new alternating conjugated polymer (**P-BNBP-BNTT**), based on BNBP and B←N bridged thienylthiazole, exhibited a broad spectral response (300–700 nm) and favorable energy levels matched with PTB7-Th, and the corresponding device based on PTB7-Th:**P-BNBP-BNTT** blend gave a PCE of 2.37%. It is generally believed that polymeric NFAs with narrow bandgap and broad absorption spectra were playing a vital role in harvesting more sunlight. Later, DPP-incorporated copolymer (**P-BNBP-DPP**) enhanced the absorption maxima (~150 nm) with a broad spectral response from 400 to 800 nm more than thiophene-based polymer (**P-BNBP-T**) [138]. Active blend PTB7:**P-BNBP-DPP** exhibited worm-like fibrous nanostructure and “face-on” oriented crystallites which help to achieve high electron mobility of  $2.1 \times 10^{-4} \text{ cm}^2 \text{ V}^{-1} \text{ s}^{-1}$  and then a PCE of 2.69%. The PCE of BNBP-based polymeric NFAs was continuously growing, among them, the fluorine-substituted polymeric NFA **P-BNBP-fBT** achieved the highest PCE up to 6.26%. Apparently, there is room to increase the PCE by suitable structural engineering on BNBP-based polymers.

## 2.5. Miscellaneous polymeric acceptors

The structures of miscellaneous polymeric NFAs are displayed in Fig. 15, and their optical and device data are collected in Table 6. In 1998, Heeger et al. synthesized poly(3,4-dicyanothiophene) (**PDCTh**) with suitable energy levels (HOMO; 6.70 and LUMO; 3.60) as NFA blending with MEH-PPV donor in a bi-layer OSC configuration to perform a photovoltaic effect [139]. Later, poly

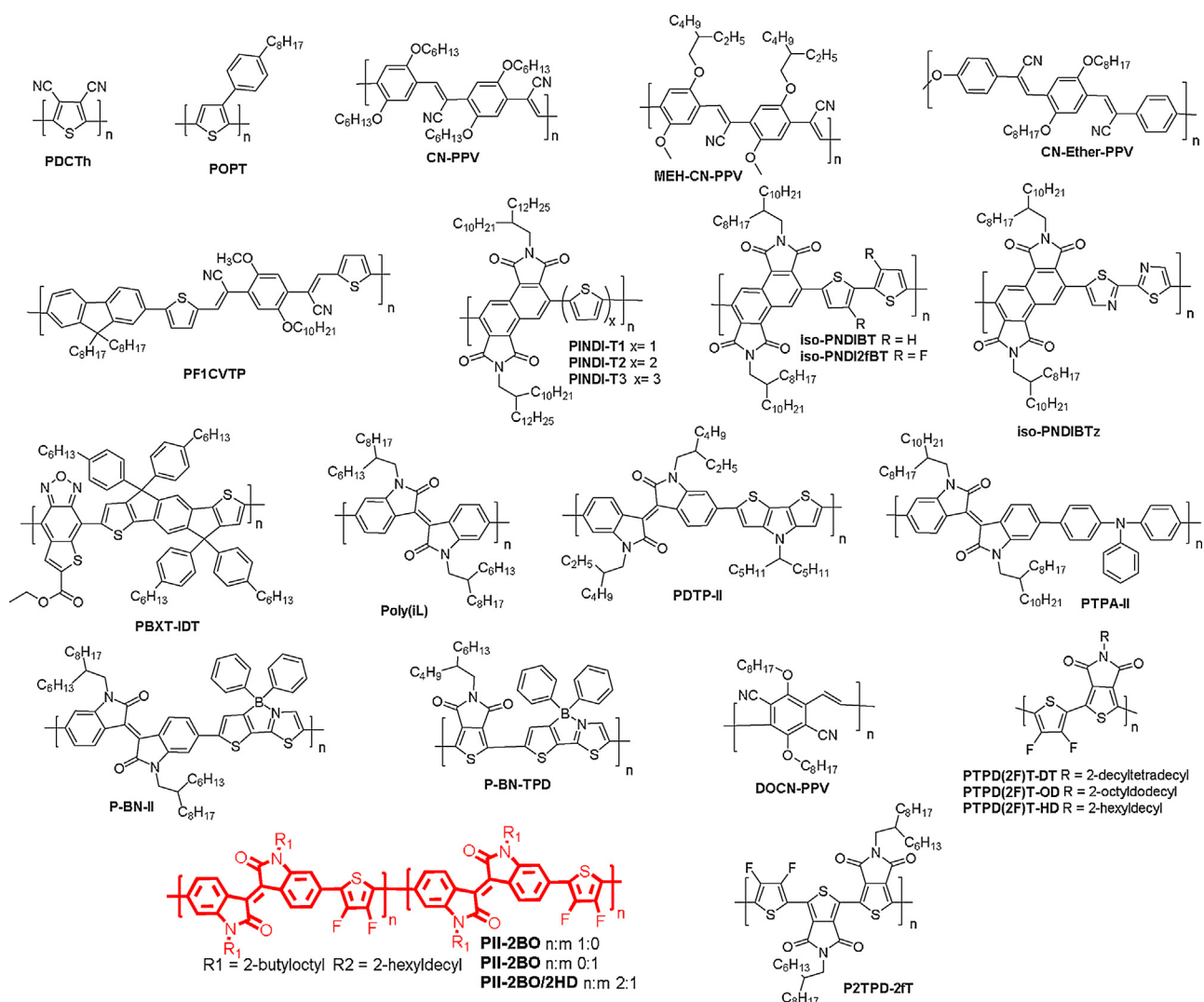


Fig. 15. Chemical structures of miscellaneous polymeric NFAs [141–154].

**Table 6**  
Photo-physical and photovoltaic properties of miscellaneous polymeric NFAs.

NFA	$\lambda_{max}$ (nm)	HOMO (eV)	LUMO (eV)	Donor	$V_{oc}$ (mV)	$J_{sc}$ ( $\text{mA Cm}^{-2}$ )	FF	PCE (%)	Refs.
<b>CN-ether-PPV</b>		6.05	3.35	M3EH-PPV	1.36	3.57	0.35	1.70	[141]
<b>DOCN-PPV</b>	460	5.75	3.65	PTZV-PT	0.75	2.02	0.29	0.80	[142]
<b>PF1CVTP</b>	473	5.35	3.05	MMDMO-PPV	1.40	3.00	0.37	1.50	[144]
<b>P3CN4HT</b>	369	6.10	3.60	MMDMO-PPV	0.62	0.09	0.26	0.01	[145]
<b>PINDI-T1</b>	412	5.98	3.77	P3HT	0.82	1.09	0.36	0.32	[146]
<b>PINDI-T2</b>	505	5.75	3.76	P3HT	0.91	0.67	0.47	0.29	[146]
<b>PINDI-T3</b>	516	5.62	3.72	P3HT	0.94	0.60	0.44	0.25	[146]
<b>iso-PNDIBT</b>	513	5.80	3.50	P3HT	0.90	0.52	0.57	0.27	[147]
<b>iso-PNDI2fBT</b>	500	6.12	3.69	P3HT	0.87	0.26	0.45	0.10	[147]
<b>iso-PNDIBTz</b>	461	6.21	3.62	P3HT	0.88	0.26	0.46	0.11	[147]
<b>PBXT-IDT</b>	740	5.33	3.64	P3HT	0.83	2.54	0.47	1.09	[148]
<b>Poly(IL)</b>	690	5.54	3.84	P3HT	1.91	0.62	0.41	0.47	[149]
<b>PDTp-II</b>	800	4.77	2.69	P3HT	0.85	2.49	0.36	0.74	[150]
<b>PTPA-II</b>	580	5.57	3.68	P3HT	0.67	0.98	0.37	0.26	[151]
<b>P-BN-II</b>	695	5.84	3.80	PTB7-Th	0.92	11.37	0.48	5.04	[152]
<b>P-BN-II</b>				PTB7	0.93	9.05	0.45	3.80	[152]
<b>P-BN-TPD</b>	609	5.85	3.73	PTB7-Th	1.08	0.51	0.22	0.12	[152]
<b>P-BN-TPD</b>				PTB7	1.00	2.48	0.30	0.70	[152]
<b>PTPD[2F]T-HD</b>	554	6.34	3.87	PTB7-Th	1.10	8.40	0.44	4.40	[153]
<b>PTPD[2F]T-OD</b>	550	6.36	3.84	PTB7-Th	1.00	6.50	0.37	2.90	[153]
<b>PTPD[2F]T-DT</b>	551	6.34	3.83	PTB7-Th	0.80	2.10	0.30	0.70	[153]
<b>P2TPD[2F]T</b>	554	5.97	4.05	PBDT-TS1	1.10	6.00	0.41	2.60	[122]
<b>PII-2BO</b>	624	6.20	4.00	PBDTT-FTAZ	0.97	13.20	0.55	7.30	[154]

(3-cyano-4-hexylthiophene) (**P3CN4HT**) and poly(3-(4-n-octyl)-phenylthiophene) (**POPT**) NFAs were developed to enhance spectral response and PCE (2.0%) [140]. Kietzke et al. reported an NFA **CN-ether-PPV** blended with M3EH-PPV donor, resulting in a high  $J_{SC}$  of  $3.57 \text{ mA cm}^{-2}$  and then a PCE of 1.70% attributed to the formation of vertical composition graded layer of blend film during spin coating [141]. Friend et al. observed the photoelectric effect for the blend film composed of poly(*p*-phenylene vinylene) (CN-PPV) and polymer donor, but its charge collection and PCE were limited by small exciton diffusion range [143]. Blend film composed of polyfluorene as NFA and MDMO-PPV donor exhibited a higher external quantum efficiency and PCE of 1.50% [144]. Typically, polymers with an increased number of thiophene units can enhance absorption character with high LUMO energy level, but gave inferior external quantum efficiency and decreased  $J_{SC}$  and PCE values. Chen et al. designed and synthesized a polymer (**PBXT-IDT**) composed of thiophene-fused benzoxadiazole and IDT. **PBXT-IDT** showed drastic red-shifted absorption (740 nm), the device based on **PBXT-IDT:P3HT** blend film only showed a PCE of 1.09% [148]. Reynolds et al. synthesized low bandgap isoindigo polymer for broad absorption spectra and its all polymer solar cell with P3HT donor showed a PCE of 0.5% [149]. Later, isoindigo polymers, **PDTPII** [150], **PTPA-II** [151] and **P-BN-II** [152], were synthesized by conjugating the isoindigo unit with dithienopyrrole, triphenylamine and bithiophene containing  $B \leftarrow N$  units, respectively. Among them, **PDTPII** displayed red-shifted absorption maximum (800 nm) because electron rich dithienopyrrole rendered strong intra-molecular charge transfer interaction. When they blend with PTB7-Th donor, **P-BN-II** exhibited a superior PCE of 5.04% because the well-mixed active blend with the formation of favorable morphology for enhanced electron mobility ( $1.88 \times 10^{-4} \text{ cm}^2 \text{ V}^{-1} \text{ s}^{-1}$ ).

Beaujuge et al. developed alkyl-substituted thieno[3,4-*c*]pyrrole-4,6-dione-alt-3,4-difluorothiophene-based polymers (**PTPD[2F]T**) and demonstrated the effect of branched alkyl chains on blend morphology and charge transport properties of the devices. Hence, a device based on PTB7-Th:**PTPD[2F]T-2HD** blend film exhibited a PCE as high as 4.40% [153]. Later, they synthesized **P2TPD[2F]T** which contains excess thieno[3,4-*c*]pyrrole-4,6-dione unit to the parent polymer **PTPD[2F]T**. But the device based on **PBDT-TS1:P2TPD[2F]T** blend film showed an inferior PCE of 2.60% as compared to a corresponding device based on NFAs such as **PTPD[2F]T-HD** and **P2TPDBT[2F]T**. This can be attributed to the 1-hexyldecyl chain that led to the blend film with optimized morphology [122]. Beaujuge et al. synthesized isoindigo-3,4-difluorothiophene based polymeric NFA **PII-2BO** which showed longer absorption maximum and high LUMO level. Active blend based on **PBFTAZ:PII-2BO** achieved high  $J_{SC}$  of  $13.20 \text{ mA cm}^{-2}$  and high PCE of 7.30% [154]. Overall, in this miscellaneous classification, **PII-2BO** NFA based on isoindigo unit exhibited the highest PCE of 7.30% as blended with **PBFTAZ** donor.

Among various categories of polymeric NFAs, so far, OSCs adopting NDI-based polymer **N2200** delivered the best PCE up to 10.1% after subtle optimizations of processing solvents as well as molecular weight of polymers. However, PDI and BNBP-based polymers were also potentially promising NFAs. Based on the collected information in this review, further new structural designs on polymeric NFAs to give broad absorption, suitable energy levels and favorable molecular packing in combination with new polymeric donors would expect to deliver higher PCEs in the near future.

### 3. Small molecular acceptors

Along the track of developing polymeric NFAs for OSCs, SM NFAs were also extensively studied and showed comparable PCEs

to their polymeric counterparts. There is a significant growth in this research area mainly due to flexible and easy molecular designing and less purification efforts. The optical and energetic levels, as well as miscibility and morphology towards donor counterparts in blend film can be effectively tuned to impart the high performance solar cell. More importantly, their fixed geometry/shape and definite molecular weight provide favorable molecular interactions with donor, and then feasibly leads to nano-phase segregation and better morphological stability. With a judicious selection of donor counterpart depending on their complimentary absorption and suitable energy levels, promising photovoltaic devices can be reasonably achieved. Up to date, a huge number of SMs NFAs were reported, and they were classified into several classes depending on their structural features of the main chromophore used for the construction of NFAs.

#### 3.1. Co-planar aromatic hydrocarbons

Co-planar aromatic hydrocarbons are  $\pi$ -aromatics possessing ladder-type structure for suitable  $\pi$ - $\pi$  intermolecular interactions, giving better molecular packing in solid state and then good charge transporting properties. They can be easily functionalized at aromatic sites via halogenations followed by various coupling reactions. Their high thermal stability and glass transition temperature enable their potentiality in organic electronic applications. We have classified them into several categories depending on the structural features, and each one displayed unique optical and electronic properties, and device performance.

##### 3.1.1. Fluorene-based small molecular acceptors

Fluorene-based SM NFAs gave OSCs promising PCEs possibly attributed to the high charge-transporting property. The easy functionalization at 2 and 7 positions of fluorene offers high flexibility to tune physical properties. In most of the cases, fluorene is used as a central linker flanked with various acceptor units to enhance the spectral response and uplift the LUMO level. Several fluorene-based NFAs were reported (Fig. 16) and their optical and device parameters were summarized in Table 7.

Lim et al. synthesized **Flu-RH** based on fluorene and thiophene-rhodanine. The device based on **Flu-RH:P3HT** blend showed high  $V_{OC}$  of 1.03 V and PCE of 3.08% due to the broad spectral response and higher LUMO level [155]. The incorporation of branched 2-ethylhexyl chain on fluorene and indanone terminal acceptors (**FEH-In**) can optimize blend morphology to enhance  $J_{SC}$  ( $4.82 \text{ mA cm}^{-2}$ ) and PCE (2.43%) when compared to linear alkyl-substituted NFA **Flu-In** [157]. Chen et al. replaced the terminal end group of **Flu-In** with dicyanomethylene-3-indanone, the resulting dye **DICTF** exhibited red-shifted absorption (70 nm), which is highly beneficial for improving the device efficiency. When **DICTF** blended with PTB7-Th, a high  $J_{SC}$  of  $16.61 \text{ mA cm}^{-2}$  and then a high PCE of 7.83%, which is far higher as compared with the corresponding device based on PC<sub>70</sub>BM acceptor, was obtained [158]. Gao et al. reported that **IFTIC** based on indenofluorene showed red-shifted absorption with the peak maximum centered at 603 nm. As a result, polymer solar cell based on PTB7-Th:**IFTIC** blend achieved a PCE of 6.56% [160].

Chen et al. combined fluorene and thiobarbituric acid end groups to make **DTBTF** with high LUMO level, which is useful to enhance  $V_{OC}$  of the device. After blending with SM donor **DR3TSBDT**, the device exhibited a PCE of 3.84% with high  $V_{OC}$  of 1.15 V [165]. In 2011, Meredith et al. reported a fluorene-based NFA (**K12**) combining fluorene and dicyanomethylene BT (BT-DCN). The OSC based on P3HT:**K12** blend only showed a poor PCE of 0.73% mainly due to the poor acceptor absorption (480 nm) and phased separation of active layer [162]. Later, Beaujuge reported SM NFA **FLBDCN** consisting of two BT-DCN units that showed a slightly red-

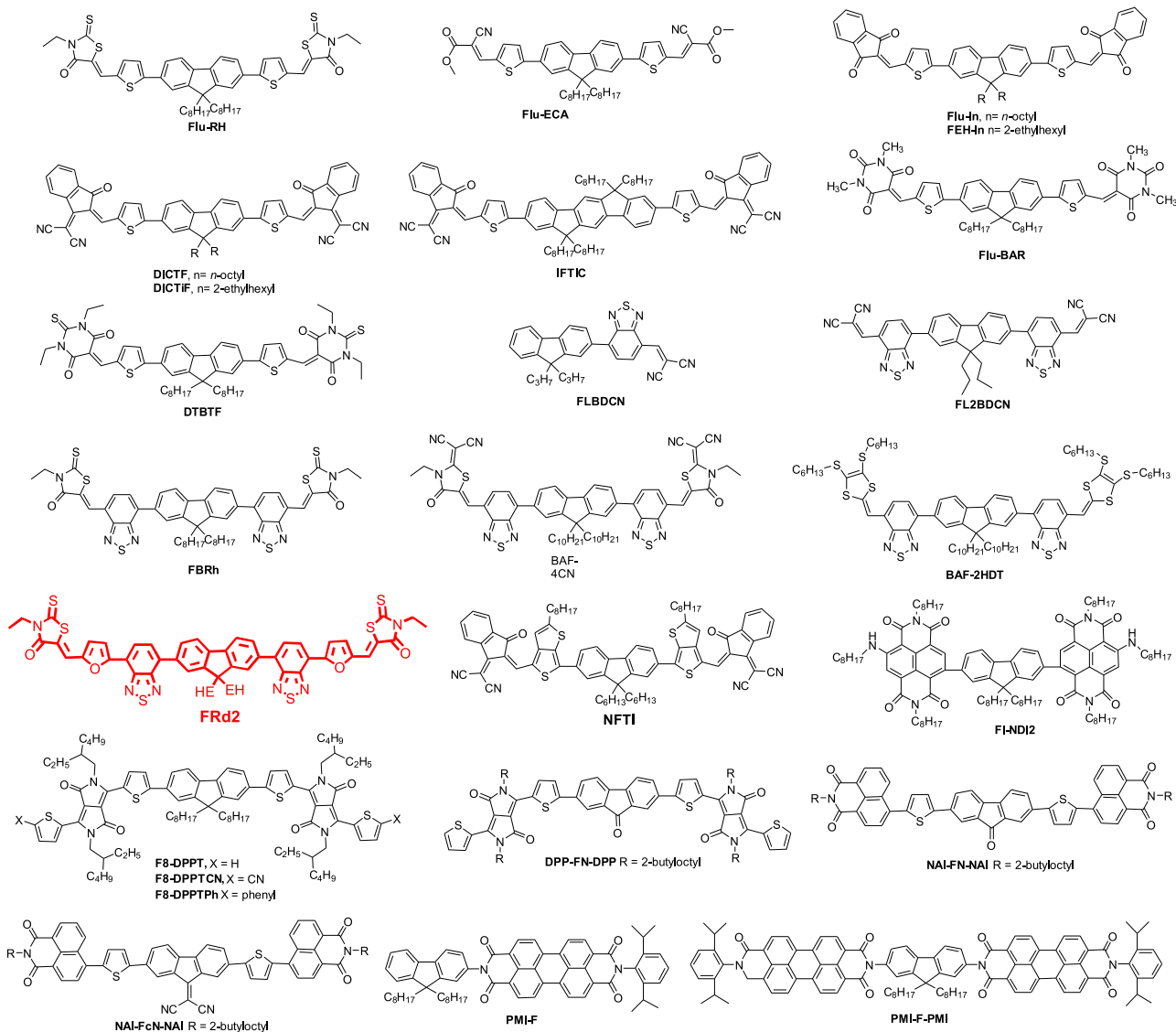


Fig. 16. Chemical structures of fluorene based SM NFAs [155–176].

shifted absorption (486 nm). The optimized device based on PTB7-Th:**FLBDCN** blend film exhibited a higher PCE of 5.1% due to the favorable blend morphology of active layer which improved  $V_{OC}$  (0.88 V) and  $J_{SC}$  (11.20 mA cm $^{-2}$ ) [163].

Holliday et al. synthesized **FBRh** based on fluorene and rhodanine bridged through BT unit. **FBRh** showed a longer absorption than **Flu-RH**, which was attributed to the incorporation of electron deficient and quinoidal BT unit, which enhances intramolecular charge transfer transitions. As a result, the active blend P3HT:**FBRh** gave the OSC a higher PCE of 4.11% than **Flu-RH** [164]. Singh et al. modified the terminal end group with 2-(1,1-dicyanomethylene)rhodanine unit (**BAF-4CN**) to uplift the LUMO level. The device based on blend film PffBT4T-2OD:**BAF-4CN** showed a high PCE up to 8.40% with high  $J_{SC}$  (15.52 mA cm $^{-2}$ ),  $V_{OC}$  (0.77 V) and FF (0.77) [165]. Later, the same group further used dithiafulvalene as end group resulting in a new acceptor **BAF-2HDT** with red-shifted absorption. The polymer solar cell based on blend PffBT4T-2OD:**BAF-2HDT** delivered a PCE of 5.51%, which was improved to 7.13% after thermal annealing [166]. They also reported SM NFA **FRd2** contains furan and rhodanine end groups that showed high LUMO energy level. BHJ device with blend film PTB7-Th:**FRd2** exhibited a PCE as high as 9.40%, which was

attributed to better complimentary absorption of donor and acceptors in blend film, and the high LUMO of acceptor which increased the  $J_{SC}$  and  $V_{OC}$  of the device [167]. Zhu et al. reported NFA **NFTI** based on fluorene and thieno[3,4-*b*]thiophene and showed longer absorption maxima at 706 nm due to quinoidal-resonance character of thieno[3,4-*b*]thiophene. Active blend based on PBDB-T:**NFTI** exhibited higher  $J_{SC}$  of 17.82 mA cm $^{-2}$  and PCE of 9.02% due to the formation of finer nanoaggregates in active blend [168].

McNeill utilized fluorenone as central unit decorated with DPP end groups to make **DPP-FN-DPP**. The device with P3HT:**DPP-FN-DPP** blend as active layer gave an enhanced  $V_{OC}$  of 0.97 V [170]. Chen et al. incorporated phenyl end-capped DPP unit as terminal groups on both sides of fluorene to make an acceptor **F8-DPPTPh** which showed drastic red shift and favorable HOMO and LUMO levels [172]. Polymer solar cell based on P3HT:**F8-DPPTPh** blend showed nanoscale morphology (20–30 nm) which favors high charge transportation and then high  $J_{SC}$  (5.35 mA cm $^{-2}$ ) and high  $V_{OC}$  (1.14 V), resulting in a PCE of 3.17%. Later, the same group replaced the phenyl end-capping unit with cyano group (**F8-DPPTCN**) to red shift the absorption maximum about 20 nm, which is useful for large photocurrent, but the lower LUMO energy (0.24 eV)

**Table 7**

Photo-physical and photovoltaic properties of fluorene based SM NFAs.

NFA	$\lambda_{max}$ (nm)	HOMO (eV)	LUMO (eV)	Donor	$V_{OC}$ (mV)	$J_{SC}$ ( $\text{mA cm}^{-2}$ )	FF	PCE (%)	Refs.
<b>Flu-RH</b>	500	5.58	3.53	P3HT	1.03	5.70	0.52	3.08	[155]
<b>Flu-ECA</b>	459	5.70	3.48	P3HT	1.03	2.82	0.44	1.26	[156]
<b>Flu-In</b>	518	5.70	3.58	P3HT	0.92	3.40	0.42	1.32	[156]
<b>FEH-In</b>	500	5.95	3.75	P3HT	0.95	3.82	0.67	2.43	[157]
<b>8DICTF</b>	587	5.67	3.79	PTB7-Th	0.86	16.61	0.56	7.83	[158]
<b>DICTiF</b>	589	5.55	3.62	PBDT-T	0.98	11.20	0.65	6.97	[159]
<b>IFTIC</b>	603	5.42	3.85	PTB7-Th	0.92	12.96	0.55	6.56	[160]
<b>Flu-BAR</b>	506	5.81	3.53	P3HT	0.90	2.49	0.57	1.28	[161]
<b>DTBTf</b>	540	5.68	3.62	DR3TSBDT	1.15	7.42	0.45	3.84	[155]
<b>FLBDCN</b>	480	6.20	3.60	P3HT	0.62	2.40	0.50	0.73	[162]
<b>FL2BDCN</b>	486	6.18	3.67	PTB7-Th	0.88	11.20	0.51	5.10	[163]
<b>FBRh</b>	509	5.70	3.57	P3HT	0.82	7.95	0.63	4.11	[164]
<b>BAF-4CN</b>	498	5.71	3.55	PffBT4T-2OD	0.77	15.52	0.71	8.40	[165]
<b>BAF-2HDT</b>	509	5.70	3.60	PffBT4T-2OD	0.77	14.64	0.64	7.13	[166]
<b>FRd2</b>	509	5.67	3.58	PTB7-Th	0.83	15.70	0.72	9.40	[167]
<b>NFTI</b>	706	5.46	3.77	PBDT-T	0.90	17.82	0.56	9.02	[168]
<b>FI-NDI2</b>	538	6.00	4.04	P3HT	0.58	3.69	0.54	1.16	[169]
<b>DPP-FN-DPP</b>	585	5.56	3.81	P3HT	0.97	3.30	0.37	1.30	[170]
<b>F8-DPPT</b>	599	5.30	3.50	P3HT	1.10	2.42	0.45	1.20	[171]
<b>F8-DPPTPh</b>	625	5.21	3.39	P3HT	1.18	5.35	0.51	3.17	[172]
<b>F8-DPPTCN</b>	643	5.31	3.65	P3HT	0.97	6.25	0.39	2.37	[173]
<b>NAI-FN-NAI1</b>	411	6.07	3.96	P3HT	0.88	9.12	0.45	3.80	[174]
<b>NAI-FCN-NAI</b>	586	6.14	4.21	P3HT	0.56	3.25	0.36	0.80	[174]
<b>PMI-F</b>	520	5.72	3.56	P3HT	1.00	3.42	0.39	1.35	[175]
<b>PMI-F-PMI</b>	533	5.74	3.54	P3HT	0.98	5.61	0.42	2.30	[175]
				PTZ1	1.30	7.00	0.63	6.00	[176]

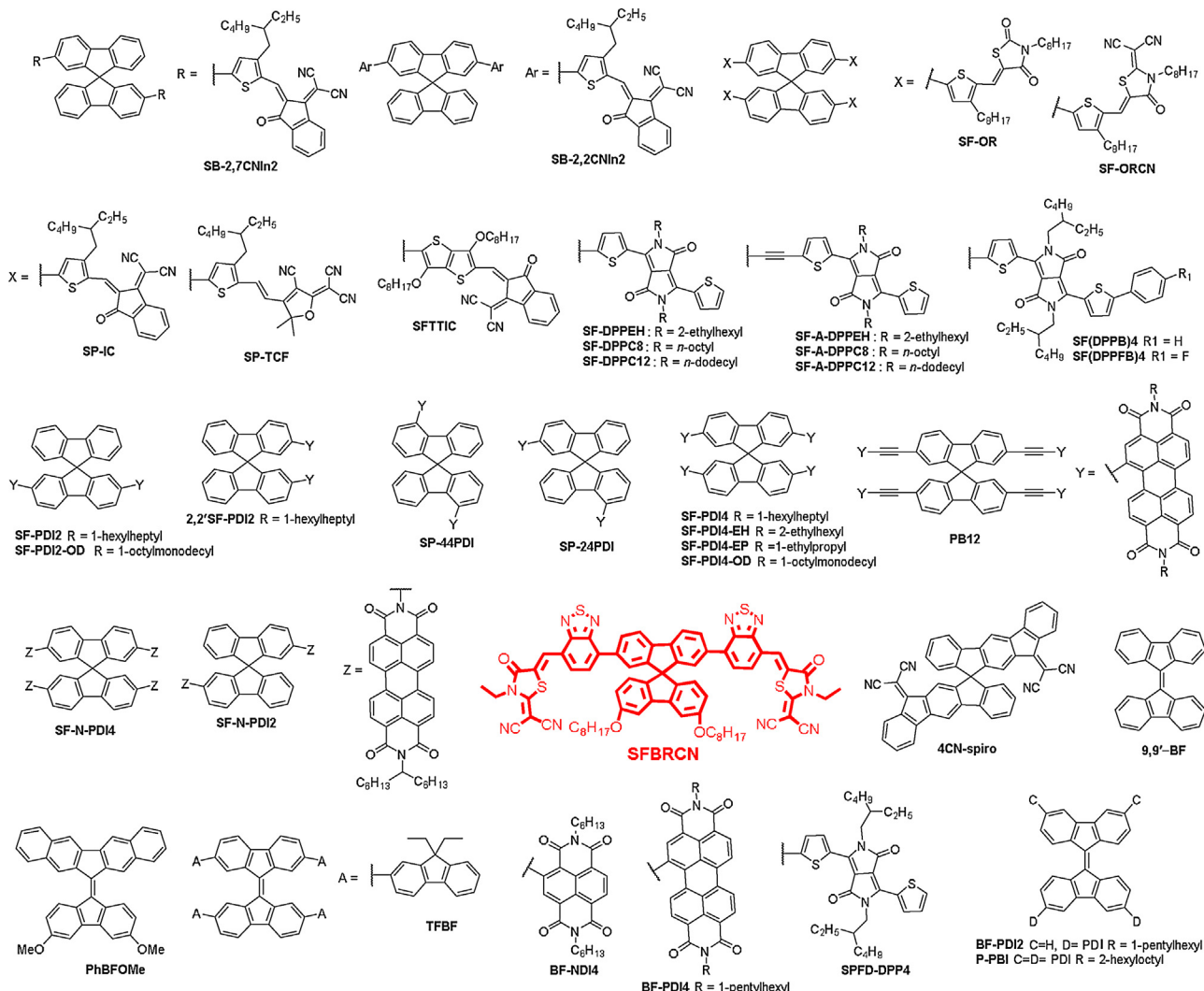
decreased the  $V_{OC}$  of the device [173]. This result indicates that the subtle modification of the acceptor unit significantly changes the energy levels that can minimize the energy loss in the device. Sonar co-workers utilized fluorene and naphthalimide (NI) units to synthesize **NAI-FN-NAI** and **NAI-FCN-NAI**. Among them, **NAI-FN-NAI** showed nanoscale morphology and thus produced high  $V_{OC}$  and PCE of 3.80% as blended with P3HT donor [174]. Later, fluorene connected through imide of PDI (**PMI-F** and **PMI-F-PMI**) to produce high LUMO level and high  $V_{OC}$  values, and **PMI-F-PMI** achieved highest PCE of 3.3% when blended with P3HT donor [175]. Later they choose complimentary absorbing PTZ1 as donor to blend with **PMI-F-PMI** and achieved a high PCE of 6.0% [176]. This result also revealed that the solvent additive can decrease the aggregation of the donor and acceptor materials and then well-distributed nanofibrillar structures were observed, which then increased charge mobility and photovoltaic parameters [176]. In a short summary, fluorene effectively serves as a promising core skeleton for linking various functional terminal groups, leading to a variety of fluorene-based SM NFAs. Among them, OSC using PTB7-Th as donor together with NFA **FRd2** which is composed of BT-furan and rhodanine end groups achieved the best PCE up to 9.4%.

### 3.1.2. Spirobifluorene-based small molecular acceptors

Spirobifluorene with the flexibility for multiple functionalization at various positions was an extensively studied building block due to its high isotropic optical and charge-transporting properties. The cross-shaped geometry suppresses the aggregation while retains required  $\pi-\pi$  intermolecular interactions for charge transport. SM NFAs based on spirobifluorene as a core have been developed by introducing various electron-withdrawing chromophore units. Typically, the OSCs employing spirobifluorene-based NFAs exhibited high  $V_{OC}$  values thanks to its uplifted LUMO levels. Fig. 17 displayed the structures of spirobifluorene-based NFAs, and their optical and photovoltaic data was collected in Table 8. Zhan et al. synthesized spirobifluorene-based isomeric acceptors (**SB-2,7'CNIn2** and **SB-2,2'CNIn2**) based on dicyanomethylene-3-indanone as end groups. Molecular configuration of these molecules affected the optical properties. The device employed **SB-2,2'CNIn2** blended with PBTTT-C-T donor exhibited higher electron mobility resulting in

a higher PCE (0.97%) than its isomer **SB-2,7'CNIn2** [177]. Chen et al. reported spirobifluorene-based tetra-substituted acceptors (**SF-OR** and **SF-ORCN**) with rhodanine, and 2-(1,1-dicyanomethylene) rhodanine units as terminal groups. These molecules exhibited desirable high molar extinction coefficient. The presence of dicyanomethylene unit in **SF-ORCN** decreases planarity and co-facial stacking and gives good phase separation and better electron transport [178]. Later, spirobifluorene conjugated with various terminal electron-accepting groups, such as thiophene/thienothiophene-functionalized dicyanomethylene-3-indanone, were reported [179,180]. The resulted drastic red-shifted absorption and the effective suppression of aggregation lead to better film morphology. Among them, the device employed PTB7-Th:**PBDB-T** blend as active layer exhibited a PCE of 5.66%, which is superior to other dyes, due to long absorption maximum with high molar absorptivity and high morphological stability of the blend. Later, they reported DPP-decorated spirobifluorene NFAs containing various alkyl chains attached to the DPP unit. These molecules showed a twisted X-shaped geometry and helped to reduce aggregation, while the nature of alkyl chain played a crucial role in crystallization of the blend. However, 2-ethylhexyl-substituted spirobifluorene dye (**SF-DPPEH**) showed moderate crystallinity in the active blend, decreased geminate recombination, and then increased  $J_{SC}$  ( $6.96 \text{ mA cm}^{-2}$ ) and PCE of 3.63% as it blended with donor P3HT [181].

The incorporation of DPP units into spirobifluorene core through acetylene bond leads to drastically different morphological features and inferior device performance. Later, the subtle molecular engineering on four arms of DPP unit by incorporating phenyl end-cap units resulted in **SF(DPPB)4**, which exhibited red-shifted absorption and high LUMO level. The device based on **SF(DPPB)4:P3HT** blend produced superior PCE of 5.16% with high  $V_{OC}$  of 1.14 V [182]. Surprisingly, Peng et al. reported that an interesting NFA **SFBRCN** contains BT-DCN units at 2 and 7 positions of spirobifluorene. The device based on **SFBRCN** as NFA exhibited the highest PCE up to 10.30% with high  $V_{OC}$  (0.91 V),  $J_{SC}$  17.54 ( $\text{mA cm}^{-2}$ ) and FF (0.64) when blended with PTB7-Th [184]. It can be attributed to the complimentary absorption, favorable energy levels and optimal nanosized morphology.

**Fig. 17.** Chemical structures of spirobifluorene based SM NFAs [177–202].

Zhao et al. incorporated PDI units at isomeric positions (2,7 and 2,2') of spirobifluorene to give **SF-PDI2** and **2,2'SF-PDI2**, respectively, for mitigating the self-aggregation and crystallization properties of PDI [185]. However, **SF-PDI2** showed better crystalline packing and morphology resulting in high charge mobility and FF in device. Promising features of **SF-PDI2** motivated researchers to study the OSC device performance with different donor materials (PffBT4T-2DT, PTB7-Th, FTAZ, PyCNTAZ, PTB7-Th and PffBT4T-2OD) [14,186]. Overall, the device based on optimized blend film with PffBT4T-2DT donor exhibited an impressive PCE of 6.30% with high  $J_{SC}$  of  $10.70\text{ mA cm}^{-2}$  and  $V_{OC}$  of 0.98 V as compared to other donor materials. This can be attributed to the strong absorption and favorable energy levels of PffBT4T-2DT donor that well matched with **SF-PDI2** and smooth blend morphology, which led to better charge transport properties. Later, tetra-substituted spirobifluorene with PDI units (**SF-PDI4**) attracted immense attention due to its strong absorption, 3D interlocking geometrical structure and high solubility [187–193]. **SF-PDI4** showed red-shifted absorption properties, high LUMO level, high thermal properties and isotropic electron charge transport like fullerene-based acceptors. As a result, its active blend with donor possesses better intermixed homogenous domains. Several donor materials were used to blend with **SF-PDI4**, and out of them a low bandgap polymer donor PV4T2FBT

produced PCE as high as 5.82% with high  $J_{SC}$  of  $12.02\text{ mA cm}^{-2}$  and  $V_{OC}$  of 0.90 V [191]. This can be attributed to the thin film blend based on PV4T2FBT donor that displayed “face-on” oriented crystalline behavior, which is beneficial for vertical charge transport and increased mobility and  $J_{SC}$ .

Cho et al. have synthesized **SF-N-PDI2** and **SF-N-PDI4** containing spirobifluorene core linked with PDI unit through imide linkage and studied the effect of di- and tetra-PDI substitution on physical properties and device performance. As compared to **SF-N-PDI4**, **SF-N-PDI2** showed a higher LUMO level which helps the device to have an increased  $V_{OC}$  and then a higher PCE 5.31% due to the closer intermolecular packing and better intercalation of di-substituted acceptor with donor [194]. Müllen et al. synthesized fused polycyclic spirobifluorene-based acceptor **4CN-spiro**, which contains four dicyanomethylene units, and raised LUMO suitable as acceptor to construct solar cells. However, when it blended with PTB7 donor, a lower PCE was obtained due to incomplete exciton quenching and fast geminate recombination [195].

Hwang et al. introduced a similar acceptor, 9,9'-bifluorenylidene (**9,9'-BF**), which showed a strong electron-accepting nature because **9,9'-BF** will transform into aromatic by accepting an electron from a donor. The device with blend film of P3HT:**9,9'-BF** exhibited a PCE of 2.28% with high  $V_{OC}$  of 1.07 V [196]. In addition,

**Table 8**

Photo-physical and photovoltaic properties of spirobifluorene based SM NFAs.

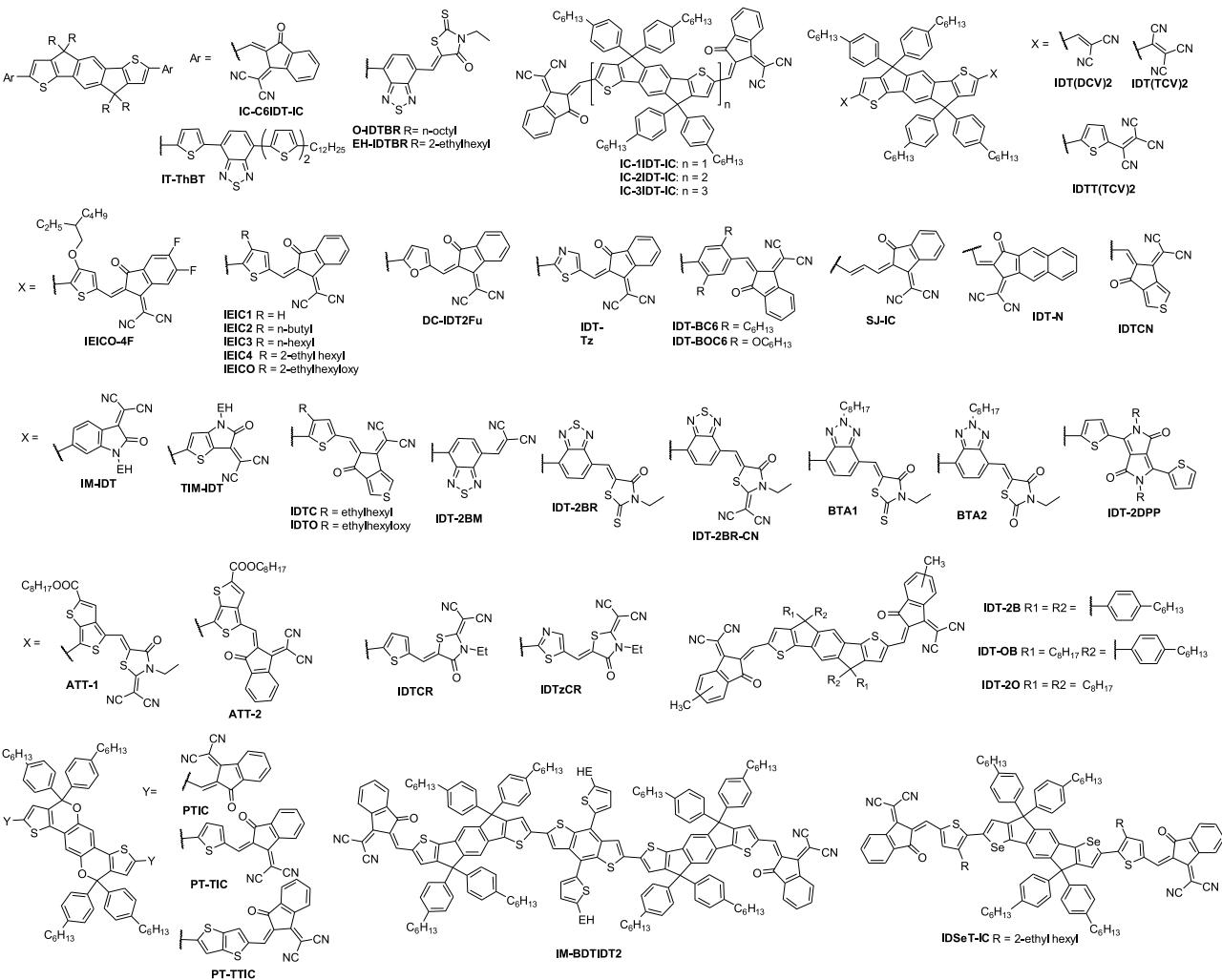
NFA	$\lambda_{\text{max}}$ (nm)	HOMO (eV)	LUMO (eV)	Donor	$V_{\text{OC}}$ (mV)	$J_{\text{SC}}$ (mA Cm $^{-2}$ )	FF	PCE (%)	Refs.
<b>SB-2,7'CNIn2</b>	514	5.94	3.78	PBDTTT-C-T	0.86	2.25	0.33	0.63	[177]
<b>SB-2,2'CNIn2</b>	530	5.96	3.86	PBDTTT-C-T	0.87	3.34	0.33	0.97	[177]
<b>SF-OR</b>	504	5.50	3.25	P3HT	0.97	7.50	0.63	4.66	[178]
<b>SF-ORCN</b>	520	5.55	3.29	P3HT	0.91	7.74	0.61	3.63	[178]
<b>SP-IC</b>	539	5.88	3.91	PTB7-Th	0.88	11.46	0.45	4.50	[179]
<b>SP-TCF</b>	524	5.90	3.97	PTB7-Th	0.75	2.51	0.52	0.97	[179]
<b>SFTTIC</b>	622	5.46	3.65	PBDB-T	0.96	9.28	0.63	5.66	[180]
				PTB7-Th	0.91	12.42	0.41	4.65	[180]
<b>SF-DPPEH</b>	597	5.26	3.60	P3HT	1.10	6.96	0.47	3.63	[181]
<b>SF-DPPC8</b>	598	5.24	3.55	P3HT	0.88	5.21	0.41	1.87	[181]
<b>SF-DPPC12</b>	597	5.23	3.57	P3HT	0.91	3.88	0.40	1.42	[181]
<b>SF-A-DPPEH</b>	588	5.30	3.58	P3HT	0.75	2.37	0.43	0.76	[181]
<b>SF-A-DPPC8</b>	590	5.29	3.56	P3HT	0.79	1.21	0.29	0.28	[181]
<b>SF-A-DPPC12</b>	590	5.29	3.57	P3HT	0.70	1.96	0.33	0.45	[181]
<b>SF(DPPB)4</b>	625	5.26	3.51	P3HT	1.14	8.29	0.55	5.16	[182]
<b>SF(DPPFB)4</b>	620	5.27	3.55	P3HT	1.04	8.48	0.50	4.42	[183]
<b>SFBRCN</b>	495	5.93	3.86	PTB7-Th	0.91	17.54	0.64	10.30	[184]
<b>SF-PDI2</b>		5.71	3.71	P3HT	0.61	5.92	0.65	2.35	[185]
				PffBT4T-2DT	0.98	10.70	0.57	6.30	[186]
				PTB7-Th	1.00	7.40	0.39	3.00	[186]
				FTAZ	0.94	6.70	0.37	2.30	[14]
				PyCNTAZ	1.15	8.15	0.47	4.37	[14]
<b>PB12</b>	562	5.89	3.87	PBDB-T	0.85	8.52	0.59	4.27	[187]
<b>SF-PDI2-OD</b>		5.83	3.88	PTB7-Th	0.90	4.77	0.39	1.66	[188]
<b>2,2'SF-PDI2</b>		5.71	3.71	P3HT	0.61	6.27	0.60	2.28	[185]
<b>SP-44PDI</b>	529	5.91	3.81	PTB7-Th	0.90	9.27	0.46	3.91	[189]
<b>SP-24PDI</b>	529	5.85	3.80	PTB7-Th	0.94	10.36	0.46	4.56	[189]
<b>SF-PDI4</b>				PffBT4T-2OD	0.91	5.86	0.56	2.97	[188]
<b>SF-PDI4-EH</b>	535	6.24	4.11	PTB7-Th	0.85	13.08	0.48	5.34	[190]
<b>SF-PDI4-OD</b>	540	5.86	3.87	PffBT4T-2OD	0.80	12.00	0.46	4.82	[188]
<b>SF-PDI4-OD</b>				PffBT4T-2OD	0.94	8.21	0.51	3.89	[188]
<b>SF-PDI4</b>	531	5.97	3.78	PffBT4T-2DT	0.93	11.03	0.51	5.11	[191]
				PV4T2FBT	0.90	12.02	0.54	5.82	[191]
<b>SF-PDI4-EP</b>		5.86	3.70	PTB7	0.75	5.90	0.36	1.57	[192]
<b>SF-PDI4</b>		6.08	3.80	PTB7-Th	0.80	4.88	0.60	2.35	[193]
<b>SF-N-PDI2</b>	526	5.99	3.82	PTB7-Th	0.84	10.53	0.60	5.31	[194]
<b>SF-N-PDI4</b>	525	6.01	3.85	PTB7-Th	0.82	11.36	0.50	4.68	[194]
<b>4CN-spiro</b>	500	5.80	3.63	PTB7	0.89	1.41	0.48	0.80	[195]
<b>9,9'-BF</b>	460	5.62	3.48	P3HT	1.07	5.04	0.42	2.28	[196]
<b>TFBF</b>	475	5.81	3.49	P3HT	0.70	1.20	0.30	0.26	[197]
<b>BF-NDI4</b>	459	6.00	3.70	PTB7-Th	0.83	7.29	0.39	2.28	[198]
				459	6.00	3.49	0.38	1.08	[198]
				PTB7-Th	0.82	9.35	0.46	3.64	[198]
				PTB7	0.81	7.21	0.42	2.53	[198]
<b>BF-PDI2</b>	530	5.77	3.83	PTB7-Th	0.90	6.38	0.43	2.46	[198]
<b>BF-PDI4</b>	532	5.86	3.92	PTB7-Th	0.87	9.59	0.53	4.43	[199]
<b>SPFD-DPP4</b>	517	5.51	3.84	P3HT	1.17	7.74	0.60	5.42	[199]
<b>p-PBI</b>	611	5.42	3.78	PTB7-Th	0.82	12.32	0.59	5.95	[200]
<b>PhBFOMe</b>	517	5.17	3.24	P3HT	1.10	3.90	0.40	1.70	[201,202]

the device based on **BF-PDI4** as NFA exhibited a superior PCE of 3.64% as blended with PTB7-Th, which is higher than that of **BF-NDI4** based device due to its poor morphological stability [198]. Later, its isomeric NFA **p-PBI**, contains isomeric linkage of 9,9'-bifluorenylidene with PDI units, improved PCE (5.95%) as blended with PTB7-Th donor due to nanoscale phase separation in blend film that favors charge transporting property [200]. Later, Ong et al. found that the number of PDI units substituted on 9,9'-bifluorenylidene affected the PCE. The tetra-substituted derivative (**BF-NDI4**) exhibited a better external quantum efficiency and showed a superior PCE of 4.43% over di-substituted derivative **BF-NDI2** [198]. Gupta et al. incorporated four DPP units onto 9,9'-bifluorenylidene, and the resulting **SPFD-DPP4** displayed excellent solubility, thermal stability and suitable energy levels towards a classical P3HT donor. Polymer solar cell based on P3HT:**SPFD-DPP4** blend exhibited a PCE of 5.42% with high  $V_{\text{OC}}$  of 1.17 V. A superior PCE of device employing **SPFD-DPP4** as NFA was due to favorable morphology, good electron mobility over **TFBF**, **BF-PDI4** and **BF-NDI4** [199]. Wudl et al. synthesized a fused 9,9'-bifluorenylidene-

based acceptor **PhBFOMe**, and it showed red-shifted absorption and produced a PCE of 1.70% when compared to its parent compound **9,9'BF** [201,202]. In short summary, as various electron-accepting moieties can be introduced, spirobifluorene as a building block enables fine-tuning the optical and energy levels of resulting NFAs to be feasible. The 3D feature resulting from the rigid and X-shape of spirobifluorene core can effectively suppresses the aggregation, and thus a nano-separated phase in the active blend. In this class, the device based on **SFBRCN** as NFA and PTB7-Th as donor achieved the highest PCE of 10.30% attributed to strong absorption, favorable energy levels and optimal nanosized morphology.

### 3.2. Co-planar aromatic heteroacenes

Co-planar aromatic heteroacenes are analogous to co-planar aromatic hydrocarbons where C-bridge was replaced by nitrogen or sulphur atoms. They show a ladder-type structure, and N-bridge can address with pendant alkyl/aryl groups to manipulate the

**Fig. 18.** Chemical structures of indacenodithiophene (IDT) based SM NFAs [203–243].

intermolecular  $\pi$ - $\pi$  interactions and then blend morphology. Also, it shows red-shifted absorption when compared to those of aromatic hydrocarbons along with high thermal and photochemical stability. They were classified into various categories based on the structural features and heteroatom incorporated in aromatics.

### 3.2.1. Indacenodithiophene-based small molecule acceptors

IDT and its analogously fused derivative dithieno-indacenodithiophene (IDTT) are planar polyaromatic heteroacenes. They are rigid and co-planarized with favorable intermolecular  $\pi$ - $\pi$  interactions, which enhanced the  $\pi$ -conjugation in film state and then high hole mobility. Substitution of alkyl/aryl units at active methylene bridge positions improves the solubility for feasible processability. IDT or their analogs contains seven- or more member-ring exhibited strong absorption and “face-on” intermolecular  $\pi$ - $\pi$  interactions in active blend which can potentially serve as good NFAs for OSCs blending with suitable donors. However, facile functionalizations on both sides of IDT and IDTT with various electron deficient functional units have been broadly studied and several potential NFAs have been identified. The structures of reported IDT-based NFAs are shown in Fig. 18, and their related data are compiled in Table 9. We have thoroughly scrutinized and discussed the promising candidates that evaluate the structure-property-device performance relationships.

Zhan et al. reported **IC-C6IDT-IC**, composed of IDT core containing hexyl groups and dicyanomethylene-3-indanone as

end-capped units, exhibited good absorption (660 nm) and suitable HOMO and LUMO energy levels as NFA. The device based on as-cast PTDBT-T1:**IC-C6IDT-IC** blend film exhibited a high PCE of 8.71% and high J<sub>sc</sub> of 15.05 mA cm<sup>-2</sup> manifested from strong absorption, and highly ordered “face-on”  $\pi$ - $\pi$  interactions of the blend film that favors good charge transporting properties [203]. Later, different polymer donors were employed; the highest PCE up to 9.73% was obtained for DBTT-2fBTT donor due to better complimentary absorption [203,204]. Later, **O-IDTBR** based on IDT core functionalized with BT conjugated with 2-(1,1-dicyanomethylene)rhoda-nine terminal units was reported to show strong absorption and led device blended with P3HT to have a PCE of 6.30% [206]. A suitable combination of polymer donor PvBDTTAZ further improved PCE to as high as 11.60% due to better complimentary absorption and high charge transport of the active layer [209].

Zhan et al. further replaced the alkyl chain of IDT with hexylphenyl unit, resulting in a molecule **IC-1IDT-IC**, which enhances strong crystallization and  $\pi$ - $\pi$  stacking, and thus brings about a relatively high electron mobility. As a result, the device with PDBT-T1:**IC-1IDT-IC** blend film exhibited a PCE of 7.39%. In addition, the number of IDT units in IC-nIDT-IC oligomers also affected the  $\pi$ - $\pi$  stacking and crystallinity of blend films [210]. Strong absorption and favorable molecular interactions of the IDT core were utilized to synthesize several NFAs by incorporating various terminal acceptor units to fine-tune the absorption, energy levels and molecular interactions.

**Table 9**

Photo-physical and photovoltaic properties of indacenodithiophene (IDT) based SM NFAs.

NFA	$\lambda_{\text{max}}$ (nm)	HOMO (eV)	LUMO (eV)	Donor	$V_{\text{OC}}$ (mV)	$J_{\text{SC}}$ (mA Cm $^{-2}$ )	FF	PCE (%)	Refs.
<b>IC-C6IDT-IC</b>	664	5.69	3.91	PTDBT-T1	0.89	15.05	0.65	8.71	[203]
				DRTB-T	0.98	14.25	0.65	9.08	[204]
				DBTT-2fBTT	0.98	15.21	0.66	9.73	[205]
<b>O-IDTBR</b>	650	5.51	3.88	P3HT	0.72	13.90	0.60	6.30	[206]
				P3HT	0.76	12.10	0.62	6.00	[206]
<b>EH-IDTBR</b>	650	5.58	3.90	BDT3TR	0.91	11.21	0.56	7.09	[207]
				PffBT4T-2DT	1.07	15.00	0.62	9.95	[15]
				PvBDTTAZ	1.08	16.26	0.64	11.60	[209]
<b>IT-ThBT</b>	574	5.46	3.81	P3HT	0.56	1.08	24.0	0.15	[208]
				PDBT-T1	0.92	13.39	0.60	7.39	[210]
<b>IC-1IDT-IC</b>	656	5.91	3.83	PTB7-Th	0.93	12.75	0.37	4.38	[210]
				PDBT-T1	1.02	5.28	0.48	2.58	[210]
				PTB7-Th	0.91	8.51	0.47	3.63	[211]
<b>IDT(DCV)2</b>	498	5.81	3.65	PTB7-Th	0.91	8.51	0.47	3.63	[211]
<b>IDT(TCV)2</b>	561	6.04	4.18	PTB7-Th	0.49	11.02	0.53	2.84	[211]
<b>IDTT(TCV)2</b>	691	5.58	4.06	PTB7-Th	0.60	11.98	0.50	3.57	[211]
<b>IEIC1</b>	700	5.43	3.85	PBDTT-C-T	0.90	8.33	0.52	3.93	[212]
<b>IEIC1</b>	700	5.44	3.87	PTB7-Th	0.84	9.90	0.44	3.90	[213]
<b>IEIC2</b>	700	5.45	3.87	PTB7-Th	0.91	11.10	0.50	5.40	[213]
<b>IEIC3</b>	700	5.46	3.86	PTB7-Th	0.93	12.80	0.58	7.40	[213]
<b>IEIC4</b>	696	5.48	3.85	PTB7-Th	0.95	12.30	0.49	6.00	[213]
				PTB7-Th	0.97	13.55	0.48	6.31	[214]
				PTB7-TH	0.90	7.34	0.33	1.79	[215]
				PTB7-TH	0.78	9.18	0.34	2.42	[215]
				DPP -BDT-DPP	0.90	8.24	0.54	4.00	[215]
				DPP -BDT-DPP	0.94	10.87	0.59	6.03	[215]
				Pfft2-FTA2-2DT	1.00	12.20	0.59	7.20	[216]
<b>IEICO</b>	785	5.32	3.95	PBDTT-C-T	0.82	17.70	0.58	8.40	[217]
<b>IEICO-4F</b>	800	5.47	3.90	PTB7-Th	0.74	22.80	0.59	10.00	[218]
<b>IEICO-4F</b>	800	5.47	3.90	J52	0.74	21.90	0.59	9.40	[218]
<b>DC-IDT2Fu</b>	702	5.44	3.88	PBDTT-C-T	0.94	5.00	0.48	2.26	[219]
<b>IDT-Tz</b>	649	5.62	4.09	PBDB-T	0.88	13.67	0.71	8.52	[220]
<b>IDT-BC6</b>	592	5.55	3.82	PBDB-T	0.92	5.63	0.44	2.30	[221]
<b>IDT-BOC6</b>	688	5.51	3.78	PBDB-T	1.01	17.52	0.54	9.60	[221]
<b>SJ-IC</b>	743	5.61	3.94	J61	0.83	16.99	0.66	9.27	[222]
<b>IDT-N</b>	687	5.74	4.08	PBDB-T	0.7	15.88	0.71	9.00	[223]
				PBDB-TF	0.94	16.79	0.78	12.20	[224]
<b>IDTCN</b>	659	5.91	3.94	PBT1-EH	0.2	12.76	0.68	8.30	[225]
<b>IM-IDT</b>	674	5.44	4.00	PTB7-Th	0.58	4.96	0.49	1.60	[226]
<b>TIM-IDT</b>	733	5.36	4.01	PTB7-Th	0.59	6.04	0.48	1.96	[226]
<b>IDTC</b>	727	5.57	3.96	PBDB-T	0.91	16.40	0.60	9.35	[227]
<b>IDTO</b>	723	5.52	3.84	PBDB-T	0.94	15.94	0.64	10.02	[227]
<b>IDT-2BM</b>	660	5.60	3.80	PBDTT-C-T	0.77	10.10	0.55	4.26	[228]
<b>IDT-2BR</b>	636	5.52	3.69	P3HT	0.84	8.91	0.68	5.12	[229]
<b>IDT-2BR</b>	605	5.50	3.53	P3HT	0.97	7.59	0.67	4.93	[230]
<b>IDT-2BR</b>	690	5.52	3.69	PTB7-Th	0.99	13.00	0.60	7.70	[231]
<b>IDT-2BR</b>	690	5.30	3.56	PTB7-Th	1.02	13.60	0.59	8.20	[232]
<b>IDT-2BR-CN</b>		5.38	3.67	PTB7-Th	0.88	12.40	0.50	5.50	[232]
<b>BTA1</b>	593	5.51	3.55	P3HT	1.02	7.34	0.70	5.24	[233]
<b>BTA2</b>	593	5.43	3.38	P3HT	1.22	6.15	0.60	4.50	[234]
<b>ATT-1</b>	736	5.50	3.63	PTB7-Th	0.87	16.48	0.70	10.07	[235]
<b>ATT-2</b>	791	5.50	3.90	PTB7-Th	0.73	20.75	0.63	9.58	[236]
<b>IDT-2DPP</b>	640	5.11	3.32	P3HT	1.13	1.05	0.38	0.45	[237]
<b>IM-BDTIDT2</b>	665	5.53	3.89	PTB7-Th	0.97	11.28	0.49	5.53	[238]
<b>IDSeT-IC</b>	680	5.45	3.79	J51	0.91	15.20	0.62	8.58	[239]
<b>IDTzCR</b>	593	5.67	3.77	PTB7-Th	1.04	13.80	0.60	8.71	[240]
<b>IDTCR</b>	603	5.46	3.67	PTB7-Th	1.11	11.01	0.50	6.10	[240]
<b>IDT-2B</b>	654	5.80	3.84	PBDB-T	0.89	13.30	0.54	6.42	[241]
<b>IDT-OB</b>	661	5.77	3.87	PBDB-T	0.88	16.18	0.71	10.12	[241]
<b>IDT-2O</b>	668	5.73	3.85	PBDB-T	0.86	15.64	0.72	9.68	[241]
<b>PTIC</b>	<b>667</b>	5.67	3.85	PBDB-T	0.84	14.20	0.64	7.66	[242]
<b>PT-TIC</b>	707	5.33	3.89	PBDB-T	0.89	17.31	0.60	9.21	[243]
<b>PT-TTIC</b>	695	5.28	3.92	PBDB-T	0.90	10.58	0.42	4.02	[243]
<b>ITIC</b>	664	5.48	3.83	PTB7-Th	0.82	14.79	0.62	7.52	[244]
				HFQx-T	0.92	15.59	0.65	9.40	[245]
				PDTP4TFBT	0.90	14.18	0.59	7.58	[246]
				PBDB-T	0.90	16.81	0.74	11.21	[247]
				J51	0.82	16.47	0.69	9.26	[248]
				PDCBT	0.94	16.50	0.66	10.16	[249]
				PTzBI-DT	0.91	16.84	0.62	9.43	[250]
				PTzBI	0.87	18.29	0.64	10.24	[250]
				PBDT-NQx	0.87	16.21	0.65	9.11	[251]
				PBDTS-NQx	0.92	17.86	0.70	11.47	[251]
				J61	0.89	17.43	0.62	9.53	[252]
				PBDT $\beta$ NPFBT	0.90	14.67	0.56	7.33	[253]
				PBDT-2fBz	0.89	19.00	0.62	10.50	[254]
				PBDT-fBT0	0.86	14.90	0.57	7.28	[255]

**Table 9** (Continued)

NFA	$\lambda_{\text{max}}$ (nm)	HOMO (eV)	LUMO (eV)	Donor	$V_{\text{OC}}$ (mV)	$J_{\text{SC}}$ (mA Cm $^{-2}$ )	FF	PCE (%)	Refs.
<b>m-ITIC</b> <b>ITIC-EH</b>	700	5.52	3.82	PBDBS-EH-T	0.94	17.84	0.63	10.49	[256]
				HD-PBDT2FT	0.92	14.40	0.65	8.70	[257]
				OD-PBDT2FT	0.92	13.10	0.69	8.30	[257]
				PBDD4T-2F	0.94	15.04	0.61	8.69	[258]
				J71	0.94	17.32	0.70	11.41	[259]
				PffQx-PS	0.97	14.96	0.63	9.12	[260]
				J61	0.90	17.97	0.66	10.57	[261]
				J61	0.91	18.31	0.71	11.77	[261]
				PBQ-OF	0.69	16.16	0.60	6.68	[262]
				PBQ-QF	0.83	17.16	0.63	8.90	[262]
				PBQ-4F	0.95	17.87	0.67	11.34	[262]
<b>pO-ITIC</b>	679	5.49	3.71	PTZ-DO	0.92	14.56	0.67	9.03	[263]
<b>mO-ITIC</b>	674	5.50	3.74	PTZ-DO	0.92	15.18	0.66	9.28	[263]
<b>FpO-ITIC</b>	662	5.61	3.72	PTZ-DO	0.88	12.55	0.60	6.69	[263]
<b>ITIC-OE</b>	671	5.67	4.03	PBDB-T	0.85	14.80	0.67	8.50	[264]
<b>ITIC-C3</b>	669	5.86	4.05	PBDB-TF	0.04	0.60	0.22	<0.1	[265]
<b>ITIC-C6</b>	669	5.70	4.00	PBDB-TF	0.98	14.40	0.64	9.31	[265]
<b>ITIC-C9</b>	669	5.78	3.97	PBDB-TF	0.99	14.50	0.67	10.24	[265]
<b>ITIC-SC6</b>	665	5.68	3.91	PBDB-ST	0.90	13.87	0.58	7.27	[266]
<b>ITIC-SC8</b>	665	5.70	3.90	PBDB-ST	0.90	14.43	0.60	7.79	[266]
<b>ITIC-SC2C6</b>	665	5.74	3.86	PBDB-ST	0.92	15.32	0.64	9.16	[266]
<b>C8-ITIC</b>	680	5.63	3.91	PFBDB-T	0.94	19.60	0.72	13.20	[267]
<b>ITIC-Th</b>	668	5.66	3.93	PTB7-Th	0.80	15.93	0.68	8.70	[268]
				PTDBT-T1	0.88	16.24	0.67	9.60	[268]
				PTFB-O	0.93	17.60	0.69	10.88	[269]
<b>ITCPTC-Th</b>	684	5.68	4.03	PBDB-T	0.86	17.05	0.72	10.61	[270]
<b>ITIC-Th1</b>	677	5.74	4.01	FTAZ	0.85	19.33	0.73	12.10	[271]
<b>ITCPTC-Se</b>	684	5.65	4.00	PBDB-T	0.86	15.20	0.68	9.02	[270]
<b>IT-M</b>	700	5.58	3.98	PBDB-T	0.94	17.44	0.74	12.05	[272]
<b>IT-DM</b>	692	5.56	3.93	PBDB-T	0.97	16.48	0.71	11.29	[272]
<b>IT-M</b>	700	5.58	3.98	PDCBT-2F	0.94	10.43	0.56	6.60	[273]
				PB3T	1.00	18.90	0.63	11.90	[274]
				PB2T	0.56	0.08	0.26	0.01	[274]
<b>ITOM1</b>	650	5.50	3.76	PBDB-T	1.01	12.31	0.51	6.30	[275]
<b>ITOM2</b>	678	5.49	3.86	PBDB-T	0.93	17.53	0.73	11.90	[275]
<b>ITOM3</b>	664	5.52	3.80	PBDB-T	0.97	16.38	0.68	10.80	[275]
<b>ITOM4</b>	676	5.49	3.81	PBDB-T	0.96	14.69	0.56	7.90	[275]
<b>IT-01</b>	668	5.38	3.33	PBDB-T	0.93	17.35	0.72	11.60	[276]
<b>IT-02</b>	668	5.37	3.31	PBDB-T	0.97	15.34	0.62	9.30	[276]
<b>IT-03</b>	668	5.36	3.31	PBDB-T	0.98	9.80	0.51	4.90	[276]
<b>IT-04</b>	668	5.35	3.30	PBDB-T	0.95	9.16	0.47	4.20	[276]
<b>IT-4F</b>	717	5.66	4.14	PBDB-T-SF	0.88	20.88	0.71	13.10	[277]
<b>H-ITIC</b>		5.61	4.02	PBDTTTPD	1.04	10.60	0.58	6.40	[278]
<b>F-ITIC</b>		5.65	4.09	PBDTTTPD	0.94	14.10	0.66	8.80	[278]
<b>Cl-ITIC</b>		5.70	4.14	PBDTTTPD	0.94	15.60	0.65	9.50	[278]
<b>Br-ITIC</b>		5.73	4.20	PBDTTTPD	0.93	15.40	0.66	9.40	[278]
<b>I-ITIC</b>		5.68	4.14	PBDTTTPD	0.95	14.50	0.65	8.90	[278]
<b>ITVIC</b>	755	5.46	3.97	J71	0.89	14.47	0.57	7.34	[279]
<b>ITVfIC</b>	780	5.56	4.01	J71	0.84	19.73	0.59	9.72	[279]
<b>ITVffIC</b>	780	5.58	4.04	J71	0.81	20.60	0.63	10.54	[279]
<b>ITIC-th</b>	730	5.28	3.82	PBDB-T1	0.92	15.93	0.62	9.12	[280]
<b>ITThC</b>	640	5.47	3.76	PBDB-T	1.01	15.90	0.71	11.40	[281]
<b>MeIC</b>	674	5.57	3.92	J71	0.92	18.41	0.74	12.54	[282]
<b>IDT-T-N</b>	734	5.58	4.06	PBDB-T	0.94	14.03	0.56	7.40	[223]
<b>ITThIC</b>	699	5.49	3.85	HFQx-T	0.88	16.49	0.71	10.40	[283]
<b>IDTT-2BM</b>	672	5.50	3.80	PBDTT-C-T	0.85	9.87	0.57	4.81	[228]
<b>INIC0</b>	692	5.45	3.88	FTAZ	0.96	13.51	0.58	7.70	[284]
<b>INIC1</b>	710	5.54	3.97	FTAZ	0.93	16.63	0.64	10.10	[284]
<b>INIC2</b>	704	5.52	3.98	FTAZ	0.90	17.56	0.67	10.80	[284]
<b>INIC3</b>	710	5.52	4.02	FTAZ	0.86	19.44	0.67	11.50	[284]
<b>DTNIC6</b>	638	5.87	3.92	PBDB-T	0.96	7.71	0.45	3.39	[285]
<b>DTNIC8</b>	634	5.91	3.93	PBDB-T	0.96	12.92	0.72	9.03	[285]
<b>DTNR</b>	618	5.94	3.94	PTB7-Th	1.08	15.72	0.56	9.51	[286]
<b>NTIC</b>	650	3.76	5.58	PBDB-T	0.94	13.55	0.68	8.63	[287]
<b>NTIC-Me</b>	647	3.73	5.53	PBDB-T	0.96	13.03	0.66	8.30	[287]
<b>NTIC-OMe</b>	651	3.70	5.53	PBDB-T	0.96	13.52	0.66	8.61	[287]
<b>NTIC-F</b>	657	3.77	5.52	PBDB-T	0.81	15.04	0.66	8.10	[287]
<b>IHIC-N</b>	641	5.57	3.80	PTB7	0.85	13.50	0.61	6.91(11.9)	[288]
<b>FTIC-C8C8</b>	665	5.43	3.71	PBDB-T	0.94	15.81	0.66	10.06	[289]
<b>FTIC-C8C6</b>	666	5.62	3.83	PBDB-T	0.92	16.69	0.68	10.45	[290]
<b>FTIC-C6C6</b>	666	5.60	3.81	PBDB-T	0.92	17.44	0.64	10.26	[290]
<b>FTIC-C6C8</b>	666	5.64	3.81	PBDB-T	0.93	18.55	0.65	11.12	[290]
<b>DTF-IC</b>	663	3.80	5.40	PTB7-Th	0.87	14.35	0.54	6.70	[291]
<b>DTC-IC</b>	679	3.81	5.41	PTB7-Th	0.86	14.12	0.56	6.80	[291]
<b>FDNCTF</b>	697	5.42	3.73	PBDB-T	0.93	16.30	0.72	11.20	[292]
<b>DTCC-IC</b>	669	5.50	3.87	PTB7-Th	0.95	11.05	0.55	5.74	[293]
<b>CDTCN</b>	704	5.39	3.80	PBDB-T	0.96	11.26	0.58	6.23	[151,291]

**Table 9** (Continued)

NFA	$\lambda_{\text{max}}$ (nm)	HOMO (eV)	LUMO (eV)	Donor	$V_{\text{OC}}$ (mV)	$J_{\text{SC}}$ (mA cm $^{-2}$ )	FF	PCE (%)	Refs.
<b>DTC8-IC</b>	654	5.46	3.65	PBDB-T	0.97	14.27	0.67	9.48	[245]
<b>4TIC</b>	740	5.28	3.87	PTB7-Th	0.77	18.40	0.70	10.43	[294]
<b>4TIC</b>	740	5.28	3.87	PTB7-Th	0.75	18.75	0.67	9.77	[295]
<b>BDT-IC</b>	703	5.40	3.83	PBDB-T	0.87	17.85	0.67	10.42	[296]
<b>BDT-IC</b>	703	5.40	3.83	J71	0.92	17.30	0.65	10.50	[297]
<b>BDT-IC-EO</b>	718	5.32	3.85	J61	0.87	16.35	0.67	9.56	[298]
<b>BDT-IC-EO</b>	718	5.32	3.85	J71	0.90	17.75	0.66	10.46	[298]
<b>NCBDT</b>	730	5.36	3.89	PBDB-T	0.84	20.33	0.71	12.12	[299]
<b>BDTTT-M</b>	700	5.40	3.85	PBDB-T	0.90	17.56	0.71	11.31	[300]
<b>BDTTThIT-M</b>	710	5.35	3.82	PBDB-T	0.94	18.03	0.71	12.12	[300]
<b>IDTIDT-IC</b>	696	5.42	3.82	PTB7-Th	0.94	14.49	0.48	6.48	[301]
<b>IDTIDSe-IC</b>	701	5.41	3.81	J51	0.91	15.16	0.58	8.02	[302]
<b>BT-CIC</b>	765	5.49	4.09	PCE-10	0.70	22.50	0.71	11.20	[303]
<b>IUIC</b>	772	5.45	3.87	PTB7-Th	0.80	21.74	0.65	11.20	[304]
<b>NSTI</b>	668	5.54	3.87	PBDBT	0.83	16.47	0.75	10.33	[305]
<b>NIDBT</b>	593	5.48	3.83	PTB7-Th	0.83	11.31	0.46	4.35	[306]
<b>IHIC2</b>	659	5.69	3.86	FTAZ	0.77	16.10	0.59	7.31	[307]
<b>IOIC2</b>	696	5.41	3.78	FTAZ	0.90	19.70	0.69	12.30	[307]
<b>FOIC</b>	782	5.36	3.92	PTB7-Th	0.74	24.00	0.67	12.00	[308]

Choi et al. synthesized **IDT(DCV)2** and **IDT(TCV)2** by incorporation of dicyanomethylene and tricyanomethylene terminal acceptors, respectively. It was found that the devices with active blends based on PTB7-Th donor exhibited superior self-life stability more than 1000 h due to its robust internal morphologies [211]. Later, analogous NFA **IEIC** exhibited a strong absorption due to the extension of  $\pi$ -conjugation, and OSCs based on PBDTTT-C-T: **IEIC1** blend showed a PCE of 3.93% [212]. A variety of alkyl chains such as butyl (**IEIC2**), hexyl (**IEIC3**), 2-ethylhexyl (**IEIC4**) and 2-ethylhexyloxy (**IEICO**) were incorporated on thiophene unit and their effects on absorption, molecular interactions and device performance were studied [213–217]. In particular, alkyl chains affected the distribution of domain spacing in the blend and then charge-transporting properties. Among them, polymer solar cells based on PffT2-FTAZ-2DT: **IEIC4** blend exhibited the highest PCE of 7.20% due to better packing and small domain size in the blend which contributes to a high  $J_{\text{SC}}$  of 12.20 mA cm $^{-2}$  and high  $V_{\text{OC}}$  of 1.00 V [216]. However, the alkoxy chain containing NFA **IEICO** showed absorption maxima at 785 nm, which helps to increase  $J_{\text{SC}}$  up to 17.70 mA cm $^{-2}$  and PCE of 8.40% when blended with PBDTTT-C-T donor [217]. Fluorine-incorporated NFA **IEICO-4F** showed red-shifted absorption with maxima to 800 nm, and the high LUMO level (3.90 eV) enables low energy loss (0.50 eV), leading to the highest  $J_{\text{SC}}$  of 22.80 mA cm $^{-2}$  and a high PCE of 10.00% [218].

Later, several molecules were reported by replacing thiophene with various aromatic units such as furan (**DC-IDT2Fu**), thiazole (**IDT-Tz**), alkoxyphenyl (**IDT-BOC6**) and vinyl (**SJ-IC**) units [219–222]. Among them, the PBDB-T donor-based device employing **IDT-Tz** and **IDT-BOC6** as NFAs achieved the highest PCE of 8.52% and 9.60%, respectively, because its heteroatom (S and O) facilitates the supra-molecular conformational lock for enhancing absorption as well as electron mobility. Subsequently, Yang et al. synthesized **IDTC** and **IDTO** by incorporating new terminal acceptors, which enables strong absorption, balanced charge transportation and led to higher PCEs of 9.35% and 10.02%, respectively, when blended with the polymer donor PBDB-T [227]. To enhance the spectral response and raised the LUMO of the molecules, BT/BTz building blocks end-capped with dicyanomethylene, rhodanine and 2-(1,1-dicyanomethylene)rhodanine units attached to both sides of the IDT central linker were synthesized [228–233]. Among them, **IDT-2BR** showed a strong absorption which was tested with several polymer donors for OSCs, and the device employing PTB7-Th as donor achieved highest PCE of 8.20%, which was attributed to strong absorption and well-matched energy levels with low energy loss (0.59 eV) [232]. However, polymer solar cells based on SM

NFAs containing BTz units (**BTA1** and **BTA2**) blended with P3HT can achieve a high  $V_{\text{OC}}$  up to 1.22 eV due to uplifted LUMO as well as high charge transporting properties [233,234].

Zhu et al. reported thienothiophene-based molecules, **ATT-1** and **ATT-2**, and made OSCs blended with PTB7-Th donor to deliver high PCEs of 10.07% and 9.58%, respectively, due to their strong and complimented absorption [235,236]. The strong absorption of **ATT-2** produced the high  $J_{\text{SC}}$  20.75 mA cm $^{-2}$ , while the high LUMO of **ATT-1** is responsible for high  $V_{\text{OC}}$  of 0.87 V. Choi et al. reported a low bandgap **IM-BDTIDT2**, composed of BDT unit centralized with two IDT and dicyanomethylene-3-indanone units, which showed a PCE of 5.53% as blended with PTB7-Th [238]. Polymer solar cells based on J51:**IDSeT-IC** blend exhibited a PCE of 8.58% with a minimized trade-off of  $J_{\text{SC}}$  and  $V_{\text{OC}}$  (15.20% mA cm $^{-2}$  and 0.91 V) values when compared to fullerene acceptor based-device [239]. Huang et al. synthesized IDT-based dyes, **IDTzCR** and **IDTCR**, introducing 2-(1,1-dicyanomethylene)rhodanine as end groups conjugated via thiophene and thiazole, respectively. **IDTzCR** showed more planar structure due to conformationally locked IDT and thiazole units via S . . . N bonding, which greatly reduce the molecular reorganization energy and thus balance the hole/electron mobility, leading to high FF. OSC based on **IDTzCR** blended with PTB7-Th donor exhibited high PCE of 8.71% due to high charge collection efficiency that increases  $J_{\text{SC}}$  to 13.80 mA cm $^{-2}$  as compared to the inferior NFA **IDTCR** (6.10%) [240]. Bo et al. reported **IDT-OB** containing asymmetric side chains showed high solubility, close molecular packing and thus a better phase separation led to a high PCE of 10.12% as blended with PBDB-T donor [241]. Yang et al. synthesized **PTIC** based on pyran-bridged IDT and dicyanomethylene-3-indanone terminal-groups, exhibited a PCE of 7.66% as blended with PBDB-T donor [242]. Later, Wang et al. incorporated thiophene (**PT-TIC**) and thienothiophene (**PT-TTIC**) between IDT and acceptor units to enhance the absorption maxima. Among them, PBDB-T:**PT-TIC** blend showed better crystallinity and thus favor charge transporting property, resulting high PCE of 9.21% [243].

Later, fused seven-member ring core IDTTs were designed and developed to enhance the spectral absorbance as compared to that of its congener IDT. The structures of IDTT-based NFAs were displayed in Fig. 19 with photophysical properties were compiled in Table 9. Zhan et al. reported **ITIC** as potential NFA, composed of central IDTT functionalized with dicyanomethylene-3-indanone end-capping acceptors. **ITIC** showed red-shifted absorption with absorption maxima at 664 nm as compared to that of parent dye **IC-1IDT-IC** [244]. Polymer solar cells based on PTB7-Th:**ITIC** blend

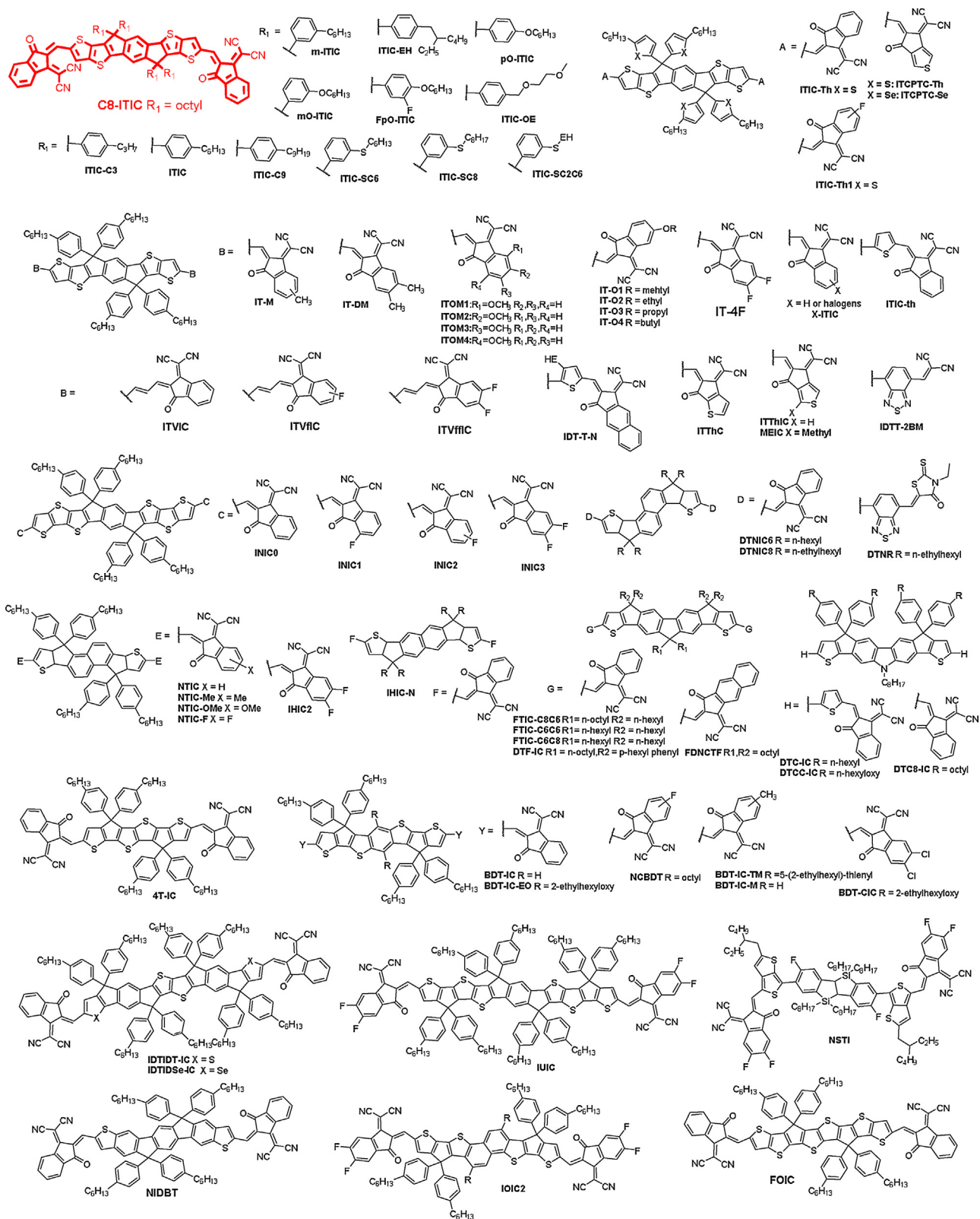


Fig. 19. Chemical structures of fused indacenodithiophene (IDT) based SM NFAs [244–308].

film exhibited high  $J_{SC}$  of 14.79 mA cm<sup>-2</sup>,  $V_{OC}$  of 0.82 V and PCE of 7.52% due to balanced charge transport and proper phase separation of the blended film [244]. Due to its strong absorption and favorable energy levels of **ITIC**, several polymer/SM donors with variable spectral responses and minimized energy loss were

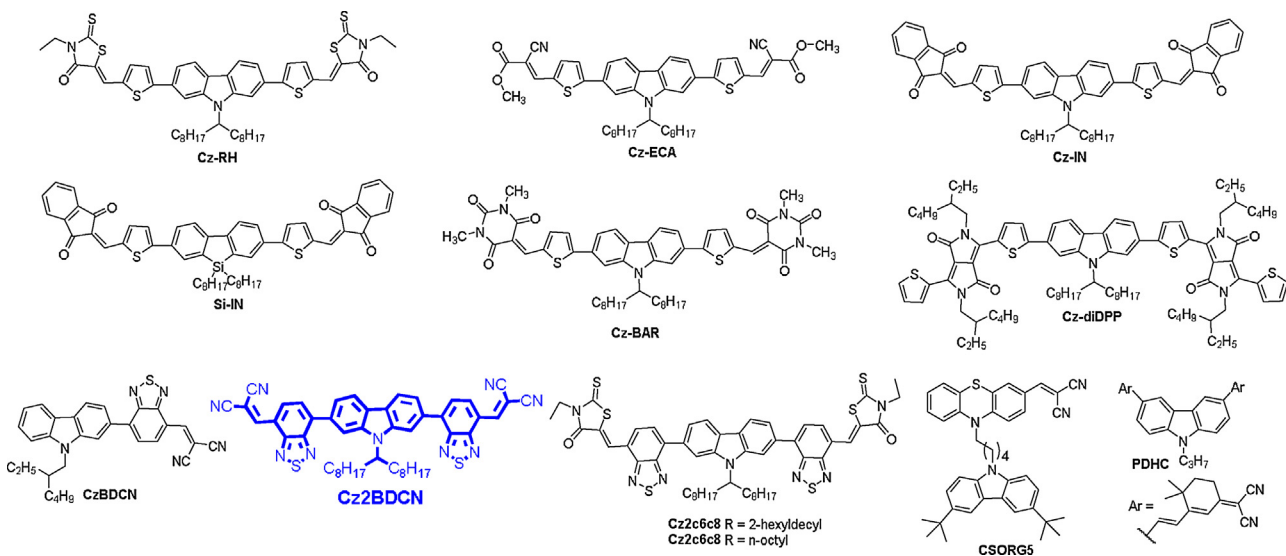
used to blend and enhance the PCE of OSCs. Among them, some potential polymer donors such as PBDB-T, PDCBT, PTzBI, PBDTS-NQx, PBDT-2fBz and PBDBS-EH-T have been used to optimize devices based on **ITIC** NFA, and drastically increased PCE up to 11.50% due to (i) better complimentary absorption spectra,

(ii) minimized energy loss and (iii) better charge transportation [245–260].

Li et al. modified the molecular structure of ITIC by side-chain engineering with *meta*-alkylphenyl substitution to give **m-ITIC**, resulting in a high PCE of 11.77% when compared to congener ITIC [261]. Though m-ITIC showed blue-shifted absorption, however, its stronger film absorptivity, good molecular packing and electron mobility were responsible for a significant improvement in the PCE. Gao et al. reported alkoxy-phenyl substituted NFA, **pO-ITIC**, **mO-ITIC** and **FpO-ITIC**, showed high molar absorptivity and raised the LUMO levels led to high  $V_{OC}$  and PCEs. Among them, **mO-ITIC** exhibited a high PCE up to 9.28% due to its better matching of absorption and frontier energy levels with PTZ-DO donor [263]. Marks et al. proved that increasing alkyl chain length on IDTT core enhanced the crystallinity and carrier mobility of the corresponding blend [265]. Similarly, Heeney et al. incorporated octyl side chain on central core (**C8-ITIC**) improves the molar absorptivity and crystallization propensity of blend, leading to the highest PCE of 13.2% as blended with fluorinated PBDB-T donor [267]. Later, efficient acceptor **ITIC-Th** was reported by Zhan and co-workers to stabilize LUMO and increase the electron mobility due to S-S intermolecular interactions. Hence, the device based on blend film of ITIC-Th:ITIC-Th produced a high PCE of 9.60% due to high  $J_{SC}$  of  $16.24 \text{ mA cm}^{-2}$ , which stems from its high electron mobility of blend films [268]. However, the NFAs with strong absorptions such as **ITCPTC-Se** and **ITCPTC-Th** led the device blended with donor PBDB-T to exhibit a higher PCE of 10.61% because thiophene side group facilitates good morphology and  $\pi$ - $\pi$  stacking in blend films [270]. Later, Wang et al. incorporated fluorine atoms on terminal acceptor groups (**ITIC-Th1**) to improve the intermolecular interactions and reduced optical band gap. As a result, blend film based on FTAZ:ITIC-Th1 exhibited high PCE of 12.10% due to effective exciton dissociation and reduced molecular recombinations [271]. Hou et al. subtly modified the molecular structure of **ITIC** by incorporating mild electron-donating methyl and dimethyl groups onto terminal acceptor units to make new acceptors **IT-M** and **IT-DM** to uplifted LUMO levels by 0.04 eV and 0.09 eV, respectively [272]. Hence, active blends based on PBDB-T:IT-M and PBDB-T:IT-DM achieved higher  $V_{OC}$  values (0.94 V and 0.97 V) and then a higher PCE (12.05% and 11.29%) when compared to those of parent **ITIC**-based devices. The nature and position of the alkyl/alkoxy substitution manipulate the  $\pi$ - $\pi$  stacking interactions, in which 5-methoxyl-substituted NFA (**IT-OM2**) exhibited the highest degree of molecular ordering, and thus the highest electron mobility when compared to other congener acceptors [275]. Hence, the OSC device with active blend PBDB-T:IT-OM2 achieved the PCE of 11.90% with  $J_{SC}$  of  $17.53 \text{ mA cm}^{-2}$ , which is higher than other isomeric acceptors. Later, the introduction of fluorine atoms onto the end group to give new acceptor **IT-4F**, which showed drastic red-shifted absorption. The corresponding PBDB-T-SF:IT-4F blend film showed a significant improvement in  $J_{SC}$  ( $20.88 \text{ mA cm}^{-2}$ ) and yielded the highest PCE up to 13.10% [277]. Modification of terminal acceptors also greatly influenced the absorption, molecular packing and then PCEs of the corresponding acceptor-based blend films. In this context, end group modification with thiényl-fused group results in a new acceptor **ITThC**, which greatly raise the LUMO level and facilitates closer  $\pi$ - $\pi$  stacking distance and then higher electron mobility. Hence, polymer solar cells based on blend film of PBDB-T:ITThC exhibited high  $V_{OC}$  of 1.01 V with an impressive PCE of 11.40% [281]. Zhan et al. reported a series of NFAs (**INIC0-INIC4**) based on non-fluorinated or fluorinated dicyanomethylene-3-indanone terminal units. They showed strong absorption and the corresponding blend film achieved higher  $J_{SC}$  and PCE values when compared to non-fluorinated dyes [285]. Polymer solar cell based on di-fluorinated dye **INIC3** blended with

FTAZ donor yields a best PCE as high as 11.50%, which is higher than other isomeric dyes.

Zheng et al. reported two dyes **DTNIC6** and **DTNIC8** contain hexyl and 2-ethylhexyl chains to optimize blend phase morphology for efficient exciton dissociation and reduced bimolecular recombination, balanced charge carrier mobility [285]. As a result, the device based on PBDB-T:DTNIC8 blend films gave high FF of 0.77 and PCE of 9.03% as compared to **DTNIC6**-blended film having PCE of 3.39%. Later, they made BT rhodanine functionalized **DTNR** to blend with PTB7-Th donor, the targeted device exhibited the PCE of 9.51% due to minimum energy loss of 0.55 eV, achieving the  $V_{OC}$  up to 1.08 V [286]. Chen et al. reported isomeric dithienonaphthalene-based acceptor (**NTIC**), which exhibited a strong absorption because the structure facilitated better conjugation between the terminal acceptors and the device achieved a PCE of 8.63% as **NTIC** blended with polymer donor PBDB-T [287]. In this context, dithieno-fused fluorene/cbazole-based acceptors were made to enhance the spectral response in addition to the incorporation of alkyl chains at fluorene/cbazole that can also modulate the morphology of corresponding blend film [291–293]. A device based on PBDB-T:**FTIC-C6C8** blend film achieved best PCE of 11.12% owing to strong absorption and optimized nanoscale morphology of the photoactive layers [292]. Later, Liu et al. reported a narrow bandgap acceptor (**4TIC**) and showed red-shifted absorption centered at 740 nm. In addition, the rigid central building block offers a lower reorganization energy, which facilitates lower  $V_{OC}$  energy loss [294,295]. As a result, the device based on PTB7-Th:**4TIC** blend film achieved a high PCE of 10.42% with a high  $J_{SC}$  of  $18.40 \text{ mA cm}^{-2}$ . Chen et al. reported **BDT-IC**, based on heptycyclicbenzodi-cyclopentadithiophene as central unit and dicyanomethylene-3-indanone as terminal acceptors [296]. The optimized device based on PBDB-T:**BDT-IC** blend produced a PCE of 10.42% with a remarkable  $J_{SC}$  of  $17.85 \text{ mA cm}^{-2}$ , which was manifested from a broad spectral coverage of the blend film. Later, **BDT-IC-EO** was reported with the incorporation of alkoxy chain on the central core for better packing and optimal morphology [298]. As a result, OSCs based on J71:**BDT-IC-EO** blend showed improved PCE to reach to 10.46% due to a significant increment in  $V_{OC}$  (0.90 V). Later, Chen et al. fine tune the energy level of NFA **NCBDT** by introducing alkyl chain on central linker and fluorine atoms on terminal acceptor, respectively. Blend film based on PBDB-T:**NCBDT** exhibited efficient charge generation, high charge extraction and low bimolecular recombination led to high  $J_{SC}$  ( $20.0 \text{ mA cm}^{-2}$ ) and PCE (12.12%) [299]. Liao et al. reported fused deca-heterocyclic-based acceptor (**IDTIDT-IC**) and showed excellent co-planarity and enhanced effective conjugation length when compared to previous fused IDT acceptors [301]. Hence, polymer solar cell based on PTB7-Th:**IDTIDT-IC** blend exhibited a PCE of 6.48% with a high  $V_{OC}$  of 0.94 V due to minimal energy loss of 0.59 eV. Later, the same group inserted selenium atoms as bridge, resulting in a new NFA **IDTIDSe-IC**, showed enhanced PCE of 8.02% attributed to the red-shifted absorption and high charge carrier mobility of corresponding blend films with J51 donor [302]. Forrest et al. reported chlorinated NFA, **BT-CIC**, displayed strong absorption maximum at 765 nm leading to high  $J_{SC}$  of  $22.50 \text{ mA cm}^{-2}$  and PCE up to 11.20% as blended with PCE-10 donor [303]. Later Zhan et al. synthesized fused-undecacyclic NFA, **IUIC**, having dicyanomethylene-3-indanone terminal units to enhance absorption and raise LUMO level, leading to higher PCE of 11.20% as blend with PTB7-Th donor [304]. Recently, Zhu et al. reported **NSTI** based on bis-silicon-bridged stilbene and thienothiophene exhibits longer absorption due to quinoidal interactions. Its blend film with donor PBDBT and showed high  $J_{SC}$  of  $16.47 \text{ mA cm}^{-2}$  and PCE of 10.33% [305]. Lin et al. reported NFAs **IHIC2** and **IOIC2** based on naphthodithiophene fused octacyclic building block showed high absorption as well as higher LUMO level which favors  $J_{SC}$  and  $V_{OC}$  for OSC device based on the

**Fig. 20.** Chemical structures of carbazole based SM NFAs [155,156,161,163,311–315].

corresponding blend film. Blend film based on **FTAZ:IOIC2** exhibited high PCE of 12.3% due to its high electron mobility than **IHC2 NFA** [307]. Recently, Zhan et al. reported **FOIC** based on fused tris(thienothiophene) showed longer absorption maximum up to 782 nm, higher LUMO level and exhibited a PCE of 12.0% as blended with PTB7-Th donor due to effective exciton separation, charge collection and negligible bimolecular recombinations [308].

Overall, IDT-derived acceptors displayed strong absorption and favorable energy levels to well matched with various polymer donors. Also, the co-planar motif of IDT unit allows suitable “face-on” molecular  $\pi$ - $\pi$  stacking which facilitates the formation of optimum morphology in blend film for better charge transportation and reduced charge recombination. Subtle modification of terminal acceptors greatly modulates the optoelectronic properties and the best foresee PBDB-T-SF. Over all, **C8-ITIC** NFA based on IDTT exhibited the highest PCE of 13.20% in combination with PFBD-T donor. It will be optimistic to foresee the great advance of NFA developments based on fused IDT cores. With suitable molecular engineering on terminal acceptors along with a new class of fused IDT cores, OSCs based on this class of NFAs with improved PCEs can be anticipated.

### 3.2.2. Carbazole-based small molecular acceptors

Carbazole is an aromatic heteroacene that contains N-atom bridge, which is analogous to fluorene, showed pronounced thermal stability and high charge transporting properties. The carbazole core offers flexibility for functionalization at various

positions (C1, C2, C3, C6, C7 and N9), while N-functionalization with alkyl or aryl substituents can further control the molecular interactions and packing. Carbazole derivatives typically possess high glass transition temperature for morphological stability and uplifted LUMO, which was beneficial for high  $V_{OC}$  and then PCE as they are employed as NFAs in OSCs. Carbazole can provide a better electronic communication via 2 and 7 substitutions with various electron-withdrawing groups [309]. Fig. 20 displayed the structures of carbazole-based NFAs and their properties and device data was compiled in Table 10.

Lim et al. synthesized **Cz-RH** containing carbazole as central block and rhodanine end groups, which exhibited red-shifted absorption and higher LUMO energy than **Flu-RH** [155]. After blending with P3HT, a PCE of 2.56% was achieved with high  $V_{OC}$  of 1.03 V. In NFAs, the end groups strongly influence the blend morphology and manipulate charge transport properties. In this context, they replaced the rhodanine end group with both cyanoethylacetate and 1,3-indanedione, resulting in **Cz-ECA** and **Cz-IN**, respectively [156]. The incorporation of indanone red-shifted the absorption (20 nm), while cyanoethylacetate uplifted the LUMO energy. However, the device employed P3HT:**Cz-ECA** as active blend exhibited a PCE of 1.03% with high  $V_{OC}$  of 1.00 V. Bhosale et al. reported **Si-IN** based on dibenzosilole core which showed higher PCE of 2.76% than **Cz-IN** due to its good nanoscale interpenetrating network in the active blend [310]. For a broad spectral response, Bhosale et al. incorporated DPP as end units of carbazole, resulting in a new NFA **Cz-diDPP**, which exhibited

**Table 10**

Photo-physical and photovoltaic properties of carbazole based SM NFAs.

NFA	$\lambda_{max}$ (nm)	HOMO (eV)	LUMO (eV)	Donor	$V_{OC}$ (mV)	$J_{SC}$ (mA cm <sup>-2</sup> )	FF	PCE (%)	Refs.
<b>Cz-RH</b>	500	5.53	3.50	P3HT	1.03	4.69	0.53	2.56	[155]
<b>Cz-ECA</b>	465	5.63	3.48	P3HT	1.00	2.34	0.44	1.03	[156]
<b>Cz-IN</b>	519	5.57	3.58	P3HT	0.61	0.13	0.26	0.02	[156]
<b>Si-IN</b>	492	5.71	3.64	P3HT	0.78	7.61	0.46	2.76	[310]
<b>Cz-BAR</b>	509	5.63	3.51	P3HT	0.88	3.06	0.58	1.57	[161]
<b>Cz-diDPP</b>	599	5.56	3.74	P3HT	0.61	8.46	0.62	3.15	[311]
<b>CzBDCN</b>	463	5.90	3.60	P3HT	0.54	1.06	0.40	0.20	[312]
<b>Cz2BDCN</b>	497	6.10	3.64	PTB7-Th	0.88	10.60	0.53	5.30	[163]
<b>CzC6C8</b>	494	5.79	3.79	PBT	0.99	8.24	0.41	3.30	[313]
<b>Cz8</b>	489	5.72	3.74	PBT	1.03	9.00	0.50	4.64	[313]
<b>Cz8</b>				PTB7-Th	0.98	11.24	0.45	4.91	[313]
<b>PDHC</b>	490	5.47	3.42	P3HT	1.14	0.70	0.27	0.20	[314]
<b>CSORG5</b>	445	5.38	3.40	P3HT	0.98	5.96	0.56	2.80	[315]

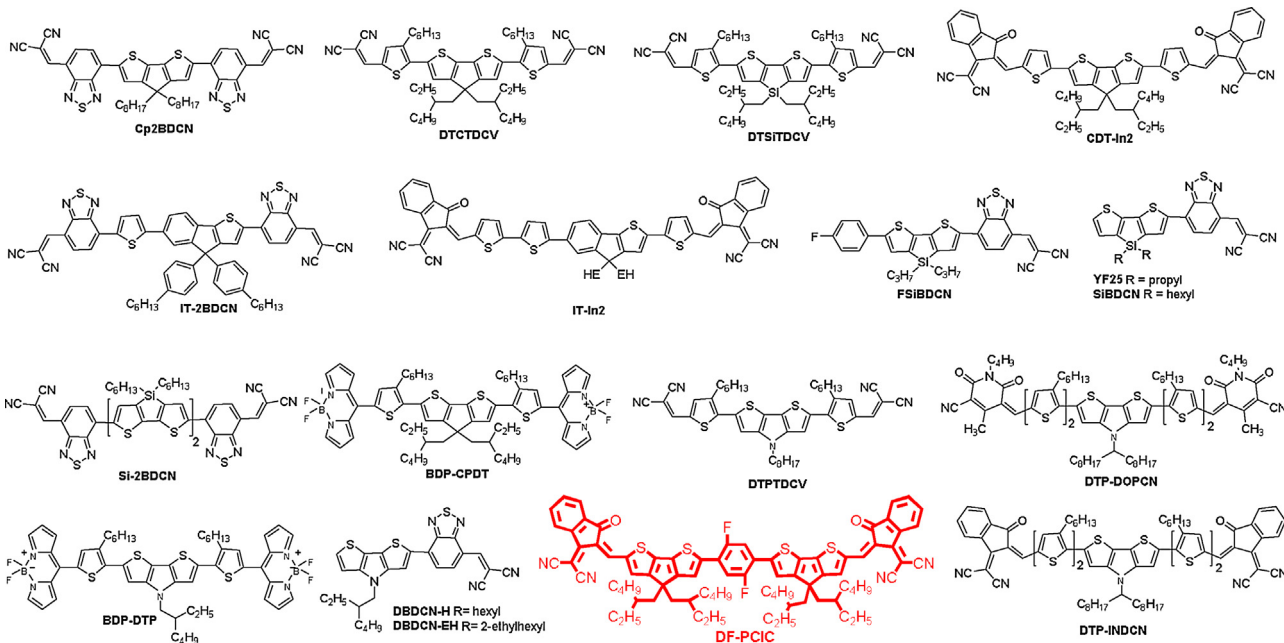


Fig. 21. Chemical structures of dithieno-fused heterocyclic SM NFAs [316–323].

drastically red-shifted absorption maximum located at 599 nm, which can help to produce a large photocurrent. After blending with P3HT, the device showed a higher PCE of 3.15% than those of device based on **Cz-RH**, **Cz-In** and **Cz-BAR** [311].

**Cz2BDCN** composed of carbazole and BT-DCN end-capping unit displayed red-shifted absorption as compared to mono-substituted acceptor **CzBDCN** [163]. Even **Cz2BDCN** has moderate absorption spectral coverage, as blended with PTB7-Th, the device achieved a PCE of 5.30% with high  $J_{SC}$  of  $10.60 \text{ mA cm}^{-2}$ , which is better than **FL2BDCN** and **Cp2BDCN**. Mainly, a high electron mobility of **Cz2BDCN** was responsible for the enhancement of  $V_{OC}$  and FF than other dyes. Later, Bo et al. modified the terminal dicyanomethylene unit by rhodanine, resulting in a new acceptor **CzC8**, which showed comparable absorption and uplifted HOMO and LUMO energy levels. The device based on the corresponding blend film with PTB7-Th donor gave a PCE of 4.91% [313]. Tian et al. synthesized **PDHC**, which was blended with P3HT donor to give a device exhibited a higher  $V_{OC}$  of 1.14 V as compared to that of corresponding devices based on fullerene acceptor. Chandrasekharam et al. synthesized phenothiazine-based acceptor **CSORG5**, which showed high LUMO level and moderate absorption properties [315]. Optimized device based on P3HT:**CSORG5** exhibited  $V_{OC}$  of 0.98 V and then achieved a moderate PCE of 2.80%, and after the insertion of a  $\text{TiO}_2$  layer in the device architecture, the PCE increased to 4.80%. Overall, the NFA **Cz2BDCN** based on carbazole core conjugated with BT-DCN units can deliver the highest PCE due to its broad spectral response and high electron mobility.

### 3.2.3. Dithieno-fused heterocycle-based small molecular acceptors

Dithieno-fused heterocyclic systems such as cyclopentadithiophene, dithienopyrrole and dithienosilole were analogous heteroaromatic cores where carbon atom was replaced by N- or Si-atom, respectively. They can be easily functionalized by simple bromination and followed by typical metal-catalyzed coupling reactions. Their derivatives generally show high electron richness and thermal stability. They provide available sites for alkylation, which improves solubility and optimizes the molecular packing in the thin film state. Their derivatives with suitable electron-

withdrawing groups facilitate strong intramolecular donor-acceptor interactions, which lead to NFAs with NIR-absorption. The structures were shown in Fig. 21, and their corresponding optical and device parameters were displayed in Table 11.

Ma et al. synthesized a set of acceptors (**DTCTDCV**, **DTSiTDCV** and **DTPTDCV**) based on cyclopentadithiophene, dithienosilole and dithienopyrrole as cores and end-capped with dicyanomethylene groups. These molecules showed broader absorption spectra (300–700 nm) and suitable high LUMO energy level compatible with conventional P3HT donor [316]. After blending with P3HT, **DTSiTDCV**-based device exhibited a higher PCE (1.56%) due to its highly crystalline blend, which favored better charge-transporting properties and thus high  $J_{SC}$  and  $V_{OC}$  than other NFA blends in this class. Later, Zheng et al. developed cyclopentadithiophene-based NFA (**CDT-In2**), for comparison, indenothiophene-based acceptor (**IT-In2**) was also synthesized. **IT-In2** exhibited a superior PCE of 7.82% as blended with PBDB-T due to crystalline blend morphology-enhanced electron mobility [317].

Meredith et al. aimed to attain a broad spectrum with narrow bandgap acceptors based on dithienopyrrole (**DBDCN-H**) and dithienosilole (**FSiBDCN** and **YF25**) cores conjugated with BT-DCN units [312,320]. They exhibited red-shifted absorption and high LUMO energy levels. Optimized devices based on P3HT:**FSiBDCN** blend exhibited a moderate PCE of 1.50% which is superior to **DBDCN-H**-based counterpart due to good blend morphology and high incident photon conversion efficiency. Later, Burn et al. developed monomeric and dimeric dithienosilole equipped with BT-DCN units (**SiBDCN** and **Si-2BDCN**). They found that dimeric **Si-2BDCN** exhibited better phase separation allowing efficient exciton formation, while monomeric **SiBDCN** exhibited a strong tendency to intermix with the P3HT donor without phase separation in the blend [321]. As a result, **Si-2BDCN** produced better performance than **SiBDCN**.

Beaujuge et al. synthesized **Cp2BDCN** based on cyclopentadithiophene containing two BT-DCN units on both sides. **Cp2BDCN** showed red-shifted absorption due to its electron-rich core compared to fluorene and carbazole analogous molecules (**FL2BDCN** and **Cz2BDCN**). As a result, the device based on **Cp2BDCN** blended with PTB7-Th donor exhibited a PCE of 4.6%

**Table 11**

Photo-physical and photovoltaic properties of dithienofused heterocycle based SM NFAs.

NFA	$\lambda_{\text{max}}$ (nm)	HOMO (eV)	LUMO (eV)	Donor	$V_{\text{OC}}$ (mV)	$J_{\text{SC}}$ ( $\text{mA cm}^{-2}$ )	FF	PCE (%)	Refs.
<b>DTCTDCV</b>	577	5.62	3.74	P3HT	0.58	1.76	0.31	0.32	[316]
<b>DTSiTDCV</b>	559	5.69	3.82	P3HT	1.01	3.56	0.43	1.56	[316]
<b>DTPTDCV</b>	584	5.55	3.77	P3HT	0.78	2.60	0.32	0.65	[316]
<b>CDT-In2</b>	720	5.75	4.26	PBDB-T	0.86	7.89	0.37	2.54	[317]
<b>IT-In2</b>	647	5.89	4.18	PBDB-T	0.94	13.94	0.59	7.82	[317]
<b>IT-2BDCN</b>	606	5.50	3.78	PTB7-Th	0.76	14.07	0.62	6.57	[318]
<b>BDP-CPDT</b>	516	5.16	3.82	P3HT	0.62	3.90	0.63	1.51	[319]
<b>BDP-DTP</b>	516	5.14	3.74	P3HT	0.57	3.28	0.63	1.18	[319]
<b>FSiBDCN</b>	604	5.70	3.70	P3HT	0.55	5.88	0.46	1.50	[312]
<b>DBDCN-H</b>	602	5.70	3.60	P3HT	0.58	2.41	0.40	0.30	[312]
<b>DBDCN-EH</b>	603	5.70	3.60	P3HT	0.52	2.07	0.39	0.40	[312]
<b>YF25</b>	575	5.40	3.70	P3HT	0.54	4.85	0.55	1.43	[320]
<b>SiBDCN</b>	575	5.60	3.80	P3HT	0.48	0.33	0.30	0.05	[321]
<b>Si-2BDCN</b>	685	5.50	3.90	P3HT	0.40	0.78	0.53	0.17	[321]
<b>Cp2BDCN</b>	681	5.79	3.90	PTB7-Th	0.66	11.90	0.60	5.00	[163]
<b>DTP-DOPCN</b>	648	5.27	4.00	PBDT-TBT	0.83	10.53	0.56	4.89	[322]
<b>DTP-INDCN</b>	680	5.24	4.05	PBDT-TBT	0.80	13.77	0.63	6.94	[322]
<b>DF-PCIC</b>	696	5.49	3.77	PBDB-T	0.91	15.66	0.72	10.14	[323]

with a  $J_{\text{SC}}$  of  $11.70 \text{ mA cm}^{-2}$ . The additive treatment improved the PCE (5.0%) due to better blend morphology and then good charge-transporting properties [163]. Thayumanvan et al. modified terminal end groups by incorporation of BODIPY unit on cyclopentadithiophene and dithienopyrrole to form acceptors **BDP-CPDT** and **BDP-DTP**, respectively. They showed weak absorption than related core-based molecules (**DTCTDCV** and **DTPTDCV**) having dicyanomethylene end group. But, devices based on **BDP-CPDT** (1.51%) and **BDP-DTP** (1.18%) exhibited slightly high PCEs due to the ordered blend morphology and thus high electron mobility [319]. Mishra et al. reported dithienopyrrole-based acceptors (**DTP-DOPCN** and **DTP-INDCN**), which can generate significantly large photocurrent up to 1000 nm region with exceptional high external quantum efficiency (EQE) of 69% at 880 nm [322]. The device with PBDT-TBT:**DTP-INDCN** blend produced a  $V_{\text{OC}}$  of 0.84 V and PCE of 6.94% which is higher than **DTP-DOPCN** [322]. Chen et al. synthesized **DF-PCIC** based on unfused core containing two cyclopentadithiophene and one 2,5-difluorobenzene unit which posses F···H interactions to keep more planar geometry for effective donor-acceptor interactions and then longer absorption maximum. As a result, blend film based on PBDB-T:**DF-PCIC** achieved high PCE of 10.14% with excellent morphological and device stability [323]. Overall, the OSC based on dithienopyrrole-based NFA (**DF-PCIC**) end-capped with dicyanomethyleneindan-1-one exhibited a highest PCE up to 10.14% in blend with polymer PBDB-T donor in this classification. Again, these electron-rich structures are promising cores for the development of NFAs by suitable molecular engineering on end groups.

### 3.3. Aromatic (di)imides-based small molecular acceptors

Aromatic imides/diimides possess a strong electron-accepting ability, thermal and photochemical and redox stability. They can easily be functionalized at various positions to modulate the molecular packing and crystallinity of the resulting aromatic diimide-based acceptors. The majority of research reports regarding NFAs came from this building block before the most successful IDT and/or IDTT-based NFAs have been reported. They were classified into various categories depending on the structural features.

#### 3.3.1. Phthalimide-based small molecular acceptors

Phthalimide has been used in organic electronic applications because their extremely facile synthesis. Their varied substitutions

at the imide nitrogen can be utilized to manipulate solubility, packing, and morphology. Fig. 22 displayed the structures of phthalimide-based NFAs and the related physical property and device data was compiled in Table 12.

Sellinger et al. reported an NFA, namely **PI-BT** based on BT linked with vinyl phthalimide units showed strong visible absorption, high LUMO level and planar structure, which favors the formation of a suitable crystalline network [324]. As a result, the device with blend film based on P3HT:**PI-BT** exhibited a PCE of 2.54%. Later, several acceptors were reported based on BT and thiazolothiazole flanked with phthalimide through acetylene linkage [325,326]. Various substitutions of alkyl groups on imide nitrogen strongly influence the photophysical properties and crystallinity. Among them, **Ph-EH** contains branched 2-ethylhexyl chain that showed better charge separation in blend film of the corresponding OSCs device. Later, Chen et al. developed several acceptors by various electron-deficient central linkers flanked with phthalimide units to establish the relation of the optoelectronic energy levels with the molecular planarity of the acceptors [327]. Finally, the device with better planar acceptor **BT-TTI-n12** blended with SM donor DPP-Pyr as active layer exhibited a high  $V_{\text{OC}}$  of 1.05 V and PCE as high as 2.4% because nanoscale morphologies of the blend films promote efficient exciton diffusion and dissociation.

Later, Wang et al. reported **FFI-1** based on cyano fluoranthene-fused phthalimide and thiophene units showed good thermal and photochemical stability [330]. Polymer solar cells based on P3HT:**FFI-1** exhibited a PCE of 2.25% though they have amorphous blend morphology and low electron mobility. However, changing thiophene linker with methoxyphenyl and naphthalene units raised LUMO level, which favors the  $V_{\text{OC}}$  of the corresponding blend film [331,332]. Fused phthalimide-based acceptors showed better PCEs in this class, the device based on blend film of P3HT:**o-CH3Ph-CN** exhibited a PCE of 2.90% when compared to other congener NFAs. Molecular engineering on the fused phthalimide core can facilitate a broad spectral response and favorable LUMO level to boost  $J_{\text{SC}}$ ,  $V_{\text{OC}}$  and then PCE of phthalimide-based acceptors.

#### 3.3.2. Naphthalene (di)imides-based small molecular acceptors

The aforementioned benefits of the naphthalene diimides (see Section 1.2) attracted immense research attention, and several SM NFAs were developed based on NI/NDI as terminal or central linker units. Naphthalene can fuse with mono- and diimides, resulting in NI and NDI building blocks, respectively. When compared to NI,

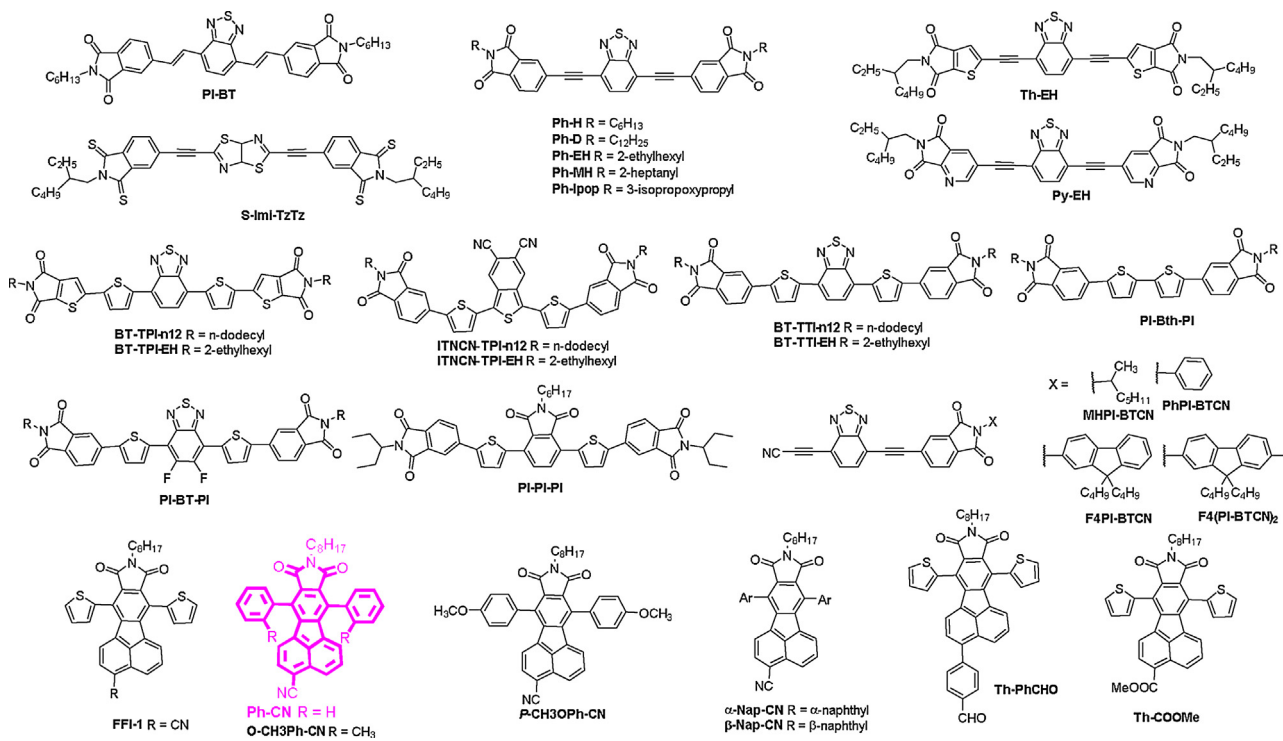


Fig. 22. Chemical structures of phthalimide based SM NFAs [324–332].

Table 12

Photo-physical and photovoltaic properties of phthalimide based SM NFAs.

NFA	$\lambda_{max}$ (nm)	HOMO (eV)	LUMO (eV)	Donor	$V_{OC}$ (mV)	$J_{SC}$ ( $\text{mA cm}^{-2}$ )	FF	PCE (%)	Refs.
<b>PI-BT</b>	448	5.80	3.30	P3HT	0.96	4.70	0.56	2.54	[324]
<b>Ph-EH</b>	413	6.21	3.32	P3HT	0.89	3.99	0.45	1.58	[325]
<b>S-Imi-TzTz</b>	473	6.37	3.73	P3HT	0.23	0.10	0.35	0.01	[325]
<b>Ph-H</b>	412	6.02	3.32	P3HT	0.69	2.52	0.44	0.77	[326]
<b>Ph-D</b>	412	6.02	3.32	P3HT	0.51	1.03	0.31	0.16	[326]
<b>Ph-EH</b>	412	6.02	3.32	P3HT	0.89	3.99	0.45	1.58	[326]
<b>Ph-MH</b>	412	6.01	3.31	P3HT	0.76	5.59	0.48	2.05	[326]
<b>Ph-Ipop</b>	412	6.02	3.32	P3HT	0.66	0.55	0.29	0.11	[326]
<b>Th-EH</b>	435	5.98	3.40	P3HT	0.72	1.44	0.36	0.38	[326]
<b>Py-EH</b>	409	6.18	3.42	P3HT	0.47	1.44	0.42	0.32	[326]
<b>BT-TPI- n12</b>	5.93	3.47	DPP-Pyr	1.01	1.44	0.54	0.85	[327]	
<b>BT-TPI-EH</b>	5.86	3.55	DPP-Pyr	1.07	0.46	0.41	0.23	[327]	
<b>ITNCN-TPI- n12</b>	5.81	3.96	DPP-Pyr	0.92	1.77	0.47	0.82	[327]	
<b>ITNCN-TPI-EH</b>	5.85	3.89	DPP-Pyr	0.89	3.13	0.46	1.44	[327]	
<b>BT-TTI- n12</b>	5.99	3.53	DPP-Pyr	1.05	3.72	0.60	2.40	[327]	
<b>BT-TTI-EH</b>	5.96	3.61	DPP-Pyr	0.95	3.37	0.49	1.71	[327]	
<b>PI-Bth-PI</b>	424	3.03	5.60	P3HT	1.23	1.20	0.46	0.32	[328]
<b>PI-PI-PI</b>	395	2.98	5.92	P3HT	0.92	1.70	0.50	0.31	[328]
<b>PI-BT-PI</b>	464	3.29	5.66	P3HT	0.94	0.84	0.22	0.28	[328]
<b>MHPI-BTCN</b>	418	6.45	3.48	P3HT	0.19	0.93	0.57	0.36	[329]
<b>PhPI-BTCN</b>	418	6.44	3.47	P3HT	0.12	1.39	0.23	0.37	[329]
<b>F4PI-BTCN</b>	420	6.43	3.48	P3HT	0.32	1.45	0.53	0.41	[329]
<b>F4(PI-BTCN)2</b>	422	6.42	3.48	P3HT	0.28	1.34	0.47	0.45	[329]
<b>FFI-1</b>	410	6.10	3.50	P3HT	0.76	4.40	0.56	1.86	[330]
<b>FFI-1</b>	6.23	3.48	P3HT	0.88	4.83	0.53	2.25	[331]	
<b>Ph-CN</b>	6.24	3.43	P3HT	0.96	5.60	0.49	2.61	[331]	
<b>o-CH3Ph-CN</b>	6.27	3.44	P3HT	0.95	6.35	0.48	2.90	[331]	
<b>p-CH3OPh-CN</b>	6.04	3.40	P3HT	0.96	4.63	0.48	2.12	[331]	
<b><math>\alpha</math>-Naph-CN</b>	6.15	3.43	P3HT	0.94	5.85	0.47	2.58	[331]	
<b><math>\beta</math>-Naph-CN</b>	6.12	3.43	P3HT	0.93	4.59	0.49	2.11	[331]	
<b>Th-PhCHO</b>	422	6.12	2.67	P3HT	1.03	5.14	0.45	2.40	[332]
<b>Th-COOMe</b>	411	6.18	2.72	P3HT	1.02	3.50	0.45	1.61	[332]

NDI showed strong electron-withdrawing nature, high electron affinity and high LUMO value. The structures of NI/NDI-based NFAs were displayed in Fig. 23 and related photophysical and photovoltaic data was compiled in Table 13.

Zhan et al. reported **NI-NI**, composed of two NI units that conjugated each other by a single bond, but showed a low PCE due to its poor absorption spectra [333]. Bo et al. reported **NI-A-C4**, **NI-A-C6** and **NI-A-C8** composed of two NI units with various alkyl

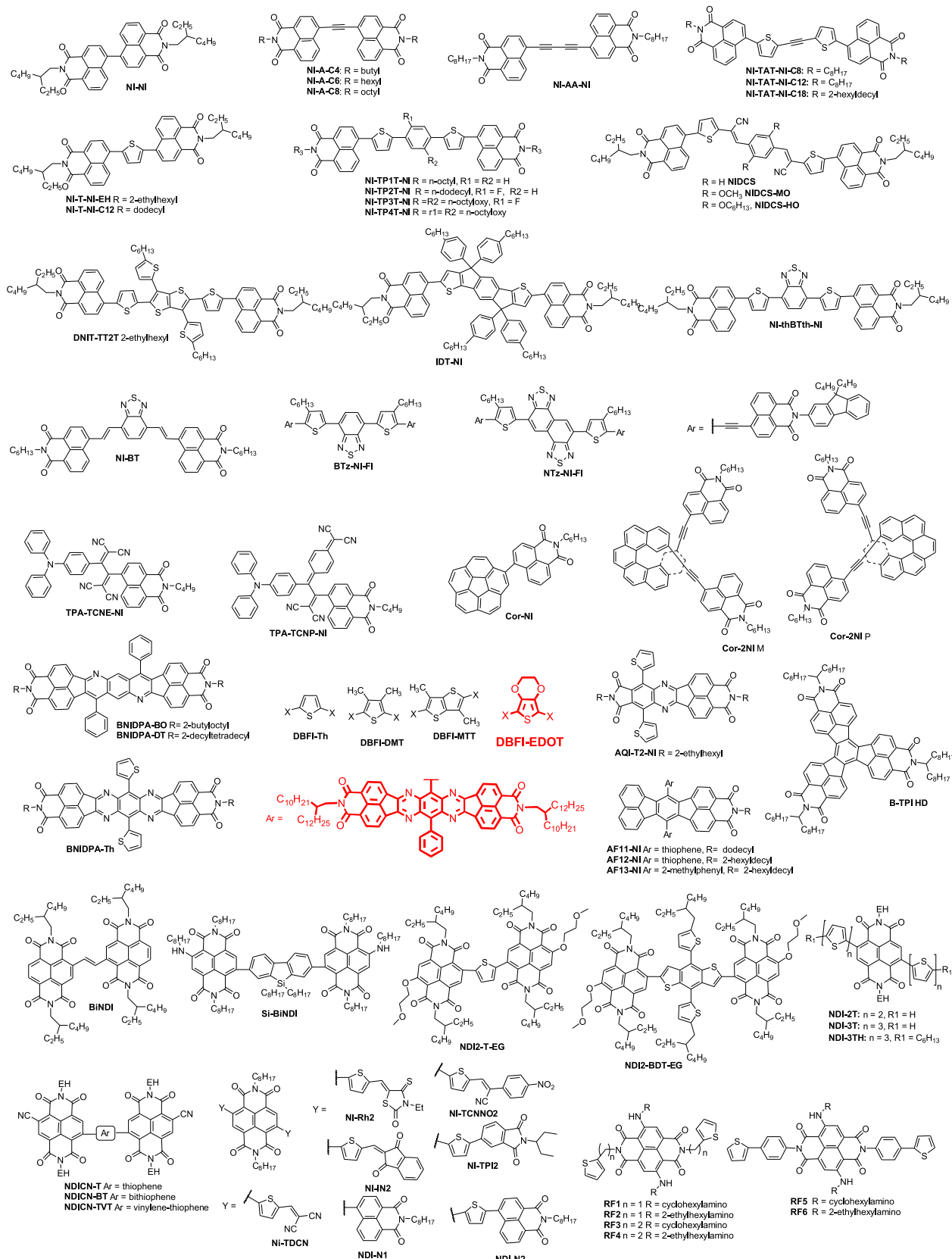


Fig. 23. Chemical structures of naphthalene (di)imide (NI/NDI) based SM NFAs [333–364].

**Table 13**

Photo-physical and photovoltaic properties of naphthalene diimide (NDI) based SM NFAs.

NFA	$\lambda_{max}$ (nm)	HOMO (eV)	LUMO (eV)	Donor	$V_{OC}$ (mV)	$J_{SC}$ (mA Cm <sup>-2</sup> )	FF	PCE (%)	Refs.
<b>NI-NI</b>	358	6.18	3.59	P3HT	0.79	0.79	0.45	0.28	[333]
<b>NI-A-C4</b>	426	6.05	3.54	PCDTBT-C12	1.09	1.34	0.10	0.15	[334]
<b>NI-A-C6</b>	426	6.04	3.48	PCDTBT-C12	1.06	6.24	0.61	4.05	[334]
<b>NI-A-C8</b>	426	6.02	3.47	PCDTBT-C12	1.07	5.19	0.60	3.34	[334]
<b>NI-AA-NI</b>	429	6.00	3.57	PCDTBT-C12	1.06	4.10	0.43	1.87	[335]
				PCDTBT-F	1.07	6.29	0.55	3.71	[335]
<b>NI-TAT-NI-C8</b>	410	5.84	3.41	PCDTBT-C12	1.24	2.16	0.30	0.82	[336]
<b>NI-TAT-NI-C12</b>	410	5.83	3.39	PCDTBT-C12	1.22	3.71	0.36	1.68	[336]
<b>NI-TAT-NI-C16</b>	410	5.95	3.49	PCDTBT-C12	1.20	0.90	0.22	0.24	[336]
<b>NI-T-NI-EH</b>	396	5.95	3.62	P3HT	0.80	1.47	0.49	0.58	[333]
<b>NI-T-NI-C12</b>	399	6.07	3.53	PCDTBT-C12	1.30	2.91	0.53	2.01	[337]
<b>NI-TP1T-NI</b>	428	5.93	3.50	PCDTBT-C12	1.04	4.79	0.56	2.78	[338]
<b>NI-TP2T-NI</b>	424	5.98	3.62	PCDTBT-C12	1.11	2.21	0.30	0.74	[338]
<b>NI-TP3T-NI</b>	437	5.95	3.68	PCDTBT-C12	1.09	1.71	0.30	0.56	[338]
<b>NI-TP4T-NI</b>	458	5.80	3.65	PCDTBT-C12	1.24	0.37	0.28	0.13	[338]
<b>NIDCS</b>	430	5.90	3.42	P3HT	0.73	8.04	0.46	2.71	[339]
<b>NIDCS-MO</b>	476	5.75	3.66	DTS(FBTTh <sub>2</sub> )	0.85	9.62	0.64	5.30	[340]
				P3HT	0.67	8.15	0.47	2.55	[339]
				PPDT2FBT	1.03	11.88	0.63	7.64	[341]
<b>DNIT-TT2T</b>	448	5.94	3.75	P3HT	0.88	3.28	0.43	1.25	[342]
<b>IDT-NI</b>	482	5.67	3.68	P3HT	1.06	4.85	0.46	2.36	[333]
<b>NI-BT</b>	467	5.7	3.40	P3HT	0.65	0.50	0.40	0.12	[324]
<b>NI-thBTth-NI</b>	480	5.50	3.35	PTB7-Th	1.02	3.84	0.31	1.23	[343]
<b>BTz-NI-FI</b>	517	5.95	3.44	P3HT	0.94	3.52	0.46	1.53	[344]
<b>NTz-NI-FI</b>	533	6.01	3.60	P3HT	0.90	5.18	0.60	2.81	[344]
<b>TPA-TCNE-NI</b>	451	5.56	3.92	PDTSi-FTz	0.98	8.02	0.40	3.14	[345]
<b>TPA-TCNP-NI</b>	722	5.44	3.98	PDTSi-FTz	0.92	11.26	0.59	6.11	[345]
<b>Cor-NI</b>		6.28	3.24	P3HT	0.82	2.75	0.46	1.03	[329]
<b>Cor-2NI M</b>	420	6.40	3.80	P3HT	0.62	6.91	0.49	2.09	[346]
<b>Cor-2NI P</b>	420	6.40	3.80	P3HT	0.62	6.85	0.47	2.00	[346]
<b>BNIDPA-BO</b>	380	5.80	3.60	PSEHTT	0.94	6.64	0.48	3.02	[347]
				PBDTTT-C-T	0.96	9.02	0.35	3.00	[347]
				PTB7	0.98	8.13	0.39	3.08	[347]
<b>BNIDPA-DT</b>	380	5.80	3.60	PSEHTT	0.95	2.67	0.50	1.26	[347]
				PBDTT-FTTE	0.90	5.20	0.36	1.71	[347]
				PTB7	0.95	4.12	0.36	1.42	[347]
<b>BNIDPA-Th</b>	550	5.29	3.70	PSEHTT	0.79	5.14	0.44	0.44	[348]
<b>DBFI-Th</b>	600	5.80	3.80	PSEHTT	0.82	9.02	0.57	4.24	[349]
<b>DBFI-DMT</b>	498	5.82	3.66	PSEHTT	0.92	12.56	0.55	6.40	[350]
<b>DBFI-Th</b>	583	5.74	3.70	PSEHTT	0.82	5.61	0.57	2.60	[350]
<b>DBFI-MTT</b>	546	5.76	3.67	PSEHTT	0.94	8.33	0.57	3.94	[350]
<b>DBFI-EDOT</b>	615	5.76	3.65	PSEHTT	0.93	13.82	0.63	8.10	[351]
				PTB7-Th	0.95	13.99	0.51	6.70	[351]
<b>AF11-NI</b>	502	6.03	3.55	P3HT	0.71	2.65	0.55	1.03	[352]
<b>AF12-NI</b>	501	6.03	3.55	P3HT	0.81	3.40	0.60	1.64	[352]
<b>AF13-NI</b>	504	5.99	3.52	P3HT	0.96	5.21	0.47	2.37	[352]
<b>AQI-T2-NI</b>	481	5.55	3.64	PTB7-Th	0.86	2.04	43.9	0.77	[353]
<b>B-TPI HD</b>	433	5.81	3.61	P3HT	0.58	4.87	0.57	1.60	[354]
				P3HT	0.61	4.30	0.55	1.45	[355]
				P-DTSi-BT	0.73	5.70	0.32	1.32	[355]
				PBDTTPD-O	1.05	4.60	0.30	1.47	[355]
				PCDTBT	0.93	2.90	0.28	0.75	[355]
<b>BiNDI</b>	380	6.74	4.35	PTB7	0.75	5.28	0.59	2.31	[356]
<b>Si-BINDI</b>	552	5.92	3.96	P3HT	0.64	3.40	0.53	1.16	[357]
<b>NDICN-T</b>	658	5.39	3.98	DTS(FBTTh <sub>2</sub> ) <sub>2</sub>	0.73	5.24	0.47	1.81	[358]
<b>NDICN-BT</b>	686	5.26	3.92	DTS(FBTTh <sub>2</sub> ) <sub>2</sub>	1.00	0.43	0.30	0.13	[358]
<b>NDICN-TVT</b>	667	5.27	3.89	DTS(FBTTh <sub>2</sub> ) <sub>2</sub>	0.75	7.10	0.56	3.01	[358]
<b>BNDI-T-EG</b>	500	5.88	3.80	PBDTTT-C-T	0.96	2.70	0.51	1.31	[359]
<b>NDI-T-EG</b>	598			PTB7	0.93	1.10	0.45	0.46	[359]
				DTS(FBTTh <sub>2</sub> ) <sub>2</sub>	0.92	0.84	0.40	0.32	[359]
				DPP-BDT-DPP	0.82	1.47	0.37	0.45	[359]
<b>NDI-2T</b>	570	5.80	4.12	P3HT	0.71	0.81	0.34	0.17	[360]
<b>NDI-3T</b>	607	5.60	4.14	P3HT	0.64	0.45	0.33	0.09	[360]
<b>NDI-3TH</b>	632	5.50	4.10	P3HT	0.82	3.43	0.53	1.45	[360]
<b>NI-Rh2</b>	417	5.76	3.97	P3HT	0.87	8.87	0.60	4.62	[361]
<b>NI-In2</b>	404	5.54	3.67	P3HT	0.91	6.69	0.58	3.52	[361]
<b>NI-TDCN</b>	340	5.73	3.46	P3HT	1.02	2.15	0.36	0.79	[362]
<b>NI-TCNNO2</b>	387	5.92	3.89	P3HT	0.87	6.77	0.38	2.24	[362]
<b>NI-TPI2</b>	364	5.92	3.82	P3HT	0.49	0.29	0.06	0.39	[359]
<b>NDI-N1</b>	420	5.95	3.69	P3HT	0.84	6.13	0.56	2.91	[363]
<b>NDI-N2</b>	470	5.86	4.10	P3HT	0.81	8.58	0.58	4.04	[363]
<b>RF1</b>	630	5.69	3.71	P3HT	0.97	1.40	0.35	0.48	[364]
<b>RF2</b>	630	5.71	3.71	P3HT	0.77	0.45	0.30	0.10	[364]
<b>RF3</b>	630	5.67	3.67	P3HT	0.84	0.06	0.23	0.01	[364]
<b>RF4</b>	630	5.69	3.67	P3HT	0.93	0.81	0.31	0.24	[364]
<b>RF5</b>	630	5.69	3.72	P3HT	1.40	0.92	0.34	0.43	[364]
<b>RF6</b>	630	5.72	3.74	P3HT	0.72	0.67	0.35	0.17	[364]

chains conjugated by acetylene unit, showed more planar, and crystalline structure that facilitates better electron transport, in addition to high  $V_{OC}$  due to higher LUMO values. As a result, the device with a blend film of PCDTBT-C12:**NI-A-C6** exhibited a PCE up to 4.05% and high  $V_{OC}$  of 1.06 V [334]. It indicates that high crystalline blend morphology greatly improves the device parameters ( $V_{OC}$  and  $J_{SC}$ ).

Later, the same group reported **NI-AA-NI** which contains two acetylene units and exhibited comparable PCE with congener NFA (**NI-A-C6**) [335]. To further red shift the absorption, they made a series of NI-based molecules comprising central benzene and thiophene bridges flanked with NI terminal units. Polymer solar cells based on blend film of PCDTBT-C12:**NI-TP1T-NI** exhibited a PCE of 2.78% because alkyl chain on central benzene core facilitate suitable film morphology and then higher electron mobility than other alkyl chains [338]. Park et al. reported new acceptors (**NIDCS**, **NIDCS-MO** and **NIDCS-HO**) based on dicyanodistyrylbenzene, thiophene units and NI terminal acceptors. The substitution of alkoxy chain in the molecular backbone (benzene) red-shifted the absorption maxima and optimized blend film morphology. As a result, the device based on a blend film of P3HT:**NIDCS** exhibited a PCE of 2.71% and  $J_{SC}$  of 8.04 mA cm $^{-2}$ ,  $V_{OC}$  of 0.73 V, and FF of 0.46 due to balanced aggregation and optimal nano-morphology [339]. However, the devices based on blend films of DTS(FBTTh2):**NIDCS-MO** and PPDT2FBT:**NIDCS-HO** exhibited improved PCE of 5.30% and 7.64%, respectively, which was ascribed to better complimentary absorption, nanoscale phase separation of the blend film [340,341].

In addition, fused thiophene linkers such as thienothiophene and IDT hybridized with NI units resulting in new acceptors **DNIT-TT2T** and **IDT-NI**, respectively, showed red-shifted absorption due to electron-rich linker allowing strong intramolecular donor-acceptor interactions. The corresponding blend film based on P3HT:**IDT-NI** led a device to exhibit a PCE of 2.36% [333,342]. On the other hand, Aso et al. made acceptors (**BTz-NI-FI** and **NTz-NI-FI**) by incorporating BT or naphthobisthiadiazole units with NI units, respectively. **NTz-NI-FI** showed red-shifted absorption and increased crystallinity in the blend film (P3HT:**NTz-NI-FI**), resulting in a better PCE (2.81%) as compared to **BTz-NI-FI** [344]. Mishra et al. reported NI-based acceptors **TPA-TCNE-NI** and **TPA-TCNP-NI** configured with NI and tetracyanobutadiene/dicyanoquino-dimethane units, respectively. These acceptors showed strong NIR absorption and high LUMO level,  $J_{SC}$  (11.26 mA cm $^{-2}$ ),  $V_{OC}$  (0.92 V) and then a good PCE of 6.11% was achieved for the corresponding blend film based on PDTSi-FTz donor [345]. Later, a series of NI-based acceptors containing helicene units was reported with higher LUMO level, which is useful for obtaining high  $V_{OC}$  with their blend films with P3HT donor [346]. Jeneckhe et al. made new acceptors based on a fused NI derivative such as bis(naphthalene imide)-3,6-diphenyl-trans-antrazoline unit, which displays higher LUMO level favorable to have high  $V_{OC}$  for the blend film. The nature of the attached alkyl chains on fused NI unit greatly influenced the morphology, charge transport and photovoltaic properties. Judicious selection of donor PTB7 for the acceptor **BNIIDPA-BO** with optimized alkyl unit to make OSC device gave a PCE of 3.08% [347]. Later, they used ladder-type tetraazabenzodifluoranthene diimide units to facilitate desirable solid-state molecular packing, and introduced various aromatics (phenyl, thiophene and thienothiophene) as central and/or terminal units to synthesize several NFAs [349,350]. Among them, **DBFI-EDOT** containing ethylenedioxothiophene as central linker showed the highest PCE up to 8.10%, which is attributed to its broad spectral response and rational twisting of the molecule with optimum molecular packing as blended with donor PSEHTT [351]. Fused decacyclene triimide (**B-TPI HD**) acceptor showed a strong electron-accepting capability and is prone to self-assembly in a

solid state, leading to nano-sized crystalline columns or fibers [355]. The device with the blend film of PBDTTPD-O:**B-TPI HD** exhibited a PCE of 1.47% due to the better matching of absorption and energy levels of donor and acceptors of blend film.

Russell et al. synthesized **BiNDI** by linking two NDI monomers via a vinyl conjugation. The device employing **BiNDI**:PTB7 blend exhibited a PCE of 2.31% due to the formation of a nano-fibrillar crystal in active blend which increased the charge-transporting properties [356]. Later, several  $\pi$ -conjugation linkers were incorporated such as thiophene, thienothiophene, vinyl-thiophene, dibenzosilole and DBT flanked with two NDI units, resulting in different degrees of red-shifted absorption depending on the nature of electron rich central linker [357–359]. However, the device based on P3HT:**Si-BiNDI** blend achieved a PCE of 1.16% due to the formation of a good nanoscale interpenetrating networks in blend films, which is beneficial for charge separation [357]. NDI, flanked with oligothiophenes terminal units, showed red-shifted absorption as compared to those of other previously reported NDI-based NFAs [360]. Blend film P3HT:**NDI-3TH** showed a PCE 1.45% due to slipped “face-on”  $\pi$ -stacking that enabled facile self-assembly and nanophase separation of blend film. Later, a series of NFAs incorporating various terminal acceptor units were reported. Among them, the device using P3HT:**NI-Rh2** blend exhibited a superior PCE of 4.62% due to broad spectral response and excellent electron mobility of blend film [361]. Furthermore, NDI was used as a central linker and connected with thiophene via with alkyl/phenyl units, resulting in dyes (**RF1-RF6**) that exhibited strong absorption profiles, but poor device PCEs were obtained due to low charge carrier mobility of blend film [364]. In short, NFAs based on NI as terminal units and fused-NI building blocks typically give higher  $V_{OC}$  and PCE due to its higher LUMO energy levels. In this class, the champion NFA **DBFI-EDOT** achieved the highest PCE of 8.10% when blended with the P3HT donor.

### 3.3.3. Perylene diimide-based small molecular acceptors

The variable positions (bay, *ortho* and imide) available for further functionalizations allowed making several varieties of PDI-based NFAs. After Tang introduced PDI derivative in 1986 as an NFA, several molecular PDI derivatives were developed and achieved OSCs with a high PCE up to 9.3%. Initially, research focused on imide functionalization followed by functionalized bay position to manipulate the crystallite size. Currently, twisted geometrical designs giving 3D structures were used to balance the aggregation and  $\pi$ - $\pi$  molecular interactions of PDI-based molecular acceptors. The number of PDI units and linkage/geometry played a crucial role in aggregation and crystalline formation in the solid state. In this context, for better understanding of the aggregation and crystalline effects, we discussed PDI NFAs depending on the number of PDI units, i.e. monomers, dimers, trimers and tetramers.

PDI has been extensively studied with various functional units at bay, *ortho* and imide positions. Simply introduce various alkyl chains on both imide position of PDI can optimize the  $\pi$ - $\pi$  molecular interactions and aggregation in the solid state. These PDI derivatives work well as NFAs in combination with low bandgap polymer donor to match complimentary absorption. The structures of monomeric PDI NFAs were displayed in Fig. 24 and their optical and device parameters were compiled in Table 14. Laquai et al. successfully used N-alkylated PDIs (**PDI-C2** and **PDI-C7**) as NFA blended with P3HT donor to give a OSC with a limited PCE (0.25%). They found that the nature of alkyl chain greatly influences the molecular packing and blend morphology [365]. Later, a judicious selection of the well-matched absorbing donors DTS(FBTTh2)2 and PBDTTT-CT enhanced spectral response and then PCE was enhanced up to 3.00% and 3.71%, respectively, mainly due to better complimentary donor and acceptor absorption in blend film [366,367]. Later, Wang et al. functionalized bay positions of PDI

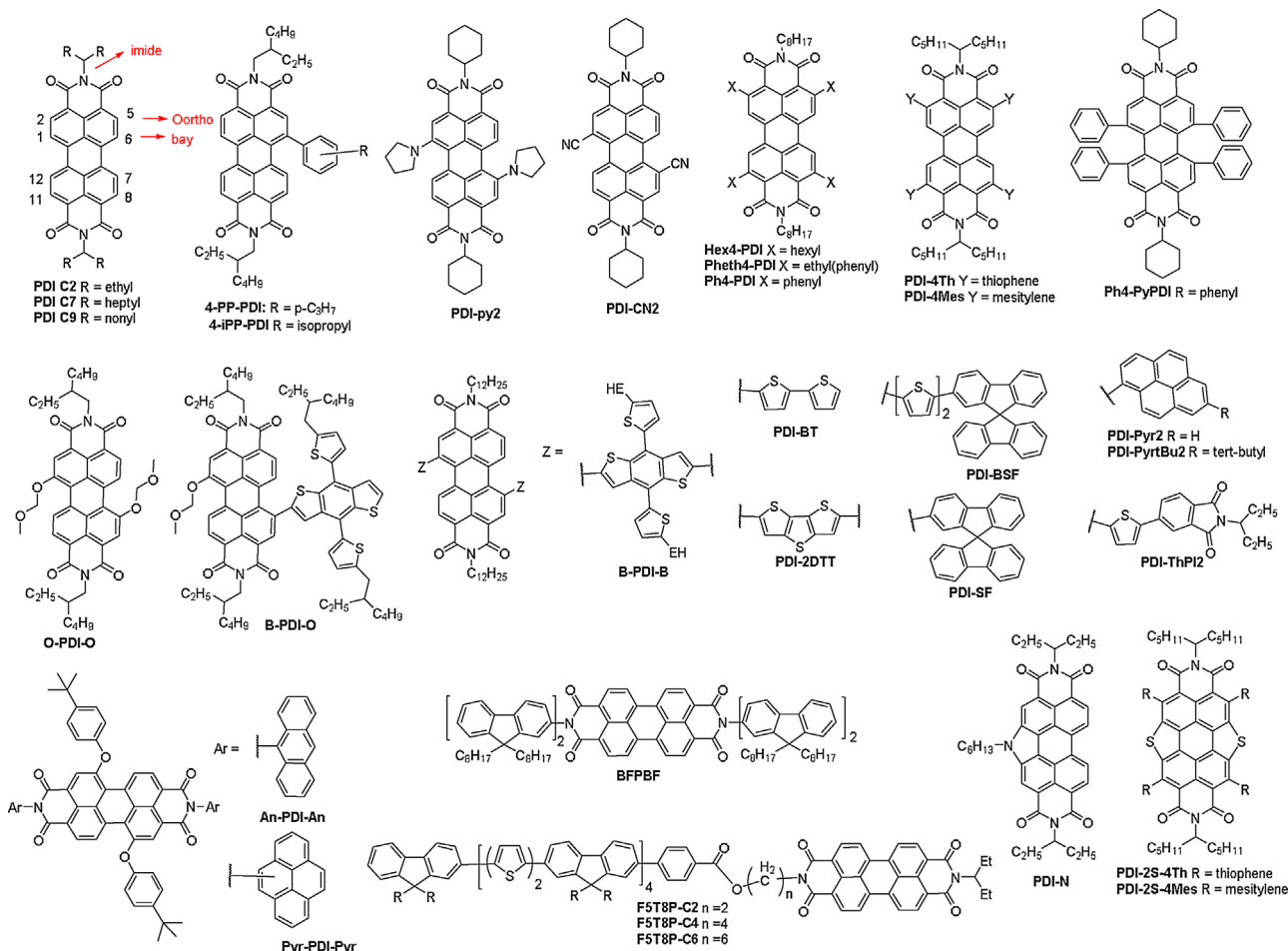


**Fig. 24.** Chemical structures of perylenediimide (PDI) monomer based SM NFAs [365–382].

**Table 14**

**Table 11**  
Photo-physical and photovoltaic properties of perylene diimide based SM NFAs

NFA	$\lambda_{max}$ (nm)	HOMO (eV)	LUMO (eV)	Donor	$V_{OC}$ (mV)	$J_{SC}$ (mA Cm $^{-2}$ )	FF	PCE (%)	Refs.
<b>PDI-C2</b>	530	5.32	3.29	P3HT	0.48	1.49	0.35	0.25	[365]
				DTS(FBTTh2)2	0.78	7.40	0.52	3.00	[366]
				PBDTTT-CT	0.80	8.10	0.52	3.71	[367]
<b>4-PP-PDI</b>	536	6.10	4.07	P3HT	0.65	1.52	0.40	0.40	[368]
<b>4-Ipp-PDI</b>	535	6.09	4.09	P3HT	0.65	1.96	0.64	0.82	[369]
<b>PDI-Py2</b>	701	5.00	3.40	P3HT	0.66	0.26	0.25	0.04	[370]
<b>PDI-CN2</b>	526	6.04	4.07	P3HT	0.13	0.13	0.30	0.01	[370]
<b>Ph4-PDI</b>	527	5.79	3.78	P-3T-TI	0.96	5.53	0.52	2.77	[371]
<b>Ph4-PDI</b>	527	5.79	3.78	PTB7-Th	0.87	5.34	0.52	2.42	[371]
<b>Hex4-PDI</b>	541	5.90	3.83	PBT13T	1.08	1.51	0.39	0.65	[372]
<b>Pheth4-PDI</b>	542	5.92	3.91	PBT13T	1.02	2.44	0.48	1.20	[372]
<b>Ph4-PDI</b>	577	6.02	4.01	PBT13T	1.02	6.56	0.55	3.67	[372]
<b>PDI-4Mes</b>	521	5.91	3.63	PTB7-Th	0.97	6.17	0.43	2.55	[373]
<b>PDI-4Th</b>	533	5.94	3.76	PTB7-Th	0.85	7.38	0.47	2.97	[373]
<b>Ph4-PyPDI</b>	603	5.69	3.82	PTB7-Th	0.87	10.10	0.46	4.10	[374]
<b>O-PDI-O</b>	566	5.93	3.78	P3HT	0.57	1.60	0.39	0.35	[374]
<b>B-PDI-O</b>	558	5.68	3.81	P3HT	0.61	3.50	0.58	1.25	[375]
<b>B-PDI-B</b>	554	5.57	3.95	P3HT	0.44	0.02	0.53	0.01	[376]
<b>PDI-SF</b>	570	5.63	3.70	P3HT	0.77	3.61	0.57	1.58	[376]
<b>PDI-BSF</b>	630	5.38	3.81	P3HT	0.71	3.11	0.53	1.18	[376]
<b>PDI-BT</b>	595	5.64	3.94	P3HT	0.52	3.05	0.51	0.81	[376]
<b>PDI-Pyr2</b>	491	5.62	3.77	PBDTTT-C-T	0.88	2.89	0.34	0.88	[377]
<b>PDI-PyrtBu2</b>	495	5.62	3.77	PBDTTT-C-T	0.89	1.54	0.33	0.45	[377]
<b>PDI-Pyr2</b>	491	5.62	3.77	PTB7	0.89	3.87	0.39	1.35	[377]
<b>PDI-PyrtBu2</b>	495	5.62	3.77	PTB7	0.90	1.36	0.33	0.41	[377]
<b>PDI-2DTT</b>	610	5.80	3.90	PBDTTT-C-T	0.76	1.04	0.33	0.28	[378]
<b>PDI-2DTT</b>	610	5.80	3.90	DTS(FBTTh2)2	0.76	7.21	0.42	2.52	[378]
<b>Pyr-PDI-Pyr</b>	476	5.90	3.80	BTD-TNP	0.95	6.30	0.53	3.17	[379]
<b>An-PDI-An</b>	525	6.00	3.85	BTD-TNP	0.92	6.60	0.47	2.85	[380]

**Table 14** (Continued)

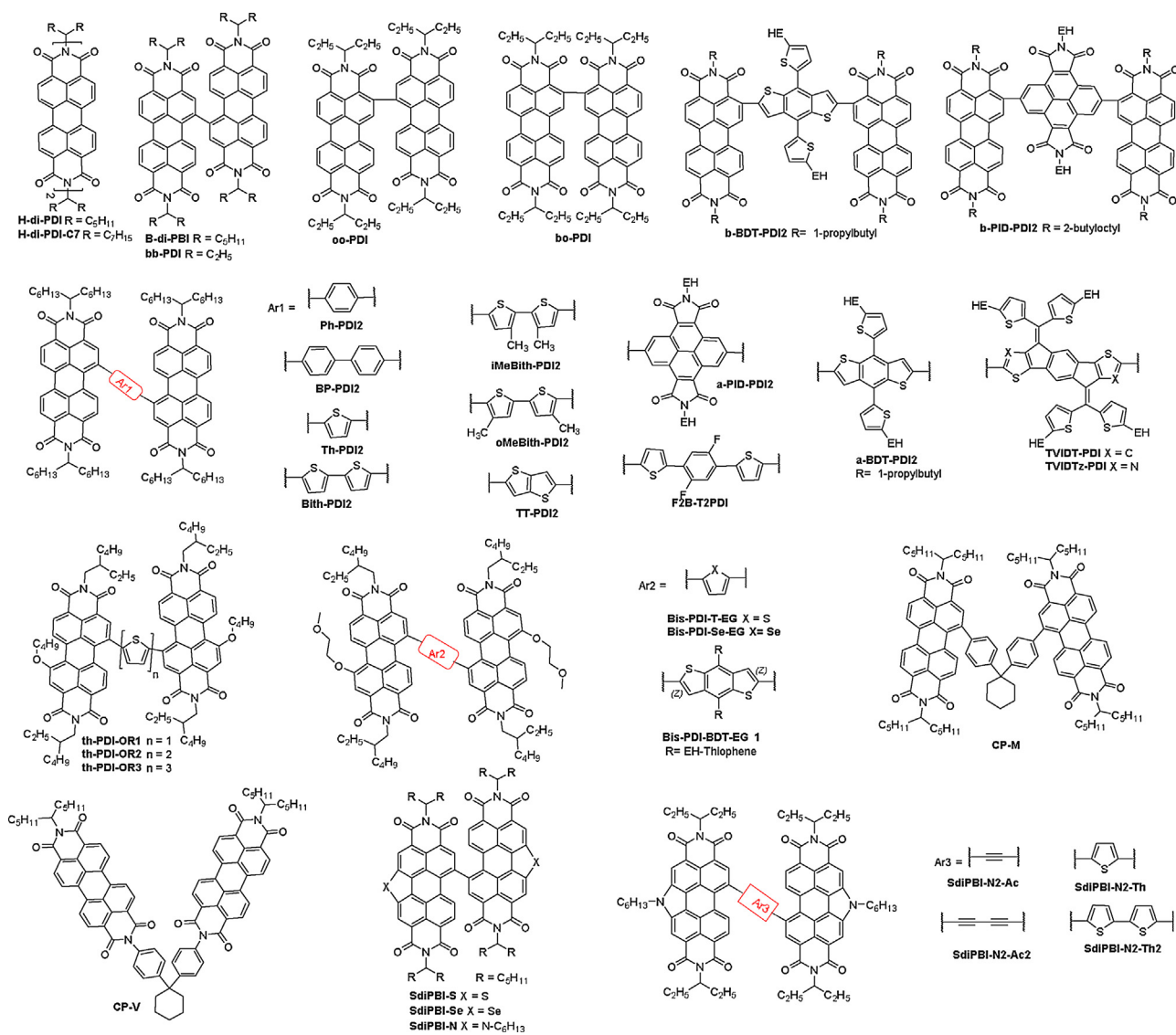
NFA	$\lambda_{\text{max}}$ (nm)	HOMO (eV)	LUMO (eV)	Donor	$V_{\text{OC}}$ (mV)	$J_{\text{SC}}$ (mA Cm $^{-2}$ )	FF	PCE (%)	Refs.
<b>F5T8P-C2</b>	526	5.27	3.86	PEDOT	1.00	4.30	0.43	1.86	[381]
<b>F5T8P-C4</b>	525	5.28	3.89	PEDOT	1.04	4.82	0.47	2.33	[381]
<b>F5T8P-C6</b>	525	5.29	3.87	PEDOT	0.96	4.60	0.46	2.04	[381]
<b>PDI-N</b>	525	5.70	3.50	PTB7	1.00	5.18	0.35	1.81	[382]
<b>PDI-2S-4Mes</b>	485	6.08	3.62	PTB7-Th	1.04	3.37	0.37	1.30	[373]
<b>PDI-2S-4th</b>	525	5.90	3.70	PTB7-Th	0.88	11.71	0.49	5.07	[373]
<b>H-di-PDI-C7</b>	540	5.90	4.10	PBDTTT-C-T	0.76	9.50	0.46	2.78	[383]
<b>H-di-PDI-C7</b>	540	6.02	4.06	PBDTTT-CT	0.77	9.00	0.46	3.20	[384]
<b>H-di-PDI</b>	581	5.81	3.75	D1	0.85	5.62	0.48	2.27	[371]
				D2	0.71	9.36	0.51	3.37	[371]
				PTB7	0.79	3.66	0.51	1.69	[385]
				PTB7-Th	0.79	13.12	0.60	6.41	[385]
<b>B-di-PBI</b>	534	5.87	3.76	PTB7	0.78	10.51	0.58	5.00	[385]
				PTB7-Th	0.79	12.86	0.54	5.56	[385]
				PTB7-Th	0.76	10.22	0.51	4.21	[386]
				PBDTPD	1.04	6.80	0.47	3.37	[387]
				PTB7-Th	0.77	11.50	0.50	4.48	[387]
				P-DTSi-BT	0.68	6.40	0.38	1.67	[387]
				PBDT-TS1	0.78	13.14	0.51	5.09	[388]
				PBDTS-TTffBT	0.92	10.89	0.65	6.51	[389]
				PCLDPP	0.92	6.10	0.42	2.40	[390]
<b>bo-2PDI</b>	529	6.23	4.02	PTB7-Th	0.67	7.63	0.39	2.01	[391]
<b>oo-2PDI</b>	529	6.15	3.90	PTB7-Th	0.80	18.79	0.55	8.30	[391]
<b>Ph-PDI2</b>		5.81	3.74	P3HT	0.54	4.24	0.55	1.27	[185]
<b>BP-PDI2</b>		5.81	3.72	PTB7-Th	0.39	8.60	3.13	2.42	[392]
<b>Th-PDI2</b>		5.68	3.77	P3HT	0.46	4.18	0.46	0.95	[185]
<b>Th-PDI2</b>				DTS(FBTTh2) <sub>2</sub>	0.66	7.54	0.74	3.70	[393]
<b>Bith-PDI2</b>		5.54	3.75	P3HT	0.52	5.20	0.58	1.56	[185]
<b>iMeBith-PDI2</b>	497	5.82	3.57	PffBT4T-2DT	0.91	8.00	0.56	4.10	[394]
<b>oMeBith-PDI2</b>	497	5.64	3.54	PffBT4T-2DT	0.89	6.80	0.51	3.10	[394]
<b>An-PDI2</b>	562	5.82	3.49	PTB7-Th	0.83	10.88	0.60	5.42	[395]
<b>TT-PDI2</b>	535	6.16	4.14	PBDTT-FITTE	0.87	5.55	0.42	2.02	[396]
<b>F2B-T2PDI</b>	489	5.94	4.17	PTB7-Th	0.84	10.60	0.57	5.05	[397]
<b>Bith-PDI2</b>	492	5.80	4.11	PTB7-Th	0.82	8.95	0.49	3.63	[397]
<b>a-PID-PDI2</b>	495	5.86	3.84	PTB7-Th	0.77	10.15	0.44	3.61	[398]
<b>b-PID-PDI2</b>	495	5.87	3.79	PTB7-Th	0.78	9.14	0.45	3.47	[398]
<b>a-BDT-PDI2</b>	495	5.60	3.78	PTB7-Th	0.81	12.74	0.46	4.92	[398]
<b>b-BDT-PDI2</b>	495	5.64	3.76	PTB7-Th	0.81	9.80	0.44	3.53	[398]
<b>TVIDTPDI</b>	521	5.48	3.85	PBDB-T	0.76	6.88	0.40	2.09	[399]
<b>TVIDTzPDI</b>	519	5.50	3.86	PTB7-Th	0.76	5.95	0.35	1.58	[399]
<b>th-PDI-OR1</b>	558	5.65	3.84	PBDTTT-C-T	0.78	9.99	0.53	4.22	[400]
<b>th-PDI-OR1</b>	552	5.66	3.72	PBDTTT-C-T	0.89	7.78	0.52	3.61	[401]
<b>th-PDI-OR2</b>	570	5.63	3.76	PBDTTT-C-T	0.83	3.05	0.31	0.77	[401]
<b>th-PDI-OR3</b>	568	5.61	3.75	PBDTTT-C-T	0.78	3.38	0.35	0.91	[401]
<b>Bis-PDI-T-EG</b>	560	5.65	3.84	PBDTTT-C-T	0.85	8.86	0.54	4.03	[402]
				PBDTTT-C-T	0.85	8.86	0.54	3.91	[403]
				BDT-O-2DPP	0.95	3.46	0.41	1.34	[403]
				DPP-BDT-DPP	0.92	4.66	0.47	2.01	[403]
				BDT-T-2T-DPP	0.83	4.60	0.43	1.62	[403]
				DPP-BDT-T	0.83	3.79	0.51	1.62	[404]
				PBDTTT-C-T	0.84	12.83	0.56	6.08	[405]
<b>bis-PDI-Se-EG</b>	562	5.61	3.84	PBDTTT-C-T	0.79	10.60	0.48	4.01	[406]
<b>BDTPDI2-EG</b>	566	5.48	3.84	P3HT	0.68	5.83	0.49	1.95	[407]
<b>CP-M</b>	536	5.92	3.85	PPDT2FBT	0.89	6.04	0.40	2.14	[408]
<b>CP-V</b>	528	6.16	3.98	PPDT2FBT	0.86	9.03	0.60	4.68	[408]
<b>SdiPBI-N</b>	525	5.37	3.57	P3TEA	1.13	11.03	0.61	7.55	[382]
				PTB7-Th	0.96	11.54	0.47	5.23	[409]
				PTB7-Th	0.97	11.30	0.43	4.80	[410]
<b>SdiPBI-S</b>	504	5.95	3.85	PDBT-T1	0.90	11.65	0.66	7.16	[411]
				PBDTS-Se	0.91	12.80	0.69	8.22	[412]
				PCLDPP	0.96	6.70	0.53	3.50	[391]
<b>SdiPBI-Se</b>	510	6.09	3.87	PDBT-T1	0.95	12.48	0.70	8.42	[413]
<b>SdiPBI-S</b>	506	6.07	3.87	DR3TBDTT	0.91	11.12	0.57	5.81	[414]
<b>SdiPBI-Se</b>	512	6.08	3.86	DR3TBDTT	0.92	11.55	0.59	6.22	[414]
<b>SdiPBI-N2-Ac</b>	676	5.84	3.80	PTB7-Th	0.97	4.33	0.29	1.22	[409]
<b>SdiPBI-N2-Ac2</b>	644	5.98	3.8	PTB7-Th	0.95	4.41	0.32	1.34	[409]
<b>SdiPBI-N2-Th</b>	534	5.69	3.47	PTB7-Th	0.99	5.53	0.36	2.00	[415]
<b>SdiPBI-N2-Th2</b>	533	5.58	3.54	PTB7-Th	1.05	6.97	0.36	2.60	[415]
<b>SdiPBI-BT</b>	508	5.86	3.79	PDT-T1	0.95	10.32	0.68	6.71	[416]
<b>diPBI-BT</b>	501	5.79	3.67	PDT-T1	0.99	9.67	0.60	5.84	[416]
<b>BDT-TDI2</b>	469	5.59	3.59	PTDBT-T1	1.02	7.55	0.54	4.52	[417]
<b>PDI-T</b>	532	5.95	4.02	PTB7-Th	0.88	9.74	0.41	3.54	[418]
<b>FPDI-F</b>	461	6.01	3.80	PTB7-Th	0.92	8.71	0.40	3.20	[418]
<b>FPDI-T</b>	469	5.98	3.77	PTB7-Th	0.93	11.95	0.58	6.48	[418]
<b>FPDI-Se</b>	471	5.96	3.76	PTB7-Th	0.92	11.19	0.55	5.59	[418]
<b>Th-PDI2</b>	500	6.17	4.12	PBDTT-FITTE	0.87	6.24	0.40	2.19	[396]
<b>Fus-Th-PDI2</b>	520	6.35	4.01	PBDTT-FITTE	0.92	7.52	0.50	3.44	[396]

**Table 14 (Continued)**

NFA	$\lambda_{\text{max}}$ (nm)	HOMO (eV)	LUMO (eV)	Donor	$V_{\text{OC}}$ (mV)	$J_{\text{SC}}$ ( $\text{mA Cm}^{-2}$ )	FF	PCE (%)	Refs.
<b>Ph-PDI2</b>	525	6.22	4.07	PBDTT-FTTE	0.91	5.50	0.41	2.19	[396]
<b>Fus-mPh-PDI2</b>	500	6.36	4.03	PBDTT-FTTE	0.93	7.68	0.54	3.89	[396]
<b>Fus-Ph-PDI2</b>	550	6.18	4.04	PBDTT-FTTE	0.89	1.51	0.29	0.23	[396]
<b>Fus-TT-PDI2</b>	535	6.20	3.99	PBDTT-FTTE	0.98	3.95	0.39	1.50	[396]
<b>Fus-mPh-PDI2</b>		6.40	4.00	D1	0.98	7.00	0.50	3.42	[371]
				D2	0.93	11.81	0.48	5.21	[371]
				PBTZF2	9.21	0.99	0.40	3.68	[419]
				PBTZF4	1.12	10.02	0.50	5.55	[419]
<b>Fus-TF-PDI2</b>	495	5.85	3.75	PBDB-T	1.10	0.42	0.29	0.13	[109]
<b>cis- Fus-TT-PDI2</b>	490	5.93	3.74	PBDB-T	1.00	11.9	0.64	7.60	[109]
<b>di-PBI</b>	532	5.93	3.83	PBDTT-C-T	0.72	8.86	0.40	2.54	[420]
<b>bay-di-PBI1</b>	530	6.08	3.84	PBDTT-C-T	0.74	5.76	0.36	1.54	[420]
<b>bay-di-PBI2</b>	680	5.93	4.16	PBDTT-C-T	0.46	5.77	0.51	1.36	[420]
<b>Helical PDI</b>	545	6.04	3.77	PTB7	0.79	11.00	0.59	5.14	[421]
				PBDTT-IT	0.80	13.50	0.55	5.94	[421]
<b>IDT-2PDI</b>	532	5.53	3.83	P3HT	0.70	5.58	0.66	2.61	[422]
<b>Fus-IDT-2PDI</b>	640	5.48	3.75	PTB7-Th	0.99	13.24	0.56	7.33	[423]
<b>H-tri-PDI</b>	537	6.01	3.93	PBDTT-TS1	0.73	16.52	0.60	7.25	[424]
<b>bbb-3PDI</b>	529		3.99	PTB7-Th	0.76	18.13	0.51	7.12	[425, 426]
<b>obo-3PDI</b>	530		4.08	PTB7-Th	0.75	12.61	0.48	4.55	[425, 426]
<b>TPAPPDI</b>	409	5.47	3.59	PBT1-EH	1.21	6.75	0.61	5.10	[427]
<b>B(PDI)3</b>	540	6.00	3.86	PTB7-Th	0.83	13.12	0.52	5.65	[428]
<b>Tz-PDI3</b>	530	6.03	3.81	PTB7-Th	0.78	17.10	0.68	9.15	[429]
<b>TRIP-3PDI-C6</b>	543	5.97	3.81	PBDT-TS1	0.96	10.26	0.46	4.53	[430]
<b>TRIP-3PDI-C8</b>	540	6.06	3.97	PTB7-Th	0.86	9.54	0.39	3.16	[431]
<b>TPA-PDI3</b>	536	5.40	3.70	PBDTT-C-T	0.87	11.27	0.33	3.22	[432]
<b>TPA-ThPDI3</b>	550	5.60	3.80	PBDTT-C-T	0.90	5.36	0.39	1.92	[433]
<b>TPA-PDI3</b>	520	5.72	3.88	PTDBT-T1	0.94	9.80	0.47	4.30	[434]
<b>TPA-PDI3-S</b>	497	5.73	3.79	PTDBT-T1	1.00	9.42	0.59	5.56	[434]
<b>TPA-PDI3-Se</b>	501	5.74	3.80	PTDBT-T1	1.00	10.24	0.58	5.96	[434]
<b>TPH-C5</b>	516	6.34	3.80	DRCN5T	1.04	11.59	0.51	6.16	[435]
<b>TPH-C4</b>	516	5.88	3.84	PDBT-T1	0.96	12.22	0.68	7.97	[436]
<b>TPH-C5</b>	516	5.86	3.82	PDBT-T1	0.96	12.17	0.68	8.02	[436]
<b>TPH-C6</b>	516	5.85	3.80	PDBT-T1	0.97	12.20	0.67	7.94	[436]
<b>TPH-C7</b>	516	5.88	3.82	PDBT-T1	0.98	12.58	0.69	8.54	[436]
<b>TPH-C5</b>	516	6.02	3.83	PDBT-T1	0.97	12.01	0.70	8.28	[437]
<b>TPH-C5-Se</b>	528	5.97	3.80	PDBT-T1	1.00	12.53	0.72	9.28	[437]
<b>BTT-3PDI</b>	502	5.80	3.92	PTB7-Th	0.85	6.13	0.38	2.19	[438]
<b>Fus-BTT-3PDI</b>	515	5.95	3.73	PTB7-Th	0.91	12.39	0.55	6.19	[438]
<b>TPC-PDI4</b>	530	6.00	3.75	PffBT4T-2DT	0.96	9.20	0.49	4.30	[439]
<b>TPSi-PDI4</b>	530	6.01	3.75	PffBT4T-2DT	0.94	8.50	0.53	4.20	[439]
<b>TPGe-PDI4</b>	530	5.94	3.68	PffBT4T-2DT	0.92	5.00	0.37	1.60	[439]
<b>TPSi-PDI4-HO</b>	539	5.97	4.00	PTB7	0.86	8.25	0.48	3.54	[440]
<b>TPC-PDI 4</b>	540	6.00	3.75	PffBT-ffBT	1.04	8.70	0.51	4.60	[441]
<b>Me-PDI4</b>	580	5.96	3.82	PBDTT-CT	0.77	7.83	0.45	2.73	[442]
<b>tetra-PBI-S</b>	504	6.02	3.68	PBDT-TS1	0.94	13.02	0.50	6.17	[443]
<b>BP-N-PDI4</b>	530	5.82	3.73	PTB7	0.65	0.74	0.27	0.13	[192]
<b>BP-PDI4</b>	524	5.84	3.77	PBDB-T	0.90	13.60	0.60	7.30	[444]
<b>TPE-PDI4</b>	535	5.77	3.72	PTB7-Th	0.91	11.70	0.52	5.44	[392]
				PffBT-ffBT	1.03	10.60	0.54	5.90	[441]
<b>TPPz-PDI4</b>	500	5.86	3.76	PffBT-ffBT	0.99	12.50	0.56	6.90	[441]
<b>P4N4</b>	538	5.97	3.69	PDBT-T1	0.96	9.40	0.63	5.71	[444]
<b>6T-PDI4</b>	500	5.73	4.18	PTB7-Th	0.81	8.97	0.47	3.41	[445]
<b>SCPDT-PDI4</b>	497	5.45	3.80	PTB7-Th	0.84	14.60	0.58	7.11	[446]
<b>Pyr-N-PDI4</b>		5.85	3.78	PTB7	0.72	7.65	0.37	2.02	[192]
<b>DBT-PDI4</b>	530	5.71	3.89	PTB7-Th	0.79	18.30	0.58	8.47	[448]
				PTB7-Th	0.82	11.90	0.57	5.85	[449]
<b>BPTS</b>	503	6.08	3.79	PDBT-T1	1.02	11.94	0.68	8.28	[450]
<b>fus-DBT-PDI4</b>	502	6.21	3.75	PTB7-Th	0.92	14.70	0.56	7.56	[449]
<b>hPDI3</b>				PTB7	0.77	13.20	0.63	6.40	[451]
				PTB7-Th	0.81	14.50	0.67	7.90	[451]
<b>hPDI4</b>				PTB7	0.79	12.90	0.64	6.50	[451]
				PTB7-Th	0.80	15.20	0.68	8.30	[451]
<b>Pyr-(hPDI2)2</b>	604	5.80	3.56	PTB7-Th	0.83	14.30	0.58	6.90	[452]
<b>Pyr-(hPDI2)3</b>	619	5.76	3.76	PTB7-Th	0.80	15.10	0.63	7.60	[452]
<b>FTTB-PDI4</b>	400	5.74	3.58	P3TEA	1.13	13.89	0.66	10.58	[453]
<b>SNTP</b>	555	6.13	3.95	PTB7-Th	0.77	15.22	0.60	7.17	[454]
<b>TPEPPDI</b>	409	5.46	3.50	PBT1-EH	1.24	4.52	0.38	2.24	[427]

core with alkylated phenyl units to control the aggregation of the corresponding film [370]. Many efforts have been made to disrupt the aggregation of PDI by introducing various alkyl and aryl units at *ortho*-positions, which results in a slip-stacking in the solid film and prevents excimer formation [371–373]. The device with

PBT13T:**Ph4-PDI** blend film exhibited a PCE of 3.67% due to the combined effect of effective suppression of aggregation and better absorption [372]. PDI (**Ph4-PyPDI**) with bay substitution can effectively suppress aggregation, raise LUMO, and broaden absorption spectra. As a result, the device based on blend film



**PTB7-Th:Ph4-PDI** exhibited a better PCE of 4.10% with high  $J_{SC}$  of  $10.10 \text{ mA cm}^{-2}$  [374]. The incorporation of BDT at bay positions of PDI increased absorption profile and twisted the molecular geometry for reducing aggregation [375].

A series of bay- aryl-substituted PDI-based acceptors were reported to fine-tune the absorption, electrochemical and aggregation properties. Among them, PDI with electron-rich thiophene fused  $\pi$ -aromatics gave red-shifted absorption, while the device based on **PDI-2DTT** exhibited a PCE of 2.52% when blended with DTS(FBTTh2)2 donor [378]. The spirobifluorene-substituted PDI (**PDI-SF**) balanced the charge carrier mobility, while pyrene-substituted PDI (**PDI-Pyr2**) led to favorable  $\pi$ - $\pi$  molecular interactions and blend morphology [376,377]. PDIs with aryl substitution at imide position can also suppress aggregation, restrains the geminate charge recombination, and improves the charge generation efficiency [380,381]. The device employing blend film of BTD-TNP:**Pyr-PDI-Pyr** exhibited a PCE of 3.17% due to favorable charge extraction [379]. Very interestingly, hetero-annulated PDIs showed strong donating strength and N-alkylation offered better solubility and prevented aggregation. As a result, polymer solar cell based on PTB7-Th:**PDI-2S-4th** blend exhibited a high PCE of 5.07% with high  $J_{SC}$  of  $11.71 \text{ mA cm}^{-2}$  because tetra-

substitution of S-annulated PDI effectively suppressed aggregation and increased spectral response.

In PDI dimers, two PDI units are combined together through bay, *ortho* or imide positions or through  $\pi$ -aromatics. As a result, PDI dimers typically showed red-shifted absorption, and suppressed aggregation, but the retaining  $\pi$ - $\pi$  molecular interactions leads to optimized crystallinity and film morphology. The structures of PDI-based dimers are depicted in Figs. 25 and 26, and their optical and device data are compiled in Table 14. Jen et al. made PDI dimers **B-di-PDI** and **H-di-PDI** via bay or imide connection, respectively. **B-di-PDI** and **H-di-PDI** possess twisted and pseudo-2D geometry with a twisting angle of  $70^\circ$  and  $90^\circ$ , respectively [385]. As compared to PDI-monomers, both dimers showed intense and broad absorption. When they blended with PTB7-Th, twisted **B-di-PDI** strongly disrupts the  $\pi$ - $\pi$  stacking, while rigid **H-di-PDI** maintains appropriate aggregation with donor PTB7-Th, which produces efficient exciton dissociation and suitable percolation pathways for charge transport. As a result, **H-di-PDI**-based blend film gave the device a higher PCE of 6.41% as compared with **B-di-PDI** (5.56%). Later, several donors were used to blend with **B-di-PDI** to enhance the PCE of OSCs device [386–390]. Among them, polymer donor PBDTTS-TTffBT achieved best

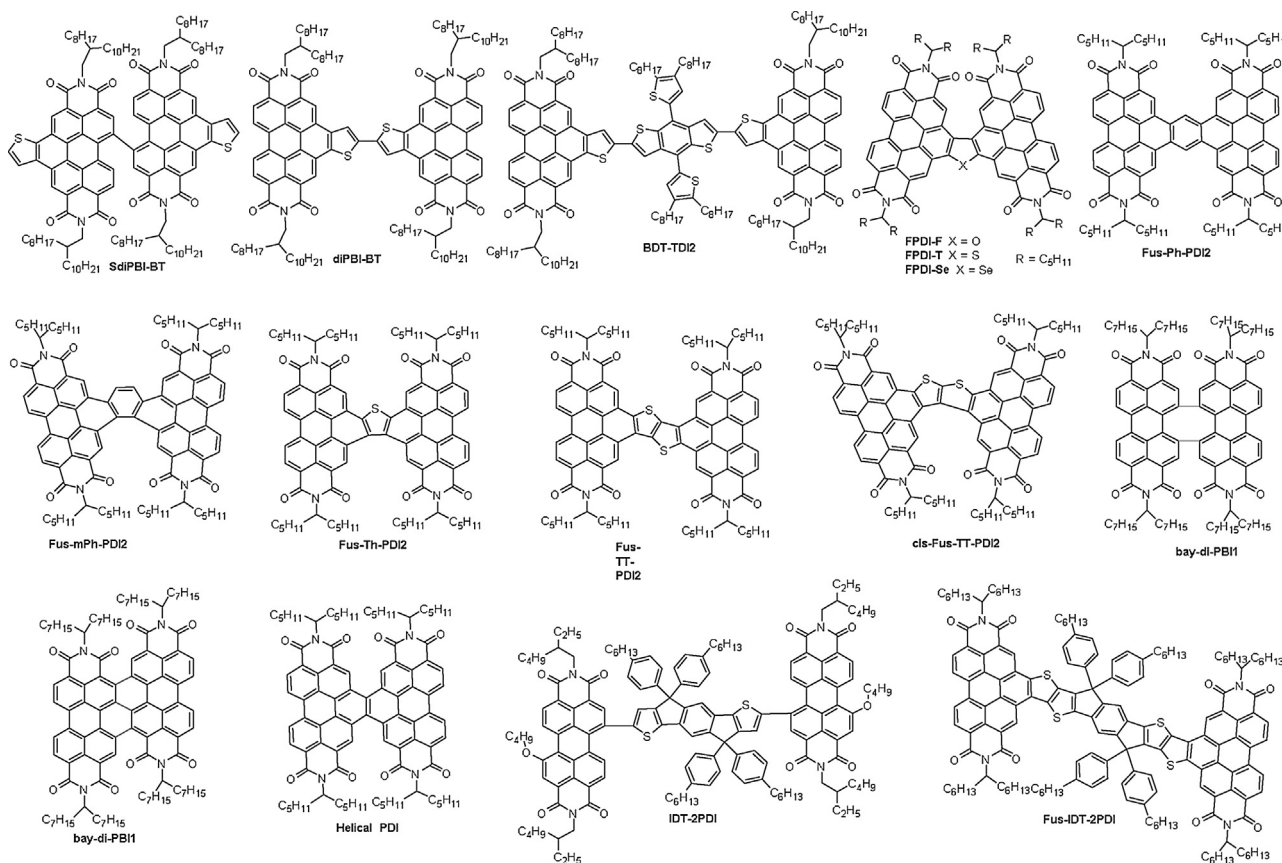


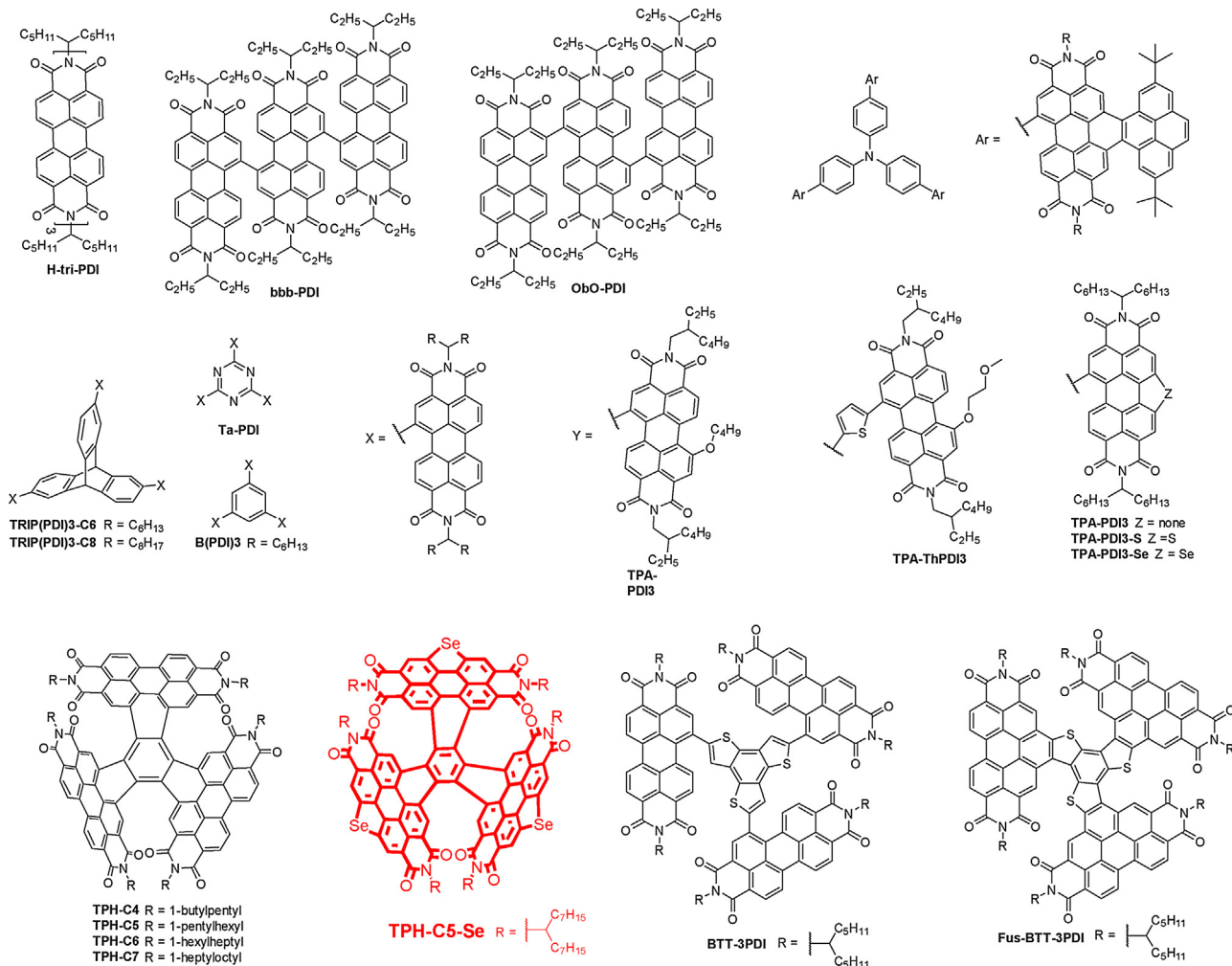
Fig. 26. Chemical structures of perylenediimide dimer based SM NFAs [416–423].

PCE of 6.51% due to better complimentary absorption and morphological blend stability [389]. However, the isomeric linkage of PDI dimer (**oo-2PDI**) achieved a better PCE (8.30%) in blend with PTB7-Th donor due to its planar geometry which can greatly optimize blend morphology and then charge carrier properties [391]. PDI dimer excellently disrupts the intermolecular stacking in thin film, but strong absorption is also a very important factor for better light-harvesting. The incorporation of aromatics between two PDI units extends the  $\pi$ -conjugation for giving longer absorption maxima. PDI unit's conjugated with (1) oligothiophene give increased absorption and then high  $J_{SC}$ . For example, the device with P3HT:**iMeBith-PDI2** blend showed a high PCE of 4.10% [185,394]; (2) anthracene unit broaden the absorption spectra and slightly suppress the aggregation of blend film PTB7-Th:**An-PDI2**, resulting in a PCE of 5.42% [395]; (3) BDT at bay or *ortho*-position of PDI, *ortho*-substituted **a-BDT-PDI2** showed red-shifted absorption with balanced planarity and aggregation produces efficient charge exciton dissociation and then a PCE of 4.91% as blended with donor PTB7-Th [398].

Alkoxy or methoxyethoxy PDI dimers containing oligothiophenes linkers showed longer absorption and significantly reduced aggregation and optimized morphology to improve the photovoltaic parameters [400–404]. In this context, the optimized device based on PBTTT-C-T:**bis-PDI-T-EG** blend exhibited a higher PCE of 6.08% due to an increase in the electron mobility and the reduced recombination loss upon solvent vapor annealing [405]. Choi et al. reported M- and V-shaped PDI-based NFAs (**CP-M** and **CP-V**) containing 1,1-diphenylcyclohexane to overcome the strong self-aggregation [408]. Polymer solar cell based on PPDT2FBT:**CP-V** blend exhibited a PCE of 4.68% because the geometry of CP-V favors good mixing with **PPDT2FBT**, resulting in nano-phase domains

that facilitate exciton dissociation and give suitable percolation pathways for charge transport.

Welch et al. developed N-annulated PDI-based dimer, **SdiPBI-N**, which showed high solubility and film-forming ability. **SdiPBI-N** blended with donor P3TEA gave the device a PCE as high as 7.55% with  $J_{SC}$  (11.03 mA cm<sup>-2</sup>) along with high  $V_{OC}$  (1.13 V) due to higher LUMO energy level [382]. Later, the same group modified the highly twisted N-annulated PDI-based dimer by introducing acetylene or thiophene linkers to make lower twisting acceptors (**SdiPBI-N2-Ac** and **SdiPBI-N2-Th**). They showed strongly red-shifted absorption, however, inferior PCEs were observed due to their severe aggregations [409,415]. In this context, Sun et al. reported S-annulated PDI-dimeric NFA **SdiPBI-S**, which showed broad absorption and higher LUMO energy. The introduction of S-atom led to more twisted molecular configuration as compared with parent PDI dimers. Blend film of PBDT-T1:**SdiPBI-S** showed a favorable phase separation and balanced carrier mobility resulting in the high PCE of 7.16%,  $J_{SC}$  of 11.65 mA cm<sup>-2</sup> and  $V_{OC}$  of 0.90 V [411]. Later, the same group replace S-atom of **SdiPBI-S** with Se-atom to give **SdiPBI-Se**, which delivered an even higher PCE of 8.42% due to a high and balanced charge carrier mobility and ultrafast charge generation processes in blend film [413]. Sun et al. utilized thienobenzene fused to the bay region of PDI subunits to give PDI dimers, **SdiPBI-BT** and **diPBI-BT**. Optimal devices based on blend film PBDT-T1:**SdiPBI-BT** exhibited a favorable phase separation which enhanced the  $V_{OC}$  to 0.95 V and the PCE of 6.71% [416]. Jen et al. reported fused PDI derivatives bridged by furan, thiophene, and selenophene units. These new NFAs showed reduced reorganization energy and extended effective  $\pi$ -conjugation, which can facilitate exciton diffusion and charge transport as compared to their parent counterparts. Among them, the device

**Fig. 27.** Chemical structures of perylenediimide (PDI) trimer based SM NFAs [424–438].

based on **FPDI-T** blended with PTB7-Th donor exhibited a superior PCE of 6.72% due to its modest twist angle that allowed more highly ordered packing and highest hole and electron mobilities than other fused PDI-based dyes [418]. Later, Marks et al. photocyclized the bay-linked PDI dimers to achieve twisted ring-fused PDI dimers (**Fus-Ph-PDI2**, **Fus-mPh-PDI2** and **Fus-TT-PDI2**), which increased the electronic coupling between two PDI units and then gave broad absorption. Blends of PBDTTT-FITTE:**Fus-mPh-PDI2** significantly decreased geminate recombination and hence increased J<sub>SC</sub> and PCE when compared to its congener PDI dimer **Ph-PDI2** [396]. Later, they blended **Fus-mPh-PDI2** with fluorinated polymer donor PBTZF4 to give a device with improved V<sub>OC</sub> (1.12 V), J<sub>SC</sub> (10.02 mA cm<sup>-2</sup>) and PCE as high as 5.55%, due to the well-matched absorption and morphology of blend [419]. Wang et al. made bay-linked (singly, doubly and triply) PDI dimers showing strong absorption, and their twisted geometry improved charge-transporting properties and PCE [420]. Fully fused PDI dimer **Fus-IDT-2PDI** composed of IDT fused with two PDI units showed red-shifted absorption and high LUMO more than unfused **IDT-2PDI** counterpart. Blend film based on PTB7-Th:**Fus-IDT-2PDI** showed favorable “face-on” orientation and higher crystallinity, hence a high PCE of 7.33% when compared to the blend PTB7-Th:**IDT-2PDI** [422,423].

In PDI trimers, three PDI units are linked together by direct conjugation (through bay, *ortho* or imide positions), or linked on both sides of π-aromatics or fused with heterocycles. PDI trimers exhibited red-shifted absorption; strong electronic coupling and

their star-shaped or twisted geometry helps to control the π-π interactions and aggregations. Fig. 27 shows the structures of trimeric PDI NFAs and the related photophysical data are compiled in Table 14.

Hou et al. made PDI trimer, namely, **H-tri-PDI**, by conjugating three PDI units through imide linkage, showed twisted geometry [424]. As a result, the device with PBDT-TS1:**H-tri-PDI** blend exhibited favorable “face-on”-oriented interactions and hence a high J<sub>SC</sub> (16.52 mA cm<sup>-2</sup>) and superior PCE (7.25%) as compared to those of PDI dimer (**H-di-PDI**) and monomer (**PDI-C2**). Also, Chen et al. reported a PDI trimers (**bbb-3PDI** and **obo-3PDI**) by conjugating PDI units (ortho and bay). Out of them, **bbb-3PDI** showed high J<sub>SC</sub> of 18.13 mA cm<sup>-2</sup> and PCE of 7.12% due to favorable morphology and balanced charge transporting properties [425,426]. Later, PDI trimers made by conjugating three PDI units with benzene (**B(PDI)3**) and triazine core (**Tz-PDI3**) gave the balance twisted geometry and suitable aggregation, leading to high PCE of 9.15% for blend film based on PTB7-Th:**Tz-PDI3** [428,429]. Aggregation of PDI trimers can be controlled by introducing triptycene and triphenylamine units, while the blend film based on PBDD-TS1:**TRIP-3PDI-C6** showed PCE of 4.53% due to effective suppression of aggregation [430]. Three PDI units conjugated to triphenylamine, resulting in highly twisted acceptor (**TPA-PDI3**) that showed strong absorption and weak intermolecular interactions and molecular aggregation. The corresponding blend with donor PBDTTT-C-T gave the device a PCE of 3.22% [432]. Star-shaped S/Se-annulated PDI trimer (**TPA-PDI3-S** and **TPA-PDI3-Se**)

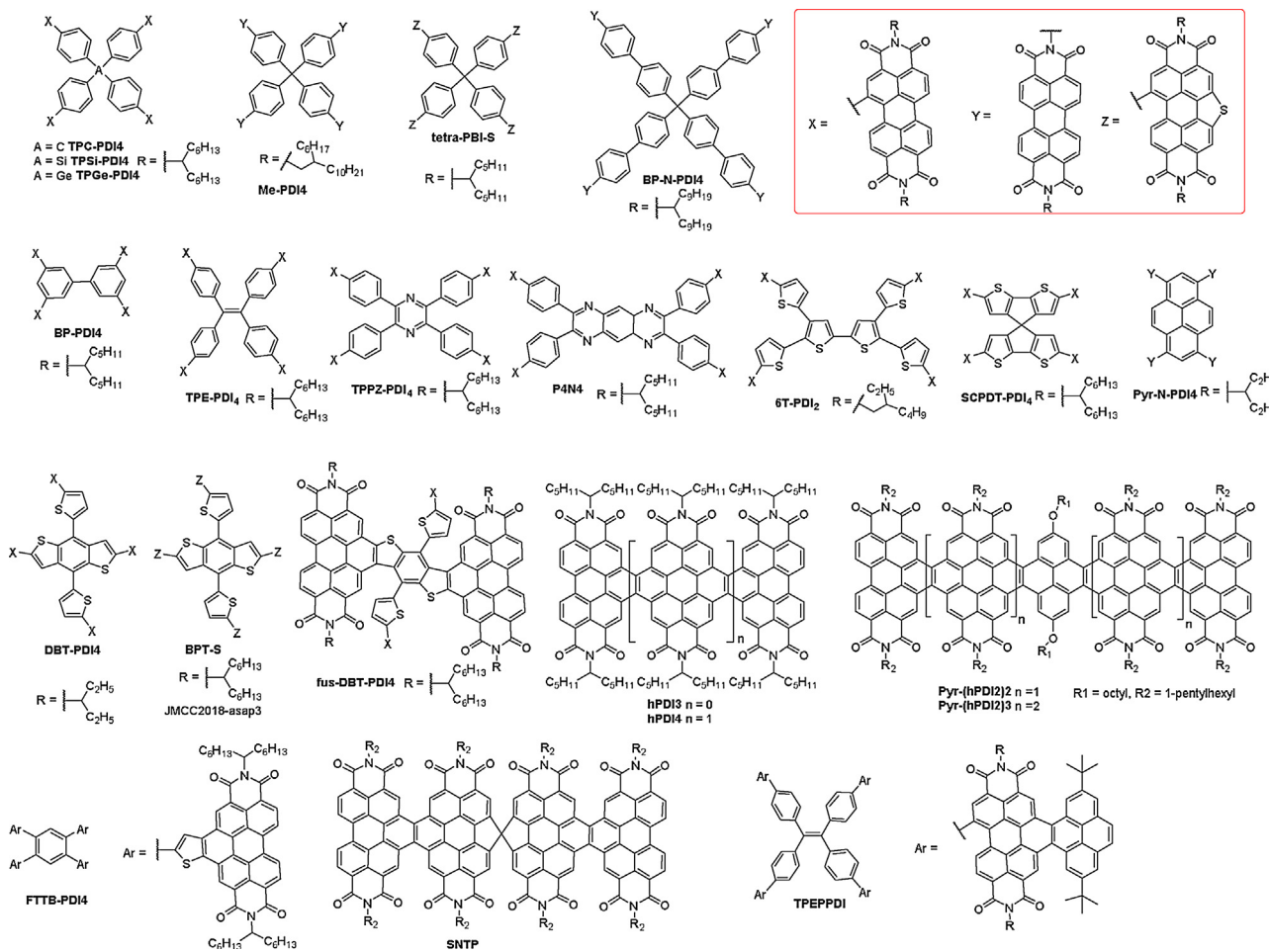


Fig. 28. Chemical structures of perylenediimide (PDI) tetramer based SM NFAs [439–454].

improved PCE due to more balanced carrier transport as compared to **TPA-PDI3** [434]. Sun et al. reported SM NFA **TPAPPD1** based on triphenylamine and pyrene fused PDI exhibited a PCE of 5.10% with highest  $V_{OC}$  (1.21 V) benefiting from the high LUMO and balanced carrier mobility of blend based on polymer donor PBT1-EH [427].

Interestingly, benzene-fused three PDI units (**TPH-C5**) and S-annulated PDI units (**TPH-C5-Se**) showed twisted three-bladed propeller configuration with broad absorption spectra and higher LUMO [435–438]. When they blended with PDBT-T1 donor, **TPH-C5-Se** showed more compact 3D network assembly because the Se···O interactions allowed better film morphology and good electron mobility, giving the device with the highest PCE of 9.28%,  $J_{SC}$  of 12.53 mA cm<sup>-2</sup> and  $V_{OC}$  of 1.00 V superior to those of **TPH-C5** [437]. Chen et al. reported **BTT-3PDI** and **Fus-BTT-3PDI** based on three PDI moieties connected to a benzotriphosphine core through single bond and ring-fusion, respectively [438]. **Fus-BTT-3PDI** exhibited a good structural rigidity and planarity as well as good electronic coupling between three PDIs and benzotriphosphine and uplifted LUMO level. As a result, the device based on PTB7-Th:**Fus-BTT-3PDI** blend exhibited the PCE of 6.19%, almost three times higher than PTB7-Th:**BTT-3PDI** blend.

In PDI tetramers, four PDI units were linked into star-shaped structures or fused with  $\pi$ -aromatics through either bay or imide position of PDI core. PDI tetramers are beneficial for strong absorption spectra, suitable energy levels and aggregation suppression, while retains favorable  $\pi$ – $\pi$  molecular interactions. The structures of tetrameric PDI NFAs are shown in Fig. 28 and their optical and device parameters are summarized in Table 14.

Yan et al. reported a series of tetraphenyl methane (**TPC-PDI4**), tetraphenyl silane (**TPSi-PDI4**) and tetraphenyl germane (**TPGe-PDI4**) core-based 3D-structure NFAs to effectively suppress aggregation [439]. When they blended with PffBT4T-2DT, **TPC-PDI4** and **TPSi-PDI4** exhibited better PCEs than **TPGe-PDI4**, which was attributed to its high geminate recombination that leads to decreased  $J_{SC}$  and  $V_{OC}$  of the device [439]. Later, Zhang et al. modified the substitution pattern from bay to imide to make terameric PDI derivative (**Me-PDI4**), which showed red-shifted absorption as compared with **TPC-PDI4** [442]. However, OSCs based on PBDTTT-CT:**Me-PDI4** blend exhibited a lower PCE due to unbalanced electron/hole mobilities. Fan et al. made **tetra-PBI-S** by integration of thiophene annulated PDI unit with tri-phenyl methane unit. This design gave a reasonably planar 3D structure that leads to a high charge transport and effective phase separation in blend film with donor PBDT-TS1 [443]. As a result, the device with PBDT-TS1:**tetra-PBI-S** blend film achieved a higher PCE of 6.17% when compared to tetra-phenyl methane/silane/germane-based acceptors.

Yan et al. reported a 3D molecule **TPE-PDI4**, composed of tetraphenyl ethylene core and four PDI peripherals via bay conjugation. **TPE-PDI4** showed weak molecular aggregation and then formed a small domain blend films and thus enables reasonably good electron-transport ability. Therefore, the device employing **TPE-PDI4** exhibited a PCE of 5.44% and  $V_{OC}$  of 0.91 V when blended with polymer donor PTB7-Th [392]. Later, the same group reported four-wing propeller-shaped molecule **TPPz-PDI4** by incorporating tetraphenyl pyrazine unit to reduce the intermolecular twisting,

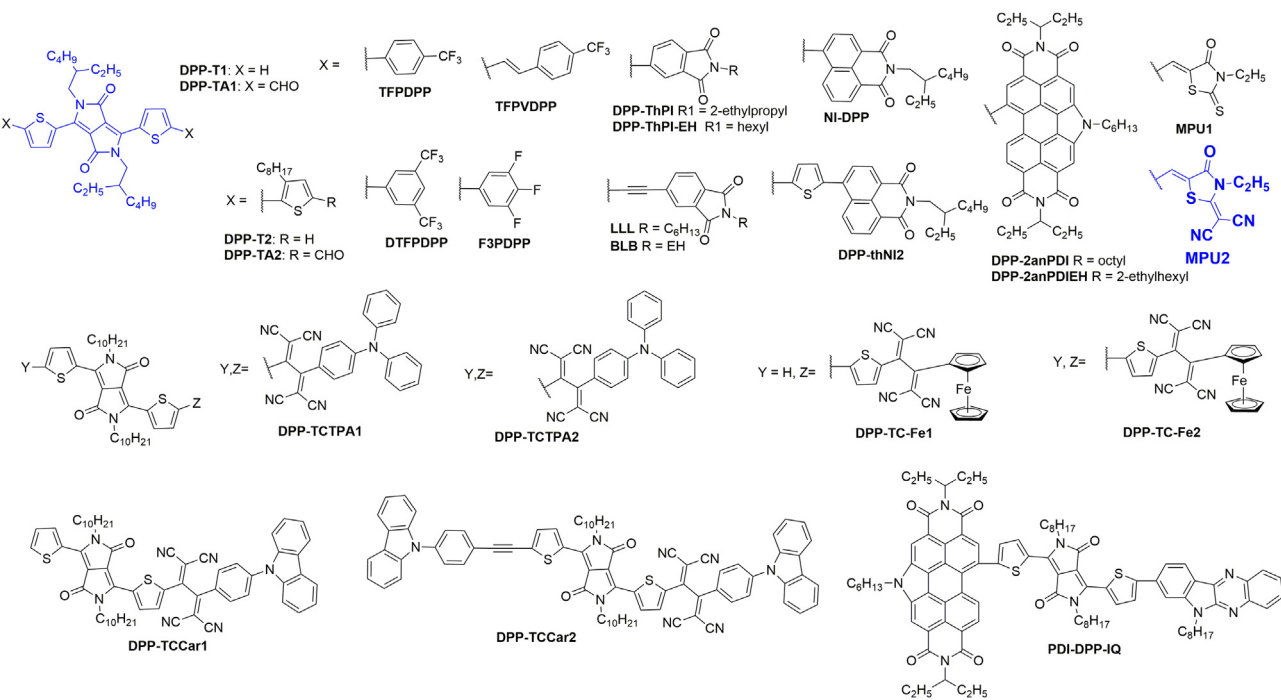


Fig. 29. Chemical structures of diketopyrrolopyrrole (DPP) based SM NFAs [455–468].

which is beneficial for the formation of small domain size in blend with PffBT-ffBT donor, resulting high PCE of 6.90% as compared to that of **TPE-PDI4** [441]. Similarly, Cao et al. made **P4N4** based on a non-planar tetraphenyl pyrazino[2,3-g]quinoxaline central linker and four PDI units. The device employing **P4N4** blended with donor PDBT-T1 exhibited a better PCE (5.71%) due to its non-planar structure minimized aggregation of the blend as compared to its di-substituted PDI based NFA (3.86%) [445]. The incorporation of a spiro-configured core unit 4,4'-spirobi[cyclopenta[2,1-*b*;3,4-*b'*]dithiophene] with four PDI peripherals decrease the strong aggregation and favor better electronic conjugation, which allowed long absorption maxima and then a better electron transporting property. As a result, the device based on PTB7-Th:**SCPDT-PDI4** blend film exhibited a high PCE of 7.11% as compared to previous star-shaped PDI tetramers [447]. Yu et al. made cross-linked molecular acceptor, **DBT-PDI4**, based on DBT, and four PDI units showed reduced aggregation. The PTB7-Th:**DBT-PDI4** blend film showed a favorable morphology and efficient charge dissociation leads to the device to have a high PCE of 8.47% [448]. Later, they fused/cyclized bay positions of PDI with DBT, resulting in a fused dye, **fus-DBT-PDI4**, which showed higher LUMO and corresponding blend films forms “face-on” orientation packing patterns that benefit the charge transport. A higher PCE was obtained as compared with **DBT-PDI4** under similar fabrication conditions [449].

Nuckolls et al. reported helical molecular acceptors (**h-PDI3** and **h-PDI4**) based on four fused PDIs. As they blended with PTB7-Th donor, the blend exhibited nano-mesh-like network for efficient exciton separation and balanced charge transport, leading the device to yield the highest PCE up to 8.30% [451]. Later, they made cove edge graphene nanoribbons (**Pyr-(hPDI2)2** and **Pyr-(hPDI2)3**) based on pyrene-fused PDI oligomers, which showed strong absorption and a high degree of twisting along the long axis. The device based on PTB7-Th:**Pyr-(hPDI2)3** blend film exhibited a high PCE of 7.60% due to broad spectral coverage as compared to PTB7-Th:**Pyr-(hPDI2)2** blend [452]. Yan et al. reported **FTTB-PDI4** composed of benzene as central linker end-capped with four

thiophene-fused PDI units, showed enhanced absorption, strong intermolecular packing and minimized energy loss with donor P3TEA [453]. As a result, the device with P3TEA:**FTTB-PDI4** blend film exhibited a high V<sub>OC</sub> of 1.18 V and then a very high PCE up to 10.58%. Later, Wang et al. made spiro-fused PDI acceptors possessing broad absorption features. More importantly, its spiro-configuration reduced aggregation and allowed rationally ordered packing in the PTB7-Th:**SNTP** blend which led the device to achieve a PCE of 7.17% [454]. Sun et al.

In short summary, PDI can successfully serve as potential chromophore due to its strong absorption, higher LUMO energy level and self-assembly nature. The number of PDI units arranged either into linear or 3D structure can manipulate the absorption and energy levels, and more importantly the aggregation behaviors in the solid state, which enables favorable morphology and then a better PCE. It is obvious that PDI dimers enhance the spectral response and then better device performance as compared to monomers. Both PDI trimers and tetramers exhibited high PCEs due to the balanced aggregation and molecular interactions, which allowed blend with suitable morphologies for better charge transporting property. Finally, the champion NFA in this regard is **TPH-C5-Se**, which achieved the highest PCE of 9.28% when blended with PDBT-T1 donor [437].

#### 3.4. Diketopyrrolopyrrole-based small molecular acceptors

DPP has attracted tremendous interest in designing and developing NFAs due to its high thermal and photochemical stability, strong absorption, and the easy for improving solubility by attaching alkyl units onto lactam N-atom. DPP-based molecules showed suitable π-π intermolecular interactions, which can be subtly modulated by various electron-rich or deficient units. DPP can be effectively used as a central core or peripheral unit and they can also be easily integrated into a 3D structure. Several potential NFAs based on DPP as central core or terminal unit were reported (Figs. 29 and 30). Their relevant physical data was compiled in Table 15. Initially, Janssen et al. developed DPP-cored molecules

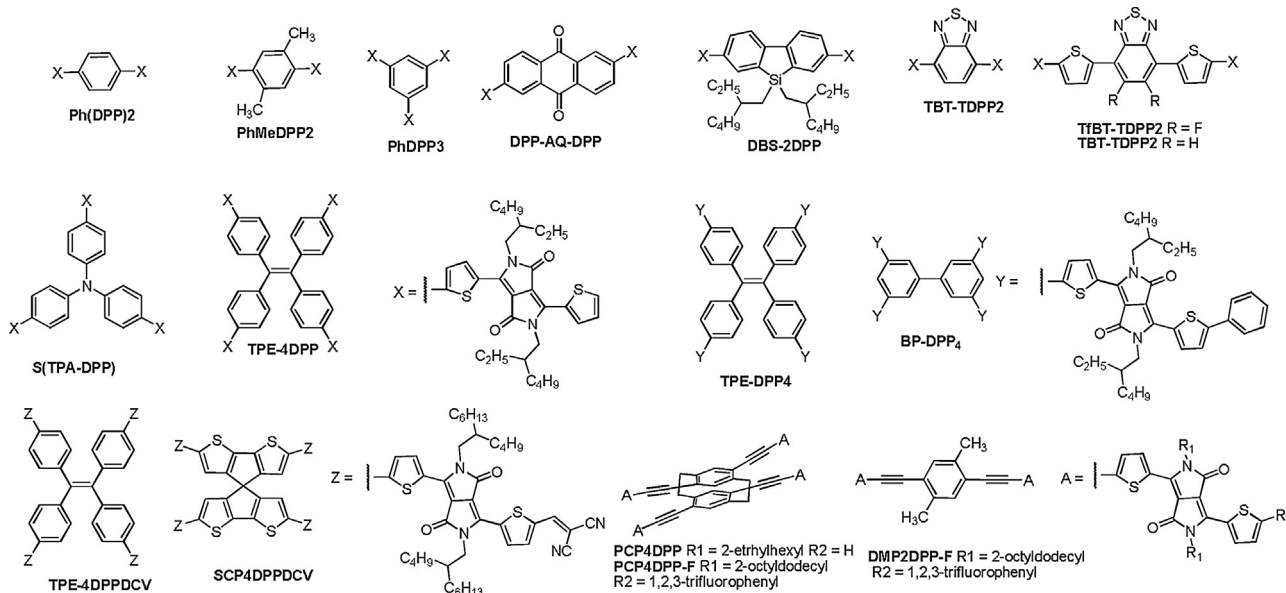


Fig. 30. Chemical structures of diketopyrrolopyrrole (DPP) based SM NFAs [469–477].

**Table 15**

Photo-physical and photovoltaic properties of ditketopyrrolopyrrole (DPP) based SM NFAs.

NFA	$\lambda_{max}$ (nm)	HOMO (eV)	LUMO (eV)	Donor	$V_{oc}$ (mV)	$J_{sc}$ ( $mA\text{ cm}^{-2}$ )	FF	PCE (%)	Refs.
DPP-T1	510	5.55	3.59	P3HT	0.85	0.79	0.25	0.17	[455]
DPP-TA1	580	5.90	4.09	P3HT	0.52	1.93	0.31	0.31	[455]
DPP-T2	615	5.39	3.68	P3HT	0.85	0.87	0.32	0.24	[455]
DPP-TA2	636	5.54	3.94	P3HT	0.60	0.86	0.29	0.15	[455]
TFPVDP	592	5.18	3.55	P3HT	0.64	1.70	0.53	0.58	[456]
TFPDPP	599	5.26	3.52	P3HT	0.81	2.36	0.52	1.00	[456]
DTFPDPP	569	5.28	3.57	P3HT	0.71	0.85	0.23	0.14	[456]
F3PDPP	595	5.31	3.68	P3HT	0.65	2.70	0.32	0.56	[456]
DPP-ThPI	616	5.80	4.10	P3HT	0.86	3.25	0.37	1.30	[457]
DPP-TzPI	614	6.10	4.30	P3HT	0.62	1.32	0.42	0.43	[457]
DPP-ThPI	611	3.44	5.23	P3HT	0.81	1.40	0.37	0.33	[328]
LLL	620	5.88	4.13	P3HT	0.89	5.91	0.50	3.28	[458]
BLB	619	5.82	3.76	P3HT	0.59	0.26	0.25	0.04	[459]
NI-DPP	576	5.51	3.55	PTB7-Th	1.06	3.12	0.46	1.64	[343]
DPP-thNI2	599	5.40	3.61	P3HT	0.70	1.91	0.45	0.60	[460]
DPP-2anPDI	685	5.30	3.70	PTB7-Th	0.97	10.42	0.49	5.60	[461]
DPP-2anPDIIEH	532	5.30	3.60	PTB7-Th	0.97	5.98	0.50	2.90	[462]
MPU1	702	5.81	3.99	P3HT	0.60	6.54	0.55	2.16	[463]
MPU2	714	5.72	4.15	PDTSi-fBT	0.98	12.37	0.62	7.52	[463]
DPP-TCTPA1	580	5.54	4.22	DT(SQxHTh2)2	1.02	11.04	0.62	6.98	[464]
DPP-TCTPA2	616	5.64	4.36	DT(SQxHTh2)2	0.94	12.15	0.68	7.76	[464]
DPP-TC-Fe1	681	5.43	3.92	PBDT-TTQ	0.92	8.15	0.52	3.90	[465]
DPP-TC-Fe2	732	5.39	4.02	PBDT-TTQ	0.86	10.28	0.56	4.95	[465]
DPP-TCCar1	695	5.52	3.83	DTB-BT-F	0.98	11.34	0.58	6.44	[466]
DPP-TCCar2	726	5.33	3.81	DTB-BT-F	0.88	12.66	0.62	6.89	[466]
PDI-DPP-IQ	535	5.20	3.70	PDTSi-fBT	0.94	10.56	0.49	4.86	[467]
PhMeDPP2	565	5.18	3.65	PDTSi-fBT	0.90	13.78	0.58	7.19	[467]
PhDPP2	600	5.16	3.52	P3HT	0.75	2.47	0.43	0.81	[468]
PhDPP3	570	5.22	3.27	P3HT	1.10	1.45	0.30	0.48	[469]
DPP-AQ-DPP	574	5.70	3.99	P3HT	1.07	1.17	0.25	0.31	[469]
DBS-2DPP	596	5.30	3.28	P3HT	0.87	2.30	0.39	0.80	[170]
TBT-TDPP2	620	5.06	3.71	P3HT	0.97	4.91	0.43	2.05	[470]
TfBT-TDPP2	620	5.70	4.18	PTB7	0.83	2.06	0.52	1.16	[471]
S(TPA-DPP)	596	5.26	3.26	P3HT	0.81	7.77	0.47	3.03	[472]
TPE-4DPP	590	5.53	3.81	P3HT	1.18	5.17	0.64	3.86	[474]
TPE-DPP4	614	5.08	3.64	P3HT	1.16	4.45	0.47	2.49	[475]
BP-DPP4	608	5.06	3.61	P3HT	1.11	2.93	0.36	1.18	[475]
TPE4DPPDCV	690	5.40	3.81	PTB7-Th	0.75	9.89	0.53	4.01	[476]
SCP4DPPDCV	765	5.31	3.89	PTB7-Th	0.70	11.69	0.51	4.20	[476]
PCP4DPP	598	5.24	3.47	P3HT	1.06	4.18	0.46	2.05	[477]
PCP4DPP-F	586	5.29	3.53	P3HT	0.90	5.88	0.51	2.69	[477]
DMP2DPP-F	578	5.22	3.52	P3HT	0.97	1.91	0.48	0.90	[477]

(**DPP-TA1** and **DPP-TA2**) decorated with aldehyde or thiophene aldehyde groups. These molecules showed strong absorption and preliminary device performance as blended with P3HT donor [455]. Later, **TFPDPP** equipped with fluorine-substituted phenyl units improved the PCE to 1% as blended with P3HT donor [456], which was attributed to the high LUMO due to fluorine substitution and better blend morphology. Later, DPP core was functionalized with phthalimide and NI units, the resulting molecules showed strong spectral response attributed to strong intra-molecular interactions [455–459]. When they blended with P3HT donor, **LLL** showed a high PCE of 3.28% due to better absorption and high  $J_{SC}$  of  $5.88 \text{ mA cm}^{-2}$  as compared to other dyes [458].

The nature of end-capping units on DPP unit influences the absorption and energy levels significantly. Welch et al. functionalized DPP core with hetero-annulated PDI, which results in a new NFA **DPP-2anPDI**, showing strong absorption (685 nm) and suitable energy levels [461,462]. OSCs based on the active layer composed of PTB7-Th:**DPP-2anPDI** showed a PCE of 5.60% attributed to strong absorption and favorable self-assembly of PDI [461]. Mishra et al. designed narrow bandgap NFAs (**MPU1** and **MPU2**) by conjugating DPP with rhodanine and dicyanorohodanine units, giving broad absorption spectra (702 to 714 nm) [463,464]. Optimized polymer solar cell based on an active layer composed of **MPU1** and PDTSi-fBT donor produced a high PCE of 7.52% and a high  $J_{SC}$  of  $12.37 \text{ mA cm}^{-2}$  [463]. However, SM-based OSCs composed of **MPU1** and **MPU2** with DTS(QxHTh2)2 donor delivered a PCE of 6.98% and 7.76%, respectively [464]. Later, they made a new type of NFAs (**DPP-TCTPA1** and **DPP-TCTPA2**) by the selective functionalization of DPP core with tetracyanobuta-1,3-diene conjugated triphenylamine units on one and both sides of DPP, respectively [465]. When they blended with polymer PBDT-TTQ donor, optimizing solar cells showed moderate PCEs.

Later, the same group replaced the end capped triphenylamine unit with ferrocene to give NFAs (**DPP-TC-Fe1** and **DPP-TC-Fe2**) showing strong absorption [466]. When blended with DTB-BT-F donor, they showed a superior PCE of 6.44% and 6.89%, respectively, due to a broad spectral coverage, better charge transport and nano-scale morphology of the active layer [466]. Similarly, tetracyanobuta-1,3-diene-conjugated carbazole dyes (**DPP-TCCar1** and **DPP-TCCar2**) were synthesized as NFAs in combination with PDTSi-fBT, which produced higher PCEs of 4.86% and 7.19%, respectively. A superior PCE of **DPP-TCCar2**-based device can be attributed to its broader absorption and balanced charge transport that enhanced  $J_{SC}$  ( $13.78 \text{ mA cm}^{-2}$ ) and FF (0.58) [467]. Later, Welch et al. designed and synthesized unsymmetrical NFAs with DPP conjugated alternatively with PDI and indoloquinoxaline units. The planarization of the molecular backbone with head-to-tail stacking induces a favorable blend morphology [468].

Conjugated molecules composed of DPP as a peripheral unit and suitable central aromatic linkers such as phenyl, triphenylamine, and spiro aromatics showed strong absorption and higher LUMO levels and thus enhanced  $J_{SC}$  and  $V_{OC}$  in OSCs applications. Yu et al. made NFA, **PhMeDPP2**, based on phenyl linker and DPP peripheral unit showed broad absorption, but a poor PCE was observed in combination with P3HT donor [469]. Later, a set of NFAs (**TBT-TDPP2** and **TfBT-TDPP2**) was reported based on BT as core and DPP terminus exhibited a strongly red-shifted absorption maximum centered at 620 nm [472]. Polymer solar cells based on an active layer of PTB7:**TfBT-TDPP2** achieved a higher PCE of 5.0% attributed to the incorporation of fluorine substitution, which enhances crystallinity and thus better electron mobility as compared to **TBT-TDPP2**. Zhan et al. made 3D star-shaped NFA **S(TPA-DPP)** based on a triphenylamine core and three DPP peripherals, which showed good absorption, and favorable LUMO, produced a high  $V_{OC}$  of 1.18 V as blended with P3HT donor [473]. Later, a set of four

directional dyes derived from tetraphenylethylene core with DPP peripherals showed a modern PCE of 3.86% due to a favorable morphology of active layer and then a high  $V_{OC}$  of 1.18 V [474]. Chen et al. reported 3D molecules (**TPE4DPPDCV** and **SCP4DPPDCV**) composed of tetraphenylethylene and spirobicyclopentadithiophene as linkers flanked with four DPP units [476]. **SCP4DPPDCV** exhibited a broader absorption and better charge-transporting ability for the corresponding blend with PTB7-Th donor, which produced a superior PCE of 4.20% as compared to congener **TPE4DPPDCV**. Dyes composed of [2,2]paracyclophane conjugated with four DPP units showed good solubility, thermal stability and favorable energy levels, resulting in a PCE of 2.69% as blended with P3HT donor [477]. Overall, the DPP unit served very well as a central linker or terminal units in conjugation with different aromatic building blocks. DPP-based molecules showed broad spectral responses and suitable higher LUMO levels, which led to higher  $J_{SC}$  and  $V_{OC}$ . So far, **MPU2** composed of DPP and rhodanine units achieved the highest PCE of 7.76% in this class. Suitable molecular designs based on DPP as a functional building block for extending absorption and high LUMO may afford potential SM NFAs for enhancing the PCE of OSCs in the near future.

### 3.3. Isoindigo-based small molecular acceptors

Recently, isoindigo have been introduced as building blocks to make low bandgap materials for organic electronics applications due to their easy synthesis, strong electron-withdrawing nature, planar structures with extended  $\pi$ -conjugation and high LUMO level. In addition, N-alkyl chains of isoindigo allow high solubility and minimize aggregation. Isoindigo can be utilized as both linker and terminal units for new molecular materials. The structures of isoindigo-based NFAs were shown in Fig. 31 and their photo-physical and photovoltaic properties were listed in Table 16. Welch et al. reported **IITH-PI** based on isoindigo and phthalimide as terminal units [328,478,479]. The optimized devices based on DTS(FBTTh2)2:**IITH-PI** blend showed a PCE of 1.01% attributed to the higher  $J_{SC}$  ( $2.60 \text{ mA cm}^{-2}$ ) than other derivative **IITH-NI** [479]. Later, Cabanetos et al. synthesized low bandgap NFA **TII-Pht2** based on thienoisoindigo and phthalimides, showed red-shifted absorption than previous isoindigo-based NFAs, but downshifted LUMO decreased the  $V_{OC}$  and PCE [458].

Welch et al. developed **TII-NanPDI** and **ISI-NanPDI** based on isoindigo/thienoisoindigo and N-annulated PDI derivative, respectively. They exhibited red-shifted absorption and a higher LUMO level than **IITH-PI** [462]. After blending with PTB7-Th, the device based on **IITH-PI** exhibited a higher PCE of 2.60%, while **TII-NanPDI** showed an inferior PCE due to the poor quantum efficiency and poor film morphology. Su et al. developed acceptors (**AN-I2**, **Py-I2**, **Si-I2** and **IDT-I2**) based on IDT and isoindigo as terminal units aromatic bridged by anthracene, pyrene, dithienosilole, respectively [480]. They showed broad spectral responses, while **IDT-I2** exhibited longer absorption, which is useful for high photocurrent and showed a PCE of 1.39% as blended with P3HT donor as compared to other analogous NFAs. Liu et al. synthesized **IID-IC** based on isoindigo and dicyanomethylene-3-indanone end groups and showed longer absorption and PCE of 2.82% as it blended with J61 donor [482]. In short summary, isoindigo-based acceptors typically faced severe aggregation and phase separation issues, which can be solved by the incorporation of suitable nonplanar/star-shaped units. Overall, **IID-IC** showed better PCE (2.82%) as it blended with J61 donor.

### 3.6. Miscellaneous small molecular acceptors

Except the various NFAs have discussed, other miscellaneous SM NFAs (Fig. 32 and Table 17) were reviewed. NFA (**BT2**) based on

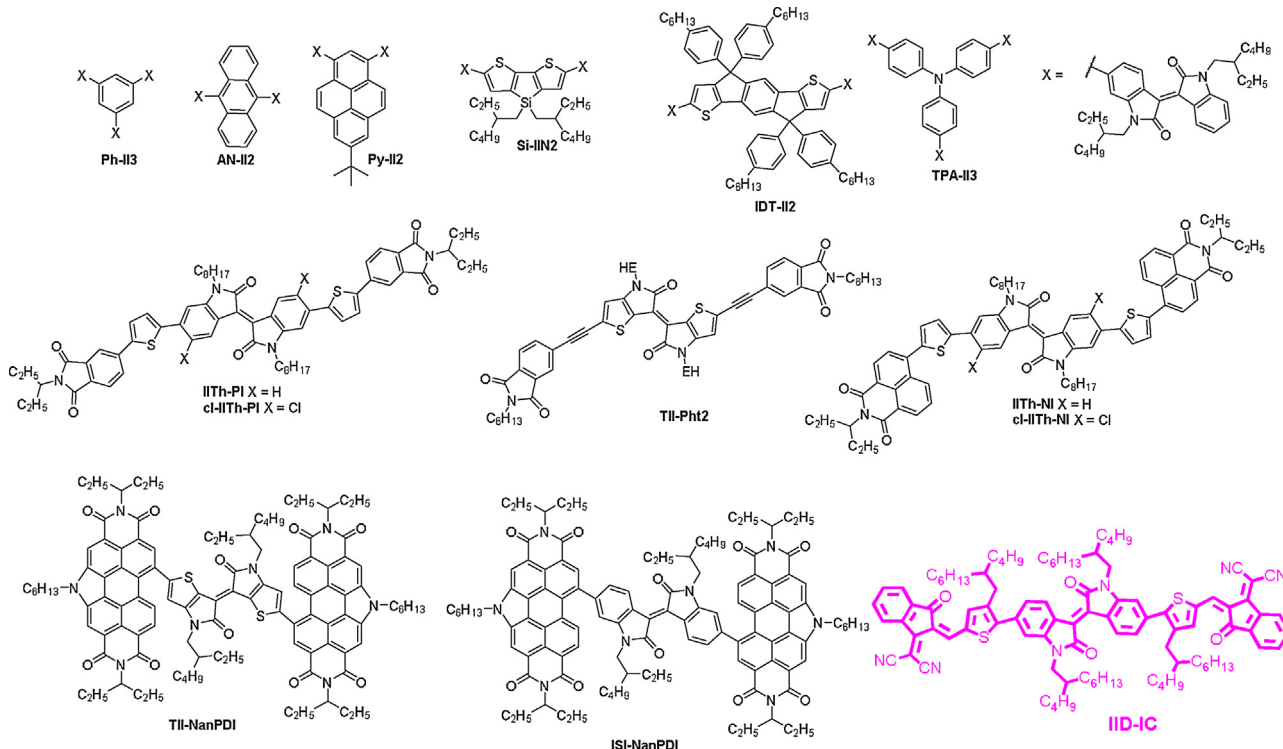


Fig. 31. Chemical structures of isoindigo based SM NFAs [478–482].

Table 16

Photo-physical and photovoltaic properties of isoindigo based SM NFAs.

NFA	$\lambda_{\text{max}}$ (nm)	HOMO (eV)	LUMO (eV)	Donor	$V_{\text{OC}}$ (mV)	$J_{\text{SC}}$ ( $\text{mA Cm}^{-2}$ )	FF	PCE (%)	Refs.
IITh-PI	440	3.64	5.47	DTS(FBTTh2)2 P3HT DTS(FBTTh2)2	0.95 0.63 0.92	1.18 0.15 2.60	0.40 0.03 0.42	0.50 0.28 1.01	[478] [245] [479]
IITh-NI	450	5.53	3.70	DTS(FBTTh2)2	0.68	1.29	0.44	0.38	[479]
cl-IITh-PI	477	5.64	3.80	DTS(FBTTh2)2	0.90	1.23	0.41	0.46	[479]
cl-IITh-NI	482	5.61	3.73	DTS(FBTTh2)2	0.87	5.27	0.42	1.93	[479]
TII-Pht2	631	5.89	4.24	P3HT	0.66	1.62	0.27	0.36	[459]
TII-NanPDI	532	5.00	3.60	PTB7-Th	0.93	1.09	0.34	0.40	[462]
ISI-NanPDI	534	5.60	3.60	PTB7-Th	1.03	6.97	0.37	2.60	[462]
AN-II2	512	5.18	2.72	P3HT	1.06	0.68	0.38	0.28	[480]
Py-II2	518	5.17	2.72	P3HT	0.92	1.49	0.39	0.54	[480]
Si-II2	614	4.98	2.82	P3HT	0.74	0.85	0.37	0.23	[480]
IDT-II2	625	4.88	2.75	P3HT	1.05	2.36	0.56	1.39	[480]
TPA-II3	537	5.54	3.77	P3HT	0.96	1.91	0.44	0.81	[481]
Ph-II3	410	5.64	3.79	P3HT	1.15	0.45	0.37	0.19	[481]
IID-IC	570	5.99	3.95	J61	0.83	6.36	0.53	2.82	[482]

benzo[b]thiophene showed a preliminary photo-response after irradiation due to favorable energy levels matched with P3HT donor [484]. Acceptor **BTh-BAR** blended with subphthalocyanine donor showed exceptionally high  $V_{\text{OC}}$  of 1.38 V, but its low external quantum efficiency limits the PCE [485]. Yamada et al. reported porphycene dimers (**DPC-mP** and **DPC-T**) that displayed broad absorption features, but their blends with P3HT donor produced poor PCEs due to over aggregation [486]. Later, **T-mBODIPY** and **B-BODIPY** incorporated BODIPY as terminal units on thiophene and DBT respectively were reported. Their high LUMO levels are beneficial for enhancing  $V_{\text{OC}}$  up to 1.12 V as blended with PTB7 [319,487]. Bhosale et al. reported the device based on P3HT:**TP-PCP3** blend film exhibited a better PCE of 4.21% [488]. Zhan et al. reported **S(TPA-BBT)** composed of star-shaped triphenylamine with bis-BT arms. The 3D structure effectively suppresses the

aggregation and raise the LUMO, which allow the corresponding blend film with P3HT donor achieving a high  $V_{\text{OC}}$  of 0.99 V [489]. Nielsen et al. reported truxenone-based molecules by the functionalization at active methylene bridges, increasing electron affinities and absorptivity. The blend film SubPc:**TRX1CNEA** led the device to achieve a high  $V_{\text{OC}}$  of 1.30 V due to favorable morphology [490,491]. However, **TrHex-3BR** based on truxene core conjugated with BT and rhodanine units broadens the absorption spectrum and raised the LUMO. As a result, the PCE of based on PTB7-Th: **TrHex-3BR** blend film was enhanced to 2.01% [492]. Bhosale et al. made a 3D acceptor **TPE-CP4** based on tetraphenylethylene core with cyanopyridone terminal units. The blend film with PTB7 gave the device a high PCE up to 6.72% [493]. A series of BT-based molecules by conjugating terminal units such as vinazene, phenazine and oligothiazoles were reported to obtain better

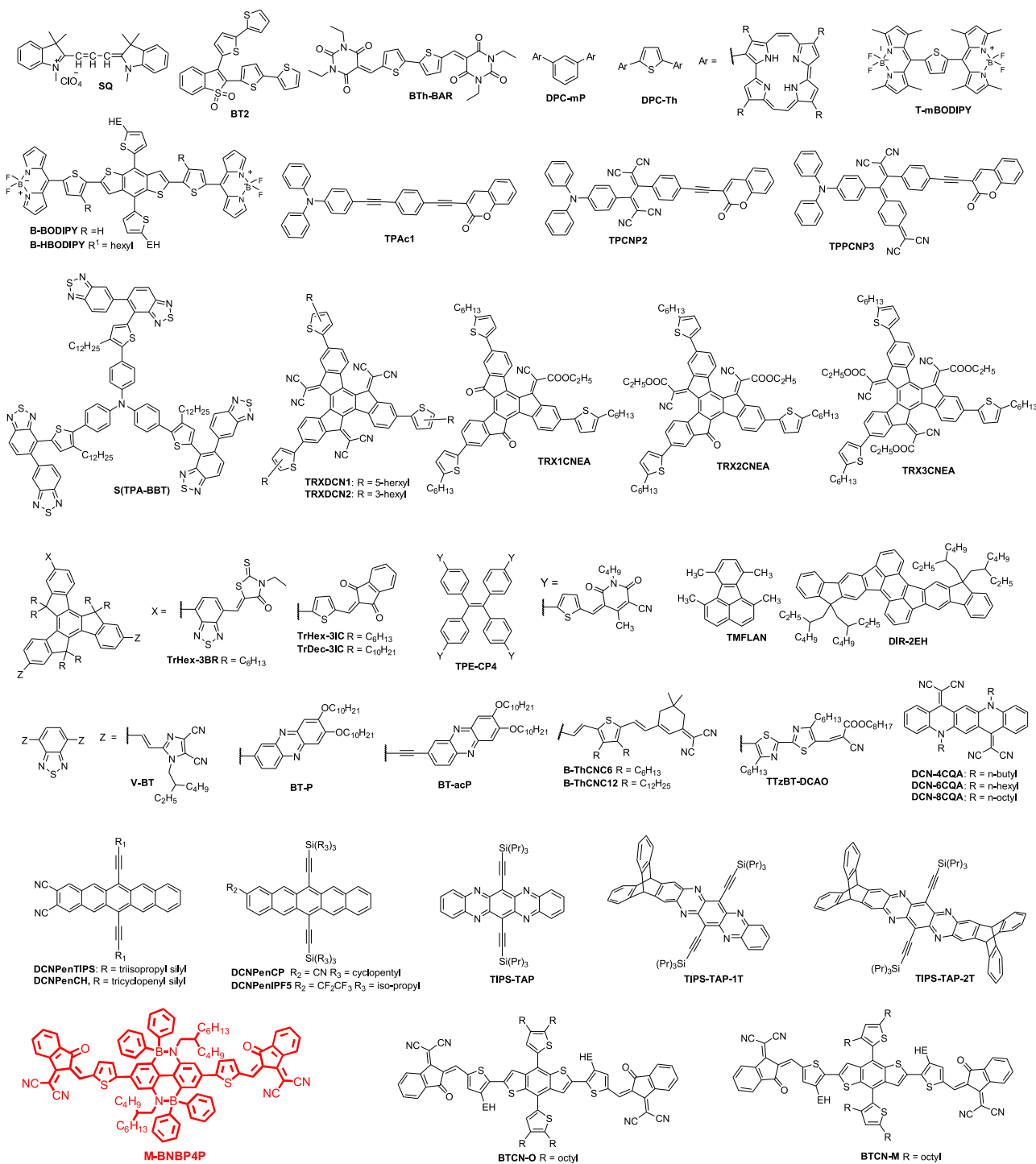


Fig. 32. Chemical structures of miscellaneous SM NFAs [483–506].

absorption spectra and higher LUMO levels [494–498]. Blend film based on PCz:**V-BT** gave the device a  $V_{OC}$  as high as 1.36 V [495].

Fused aromatic cores were utilized to construct NFAs because of the better absorption character and higher LUMO levels which meet the fundamental requirements of acceptors. For example, dicyano substituted quinacridone-based acceptor (**DCN-8CQA**), which showed a strong absorption centered at 630 nm with favorable energy levels. However, the device based on P3HT:**DCN-8CQA** blend film exhibited a poor PCE of 1.57%, which was limited by low  $V_{OC}$  [498]. Similarly, pentacene and tetraazapentacene

derivatives were also reported as NFAs. However, their blends with P3HT exhibited inferior PCEs attributed to the poor spectral response of acceptors [502–504]. Liu et al. reported **M-BNBP4P**, based on organoboron core flanked with two dicyanomethylene-3-indanone units, exhibited long absorption maximum to give OSC with high  $J_{SC}$  (14.62 mA cm<sup>-2</sup>) and PCE (7.06%) with the corresponding blend with PTB7-Th donor [505]. Hou et al. demonstrated that the position of alkyl chain substitution on the central dithienobenzene core can modulate the steric hindrance and enhance high ordered lamellar packing in the solid

**Table 17**

Photo-physical and photovoltaic properties of miscellaneous SM NFAs.

NFA	$\lambda_{max}$ (nm)	HOMO (eV)	LUMO (eV)	Donor	$V_{OC}$ (mV)	$J_{SC}$ (mA Cm $^{-2}$ )	FF	PCE (%)	Refs.
BTh-BAR	550	6.28	4.23	SubPc	1.38	2.34	0.40	1.28	[485]
DPC-mP	639	5.70	3.50	P3HT	0.33	0.89	0.28	0.08	[486]
DPC-T	641	5.60	3.50	P3HT	0.33	0.84	0.27	0.08	[486]
T-mBODIPY	519	5.53	3.49	PTB7	1.12	0.72	0.30	0.24	[487]
B-BODIPY	517	5.54	3.49	PTB7	1.08	0.10	0.34	0.04	[487]
B-HBODIPY	518	5.40	3.79	P3HT	0.65	3.09	0.60	1.21	[419]
TP-AcP1	424	5.51	3.95	P3HT	1.03	5.70	0.39	2.28	[482]
TP-TCP2	523	5.81	4.67	P3HT	0.93	6.78	0.59	3.75	[482]
TP-PCP3	661	5.64	4.48	P3HT	0.83	8.95	0.57	4.21	[482]
S(TPA-BBT)	450	5.48	3.10	P3HT	0.99	1.81	0.45	0.81	[489]
TRXDCN1	423	5.94	4.07	SubPc	0.95	1.90	0.52	1.00	[489]
TRXDCN2	415	6.17	4.08	SubPc	0.92	2.00	0.36	0.70	[489]
TRX1CNEA	368	6.00	3.90	SubPc	1.30	0.53	0.21	0.15	[491]
TRX2CNEA	397	5.90	3.90	SubPc	1.30	0.62	0.22	0.18	[491]
TRX3CNEA	416	6.00	3.90	SubPc	1.29	0.85	0.25	0.28	[492]
TrHex-3IC	570	5.92	3.94	PTB7-Th	0.88	3.71	0.38	1.23	[492]
TrDec-3IC	570	5.88	3.90	PTB7-Th	0.74	2.55	0.27	0.53	[492]
TrHex-3BR	482	5.79	3.74	PTB7-Th	1.02	5.92	0.33	2.01	[492]
TPE-CP4	514	5.72	3.90	PTB7	1.01	10.61	0.63	6.72	[493]
V-BT	448	5.87	3.49	P3HT	0.67	1.79	0.37	0.45	[494]
				PCz	1.36	1.14	0.49	0.75	[495]
BT-P		5.80	3.17	P3HT	0.49	0.57	0.60	0.17	[496]
BT-acP		5.84	3.33	P3HT	0.63	1.18	0.59	0.44	[496]
B-ThCNC6	603	5.48	3.63	P3HT	0.74	1.63	0.56	0.67	[497]
DCN-4CQA	630	5.75	4.00	P3HT	0.40	1.45	0.48	0.28	[498]
DCN-6CQA	630	5.80	4.00	P3HT	0.42	1.43	0.49	0.30	[498]
DCN-8CQA	630	5.90	4.10	P3HT	0.48	5.72	0.57	1.57	[498]
TMFLAN	373	6.07	3.77	P3HT	3.02	0.52	0.44	0.71	[499]
DIR-2EH	590	5.38	3.30	P3HT	1.22	4.29	0.58	3.05	[500]
B-ThCNC12	603	5.43	3.62	P3HT	0.82	1.80	0.35	0.52	[497]
TTzBT-DCA0		5.34	3.55	SF8TBT	1.24	0.47	0.35	0.21	[501]
DCNPenTIPS				P3HT	0.58	0.44	0.38	0.10	[502]
DCNPenCP		5.29	3.50	P3HT	0.84	3.56	0.42	1.27	[503]
DCNPenIP5		5.32	3.42	P3HT	0.67	2.07	0.33	0.46	[503]
TIPS-TAP		6.05	4.50	PTB7	0.70	2.57	0.37	0.74	[504]
TIPS-TAP-1T		5.80	4.20	PTB7	0.78	3.39	0.31	0.91	[504]
TIPS-TAP-2T		5.80	4.10	PTB7	0.85	7.51	0.36	2.51	[504]
M-BNBP4P	698	5.34	3.93	PTB7-Th	0.78	14.62	0.62	7.06	[505]
BTcn-O	626	5.59	3.95	PBDB-T	0.95	5.03	0.34	1.62	[506]
BTcn-M	622	5.69	3.95	PBDB-T	0.98	12.03	0.50	5.89	[506]

film and then better charge transporting properties [506]. Finally, in this classification, **M-BNBP4P** based on organoboron core achieved the highest PCE of 7.06% in blend with PTB7-Th donor.

#### 4. Conclusions and Prospects

In summary, the developments of NFAs were rapidly growing for the last decade. Apparently, some of them have successfully outperformed the fullerene-based counterparts in several aspects mainly due to the superior advantages such as flexible molecular designs for designated spectral coverage and morphological controls, favorable frontier energy levels, leading to low energy loss in OSCs, and impressive stability. In this review, we have summarized polymeric NFAs by classifying them into several sub-categories based on their structural features. Among them, NDI and PDI-based polymeric NFAs showed promising advance in terms of efficiency. Their strong absorption, suitable energy levels, compact molecular packing and then induce nanosize blend morphology account for the success of giving high PCE. On the other side, there is an explosive progression in small molecules NFAs. Their well-defined molecular structures allow precisely modulating many physical characteristics, particularly, the control of favorable “face-on”-oriented morphology. More importantly, the flexibility on molecular designs provided SM NFAs a wide structural spectrum, therefore, a wide space for the selection of donor counterparts for better complementary absorption, well-matched energy levels, and suitable morphological compatibility, leading to different degrees of successes. It has been witnessed that the SM NFAs based on rigid

and co-planar multi-fused aromatic cores have accomplished great achievements. Especially, the SM NFAs stemmed from the IDT core, in which many structures such as dicyanomethylene, 3-alkyl rhodanine, 2-(1,1-dicyanomethylene)rhodanine, dicyanomethylene-3-indanone, fluoro/chloro substituted dicyanomethylene-3-indanone, (2-(6-oxo-5,6-dihydro-4H-cyclopenta[c]thiophen-4-lidene)malononitrile) and thiobarbituric acid have been implemented as end-capping functional groups for well tuning not only energy levels but also blend morphology, giving the highest PCEs ever reported. Based on currently obtained results, it can be optimistically envisioned that new NFAs with suitable molecular engineering may fully replace fullerene-based acceptors in polymeric and/or molecular OSCs in the near future. Thus, understanding the structure-property-performance relationship of developed NFAs is very important for stepping forward.

Based on this review, we have learned that the absorption and molar extinction coefficient of NFAs can be finely tailored by molecular engineering on suitable cores engaged with peripherals and/or building blocks of different electronic character for inducing strong intramolecular donor-acceptor charge transfer. This basic molecular design strategy for giving better NFAs may also simultaneously consider some fundamental criteria such as suitable molecular weight in case of polymeric NFAs, optimum twisted/fused or 3D (spiro- or star-shaped) molecular geometry for suitable D/A morphological adjustment in terms of size, shape, distribution and orientation for creating multi-directional charge transport channels. In addition, the judicious selection of donors is very important for the ongoing trends in NFA-based OSCs. In this

regard, we need to continue the parallel researches of developing more promising polymeric or SM donors. Besides the efforts invested on engineering device configuration and optimizing fabrication methods such as solvent selection, solvent and/or thermal annealing, from the organic material development point of view, the current status indicates NFAs have bright future, but definitely, there are a lot of challenges ahead waiting for the better solutions, particularly, the stability if we consider their practical commercialization. We hope this review has triggered some innovative ideas for designing and developing promising NFA candidates for conquering the future challenges.

## References

- [1] N.S. Sariciftci, L. Smilowitz, A.J. Heeger, F. Wudl, *Science* 258 (1992) 1474–1476.
- [2] S. Gunes, H. Neugebauer, N.S. Sariciftci, *Chem. Rev.* 107 (2007) 1324–1338.
- [3] B.C. Thompson, J.M.J. Fréchet, *Angew. Chem. Int. Ed.* 47 (2008) 58–77.
- [4] C.W. Tang, *Appl. Phys. Lett.* 48 (1986) 183–185.
- [5] P. Heremans, D. Cheyns, B.P. Rand, *Acc. Chem. Res.* 42 (2009) 1740–1747.
- [6] M. Li, K. Gao, X. Wan, Q. Zhang, B. Kan, R. Xia, F. Liu, X. Yang, H. Feng, W. Ni, Y. Wang, J. Peng, H. Zhang, Z. Liang, H.-L. Yip, X. Peng, Y. Cao, Y. Chen, *Nat. Photonics* 11 (2016) 85–90.
- [7] J. Zhao, Y. Li, G. Yang, K. Jiang, H. Lin, H. Ade, W. Ma, H. Yan, *Nat. Energy* 1 (2016) 15027.
- [8] J.L. Wang, Z. Wu, J.S. Miao, K.K. Liu, Z.F. Chang, R.B. Zhang, H. Bin Wu, Y. Cao, *Chem. Mater.* 27 (2015) 4338–4348.
- [9] S. Zhang, L. Ye, J. Hou, *Adv. Energy Mater.* 6 (2016) 1–20.
- [10] A. Mishra, P. Bäuerle, *Angew. Chem. Int. Ed.* 51 (2012) 2020–2067.
- [11] Y. Liu, C.-C. Chen, Z. Hong, J. Gao, Y. (Michael) Yang, H. Zhou, L. Dou, G. Li, Y. Yang, *Sci. Rep.* 3 (2013) 3356.
- [12] Y.H. Chen, L.Y. Lin, C.W. Lu, F. Lin, Z.Y. Huang, H.W. Lin, P.H. Wang, Y.H. Liu, K.T. Wong, J. Wen, D.J. Miller, S.B. Darling, *J. Am. Chem. Soc.* 134 (2012) 13616–13623.
- [13] C.L. Chochos, N. Tagmatarchis, V.G. Gregorius, *RSC Adv.* 3 (2013) 7160–7181.
- [14] N. Bauer, Q. Zhang, J. Zhao, L. Ye, J.-H. Kim, I. Constantinou, L. Yan, F. So, H. Ade, H. Yan, W. You, *J. Mater. Chem. 5* (2017) 4886–4893.
- [15] D. Baran, T. Kirchartz, S. Wheeler, S. Dimitrov, M. Abdelsamie, J. Gorman, R.S. Ashraf, S. Holliday, A. Wadsworth, N. Gasparini, P. Kaienburg, H. Yan, A. Amassian, C.J. Brabec, J.R. Durrant, I. McCulloch, *Energy Environ. Sci.* 9 (2016) 3783–3793.
- [16] Y. Shimata, M. Ide, M. Tashiro, M. Katouda, Y. Imamura, A. Saeki, *J. Phys. Chem. C* 120 (2016) 17887–17897.
- [17] S.H. Chou, H.W. Kang, S.T. Chang, K.Y. Wu, G.C. Bazan, C.L. Wang, H.L. Lin, J.H. Chang, H.W. Lin, Y.C. Huang, C.S. Tsao, K.T. Wong, *ACS Appl. Mater. Interfaces* 8 (2016) 18266–18276.
- [18] M. Sévignon, J. Papillon, E. Schulz, M. Lemaire, *Tetrahedron Lett.* 40 (1999) 5873–5876.
- [19] Y. Liang, Z. Xu, J. Xia, S.T. Tsai, Y. Wu, G. Li, C. Ray, L. Yu, *Adv. Mater.* 22 (2010) 135–138.
- [20] S.H. Liao, H.J. Jhuo, Y.S. Cheng, S.A. Chen, *Adv. Mater.* 25 (2013) 4766–4771.
- [21] M. Zhang, X. Guo, W. Ma, H. Ade, J. Hou, *Adv. Mater.* 27 (2015) 4655–4660.
- [22] D. Qian, L. Ye, M. Zhang, Y. Liang, L. Li, Y. Huang, X. Guo, S. Zhang, Z. Tan, J. Hou, *Macromolecules* 45 (2012) 9611–9617.
- [23] J. Liu, S. Chen, D. Qian, B. Gautam, G. Yang, J. Zhao, J. Bergqvist, F. Zhang, W. Ma, H. Ade, O. Inganäs, K. Gundogdu, F. Gao, H. Yan, *Nat. Energy* 1 (2016) 16089.
- [24] X. Zhan, A. Facchetti, S. Barlow, T.J. Marks, M.A. Ratner, M.R. Wasielewski, S.R. Marder, *Adv. Mater.* 23 (2011) 268–284.
- [25] P. Sonar, J.P.F. Lim, K.L. Chan, *Energy Environ. Sci.* 4 (2011) 1558–1574.
- [26] Y. Lin, X. Zhan, *Mater. Horiz.* 1 (2014) 470–488.
- [27] C. Zhan, X. Zhang, J. Yao, *RSC Adv.* 5 (2015) 93002–93026.
- [28] C.B. Nielsen, S. Holliday, H.-Y. Chen, S.J. Cryer, I. McCulloch, *Acc. Chem. Res.* 48 (2015) 2803–2812.
- [29] W. Chen, Q. Zhang, *J. Mater. Chem. C* 5 (2017) 1275–1302.
- [30] G. Yu, J. Hummelen, F. Wudl, A.J. Heeger, *Science* 270 (1995) 1789–1791.
- [31] T. Kim, J.-H. Kim, T.E. Kang, C. Lee, H. Kang, M. Shin, C. Wang, B. Ma, U. Jeong, T.-S. Kim, B.J. Kim, *Nat. Commun.* 6 (2015) 8547.
- [32] C. Lee, H. Kang, W. Lee, T. Kim, K.H. Kim, H.Y. Woo, C. Wang, B.J. Kim, *Adv. Mater.* 27 (2015) 2466–2471.
- [33] G. Shen, X. Li, X. Wu, Y. Wang, H. Shan, J. Xu, X. Liu, Z. xiang Xu, F. Chen, Z.K. Chen, *Org. Electron.* 46 (2017) 203–210.
- [34] C. Lee, H. Kang, W. Lee, T. Kim, K.H. Kim, H.Y. Woo, C. Wang, B.J. Kim, *Adv. Mater.* 27 (2015) 2466–2471.
- [35] H.-H. Cho, T. Kim, K. Kim, C. Lee, F.S. Kim, B.J. Kim, *J. Mater. Chem. A* 5 (2017) 5449–5459.
- [36] Y.J. Hwang, B.A.E. Courtright, A.S. Ferreira, S.H. Tolbert, S.A. Jenekhe, *Adv. Mater.* 27 (2015) 4578–4584.
- [37] J. Oh, K. Kranthiraja, C. Lee, K. Gunasekar, S. Kim, B. Ma, B.J. Kim, S.H. Jin, *Adv. Mater.* 28 (2016) 10016–10023.
- [38] T. Earmme, Y.J. Hwang, N.M. Murari, S. Subramaniyan, S.A. Jenekhe, *J. Am. Chem. Soc.* 135 (2013) 14960–14963.
- [39] J.R. Moore, S. Albert-Seifried, A. Rao, S. Massip, B. Watts, D.J. Morgan, R.H. Friend, C.R. McNeill, H. Sirringhaus, *Adv. Energy Mater.* 1 (2011) 230–240.
- [40] N. Zhou, A.S. Dudnik, T.I.N.G. Li, E.F. Manley, T.J. Aldrich, P. Guo, H.C. Liao, Z. Chen, L.X. Chen, R.P.H. Chang, A. Facchetti, M. Olvera De La Cruz, T.J. Marks, *J. Am. Chem. Soc.* 138 (2016) 1240–1251.
- [41] D. Mori, H. Benten, I. Okada, H. Ohkita, S. Ito, *Adv. Energy Mater.* 4 (2014) 1301006.
- [42] Y. Lei, J. Sun, J. Yuan, J. Gu, G. Ding, W. Ma, *J. Mater. Sci. Technol.* 33 (2017) 411–417.
- [43] C. Mu, P. Liu, W. Ma, K. Jiang, J. Zhao, K. Zhang, Z. Chen, Z. Wei, Y. Yi, J. Wang, S. Yang, F. Huang, A. Facchetti, H. Ade, H. Yan, *Adv. Mater.* 26 (2014) 7224–7230.
- [44] L. Ye, X. Jiao, M. Zhou, S. Zhang, H. Yao, W. Zhao, A. Xia, H. Ade, J. Hou, *Adv. Mater.* 27 (2015) 6046–6054.
- [45] L. Gao, Z.G. Zhang, L. Xue, J. Min, J. Zhang, Z. Wei, Y. Li, *Adv. Mater.* 28 (2016) 1884–1890.
- [46] N. Zhou, H. Lin, S.J. Lou, X. Yu, P. Guo, E.F. Manley, S. Loser, P. Hartnett, H. Huang, M.R. Wasielewski, L.X. Chen, R.P.H. Chang, A. Facchetti, T.J. Marks, *Adv. Energy Mater.* 4 (2014) 1300785.
- [47] Y. Tang, C.R. McNeill, *J. Polym. Sci. Part B Polym. Phys.* 51 (2013) 403–409.
- [48] D. Mori, H. Benten, I. Okada, H. Ohkita, S. Ito, *Energy Environ. Sci.* 7 (2014) 2939–2943.
- [49] W. Lee, C. Lee, H. Yu, D.J. Kim, C. Wang, H.Y. Woo, J.H. Oh, B.J. Kim, *Adv. Funct. Mater.* 26 (2016) 1543–1553.
- [50] C. Li, A. Zhang, Z. Wang, F. Liu, Y. Zhou, T.P. Russell, Y. Li, W. Li, *RSC Adv.* 6 (2016) 35677–35683.
- [51] J. Yuan, W. Ma, *Org. Electron.* 39 (2016) 279–287.
- [52] Z. Tang, B. Liu, A. Melianas, J. Bergqvist, W. Tress, Q. Bao, D. Qian, O. Inganäs, F. Zhang, *Adv. Mater.* 27 (2015) 1900–1907.
- [53] J.W. Jung, T.P. Russell, W.H. Jo, *Chem. Mater.* 27 (2015) 4865–4870.
- [54] S.-Y. Liu, J.W. Jung, C.-Z. Li, J. Huang, J. Zhang, H. Chen, A.K.-Y. Jen, *J. Mater. Chem. A* 3 (2015) 22162–22169.
- [55] B. Fan, L. Ying, Z. Wang, B. He, X.-F. Jiang, F. Huang, Y. Cao, *Energy Environ. Sci.* 10 (2017) 1243–1251.
- [56] B. Fan, L. Ying, P. Zhu, F. Pan, F. Liu, J. Chen, F. Huang, Y. Cao, *Adv. Mater.* 29 (2017) 1703906.
- [57] J. Jung, W. Lee, C. Lee, H. Ahn, B.J. Kim, *Adv. Energy Mater.* 6 (2016) 1600504.
- [58] Y.J. Hwang, G. Ren, N.M. Murari, S.A. Jenekhe, *Macromolecules* 45 (2012) 9056–9062.
- [59] E. Zhou, J. Cong, M. Zhao, L. Zhang, K. Hashimoto, K. Tajima, *Chem. Commun.* 48 (2012) 5283–5285.
- [60] E. Zhou, J. Cong, K. Hashimoto, K. Tajima, *Adv. Mater.* 25 (2013) 6991–6996.
- [61] X.Z. Li, P. Sun, Y.L. Wang, H.Q. Shan, J.J. Xu, X. Song, Z.X. Xu, Z.K. Chen, *J. Mater. Chem. C* 4 (2016) 2106–2110.
- [62] J. Choi, K.H. Kim, H. Yu, C. Lee, H. Kang, I. Song, Y. Kim, J.H. Oh, B.J. Kim, *Chem. Mater.* 27 (2015) 5230–5237.
- [63] S.X. Dai, S.M. Zhang, Q.D. Ling, X.W. Zhan, *Chin. J. Polym. Sci.* 35 (2017) 230–238.
- [64] L. Xue, Y. Yang, H. Bin, Z.G. Zhang, J. Zhang, Y.X. Yang, Y. Li, *J. Polym. Sci. Part A Polym. Chem.* 55 (2017) 1757–1764.
- [65] M. Yuan, M.M. Durban, P.D. Kaziaroff, D.F. Zeigler, A.H. Rice, Y. Segawa, C.K. Luscombe, *J. Polym. Sci. Part A Polym. Chem.* 51 (2013) 4061–4069.
- [66] L. Xue, Y. Yang, Z.G. Zhang, J. Zhang, L. Gao, H. Bin, Y.X. Yang, Y. Li, *Chem. -Asian J.* 11 (2016) 2785–2791.
- [67] J.W. Jung, J.W. Jo, C.-C. Chueh, F. Liu, W.H. Jo, T.P. Russell, A.K.-Y. Jen, *Adv. Mater.* 27 (2015) 3310–3317.
- [68] M.A. Uddin, Y. Kim, R. Younts, W. Lee, B. Gautam, J. Choi, C. Wang, K. Gundogdu, B.J. Kim, H.Y. Woo, *Macromolecules* 49 (2016) 6374–6383.
- [69] P. Deng, C.H.Y. Ho, Y. Lu, H.-W. Li, S.-W. Tsang, S.K. So, B.S. Ong, *Chem. Commun.* 53 (2017) 3249–3252.
- [70] K.D. Deshmukh, R. Matsidik, S.K.K. Prasad, N. Chandrasekaran, A. Welford, L. A. Connal, A.C.Y. Liu, E. Gann, L. Thomsen, D. Kabra, J.M. Hodgkiss, M. Sommer, C.R. McNeill, *ACS Appl. Mater. Interfaces* 10 (2018) 955–969.
- [71] X. Wang, L. Lv, W. Gu, X. Wang, T. Dong, Z. Yang, H. Cao, H. Huang, *Dyes Pigm.* 140 (2017) 141–149.
- [72] L. Ye, X. Jiao, H. Zhang, S. Li, H. Yao, H. Ade, J. Hou, *Macromolecules* 48 (2015) 7156–7163.
- [73] L. Xue, Y. Yang, Z.-G. Zhang, X. Dong, L. Gao, H. Bin, J. Zhang, Y. Yang, Y. Li, *J. Mater. Chem. A* 4 (2016) 5810–5816.
- [74] F. Liu, H. Li, Y. Wu, C. Gu, H. Fu, *RSC Adv.* 5 (2015) 92151–92158.
- [75] Y. Li, Y. Yang, X. Bao, M. Qiu, Z. Liu, N. Wang, G. Zhang, R. Yang, D. Zhang, *J. Mater. Chem. C* 4 (2016) 185–192.
- [76] C. Weng, L. Gao, Z. Zhang, Z. Liu, S. Tan, Y. Li, *J. Polym. Sci. Part B Polym. Phys.* 55 (2017) 990–996.
- [77] K. Nakabayashi, H. Mori, *Macromolecules* 45 (2012) 9618–9625.
- [78] M. Schubert, D. Dolfen, J. Frisch, S. Roland, R. Steyrleuthner, B. Stiller, Z. Chen, U. Scherf, N. Koch, A. Facchetti, D. Neher, *Adv. Energy Mater.* 2 (2012) 369–380.
- [79] Z. Li, X. Xu, W. Zhang, X. Meng, W. Ma, A. Yartsev, O. Inganäs, M.R. Andersson, R.A.J. Janssen, E. Wang, *J. Am. Chem. Soc.* 138 (2016) 10935–10944.
- [80] Z. Li, W. Zhang, X. Xu, Z. Genene, D.D.C. Rasi, W. Mammo, A. Yartsev, M.R. Andersson, R.A.J. Janssen, E. Wang, *Adv. Energy Mater.* 7 (2017) 1602722.
- [81] X. Li, P. Sun, Y. Wang, H. Shan, J. Xu, C. You, Z. Xu, Z.-K. Chen, *Polym. Chem.* 7 (2016) 2230–2238.
- [82] Y. Kim, H.-H. Cho, T. Kim, K. Liao, B.J. Kim, *Polym. J.* 48 (2016) 517–524.
- [83] R. Xie, Z. Chen, Y. Liu, Z. Wang, Z. Chen, L. Ying, F. Huang, Y. Cao, *Chem. Commun.* (2018), doi:<http://dx.doi.org/10.1039/c7cc09348a>.

- [84] E. Zhou, J. Cong, Q. Wei, K. Tajima, C. Yang, K. Hashimoto, *Angew. Chem. Int. Ed.* 50 (2011) 2799–2803.
- [85] Y. Guo, Y. Li, O. Awartani, H. Han, G. Zhang, H. Ade, H. Yan, D. Zhao, *Mater. Chem. Front.* 1 (2017) 1362–1368.
- [86] Y. Guo, Y. Li, O. Awartani, J. Zhao, H. Han, H. Ade, D. Zhao, H. Yan, *Adv. Mater.* (2016) 8483–8489.
- [87] Y. Zhou, T. Kurosawa, W. Ma, Y. Guo, L. Fang, K. Vandewal, Y. Diao, C. Wang, Q. Yan, J. Reinsch, J. Mei, A.L. Appleton, G.I. Koleilat, Y. Gao, S.C.B. Mannsfeld, A. Salleo, H. Ade, D. Zhao, Z. Bao, *Adv. Mater.* 26 (2014) 3767–3772.
- [88] E. Kozma, D. Kotowski, F. Bertini, S. Luzzati, M. Catellani, *Polymer* 51 (2010) 2264–2270.
- [89] J. Hou, S. Zhang, T.L. Chen, Y. Yang, *Chem. Commun.* 49 (2008) 6034–6036.
- [90] X. Zhan, Z. Tan, B. Domercq, Z. An, X. Zhang, S. Barlow, Y. Li, D. Zhu, B. Kippelen, S.R. Marder, *J. Am. Chem. Soc.* 129 (2007) 7246–7247.
- [91] P. Cheng, L. Ye, X. Zhao, J. Hou, Y. Li, X. Zhan, *Energy Environ. Sci.* 7 (2014) 1351–1356.
- [92] X. Zhan, Z. Tan, E. Zhou, Y. Li, R. Misra, A. Grant, B. Domercq, X.-H. Zhang, Z. An, X. Zhang, S. Barlow, B. Kippelen, S.R. Marder, *J. Mater. Chem.* 19 (2009) 5794–5803.
- [93] Z. Tan, E. Zhou, X. Zhan, X. Wang, Y. Li, S. Barlow, S.R. Marder, *Appl. Phys. Lett.* 93 (2008) 073309.
- [94] S. Dai, Y. Lin, P. Cheng, Y. Wang, X. Zhao, Q. Ling, X. Zhan, *Dyes Pigm.* 114 (2015) 283–289.
- [95] Y. Zhang, X. Guo, W. Su, B. Guo, Z. Xu, M. Zhang, Y. Li, *Org. Electron.* 41 (2017) 49–55.
- [96] H. Chang, Z. Chen, X. Yang, Q. Yin, J. Zhang, L. Ying, X.F. Jiang, B. Xu, F. Huang, Y. Cao, *Org. Electron.* 45 (2017) 227–233.
- [97] I.H. Jung, D. Zhao, J. Jang, W. Chen, E.S. Landry, L. Lu, D.V. Talapin, L. Yu, *Chem. Mater.* 27 (2015) 5941–5948.
- [98] C.W. Ge, C.Y. Mei, J. Ling, J.T. Wang, F.G. Zhao, L. Liang, H.J. Li, Y.S. Xie, W.S. Li, J. *Polym. Sci. Part A Polym. Chem.* 52 (2014) 1200–1215.
- [99] Y. Zhou, Q. Yan, Y.-Q. Zheng, J.-Y. Wang, D. Zhao, J. Pei, *J. Mater. Chem. A* 1 (2013) 6609–6613.
- [100] F. Yang, C. Li, G.T. Feng, X.D. Jiang, A.D. Zhang, W.W. Li, *Chin. J. Polym. Sci.* 35 (2017) 239–248.
- [101] E. Zhou, K. Tajima, C. Yang, K. Hashimoto, *J. Mater. Chem.* 20 (2010) 2362–2368.
- [102] S. Sharma, N.B. Kolhe, V. Gupta, V. Bharti, A. Sharma, R. Datt, S. Chand, S.K. Asha, *Macromolecules* 49 (2016) 8113–8125.
- [103] S. Dai, S. Huang, H. Yu, Q. Ling, X. Zhan, *J. Polym. Sci. Part A Polym. Chem.* 55 (2017) 682–689.
- [104] Y.J. Hwang, T. Earmme, B.A.E. Courtright, F.N. Eberle, S.A. Jenekhe, *J. Am. Chem. Soc.* 137 (2015) 4424–4434.
- [105] W. Zhou, Z.G. Zhang, L. Ma, Y. Li, X. Zhan, *Sol. Energy Mater. Sol. Cells* 112 (2013) 13–19.
- [106] Y. Jiang, L. Lu, M. Yang, C. Zhan, Z. Xie, F. Verpoort, S. Xiao, *Polym. Chem.* 4 (2013) 5612–5620.
- [107] Y. Guo, Y. Li, O. Awartani, H. Han, J. Zhao, H. Ade, H. Yan, D. Zhao, *Adv. Mater.* 29 (2017) 1700309.
- [108] M. Liu, J. Yang, Y. Yin, Y. Zhang, E. Zhou, F. Guo, L. Zhao, *J. Mater. Chem. A* 6 (2018) 414–422.
- [109] X. Jiang, Y. Xu, X. Wang, F. Yang, A. Zhang, C. Li, W. Ma, W. Li, *Polym. Chem.* 8 (2017) 3300–3306.
- [110] Z. Liang, R.A. Cormier, A.M. Nardes, B.A. Gregg, *Synth. Met.* 161 (2011) 1014–1021.
- [111] J. Zhang, S. Xie, X. Zhang, Z. Lu, H. Xiao, C. Li, G. Li, X. Xu, X. Chen, Z. Bo, *Chem. Commun.* 53 (2017) 537–540.
- [112] J.A. Mikroyannidis, M.M. Stylianakis, G.D. Sharma, P. Balraju, M.S. Roy, *J. Phys. Chem. C* 113 (2009) 7904–7912.
- [113] K.S. Kim, S. Jeong, C. Kim, H. Kim, Y.S. Yang, J.H. Kim, Y. Kwon, W.P. Tai, Y.S. Han, *Mol. Cryst. Liq. Cryst.* 532 (2010) 445–454.
- [114] C.R. McNeill, A. Abrusci, J. Zaumseil, R. Wilson, M.J. McKiernan, J.H. Burroughes, J.J.M. Halls, N.C. Greenham, R.H. Friend, *Appl. Phys. Lett.* 90 (2007) 193506.
- [115] C.R. McNeill, J.J.M. Halls, R. Wilson, G.L. Whiting, S. Berkebile, M.G. Ramsey, R. H. Friend, N.C. Greenham, *Adv. Funct. Mater.* 18 (2008) 2309–2321.
- [116] D. Mori, H. Benten, H. Ohkita, S. Ito, K. Miyake, *ACS Appl. Mater. Interfaces* 4 (2012) 3325–3329.
- [117] Y. Fu, B. Wang, J. Qu, Y. Wu, W. Ma, Y. Geng, Y. Han, Z. Xie, *Adv. Funct. Mater.* 26 (2016) 5922–5929.
- [118] Q. Yang, H. Song, B. Gao, Y. Wang, Y. Fu, J. Yang, Z. Xie, L. Wang, *RSC Adv.* 4 (2014) 12579–12585.
- [119] M.-F.F. Falzon, M.M. Wienk, R.A.J. Janssen, *J. Phys. Chem. C* 115 (2011) 3178–3187.
- [120] M.C. Gwinner, T.J.K. Brenner, J.-K. Lee, C. Newby, C.K. Ober, C.R. McNeill, H. Sirringhaus, *J. Mater. Chem.* 22 (2012) 4436–4439.
- [121] Y. Cao, T. Lei, J. Yuan, J.-Y. Wang, J. Pei, *Polym. Chem.* 4 (2013) 5228–5236.
- [122] S. Liu, X. Song, S. Thomas, Z. Kan, F. Cruciani, F. Laquai, J.L. Bredas, P.M. Beaujuge, *Adv. Energy Mater.* 7 (2017) 1602574.
- [123] M.-F. Falzon, A.P. Zonkelt, M.M. Wienk, R.A.J. Janssen, *Phys. Chem. Chem. Phys.* 13 (2011) 8931–8939.
- [124] W. Li, W.S.C. Roelofs, M. Turbiez, M.M. Wienk, R.A.J. Janssen, *Adv. Mater.* 26 (2014) 3304–3309.
- [125] Y. Yu, S. Zhou, X. Wang, C. Li, G. Feng, Y. Wu, W. Ma, W. Li, *Org. Electron.* 47 (2017) 133–138.
- [126] A. Zhang, Q. Wang, R.A.A. Bovee, C. Li, J. Zhang, Y. Zhou, Z. Wei, Y. Li, R.A.J. Janssen, Z. Wang, W. Li, *J. Mater. Chem. A* 4 (2016) 7736–7745.
- [127] Z. Li, X. Xu, W. Zhang, Z. Genene, W. Mammo, A. Yartsev, M.R. Andersson, R.A.J. Janssen, E. Wang, *J. Mater. Chem. A* 5 (2017) 11693–11700.
- [128] H.-Y. Chen, M. Nikolla, A. Wadsworth, W. Yue, A. Onwubiko, M. Xiao, A.J.P. White, D. Baran, H. Sirringhaus, I. McCulloch, *Macromolecules* 51 (2018) 71–79.
- [129] Z. Ding, X. Long, C. Dou, J. Liu, L. Wang, *Chem. Sci.* 7 (2016) 6197–6202.
- [130] R. Zhao, Z. Bi, C. Dou, W. Ma, Y. Han, J. Liu, L. Wang, *Macromolecules* 50 (2017) 3171–3178.
- [131] Z. Ding, X. Long, B. Meng, K. Bai, C. Dou, J. Liu, L. Wang, *Nano Energy* 32 (2017) 216–224.
- [132] X. Long, Z. Ding, C. Dou, J. Zhang, J. Liu, L. Wang, *Adv. Mater.* (2016) 6504–6508.
- [133] C. Dou, X. Long, Z. Ding, Z. Xie, J. Liu, L. Wang, *Angew. Chem. Int. Ed.* 55 (2016) 1436–1440.
- [134] Z. Zhang, Z. Ding, X. Long, C. Dou, J. Liu, L. Wang, *J. Mater. Chem. C* 5 (2017) 6812–6819.
- [135] X. Long, Z. Ding, C. Dou, L. Wang, *Mater. Chem. Front.* 1 (2017) 852–858.
- [136] R. Zhao, Y. Min, C. Dou, J. Liu, L. Wang, *Chem. - A Eur. J.* 23 (2017) 9486–9490.
- [137] R.Y. Zhao, C.D. Dou, J. Liu, L.X. Wang, *Chin. J. Polym. Sci.* 35 (2017) 198–206.
- [138] X. Long, N. Wang, Z. Ding, C. Dou, J. Liu, L. Wang, *J. Mater. Chem. C* 4 (2016) 9961–9967.
- [139] Y. Greenwald, X. Xu, M. Fourmigu, G. Srdanov, C. Koss, F. Wudl, A.J. Heeger, *J. Polym. Sci. Part A Polym. Chem.* 36 (1998) 3115–3120.
- [140] T.W. Holcombe, C.H. Woo, D.F.J. Kavulak, B.C. Thompson, J.M.J. Fréchet, *J. Am. Chem. Soc.* 131 (2009) 14160–14161.
- [141] T. Kietzke, H. Ho, D. Neher, *Chem. Mater.* 17 (2005) 6532–6537.
- [142] G. Sang, Y. Zou, Y. Huang, G. Zhao, Y. Yang, Y. Li, *Appl. Phys. Lett.* 94 (2009) 193302.
- [143] J.J.M. Halls, C.A. Walsh, N.C. Greenham, E.A. Marseglia, R.H. Friend, S.C. Moratti, A.B. Holmes, *Nature* 376 (1995) 498–500.
- [144] M.M. Koetse, J. Sweelssen, K.T. Hoekerd, H.F.M. Schoo, S.C. Veenstra, J.M. Kroon, X. Yang, J. Loos, *Appl. Phys. Lett.* 88 (2006) 88–91.
- [145] C.L. Chochos, S.P. Economopoulos, V. Deimedev, V.G. Gregorius, M.T. Lloyd, G. G. Malliaras, J.K. Kallitsis, *J. Phys. Chem. C* 111 (2007) 10732–10740.
- [146] S.C. Chen, Q. Zheng, Q. Zhang, D. Cai, J. Wang, Z. Yin, C. Tang, *J. Polym. Sci. Part A Polym. Chem.* 51 (2013) 1999–2005.
- [147] S. Zhang, J. Liu, Y. Han, L. Wang, *Macromol. Chem. Phys.* 218 (2017) 1600606.
- [148] Y. Yang, J. Wang, X. Zhan, X. Chen, *RSC Adv.* 7 (2017) 19990–19995.
- [149] R. Stalder, J. Mei, J. Subbiah, C. Grand, L.A. Estrada, F. So, J.R. Reynolds, *Macromolecules* 44 (2011) 6303–6310.
- [150] R.G. Brandt, W. Yue, T.R. Andersen, T.T. Larsen-Olsen, M. Hinge, E. Bundgaard, F.C. Krebs, D. Yu, *J. Mater. Chem. C* 3 (2015) 1633–1639.
- [151] J. Wei, Q. Tu, Q. Zheng, *Dyes Pigm.* 144 (2017) 133–141.
- [152] R. Zhao, C. Dou, Z. Xie, J. Liu, L. Wang, *Angew. Chem. Int. Ed.* 55 (2016) 5313–5317.
- [153] S. Liu, Z. Kan, S. Thomas, F. Cruciani, J.L. Brédas, P.M. Beaujuge, *Angew. Chem. Int. Ed.* 55 (2016) 12996–13000.
- [154] S. Liu, Y. Firdaus, S. Thomas, Z. Kan, F. Cruciani, S. Lopatin, J. Bredas, P.M. Beaujuge, *Angew. Chemie. Int. Ed.* 130 (2018) 540–544.
- [155] Y. Kim, C.E. Song, S. Moon, E. Lim, V.A. Online, Y. Kim, C.E. Song, S. Moon, E. Lim, *Chem. Commun.* 50 (2014) 8235–8238.
- [156] Y. Kim, C.E. Song, S.-J. Moon, E. Lim, *RSC Adv.* 5 (2015) 62739–62746.
- [157] K.N. Winzenberg, P. Kemppinen, F.H. Scholes, G.E. Collis, Y. Shu, T.B. Singh, A. Bilic, C.M. Forsyth, S.E. Watkins, *Chem. Commun.* 49 (2013) 6307–6309.
- [158] M. Li, Y. Liu, W. Ni, F. Liu, H. Feng, Y. Zhang, T. Liu, H. Zhang, X. Wan, B. Kan, Q. Zhang, T.P. Russell, Y. Chen, *J. Mater. Chem. A* 4 (2016) 10409–10413.
- [159] H. Zhang, Y. Liu, Y. Sun, M. Li, W. Ni, Q. Zhang, X. Wan, Y. Chen, *Sci. China Chem.* 60 (2017) 366–369.
- [160] J. Zhang, B. Zhao, Y. Mi, H. Liu, Z. Guo, G. Bie, W. Wei, C. Gao, Z. An, *Dyes Pigm.* 140 (2017) 261–268.
- [161] E. Lim, *Bull. Korean Chem. Soc.* 38 (2017) 285–288.
- [162] P.E. Schwenn, K. Gui, A.M. Nardes, K.B. Krueger, K.H. Lee, K. Mutkins, H. Rubinstein-Dunlop, P.E. Shaw, N. Kopidakis, P.L. Burn, P. Meredith, *Adv. Energy Mater.* 1 (2011) 73–81.
- [163] K. Wang, Y. Firdaus, M. Babics, F. Cruciani, Q. Saleem, A.E. Labban, M.A. Alamoudi, T. Marszałek, W. Pisula, F. Laquai, P.M. Beaujuge, *Chem. Mater.* 28 (2016) 2200–2208.
- [164] S. Holliday, R.S. Ashraf, C.B. Nielsen, M. Kirkus, J.A. Röhr, C.-H. Tan, E. Collado-Fregoso, A.-C. Knall, J.R. Durrant, J. Nelson, I. McCulloch, *J. Am. Chem. Soc.* 137 (2015) 898–904.
- [165] Suman, V. Gupta, A. Bagui, S.P. Singh, *Adv. Funct. Mater.* 27 (2017) 1603820.
- [166] Suman, A. Bagui, V. Gupta, K.K. Maurya, S.P. Singh, *J. Phys. Chem. C* 120 (2016) 24615–24622.
- [167] Suman, A. Bagui, R. Dutt, V. Gupta, S.P. Singh, *Chem. Commun.* 53 (2017) 12790–12793.
- [168] H. Fan, T. Vergote, S. Xu, S. Chen, C. Yang, X. Zhu, *Mater. Chem. Front.* (2018), doi:<http://dx.doi.org/10.1039/C7QM00585G>.
- [169] A. Gupta, X. Wang, D. Srivani, B. Alford, V. Chellappan, A. Bilic, H. Patil, L.A. Jones, S.V. Bhosale, P. Sonar, S.V. Bhosale, *Asian J. Org. Chem.* 4 (2015) 800–807.
- [170] T.T. Do, K. Rundel, Q. Gu, E. Gann, S. Manzhos, K. Feron, J. Bell, C.R. McNeill, P. Sonar, *New J. Chem.* 41 (2017) 2899–2909.
- [171] H. Patil, W.X. Zu, A. Gupta, V. Chellappan, A. Bilic, P. Sonar, A. Ranananaware, S.V. Bhosale, S.V. Bhosale, *Phys. Chem. Chem. Phys.* 16 (2014) 23837–23842.

- [172] H. Shi, W. Fu, M. Shi, J. Ling, H. Chen, *J. Mater. Chem. A* 3 (2015) 1902–1905.
- [173] S. Li, J. Yan, C.-Z. Li, F. Liu, M. Shi, H. Chen, T.P. Russell, *J. Mater. Chem. A* 4 (2016) 3777–3783.
- [174] T.T. Do, H.D. Pham, S. Manzhos, J.M. Bell, P. Sonar, *ACS Appl. Mater. Interfaces* 9 (2017) 16967–16976.
- [175] Y. Zhang, Y. Xiao, Y. Xie, L. Zhu, D. Shi, C. Cheng, *Org. Electron. Phys. Mater. Appl.* 21 (2015) 184–191.
- [176] Y. Zhang, X. Guo, B. Guo, W. Su, M. Zhang, Y. Li, *Adv. Funct. Mater.* 27 (2017) 1603892.
- [177] J. Wang, S. Dai, Y. Yao, P. Cheng, Y. Lin, X. Zhan, *Dyes Pigm.* 123 (2015) 16–25.
- [178] N. Qiu, X. Yang, H. Zhang, X. Wan, C. Li, F. Liu, H. Zhang, T.P. Russell, Y. Chen, *Chem. Mater.* 28 (2016) 6770–6778.
- [179] S.Y. Park, G.E. Park, S. Choi, J.H. Lee, D.H. Lee, M.J. Cho, D.H. Choi, *Dyes Pigm.* 146 (2017) 226–233.
- [180] M. Chang, Y. Wang, N. Qiu, Y.-Q.-Q. Yi, X. Wan, C. Li, Y. Chen, *Chin. J. Chem.* 35 (2017) 1687–1692.
- [181] X.F. Wu, W.F. Fu, Z. Xu, M. Shi, F. Liu, H.Z. Chen, J.H. Wan, T.P. Russell, *Adv. Funct. Mater.* 25 (2015) 5954–5966.
- [182] S. Li, W. Liu, M. Shi, J. Mai, T.-K. Lau, J. Wan, X. Lu, C.-Z. Li, H. Chen, *Energy Environ. Sci.* 9 (2016) 604–610.
- [183] C. Yuan, W. Liu, M. Shi, S. Li, Y. Wang, H. Chen, C.Z. Li, H. Chen, *Dyes Pigm.* 143 (2017) 217–222.
- [184] G. Zhang, G. Yang, H. Yan, J.H. Kim, H. Ade, W. Wu, X. Xu, Y. Duan, Q. Peng, *Adv. Mater.* 29 (2017) 1606054.
- [185] Q. Yan, Y. Zhou, Y.-Q. Zheng, J. Pei, D. Zhao, *Chem. Sci.* 4 (2013) 4389–4394.
- [186] J. Zhao, Y. Li, H. Lin, Y. Liu, K. Jiang, C. Mu, T. Ma, J.Y. Lin Lai, H. Hu, D. Yu, H. Yan, *Energy Environ. Sci.* 8 (2015) 520–525.
- [187] C. Yu, Y. Xu, S. Liang, X. Jiang, G. Feng, C. Li, W. Li, *Chin. Chem. Lett.* (2017), doi: <http://dx.doi.org/10.1016/j.clet.2017.08.016>.
- [188] L. Yang, Y. Chen, S. Chen, T. Dong, W. Deng, L. Lv, S. Yang, H. Yan, H. Huang, *J. Power Sources* 324 (2016) 538–546.
- [189] X. Zhou, Q. Sun, W. Li, Y. Zhao, Z. Luo, F. Zhang, C. Yang, *Dyes Pigm.* 146 (2017) 151–158.
- [190] J. Yi, Y. Wang, Q. Luo, Y. Lin, H. Tan, H. Wang, C.-Q. Ma, *Chem. Commun.* 52 (2016) 1649–1652.
- [191] J. Lee, R. Singh, D.H. Sin, H.G. Kim, K.C. Song, K. Cho, *Adv. Mater.* 28 (2016) 69–76.
- [192] S. Jinnai, Y. Ie, Y. Kashimoto, H. Yoshida, M. Karakawa, Y. Aso, *J. Mater. Chem. A* 5 (2017) 3932–3938.
- [193] R. Singh, J. Lee, M. Kim, P.E. Keivanidis, K. Cho, *J. Mater. Chem. A* 5 (2017) 210–220.
- [194] K.C. Song, R. Singh, J. Lee, D.H. Sin, H. Lee, K. Cho, *J. Mater. Chem. C* 4 (2016) 10610–10615.
- [195] D. Xia, D. Gehrig, X. Guo, M. Baumgarten, F. Laquai, K. Müllen, *J. Mater. Chem. A* 3 (2015) 11086–11092.
- [196] H.U. Kim, J.-H. Kim, H. Suh, J. Kwak, D. Kim, A.C. Grimsdale, S.C. Yoon, D.-H. Hwang, *Chem. Commun.* 49 (2013) 10950–10952.
- [197] O.Y. Park, H.U. Kim, J.H. Kim, J.B. Park, J. Kwak, W.S. Shin, S.C. Yoon, D.H. Hwang, *Sol. Energy Mater. Sol. Cells* 116 (2013) 275–282.
- [198] Y. Fan, S. Barlow, S. Zhang, B. Lin, S.R. Marder, *RSC Adv.* 6 (2016) 70493–70500.
- [199] Y. Lu, B. Wu, P. Deng, F. Zhu, B.S. Ong, *New J. Chem.* 41 (2017) 6822–6827.
- [200] Y. Zhao, H. Wang, S. Xia, F. Zhou, Z. Luo, J. Luo, F. He, C. Yang, *Chem. – A Eur. J.* (2018), doi: <http://dx.doi.org/10.1002/chem.201705480>.
- [201] F.G. Brunetti, X. Gong, M. Tong, A.J. Heeger, F. Wudl, *Angew. Chem. Int. Ed.* 49 (2010) 532–536.
- [202] X. Gong, M. Tong, F.G. Brunetti, J. Seo, Y. Sun, D. Moses, F. Wudl, A.J. Heeger, *Adv. Mater.* 23 (2011) 2272–2277.
- [203] Y. Lin, Q. He, F. Zhao, L. Huo, J. Mai, X. Lu, C.J. Su, T. Li, J. Wang, J. Zhu, Y. Sun, C. Wang, X. Zhan, *J. Am. Chem. Soc.* 138 (2016) 2973–2976.
- [204] L. Yang, S. Zhang, C. He, J. Zhang, H. Yao, Y. Yang, Y. Zhang, W. Zhao, J. Hou, *J. Am. Chem. Soc.* 139 (2017) 1958–1966.
- [205] H. Bin, Y. Yang, Z.G. Zhang, L. Ye, M. Ghasemi, S. Chen, Y. Zhang, C. Zhang, C. Sun, L. Xue, C. Yang, H. Ade, Y. Li, *J. Am. Chem. Soc.* 139 (2017) 5085–5094.
- [206] S. Holliday, R.S. Ashraf, A. Wadsworth, D. Baran, S.A. Yousef, C.B. Nielsen, C.-H. Tan, S.D. Dimitrov, Z. Shang, N. Gasparini, M. Alamoudi, F. Laquai, C.J. Brabec, A. Salleo, J.R. Durrant, I. McCulloch, *Nat. Commun.* 7 (2016) 11585.
- [207] S. Badgujar, C.E. Song, S.Oh, W.S. Shin, S.-J. Moon, J.-C. Lee, I.H. Jung, S.K. Lee, *J. Mater. Chem. A* 4 (2016) 16335–16340.
- [208] X. Liu, P. Cai, D. Chen, J. Chen, S. Su, Y. Cao, *Sci. China Chem.* 57 (2014) 973–981.
- [209] S. Chen, Y. Liu, L. Zhang, P.C.Y. Chow, Z. Wang, G. Zhang, W. Ma, H. Yan, *J. Am. Chem. Soc.* 139 (2017) 6298–6301.
- [210] Y. Lin, T. Li, F. Zhao, L. Han, Z. Wang, Y. Wu, Q. He, J. Wang, L. Huo, Y. Sun, C. Wang, W. Ma, X. Zhan, *Adv. Energy Mater.* 6 (2016) 1600854.
- [211] E.Y. Ko, G.E. Park, J.H. Lee, H.J. Kim, D.H. Lee, H. Ahn, M.A. Uddin, H.Y. Woo, M.J. Cho, D.H. Choi, *ACS Appl. Mater. Interfaces* 9 (2017) 8838–8847.
- [212] H. Bai, Y. Wang, P. Cheng, J. Wang, Y. Wu, J. Hou, X. Zhan, *J. Mater. Chem. A* 3 (2015) 1910–1914.
- [213] C. Yan, Y. Wu, J. Wang, R. Li, P. Cheng, H. Bai, Z. Zhan, W. Ma, X. Zhan, *Dyes Pigm.* 139 (2017) 627–634.
- [214] Y. Lin, Z.-G. Zhang, H. Bai, J. Wang, Y. Yao, Y. Li, D. Zhu, X. Zhan, *Energy Environ. Sci.* 8 (2015) 610–616.
- [215] K. Liu, T.T. Larsen-Olsen, Y. Lin, M. Beliatis, E. Bundgaard, M. Jørgensen, F.C. Krebs, X. Zhan, *J. Mater. Chem. A* 4 (2016) 1044–1051.
- [216] H. Lin, S. Chen, Z. Li, J.Y.L. Lai, G. Yang, T. McAfee, K. Jiang, Y. Li, Y. Liu, H. Hu, J. Zhao, W. Ma, H. Ade, H. Yan, *Adv. Mater.* 27 (2015) 7299–7304.
- [217] H. Yao, Y. Chen, Y. Qin, R. Yu, Y. Cui, B. Yang, S. Li, K. Zhang, J. Hou, *Adv. Mater.* (2016) 8283–8287.
- [218] H. Yao, Y. Cui, R. Yu, B. Gao, H. Zhang, J. Hou, *Angew. Chem. Int. Ed.* 129 (2017) 3091–3095.
- [219] Y. Wang, H. Bai, X. Zhan, *J. Energy Chem.* 24 (2015) 744–749.
- [220] S. Yu, Y. Chen, L. Yang, P. Ye, J. Wu, J. Yu, S. Zhang, Y. Gao, H. Huang, *J. Mater. Chem. A* 5 (2017) 21674–21678.
- [221] Y. Liu, Z. Zhang, S. Feng, M. Li, L. Wu, R. Hou, X. Xu, X. Chen, Z. Bo, *J. Am. Chem. Soc.* 139 (2017) 3356–3359.
- [222] X. Li, T. Yan, H. Bin, G. Han, L. Xue, F. Liu, Y. Yi, Z.-G. Zhang, T.P. Russell, Y. Li, *J. Mater. Chem. A* 5 (2017) 22588–22597.
- [223] R. Li, G. Liu, M. Xiao, X. Yang, X. Liu, Z. Wang, L. Ying, F. Huang, Y. Cao, *J. Mater. Chem. A* 5 (2017) 23926–23936.
- [224] S. Li, L. Ye, W. Zhao, X. Liu, J. Zhu, H. Ade, J. Hou, *Adv. Mater.* (2017) 1704051.
- [225] D. Xie, T. Liu, T.H. Lee, W. Gao, C. Zhong, L. Huo, Z. Luo, K. Wu, W. Xiong, J.Y. Kim, H. Choi, Y. Sun, C. Yang, *Dyes Pigm.* 148 (2018) 263–269.
- [226] D. Zhao, J. Hu, Z. Liu, B. Xiao, X. Wang, E. Zhou, Q. Zhang, *Dyes Pigm.* 151 (2017) 102–109.
- [227] Z. Luo, Y. Zhao, Z.-G. Zhang, G. Li, K. Wu, D. Xie, W. Gao, Y. Li, C. Yang, *ACS Appl. Mater. Interfaces* 9 (2017) 34146–34152.
- [228] H. Bai, Y. Wu, Y. Wang, Y. Wu, R. Li, P. Cheng, M. Zhang, J. Wang, W. Ma, X. Zhan, *J. Mater. Chem. A* 3 (2015) 20758–20766.
- [229] Y. Wu, H. Bai, Z. Wang, P. Cheng, S. Zhu, Y. Wang, W. Ma, X. Zhan, *Energy Environ. Sci.* 8 (2015) 3215–3221.
- [230] B. Xiao, A. Tang, L. Cheng, J. Zhang, Z. Wei, Q. Zeng, E. Zhou, *Sol. RRL* (2017) 1700166.
- [231] B. Jia, Y. Wu, F. Zhao, C. Yan, S. Zhu, P. Cheng, J. Mai, T.K. Lau, X. Lu, C.J. Su, C. Wang, X. Zhan, *Sci. China Chem.* 60 (2017) 257–263.
- [232] Q.-Y. Li, J. Xiao, L.-M. Tang, H.-C. Wang, Z. Chen, Z. Yang, H.-L. Yip, Y.-X. Xu, *Org. Electron.* 44 (2017) 217–224.
- [233] B. Xiao, A. Tang, J. Zhang, A. Mahmood, Z. Wei, E. Zhou, *Adv. Energy Mater.* 7 (2017) 1602269.
- [234] B. Xiao, A. Tang, J. Yang, Z. Wei, E. Zhou, *ACS Macro Lett.* 6 (2017) 410–414.
- [235] F. Liu, Z. Zhou, C. Zhang, T. Vergote, H. Fan, F. Liu, X. Zhu, J. Am. Chem. Soc. 138 (2016) 15523–15526.
- [236] F. Liu, Z. Zhou, C. Zhang, J. Zhang, Q. Hu, T. Vergote, F. Liu, T.P. Russell, X. Zhu, *Adv. Mater.* 29 (2017) 1606574.
- [237] H. Bai, P. Cheng, Y. Wang, L. Ma, Y. Li, D. Zhu, X. Zhan, *J. Mater. Chem. A* 2 (2014) 778–784.
- [238] M.J. Cho, G.E. Park, S.Y. Park, Y.-U. Kim, D.H. Choi, *RSC Adv.* 7 (2017) 38773–38779.
- [239] Y. Li, L. Zhong, F.-P. Wu, Y. Yuan, H.-J. Bin, Z.-Q. Jiang, Z. Zhang, Z.-G. Zhang, Y. Li, L.-S. Liao, *Energy Environ. Sci.* 9 (2016) 3429–3435.
- [240] P. Ye, Y. Chen, J. Wu, X. Wu, S. Yu, W. Xing, Q. Liu, X. Jia, A. Peng, H. Huang, *J. Mater. Chem. C* 5 (2017) 12591–12596.
- [241] S. Feng, C. Zhang, Y. Liu, Z. Bi, Z. Zhang, X. Xu, W. Ma, Z. Bo, *Adv. Mater.* 29 (2017) 1703527.
- [242] S. Wen, Y. Wu, Y. Wang, Y. Li, L. Liu, H. Jiang, Z. Liu, R. Yang, *ChemSusChem* (2017), doi: <http://dx.doi.org/10.1002/cssc.201701917>.
- [243] L. Yang, M. Li, J. Song, Y. Zhou, Z. Bo, H. Wang, *Adv. Funct. Mater.* (2018) 1705927.
- [244] Y. Lin, J. Wang, Z.-G. Zhang, H. Bai, Y. Li, D. Zhu, X. Zhan, *Adv. Mater.* 27 (2015) 1170–1174.
- [245] Y.-T. Hsiao, C.-H. Li, S.-L. Chang, S. Heo, K. Tajima, Y.-J. Cheng, C.-S. Hsu, *ACS Appl. Mater. Interfaces* 9 (2017) 42035–42042.
- [246] M. An, F. Xie, X. Geng, J. Zhang, J. Jiang, Z. Lei, D. He, Z. Xiao, L. Ding, *Adv. Energy Mater.* 7 (2017) 1602509.
- [247] W. Zhao, D. Qian, S. Zhang, S. Li, O. Inganäs, F. Gao, J. Hou, *Adv. Mater.* (2016) 4734–4739.
- [248] L. Gao, Z.G. Zhang, H. Bin, L. Xue, Y. Yang, C. Wang, F. Liu, T.P. Russell, Y. Li, *Adv. Mater.* (2016) 8288–8295.
- [249] Y. Qin, M.A. Uddin, Y. Chen, B. Jang, K. Zhao, Z. Zheng, R. Yu, T.J. Shin, H.Y. Woo, J. Hou, *Adv. Mater.* 28 (2016) 9416–9422.
- [250] B. Fan, K. Zhang, X.F. Jiang, L. Ying, F. Huang, Y. Cao, *Adv. Mater.* 29 (2017) 1606396.
- [251] T. Yu, X. Xu, G. Zhang, J. Wan, Y. Li, Q. Peng, *Adv. Funct. Mater.* 27 (2017) 1701491.
- [252] H. Bin, Z.G. Zhang, L. Gao, S. Chen, L. Zhong, L. Xue, C. Yang, Y. Li, *J. Am. Chem. Soc.* 138 (2016) 4657–4664.
- [253] D. Liu, C. Gu, J. Wang, D. Zhu, Y. Li, X. Bao, R. Yang, E.J. Kramer, N. Coates, J.S. Moon, R. Gaudiana, H.Y. Woo, X. Zhan, *J. Mater. Chem. C* 5 (2017) 9141–9147.
- [254] Q. Fan, W. Su, X. Guo, Y. Wang, Y. Wang, J. Chen, C. Ye, M. Zhang, Y. Li, A. Salleo, B.F. Chmelka, A. Amassian, P.M. Beaujuge, M.D. McGehee, Y.M. Sun, Z. Wei, W. Ma, C. Wang, Z. Bo, O. Inganäs, Y.F. Li, X.W. Zhan, *J. Mater. Chem. C* 5 (2017) 9204–9209.
- [255] X. Gong, G. Li, S. Feng, L. Wu, Y. Liu, R. Hou, C. Li, X. Chen, Z. Bo, *J. Mater. Chem. C* 5 (2016) 937–942.
- [256] Q. Wang, S. Zhang, B. Xu, S. Li, B. Yang, W. Yuan, J. Hou, *J. Phys. Chem. C* 121 (2017) 4825–4833.
- [257] D. Xia, Y. Wu, Q. Wang, A. Zhang, C. Li, Y. Lin, F.J.M. Colberts, J.J.V. Franeker, R.A. J. Janssen, X. Zhan, W. Hu, Z. Tang, W. Ma, W. Li, *Macromolecules* 49 (2016) 6445–6454.
- [258] S. Zhang, Y. Qin, M.A. Uddin, B. Jang, W. Zhao, D. Liu, H.Y. Woo, J. Hou, *Macromolecules* 49 (2016) 2993–3000.
- [259] H. Bin, L. Gao, Z.-G. Zhang, Y. Yang, Y. Zhang, C. Zhang, S. Chen, L. Xue, C. Yang,

- M. Xiao, Y. Li, *Nat. Commun.* 7 (2016) 13651.
- [260] J. Yuan, L. Qiu, Z.G. Zhang, Y. Li, Y. Chen, Y. Zou, *Nano Energy* 30 (2016) 312–320.
- [261] Y. Yang, Z.G. Zhang, H. Bin, S. Chen, L. Gao, L. Xue, C. Yang, Y. Li, *J. Am. Chem. Soc.* 138 (2016) 15011–15018.
- [262] Z. Zheng, O.M. Awartani, B. Gautam, D. Liu, Y. Qin, W. Li, A. Bataller, K. Gundogdu, H. Ade, J. Hou, *Adv. Mater.* 29 (2017) 1604241.
- [263] B. Zhao, W. Wang, J. Xin, H. Wu, H. Liu, Z. Guo, Z. Cong, W. Ma, C. Gao, *Chem. Eng.* (2017), doi:<http://dx.doi.org/10.1021/acssuschemeng.7b03606>.
- [264] X. Liu, B. Xie, C. Duan, Z. Wang, B. Fan, K. Zhang, B. Lin, F.J.M. Colberts, W. Ma, R.A.J. Janssen, F. Huang, Y. Cao, *J. Mater. Chem. A* 6 (2018) 395–403.
- [265] T.J. Aldrich, S.M. Swick, F.S. Melkonyan, T.J. Marks, *Chem. Mater.* 29 (2017) 10294–10298.
- [266] C. Zhang, S. Feng, Y. Liu, R. Hou, Z. Zhang, X. Xu, Y. Wu, Z. Bo, *ACS Appl. Mater. Interfaces* 9 (2017) 33906–33912.
- [267] Z. Fei, F.D. Eisner, X. Jiao, M. Azzouzi, J.A. Röhr, Y. Han, M. Shahid, A.S.R. Chesman, C.D. Easton, C.R. McNeill, T.D. Anthopoulos, J. Nelson, M. Heeney, *Adv. Mater.* (2018) 1705209.
- [268] Y. Lin, F. Zhao, Q. He, L. Huo, Y. Wu, T.C. Parker, W. Ma, Y. Sun, C. Wang, D. Zhu, A.J. Heeger, S.R. Marder, X. Zhan, *J. Am. Chem. Soc.* 138 (2016) 4955–4961.
- [269] Z. Li, K. Jiang, G. Yang, J.Y.L. Lai, T. Ma, J. Zhao, W. Ma, H. Yan, *Nat. Commun.* 7 (2016) 13094.
- [270] W. Gao, Q. An, R. Ming, D. Xie, K. Wu, Z. Luo, Y. Zou, F. Zhang, C. Yang, *Adv. Funct. Mater.* 27 (2017) 1702194.
- [271] F. Zhao, S. Dai, Y. Wu, Q. Zhang, J. Wang, L. Jiang, Q. Ling, Z. Wei, W. Ma, W. You, C. Wang, X. Zhan, *Adv. Mater.* 29 (2017) 1700144.
- [272] S. Li, L. Ye, W. Zhao, S. Zhang, S. Mukherjee, H. Ade, J. Hou, *Adv. Mater.* 28 (2016) 9423–9429.
- [273] H. Zhang, S. Li, B. Xu, H. Yao, B. Yang, J. Hou, *J. Mater. Chem. A* 4 (2016) 18043–18049.
- [274] D. Liu, B. Yang, B. Jang, B. Xu, S. Zhang, C. He, H.Y. Woo, J. Hou, *Energy Environ. Sci.* 10 (2017) 546–551.
- [275] S. Li, L. Ye, W. Zhao, S. Zhang, H. Ade, J. Hou, *Adv. Energy Mater.* 7 (2017) 1700183.
- [276] J. Zhu, S. Li, X. Liu, H. Yao, F. Wang, S. Zhang, M. Sun, J. Hou, *J. Mater. Chem. A* 5 (2017) 15175–15182.
- [277] W. Zhao, S. Li, H. Yao, S. Zhang, Y. Zhang, B. Yang, J. Hou, *J. Am. Chem. Soc.* 139 (2017) 7148–7151.
- [278] F. Yang, C. Li, W. Lai, A. Zhang, H. Huang, W. Li, *Mater. Chem. Front.* 1 (2017) 1389–1395.
- [279] X. Li, H. Huang, H. Bin, Z. Peng, C. Zhu, L. Xue, Z.-G. Zhang, Z. Zhang, H. Ade, Y. Li, *Chem. Mater.* 29 (2017) 10130–10138.
- [280] Z. Zhang, W. Liu, T. Rehman, H.-X. Ju, J. Mai, X. Lu, M. Shi, J. Zhu, C.-Z. Li, H. Chen, *J. Mater. Chem. A* 5 (2017) 9649–9654.
- [281] H. Yao, L. Ye, J. Hou, B. Jang, G. Han, Y. Cui, G.M. Su, C. Wang, B. Gao, R. Yu, H. Zhang, Y. Yi, H.Y. Woo, H. Ade, J. Hou, *Adv. Mater.* 29 (2017) 1700254.
- [282] Z. Luo, H. Bin, T. Liu, Z.-G. Zhang, Y. Yang, C. Zhong, B. Qiu, G. Li, W. Gao, D. Xie, K. Wu, Y. Sun, F. Liu, Y. Li, C. Yang, *Adv. Mater.* (2018) 1706124.
- [283] Z. Zhang, L. Feng, S. Xu, J. Yuan, Z.-G. Zhang, H. Peng, Y. Li, Y. Zou, *J. Mater. Chem. A* 5 (2017) 11286–11293.
- [284] S. Dai, F. Zhao, Q. Zhang, T.-K. Lau, T. Li, K. Liu, Q. Ling, C. Wang, X. Lu, W. You, X. Zhan, *J. Am. Chem. Soc.* 139 (2017) 1336–1343.
- [285] Y. Ma, M. Zhang, Y. Yan, J. Xin, T. Wang, W. Ma, C. Tang, Q. Zheng, *Chem. Mater.* 29 (2017) 7942–7952.
- [286] Y. Ma, M. Zhang, Y. Tang, W. Ma, Q. Zheng, *Chem. Mater.* 29 (2017) 9775–9785.
- [287] Y.-Q.-Q. Yi, H. Feng, M. Chang, H. Zhang, X. Wan, C. Li, Y. Chen, *J. Mater. Chem. A* 5 (2017) 17204–17210.
- [288] J. Zhang, C. Yan, W. Wang, Y. Xiao, X. Lu, S. Barlow, T.C. Parker, X. Zhan, S.R. Marder, *Chem. Mater.* (2018), doi:<http://dx.doi.org/10.1021/acs.chemmater.7b04499>.
- [289] N. Qiu, H. Zhang, X. Wan, C. Li, X. Ke, H. Feng, B. Kan, H. Zhang, Q. Zhang, Y. Lu, Y. Chen, *Adv. Mater.* 29 (2017) 160496.
- [290] Z. Zhang, M. Li, Y. Liu, J. Zhang, S. Feng, X. Xu, J. Song, Z. Bo, H. Zhang, M. Li, Z. Hu, F. Huang, Y. Cao, Z. Liang, M. Zhang, T.P. Russell, Y. Chen, C. Wang, J. Hodgkiss, Z. Bo, O. Inganäs, Y. Li, X. Zhan, *J. Mater. Chem. A* 5 (2017) 7776–7783.
- [291] W. Guo, B. Zhao, J. Xin, H. Liu, Y. Mi, J. Zhang, Z. Guo, W. Wei, W. Ma, C. Gao, Z. An, *Dyes Pigm.* 144 (2017) 48–57.
- [292] H. Feng, N. Qiu, X. Wang, Y. Wang, B. Kan, X. Wan, M. Zhang, A. Xia, C. Li, F. Liu, H. Zhang, Y. Chen, *Chem. Mater.* 29 (2017) 7908–7917.
- [293] Q. Cao, W. Xiong, H. Chen, G. Cai, G. Wang, L. Zheng, Y. Sun, *J. Mater. Chem. A* 5 (2017) 7451–7461.
- [294] X. Shi, L. Zuo, K. Gao, F. Lin, F. Liu, A.K.Y. Jen, *Chem. Mater.* 29 (2017) 8369–8376.
- [295] W. Wang, C. Yan, T.K. Lau, J. Wang, K. Liu, Y. Fan, X. Lu, X. Zhan, *Adv. Mater.* 29 (2017) 1701308.
- [296] B. Kan, H. Feng, X. Wan, F. Liu, X. Ke, Y. Wang, Y. Wang, H. Zhang, C. Li, J. Hou, Y. Chen, *J. Am. Chem. Soc.* 139 (2017) 4929–4934.
- [297] Y. Li, L. Zhong, J.-D. Lin, F.-P. Wu, H.-J. Bin, Z. Zhang, L. Xu, Z.-Q. Jiang, Z.-G. Zhang, F. Liu, T.P. Russell, Y. Li, L.-S. Liao, S.R. Forrest, *Sol. RRL* 1 (2017) 1700107.
- [298] Y. Li, L. Zhong, B. Gautam, H.-J. Bin, J.-D. Lin, F.-P. Wu, Z. Zhang, Z.-Q. Jiang, Z.-G. Zhang, K. Gundogdu, Y. Li, L.-S. Liao, *Energy Environ. Sci.* 10 (2017) 1610–1620.
- [299] B. Kan, J. Zhang, F. Liu, X. Wan, C. Li, X. Ke, Y. Wang, H. Feng, Y. Zhang, G. Long, R.H. Friend, A.A. Bakulin, Y. Chen, *Adv. Mater.* 30 (2018) 1704904.
- [300] Q. An, W. Gao, F. Zhang, J. Wang, M. Zhang, K. Wu, X. Ma, Z. Hu, C. Jiao, C. Yang, *J. Mater. Chem. A* (2018), doi:<http://dx.doi.org/10.1039/C7TA10763C>.
- [301] Y. Li, X. Liu, F.-P. Wu, Y. Zhou, Z.-Q. Jiang, B. Song, Y. Xia, Z.-G. Zhang, F. Gao, O. Inganäs, Y. Li, L.-S. Liao, *J. Mater. Chem. A* 4 (2016) 5890–5897.
- [302] Y. Li, D. Qian, L. Zhong, J.-D. Lin, Z.-Q. Jiang, Z.-G. Zhang, Z. Zhang, Y. Li, L.-S. Liao, F. Zhang, *Nano Energy* 27 (2016) 430–438.
- [303] Y. Li, J.-D. Lin, X. Che, Y. Qu, F. Liu, L.S. Liao, S.R. Forrest, *J. Am. Chem. Soc.* 139 (2017) 17114–17119.
- [304] B. Jia, S. Dai, Z. Ke, C. Yan, W. Ma, X. Zhan, *Chem. Mater.* (2017), doi:<http://dx.doi.org/10.1002/aejm.201502529>.
- [305] Z. Zhang, X. Zhu, *Chem. Mater.* (2018), doi:<http://dx.doi.org/10.1021/acs.chemmater.7b04930>.
- [306] P. Wang, H. Fan, C. Zhang, X. Zhu, *Mater. Chem. Front.* 2 (2018) 136–142.
- [307] J. Zhu, Z. Ke, Q. Zhang, J. Wang, S. Dai, Y. Wu, Y. Xu, Y. Lin, W. Ma, W. You, X. Zhan, *Adv. Mater.* 30 (2018) 1704713.
- [308] T. Li, S. Dai, Z. Ke, L. Yang, J. Wang, C. Yan, W. Ma, X. Zhan, *Adv. Mater.* (2018) 1705969.
- [309] A. Venkateswararao, K.R.J. Thomas, C.P. Lee, C.T. Li, K.C. Ho, *ACS Appl. Mater. Interfaces* 6 (2014) 2528–2539.
- [310] H. Patil, A. Gupta, B. Alford, D. Ma, S.H. Privé, A. Bilic, P. Sonar, S.V. Bhosale, *Asian J. Org. Chem.* 4 (2015) 1096–1102.
- [311] A.M. Raynor, A. Gupta, H. Patil, A. Bilic, T.J. Rook, S.V. Bhosale, *RSC Adv.* 6 (2016) 28103–28109.
- [312] Y. Fang, A.K. Pandey, D.M. Lyons, P.E. Shaw, S.E. Watkins, P.L. Burn, S.C. Lo, P. Meredith, *ChemPhysChem* 16 (2015) 1295–1304.
- [313] D. Ma, S. Feng, J. Zhang, C. Kou, X. Gong, Q. Li, X. Xu, S. Yan, Z. Bo, *Dyes Pigm.* 146 (2017) 293–299.
- [314] Y. Zhou, J. Pei, Q. Dong, X. Sun, Y. Liu, W. Tian, *J. Phys. Chem. C* 113 (2009) 7882–7886.
- [315] G.D. Sharma, M.A. Reddy, D.V. Ramana, M. Chandrasekharam, *RSC Adv.* 4 (2014) 33279.
- [316] J. Wu, Y. Ma, N. Wu, Y. Lin, J. Lin, L. Wang, C.Q. Ma, *Org. Electron.* 23 (2015) 28–38.
- [317] Z. Kang, S.C. Chen, Y. Ma, J. Wang, Q. Zheng, *ACS Appl. Mater. Interfaces* 9 (2017) 24771–24777.
- [318] Y. Un Kim, G. Eun Park, S. Choi, D. Hee Lee, M. Ju Cho, D.H. Choi, *J. Mater. Chem. C* 5 (2017) 7182–7190.
- [319] A.M. Poe, A.M.D. Pelle, A.V. Subrahmanyam, W. White, G. Wantz, S. Thayumanavan, *Chem. Commun.* 50 (2014) 2913–2915.
- [320] Y. Fang, A.K. Pandey, A.M. Nardes, N. Kopidakis, P.L. Burn, P. Meredith, *Energy Mater.* 3 (2013) 54–59.
- [321] D.M. Stoltzfus, A.J. Clulow, H. Jin, P.L. Burn, I.R. Gentle, *Macromolecules* 49 (2016) 4404–4415.
- [322] A. Mishra, M.L. Keshtov, A. Looser, R. Singhal, M. Stolte, F. Würthner, P. Bäuerle, G.D. Sharma, *J. Mater. Chem. A* 5 (2017) 14887–14897.
- [323] S. Li, L. Zhan, F. Liu, J. Ren, M. Shi, C.-Z. Li, T.P. Russell, H. Chen, *Adv. Mater.* (2017) 1705208.
- [324] J.T. Bloking, X. Han, A.T. Higgs, J.P. Kastrop, L. Pandey, J.E. Norton, C. Risko, C.E. Chen, J.L. Brédas, M.D. McGehee, A. Sellinger, *Chem. Mater.* 23 (2011) 5484–5490.
- [325] Y. Ie, S. Jinna, M. Nitani, Y. Aso, *J. Mater. Chem. C* 1 (2013) 5373–5380.
- [326] S. Jinna, Y. Ie, M. Karakawa, T. Aernouts, Y. Nakajima, S. Mori, Y. Aso, *Chem. Mater.* 28 (2016) 1705–1713.
- [327] J.D. Douglas, M.S. Chen, J.R. Niskala, O.P. Lee, A.T. Yiu, E.P. Young, J.M.J. Fréchet, *Adv. Mater.* 26 (2014) 4313–4319.
- [328] A.D. Hendsbee, S.M. McAfee, J.-P. Sun, T.M. McCormick, I.G. Hill, G.C. Welch, *J. Mater. Chem. C* 3 (2015) 8904–8915.
- [329] Y. Ie, S. Jinna, M. Karakawa, Y. Aso, *Chem. Lett.* 44 (2015) 694–696.
- [330] Y. Zhou, L. Ding, K. Shi, Y.-Z. Dai, N. Ai, J. Wang, J. Pei, *Adv. Mater.* 24 (2012) 957–961.
- [331] Y. Zhou, Y.-Z. Dai, Y.-Q. Zheng, X.-Y. Wang, J.-Y. Wang, J. Pei, *Chem. Commun.* 49 (2013) 5802–5804.
- [332] Y.-Q. Zheng, Y.-Z. Dai, Y. Zhou, J.-Y. Wang, J. Pei, *Chem. Commun.* 50 (2014) 1591–1594.
- [333] Q. He, T. Li, C. Yan, Y. Liu, J. Wang, M. Wang, Y. Lin, X. Zhan, *Dyes Pigm.* 128 (2016) 226–234.
- [334] J.C. Zhang, H.M. Xiao, X.J. Zhang, Y. Wu, G.W. Li, C.H. Li, X.B. Chen, W. Ma, Z.S. Bo, *J. Mater. Chem. C* 4 (2016) 5656–5663.
- [335] J. Zhang, X. Zhang, G. Li, H. Xiao, W. Li, S. Xie, C. Li, Z. Bo, *Chem. Commun.* 52 (2016) 469–472.
- [336] R. Hou, S. Feng, X. Gong, Y. Liu, J. Zhang, C. Li, Z. Bo, *Synth. Met.* 220 (2016) 578–584.
- [337] X. Zhang, J. Zhang, H. Lu, J. Wu, G. Li, C. Li, S. Li, Z. Bo, *J. Mater. Chem. C* 3 (2015) 6979–6985.
- [338] J. Zhang, X. Zhang, H. Xiao, G. Li, Y. Liu, C. Li, H. Huang, X. Chen, Z. Bo, *ACS Appl. Mater. Interfaces* 8 (2016) 5475–5483.
- [339] O.K. Kwon, J.H. Park, S. Kyu Park, S.Y. Park, *Energy Mater.* 5 (2015) 1400929.
- [340] O.K. Kwon, J.-H. Park, D.W. Kim, S.K. Park, S.Y. Park, *Adv. Mater.* 27 (2015) 1951–1956.
- [341] O.K. Kwon, M.A. Uddin, J.H. Park, S.K. Park, T.L. Nguyen, H.Y. Woo, S.Y. Park, *Adv. Mater.* 28 (2016) 910–916.
- [342] M. Zhu, J. Miao, Z. Hu, Y. Chen, M. Liu, I. Murtaza, H. Meng, *Dyes Pigm.* 142 (2017) 39–50.
- [343] D. Dang, Y. Zhi, X. Wang, B. Zhao, C. Gao, L. Meng, *Dyes Pigm.* 137 (2017) 43–49.
- [344] S. Chatterjee, Y. Ie, M. Karakawa, Y. Aso, *Adv. Funct. Mater.* 26 (2016) 1161–1168.

- [345] P. Gautam, R. Sharma, R. Misra, M.L. Keshtov, S.A. Kuklin, G.D. Sharma, *Chem. Sci.* 8 (2017) 2017–2024.
- [346] P. Josse, L. Favereau, C. Shen, S. Dabos-Seignon, P. Blanchard, C. Cabanetos, J. Crassous, *Chem.- Eur. J.* 23 (2017) 6277–6281.
- [347] H. Li, T. Earmme, S. Subramaniyan, S.A. Jenekhe, *Adv. Energy Mater.* 5 (2015) 1–9.
- [348] H. Li, F.S. Kim, G. Ren, E.C. Hollenbeck, S. Subramaniyan, S.A. Jenekhe, *Angew. Chemie. Int. Ed.* 52 (2013) 5513–5517.
- [349] H. Li, T. Earmme, G. Ren, A. Saeki, S. Yoshikawa, N.M. Murari, S. Subramaniyan, M.J. Crane, S. Seki, S.A. Jenekhe, *J. Am. Chem. Soc.* 136 (2014) 14589–14597.
- [350] H. Li, Y.-J. Hwang, B.A.E. Courtright, F.N. Eberle, S. Subramaniyan, S.A. Jenekhe, *Adv. Mater.* 27 (2015) 3340.
- [351] Y.J. Hwang, H. Li, B.A.E. Courtright, S. Subramaniyan, S.A. Jenekhe, *Adv. Mater.* 28 (2016) 124–131.
- [352] L. Ding, C.Y. Yang, Y.Q. Zheng, J.Y. Wang, J. Pei, Z. Su, *Asian J. Org. Chem.* 6 (2017) 1231–1234.
- [353] L. Lan, Z. Chen, L. Ying, F. Huang, Y. Cao, *Org. Electron.* 30 (2016) 176–181.
- [354] T.V. Pho, F.M. Toma, M.L. Chabiny, F. Wudl, *Angew. Chemie. Int. Ed.* 52 (2013) 1446–1451.
- [355] T.V. Pho, F.M. Toma, B.J.T. De Villers, S. Wang, N.D. Treat, N.D. Eisenmenger, G. M. Su, R.C. Coffin, J.D. Douglas, J.M.J. Fréchet, G.C. Bazan, F. Wudl, M.L. Chabiny, *Energy Mater.* 4 (2014) 1301007.
- [356] Y. Liu, L. Zhang, H. Lee, H.W. Wang, A. Santala, F. Liu, Y. Diao, A.L. Briseno, T.P. Russell, *Energy Mater.* 5 (2015) 1500195.
- [357] A. Gupta, R.V. Hangare, X. Wang, B. Alford, V. Chellapan, L.A. Jones, A. Ranawake, A. Bilic, P. Sonar, S.V. Bhosale, *Dyes Pigm.* 120 (2015) 314–321.
- [358] J. Hong, Y.H. Ha, H. Cha, R. Kim, Y.J. Kim, C.E. Park, J.R. Durrant, S.-K. Kwon, T.K. An, Y.-H. Kim, *ACS Appl. Mater. Interfaces* 9 (2017) 44667–44677.
- [359] X. Wang, J. Huang, Z. Niu, X. Zhang, Y. Sun, C. Zhan, *Tetrahedron* 70 (2014) 4726–4731.
- [360] E. Ahmed, G. Ren, F.S. Kim, E.C. Hollenbeck, S.A. Jenekhe, *Chem. Mater.* 23 (2011) 4563–4577.
- [361] D. Srivani, A. Gupta, S.V. Bhosale, A.L. Puyad, W. Xiang, J. Li, R.A. Evans, S.V. Bhosale, *Chem. Commun.* 53 (2017) 7080–7083.
- [362] D. Srivani, A. Gupta, A.M. Raynor, A. Bilic, J. Li, S.V. Bhosale, S.V. Bhosale, *RSC Adv.* 6 (2016) 38703–38708.
- [363] D. Srivani, A. Gupta, D.D. La, R.S. Bhosale, A.L. Puyad, W. Xiang, J. Li, S.V. Bhosale, S.V. Bhosale, *Dyes Pigm.* 143 (2017) 1–9.
- [364] R. Fernando, Z. Mao, E. Muller, F. Ruan, G. Sauv , *J. Phys. Chem. C* 118 (2014) 3433–3442.
- [365] V. Kamml, G. Battaglia, I.A. Howard, W. Pisula, A. Mavrincky, C. Li, K. M llen, F. Laquai, *Energy Mater.* 1 (2011) 297–302.
- [366] A. Sharenko, C.M. Proctor, T.S.V.D. Poll, Z.B. Henson, T.Q. Nguyen, G.C. Bazan, *Adv. Mater.* 25 (2013) 4403–4406.
- [367] R. Singh, E. Aluicio-Sarduy, Z. Kan, T. Ye, R.C.I. MacKenzie, P.E. Keivanidis, *J. Mater. Chem. A* 2 (2014) 14348–14353.
- [368] J. Yi, Y. Ma, J. Dou, Y. Lin, Y. Wang, C.Q. Ma, H. Wang, *Dyes Pigm.* 126 (2016) 86–95.
- [369] J. Yi, J. Wang, Y. Lin, W. Gao, Y. Ma, H. Tan, H. Wang, C.Q. Ma, *Dyes Pigm.* 136 (2017) 335–346.
- [370] W.S. Shin, H.-H. Jeong, M.-K. Kim, S.-H. Jin, M.-R. Kim, J.-K. Lee, J.W. Lee, Y.-S. Gal, *J. Mater. Chem.* 16 (2006) 384–390.
- [371] N.D. Eastham, A.S. Dudnik, T.J. Aldrich, E.F. Manley, T.J. Fauvell, P.E. Hartnett, M.R. Wasielewski, L.X. Chen, F.S. Melkonyan, A. Facchetti, R.P.H. Chang, T.J. Marks, *Chem. Mater.* 29 (2017) 4432–4444.
- [372] P.E. Hartnett, A. Timalsina, H.S.S.R. Matte, N. Zhou, X. Guo, W. Zhao, A. Facchetti, R.P.H. Chang, M.C. Hersam, M.R. Wasielewski, T.J. Marks, *J. Am. Chem. Soc.* 136 (2014) 16345–16356.
- [373] X. Li, H. Wang, J.A. Schneider, Z. Wei, W.-Y. Lai, W. Huang, F. Wudl, Y. Zheng, *J. Mater. Chem. C* 5 (2017) 2781–2785.
- [374] Y. Cai, L. Huo, X. Sun, D. Wei, M. Tang, Y. Sun, *Energy Mater.* 5 (2015) 1500032.
- [375] X. Zhang, B. Jiang, X. Zhang, A. Tang, J. Huang, C. Zhan, J. Yao, *J. Phys. Chem. C* 118 (2014) 24212–24220.
- [376] D. Kotowski, S. Luzzati, G. Scavia, M. Cavazzini, A. Bossi, M. Catellani, E. Kozma, *Dyes Pigm.* 120 (2015) 57–64.
- [377] X. Liu, G. Luo, X. Cai, H. Wu, S.-J. Su, Y. Cao, *Rsc Adv.* 5 (2015) 83155–83163.
- [378] P. Cheng, X. Zhao, W. Zhou, J. Hou, Y. Li, X. Zhan, *Org. Electron.* 15 (2014) 2270–2276.
- [379] G.D. Sharma, P. Suresh, J.A. Mikroyannidis, M.M. Stylianakis, *J. Mater. Chem.* 20 (2010) 561–567.
- [380] G.D. Sharma, P. Balraj, J.A. Mikroyannidis, M.M. Stylianakis, *Sol. Energy Mater. Sol. Cells* 93 (2009) 2025–2028.
- [381] J. Qu, B. Gao, H. Tian, X. Zhang, Y. Wang, Z. Xie, H. Wang, Y. Geng, F. Wang, *J. Mater. Chem. A* 2 (2014) 3632–3640.
- [382] A.D. Hendsbee, J.P. Sun, W.K. Law, H. Yan, I.G. Hill, D.M. Spasyuk, G.C. Welch, *Chem. Mater.* 28 (2016) 7098–7109.
- [383] S. Rajaram, R. Shivanna, S.K. Kandappa, K.S. Narayan, *J. Phys. Chem. Lett.* 3 (2012) 2405–2408.
- [384] R. Shivanna, S. Shoaee, S. Dimitrov, S.K. Kandappa, S. Rajaram, J.R. Durrant, K. S. Narayan, *Energy Environ. Sci.* 7 (2014) 435–441.
- [385] C.H. Wu, C.C. Chueh, Y.Y. Xi, H.L. Zhong, G.P. Gao, Z.H. Wang, L.D. Pozzo, T.C. Wen, A.K.Y. Jen, *Adv. Funct. Mater.* 25 (2015) 5326–5332.
- [386] Y. Zang, C.Z. Li, C.C. Chueh, S.T. Williams, W. Jiang, Z.H. Wang, J.S. Yu, A.K.Y. Jen, *Adv. Mater.* 26 (2014) 5708–5714.
- [387] L. Ye, W. Jiang, W. Zhao, S. Zhang, Y. Cui, Z. Wang, J. Hou, *Org. Electron.* 17 (2015) 295–303.
- [388] L. Ye, K. Sun, W. Jiang, S. Zhang, W. Zhao, H. Yao, Z. Wang, J. Hou, *ACS Appl. Mater. Interfaces* 7 (2015) 9274–9280.
- [389] W. Lee, J.W. Jung, *Macromol. Chem. Phys.* 217 (2016) 2647–2653.
- [390] G. Feng, Y. Xu, J. Zhang, Z. Wang, Y. Zhou, Y. Li, Z. Wei, C. Li, W. Li, *J. Mater. Chem. A* 4 (2016) 6056–6063.
- [391] H. Wang, L. Chen, Y. Xiao, *J. Mater. Chem. A* 5 (2017) 22288–22296.
- [392] Y. Liu, C. Mu, K. Jiang, J. Zhao, Y. Li, L. Zhang, Z. Li, J.Y.L. Lai, H. Hu, T. Ma, R. Hu, D. Yu, X. Huang, B.Z. Tang, H. Yan, *Adv. Mater.* 27 (2015) 1015–1020.
- [393] Y. Chen, X. Zhang, C. Zhan, J. Yao, *ACS Appl. Mater. Interfaces* 7 (2015) 6462–6471.
- [394] J. Zhao, Y. Li, J. Zhang, L. Zhang, J.Y.L. Lai, K. Jiang, C. Mu, Z. Li, C.L.C. Chan, A. Hunt, S. Mukherjee, H. Ade, X. Huang, H. Yan, *J. Mater. Chem. A* 3 (2015) 20108–20112.
- [395] M. Park, J.W. Jung, *Dyes Pigm.* 143 (2017) 301–307.
- [396] P.E. Hartnett, H.S.S.R. Matte, N.D. Eastham, N.E. Jackson, Y. Wu, L.X. Chen, M.A. Ratner, R.P.H. Chang, M.C. Hersam, M.R. Wasielewski, T.J. Marks, *Chem. Sci.* 7 (2016) 3543–3555.
- [397] W.T. Hadjmojo, S.Y. Nam, T.J. Shin, S.C. Yoon, S.-Y. Jang, I.H. Jung, *J. Mater. Chem. A* 4 (2016) 12308–12318.
- [398] D. Zhao, Q. Wu, Z. Cai, T. Zheng, W. Chen, J. Lu, L. Yu, *Chem. Mater.* 28 (2016) 1139–1146.
- [399] Z.F. Chang, Y. Cai, K.K. Liu, X.X. Song, J.J. Liu, X. Liu, Y. Sun, R. bo Zhang, J.L. Wang, *Dyes Pigm.* 147 (2017) 31–39.
- [400] Z. Lu, B. Jiang, X. Zhang, A. Tang, L. Chen, C. Zhan, J. Yao, *Chem. Mater.* 26 (2014) 2907–2914.
- [401] J. Wang, Y. Yao, S. Dai, X. Zhang, W. Wang, Q. He, L. Han, Y. Lin, X. Zhan, *J. Mater. Chem. A* 3 (2015) 13000–13010.
- [402] X. Zhang, Z. Lu, L. Ye, C. Zhan, J. Hou, S. Zhang, B. Jiang, Y. Zhao, J. Huang, S. Zhang, Y. Liu, Q. Shi, Y. Liu, J. Yao, *Adv. Mater.* 25 (2013) 5791–5797.
- [403] J. Huang, X. Wang, X. Zhang, Z. Niu, Z. Lu, B. Jiang, Y. Sun, C. Zhan, J. Yao, *ACS Appl. Mater. Interfaces* 6 (2014) 3853–3862.
- [404] Y. Chen, A. Tang, X. Zhang, Z. Lu, J. Huang, C. Zhan, J. Yao, *J. Mater. Chem. A* 2 (2014) 1869–1876.
- [405] X. Zhang, C. Zhan, J. Yao, *Chem. Mater.* 27 (2015) 166–173.
- [406] X. Zhang, J. Yao, C. Zhan, *Chem. Commun.* 51 (2015) 1058–1061.
- [407] B. Jiang, X. Zhang, C. Zhan, Z. Lu, J. Huang, X. Ding, S. He, J. Yao, *Polym. Chem.* 4 (2013) 4631–4638.
- [408] G.E. Park, H.J. Kim, S. Choi, D.H. Lee, M.A. Uddin, H.Y. Woo, M.J. Cho, D.H. Choi, *Chem. Commun.* 52 (2016) 8873–8876.
- [409] J. Cann, S. Dayneko, J.-P. Sun, A.D. Hendsbee, I.G. Hill, G.C. Welch, *J. Mater. Chem. C* 5 (2017) 2074–2083.
- [410] S. Dayneko V, A.D. Hendsbee, G.C. Welch, *Chem. Commun.* 53 (1164) (2018) 1164–1167.
- [411] D. Sun, D. Meng, Y. Cai, B. Fan, Y. Li, W. Jiang, L. Huo, Y. Sun, Z. Wang, *J. Am. Chem. Soc.* 137 (2015) 11156–11162.
- [412] T. Liu, D. Meng, Y. Cai, X. Sun, Y. Li, L. Huo, F. Liu, Z. Wang, T.P. Russell, Y. Sun, *Adv. Sci. I* (2016) 160017.
- [413] D. Meng, D. Sun, C. Zhong, T. Liu, B. Fan, L. Huo, Y. Li, W. Jiang, H. Choi, T. Kim, J. Y. Kim, Y. Sun, Z. Wang, A.J. Heeger, *J. Am. Chem. Soc.* 138 (2016) 375–380.
- [414] R. Xin, J. Feng, C. Zeng, W. Jiang, L. Zhang, D. Meng, Z. Ren, Z. Wang, S. Yan, *ACS Appl. Mater. Interfaces* 9 (2017) 2739–2746.
- [415] A.D. Hendsbee, S.V. Dayneko, J.A. Pells, J.R. Cann, G.C. Welch, *Sustain. Energy Fuels* 1 (2017) 1137–1147.
- [416] C. Zhang, T. Liu, W. Zeng, D. Xie, Z. Luo, Y. Sun, C. Yang, *Mater. Chem. Front.* 1 (2017) 749–756.
- [417] G. Ding, A. Tang, F. Chen, K. Tajima, B. Xiao, E. Zhou, *RSC Adv.* 7 (2017) 13749–13753.
- [418] H. Zhong, C.H. Wu, C.Z. Li, J. Carpenter, C.C. Chueh, J.Y. Chen, H. Ade, A.K.Y. Jen, *Adv. Mater.* 28 (2016) 951–958.
- [419] A. Timalsina, P.E. Hartnett, F.S. Melkonyan, J. Strzalka, V.S. Reddy, A. Facchetti, M.R. Wasielewski, T.J. Marks, *J. Mater. Chem. A* 5 (2017) 5351–5361.
- [420] W. Jiang, L. Ye, X. Li, C. Xiao, F. Tan, W. Zhao, J. Hou, Z. Wang, *Chem. Commun.* 50 (2014) 1024–1026.
- [421] Y. Zhong, M.T. Trinh, R. Chen, W. Wang, P.P. Khlyabich, B. Kumar, Q. Xu, C.Y. Nam, M.Y. Sfeir, C. Black, M.L. Steigerwald, Y.L. Loo, S. Xiao, F. Ng, X.Y. Zhu, C. Nuckolls, *J. Am. Chem. Soc.* 136 (2014) 15215–15221.
- [422] Y. Lin, J. Wang, S. Dai, Y. Li, D. Zhu, X. Zhan, *Adv. Energy Mater.* 4 (2014) 1400420.
- [423] S. Li, W. Liu, C.-Z. Li, T.-K. Lau, X. Lu, M. Shi, H. Chen, *J. Mater. Chem. A* 4 (2016) 14983–14987.
- [424] N. Liang, K. Sun, Z. Zheng, H. Yao, G. Gao, X. Meng, Z. Wang, W. Ma, J. Hou, *Energy Mater.* 6 (2016) 1600060.
- [425] H. Wang, L. Chen, Y. Xiao, *J. Mater. Chem. C* 5 (2017) 12816–12824.
- [426] H. Wang, L. Chen, Y. Xiao, *J. Mater. Chem. C* 5 (2017) 8875–8882.
- [427] X. Zhan, W. Xiong, Y. Gong, T. Liu, Y. Xie, Q. Peng, Y. Sun, Z. Li, *Sol. RRL* 1 (2017) 1700123.
- [428] S. Li, W. Liu, C.-Z. Li, F. Liu, Y. Zhang, M. Shi, H. Chen, T.P. Russell, *J. Mater. Chem. A* 4 (2016) 10659–10665.
- [429] Y. Duan, X. Xu, H. Yan, W. Wu, Z. Li, Q. Peng, *Adv. Mater.* 29 (2017) 1605115.
- [430] L.-P. Zhang, W. Zhao, X. Liu, K.-J. Jiang, F.-T. Li, J. Hou, L.-M. Yang, *New J. Chem.* 41 (2017) 10237–10244.
- [431] X. Liu, Y. Cai, X. Huang, R. Zhang, X. Sun, *J. Mater. Chem. C* 5 (2017) 3188–3194.
- [432] Y. Lin, Y. Wang, J. Wang, J. Hou, Y. Li, D. Zhu, X. Zhan, *Adv. Mater.* 26 (2014) 5137–5142.
- [433] Q. Wu, W. Li, J. Hai, X. Zhang, Z. Lu, J. Yang, Y. Liu, L. Zhang, C. Zhan, *Dyes Pigm.* 132 (2016) 41–47.

- [434] Z. Luo, W. Xiong, T. Liu, W. Cheng, K. Wu, Y. Sun, C. Yang, *Org. Electron.* 41 (2017) 166–172.
- [435] N. Liang, D. Meng, Z. Ma, B. Kan, X. Meng, Z. Zheng, W. Jiang, Y. Li, X. Wan, J. Hou, W. Ma, Y. Chen, Z. Wang, *Adv. Energy Mater.* 7 (2017) 1601664.
- [436] H. Fu, D. Meng, X. Meng, X. Sun, L. Huo, Y. Fan, Y. Li, W. Ma, Y. Sun, Z. Wang, *J. Mater. Chem. A* 5 (2017) 3475–3482.
- [437] D. Meng, H. Fu, C. Xiao, X. Meng, T. Winands, W. Ma, W. Wei, B. Fan, L. Huo, N.L. Doltsinis, Y. Li, Y. Sun, Z. Wang, *J. Am. Chem. Soc.* 138 (2016) 10184–10190.
- [438] B. Wang, W. Liu, H. Li, J. Mai, S. Liu, X. Lu, H. Li, M. Shi, C.-Z. Li, H. Chen, *J. Mater. Chem. A* 5 (2017) 9396–9401.
- [439] Y. Liu, J.Y.L. Lai, S. Chen, Y. Li, K. Jiang, J. Zhao, Z. Li, H. Hu, T. Ma, H. Lin, J. Liu, J. Zhang, F. Huang, D. Yu, H. Yan, *J. Mater. Chem. A* 3 (2015) 13632–13636.
- [440] S.Y. Liu, C.H. Wu, C.Z. Li, S.Q. Liu, K.H. Wei, H.Z. Chen, A.K.Y. Jen, *Adv. Sci.* 2 (2015) 1500014.
- [441] H. Lin, S. Chen, H. Hu, L. Zhang, T. Ma, J.Y.L. Lai, Z. Li, A. Qin, X. Huang, B. Tang, H. Yan, *Adv. Mater.* (2016) 8546–8551.
- [442] W. Chen, X. Yang, G. Long, X. Wan, Y. Chen, Q. Zhang, *J. Mater. Chem. C* 3 (2015) 4698–4705.
- [443] W. Fan, N. Liang, D. Meng, J. Feng, Y. Li, J. Hou, Z. Wang, *Chem. Commun.* 52 (2016) 11500–11503.
- [444] Z. Liu, L. Zhang, M. Shao, Y. Wu, D. Zeng, X. Cai, J. Duan, X. Zhang, X. Gao, *ACS Appl. Mater. Interfaces* 10 (2018) 762–768.
- [445] X. Liu, T. Liu, C. Duan, J. Wang, S. Pang, W. Xiong, Y. Sun, F. Huang, Y. Cao, *J. Mater. Chem. A* 5 (2017) 1713–1723.
- [446] M. Yi, J. Yi, J. Wang, L. Wang, W. Gao, Y. Lin, Q. Luo, H. Tan, C.Q. Ma, H. Wang, *Dyes Pigm.* 139 (2017) 498–508.
- [447] H. Sun, P. Sun, C. Zhang, Y. Yang, X. Gao, F. Chen, Z. Xu, Z.K. Chen, W. Huang, *Chem.-Asian J.* 12 (2017) 721–725.
- [448] Q. Wu, D. Zhao, A.M. Schneider, W. Chen, L. Yu, *J. Am. Chem. Soc.* 138 (2016) 7248–7251.
- [449] Q. Wu, D. Zhao, J. Yang, V. Sharapov, Z. Cai, L. Li, N. Zhang, A. Neshchadin, W. Chen, L. Yu, *Chem. Mater.* 29 (2017) 1127–1133.
- [450] Z. Luo, T. Liu, W. Cheng, K. Wu, D. Xie, L. Huo, Y. Sun, C. Yang, *J. Mater. Chem. C* (2018), doi:<http://dx.doi.org/10.1039/C7TC05261H>.
- [451] Y. Zhong, M.T. Trinh, R. Chen, G.E. Purdum, P.P. Khlyabich, M. Sezen, S. Oh, H. Zhu, B. Fowler, B. Zhang, W. Wang, C.-Y. Nam, M.Y. Sfeir, C.T. Black, M.L. Steigerwald, Y.-L. Loo, F. Ng, X.-Y. Zhu, C. Nuckolls, *Nat. Commun.* 6 (2015) 8242.
- [452] T.J. Sisto, Y. Zhong, B. Zhang, M.T. Trinh, K. Miyata, X. Zhong, X.Y. Zhu, M.L. Steigerwald, F. Ng, C. Nuckolls, *J. Am. Chem. Soc.* 139 (2017) 5648–5651.
- [453] J. Zhang, Y. Li, J. Huang, H. Hu, G. Zhang, T. Ma, P.C.Y. Chow, H. Ade, D. Pan, H. Yan, *J. Am. Chem. Soc.* 139 (2017) 16092–16095.
- [454] G. Gao, N. Liang, H. Geng, W. Jiang, H. Fu, J. Feng, J. Hou, X. Feng, Z. Wang, *J. Am. Chem. Soc.* 139 (2017) 15914–15920.
- [455] B.P. Karsten, J.C. Bijleveld, R.A.J. Janssen, *Macromol. Rapid Commun.* 31 (2010) 1554–1559.
- [456] P. Sonar, G.-M. Ng, T.T. Lin, A. Dodabalapur, Z.-K. Chen, *J. Mater. Chem.* 20 (2010) 3626–3636.
- [457] P. Josse, P. Chávez, C. Dindault, C. Dalinot, S.M. McAfee, S. Dabos-Seignon, D. Tondelier, G. Welch, P. Blanchard, N. Leclerc, C. Cabanatos, *Dyes Pigm.* 137 (2017) 576–583.
- [458] P. Josse, C. Dalinot, Y. Jiang, S. Dabos, J. Roncali, P. Blanchard, C. Cabanatos, *J. Mater. Chem. C* (2015) 250–256.
- [459] P. Josse, A. Labrunie, C. Dalinot, S.M. McAfee, S. Dabos-Seignon, J. Roncali, G.C. Welch, P. Blanchard, C. Cabanatos, *Org. Electron.* 37 (2016) 479–484.
- [460] M. Chen, C. Du, X. Ren, M. Yi, J. Yi, C. Chen, F. Liu, M. Li, C. Ma, H. Wang, Chin. J. Chem. 35 (2017) 1140–1396.
- [461] S.M. McAfee, S.V. Dayneko, P. Josse, P. Blanchard, C. Cabanatos, G.C. Welch, *Chem. Mater.* 29 (2017) 1309–1314.
- [462] S.M. McAfee, S.V. Dayneko, A.D. Hendsbee, P. Josse, P. Blanchard, C. Cabanatos, G.C. Welch, *J. Mater. Chem. A* 5 (2017) 11623–11633.
- [463] M. Privado, V. Cuesta, P.D.L. Cruz, M.L. Keshtov, R. Singhal, G.D. Sharma, F. Langa, *ACS Appl. Mater. Interfaces* 9 (2017) 11739–11748.
- [464] M. Privado, V. Cuesta, P. de la Cruz, M.L. Keshtov, G.D. Sharma, F. Langa, *J. Mater. Chem. A* 5 (2017) 14259–14269.
- [465] Y. Patil, R. Misra, M.L. Keshtov, G.D. Sharma, *J. Phys. Chem. C* 120 (2016) 6324–6335.
- [466] Y. Patil, R. Misra, R. Singhal, G.D. Sharma, *J. Mater. Chem. A* 5 (2017) 13625–13633.
- [467] G.D. Sharma, Y. Patil, R. Misra, M.L. Keshtov, *J. Mater. Chem. A* 5 (2017) 3311–3319.
- [468] G.C. Welch, C. Risko, A.J. Payne, S. Dayneko, S. Li, *Chem. Commun.* 53 (2017) 10168–10171.
- [469] R.G. Brandt, F. Zhang, T.R. Andersen, D. Angmo, M. Shi, L. Gurevich, F.C. Krebs, J.W. Andreasen, D. Yu, *RSC Adv.* 6 (2016) 41542–41550.
- [470] Y. Lin, Y. Li, X. Zhan, *Adv. Energy Mater.* 3 (2013) 724–728.
- [471] A.M. Raynor, A. Gupta, H. Patil, A. Bilic, S.V. Bhosale, *RSC Adv.* 4 (2014) 57635–57638.
- [472] J.W. Jung, W.H. Jo, *Chem. Mater.* 27 (2015) 6038–6043.
- [473] Y. Lin, P. Cheng, Y. Li, X. Zhan, *Chem. Commun.* 48 (2012) 4773–4775.
- [474] A. Rananaware, A. Gupta, J. Li, A. Bilic, L. Jones, S. Bhargava, S.V. Bhosale, *Chem. Commun.* 52 (2016) 8522–8525.
- [475] S.Y. Liu, W.Q. Liu, C.X. Yuan, A.G. Zhong, D. Han, B. Wang, M.N. Shah, M.M. Shi, H. Chen, *Dyes Pigm.* 134 (2016) 139–147.
- [476] P. Sun, H. Sun, X. Li, Y. Wang, H. Shan, J. Xu, C. Zhang, Z. Xu, Z.K. Chen, W. Huang, *Dyes Pigm.* 139 (2017) 412–419.
- [477] Y. Yang, G. Zhang, C. Yu, C. He, J. Wang, X. Chen, J. Yao, Z. Liu, D. Zhang, *Chem. Commun.* 50 (2014) 9939–9942.
- [478] S.M. McAfee, J.M. Topple, A.J. Payne, J.P. Sun, I.G. Hill, G.C. Welch, *ChemPhysChem* 16 (2015) 1190–1202.
- [479] S.M. McAfee, J.M. Topple, J.-P. Sun, I.G. Hill, G.C. Welch, *RSC Adv.* 5 (2015) 80098–80109.
- [480] X. Liu, Y. Xie, X. Cai, Y. Li, H. Wu, S.-J. Su, Y. Cao, *RSC Adv.* 5 (2015) 107566–107574.
- [481] X. Liu, Y. Xie, H. Zhao, X. Cai, H. Wu, S.-J. Su, Y. Cao, *New J. Chem.* 39 (2015) 8771–8779.
- [482] J. Miao, B. Meng, J. Liu, L. Wang, *Chem. Commun.* 54 (2018) 303–306.
- [483] F. Meng, K. Chen, H. Tian, L. Zuppiroli, F. Nuesch, *Appl. Phys. Lett.* 82 (2003) 3788–3790.
- [484] N. Camaiorni, G. Ridolfi, V. Fattori, L. Favaretto, G. Barbarella, *J. Mater. Chem.* 15 (2005) 2220.
- [485] P. Sullivan, G.E. Collis, L.A. Rochford, J.F. Arantes, P. Kemppinen, T.S. Jones, K.N. Winzenberg, *Chem. Commun.* 51 (2015) 6222–6225.
- [486] T. Okabe, D. Kuzuhara, M. Suzuki, N. Aratani, H. Yamada, J. Porphyr. Phthalocyanines 20 (2016) 1350–1360.
- [487] W.X. Liu, J.N. Yao, C.L. Zhan, *Chin. Chem. Lett.* 28 (2017) 875–880.
- [488] P.S. Rao, A. Gupta, S.V. Bhosale, A. Bilic, W. Xiang, R.A. Evans, S.V. Bhosale, *Dyes Pigm.* 146 (2017) 502–511.
- [489] Y. Lin, H. Wang, Y. Li, D. Zhu, X. Zhan, *J. Mater. Chem. A* 1 (2013) 14627–14632.
- [490] C.B. Nielsen, E. Voroshazi, S. Holliday, K. Cnops, B.P. Rand, I. McCulloch, *J. Mater. Chem. A* 1 (2013) 73–76.
- [491] C.B. Nielsen, E. Voroshazi, S. Holliday, K. Cnops, D. Cheyns, I. McCulloch, *J. Mater. Chem. A* 2 (2014) 12348–12354.
- [492] K. Lin, B. Xie, Z. Wang, R. Xie, Y. Huang, C. Duan, F. Huang, Y. Cao, *Org. Electron.* 52 (2018) 42–50.
- [493] A. Rananaware, A. Gupta, G. Kadam, D.D. La, A. Bilic, W. Xiang, R.A. Evans, S.V. Bhosale, *Mater. Chem. Front.* 1 (2017) 2511–2518.
- [494] R.Y.C. Shin, T. Kietzke, S. Sudhakar, A. Dodabalapur, Z. Chen, A. Sellinger, *Chem. Mater.* 19 (2007) 1892–1894.
- [495] R.Y.C. Shin, P. Sonar, P.S. Siew, Z.-K. Chen, A. Sellinger, *J. Org. Chem.* 74 (2009) 3293–3298.
- [496] D.-C. Lee, Y. Jeong, L.V. Brownell, J.E. Velasco, K.A. Robins, Y. Lee, *RSC Adv.* 7 (2017) 24105–24112.
- [497] H. Li, Z.Y. Liu, X.Y. Zhang, S.Y. Yao, S.P. Wen, W.J. Tian, *Chem. Res. Chinese Univ.* 29 (2013) 596–599.
- [498] T. Zhou, T. Jia, B. Kang, F. Li, M. Fahlman, Y. Wang, *Adv. Energy Mater.* 1 (2011) 431–439.
- [499] C.P. Kanth, J. Patel, M. Chauhan, M. Aatif, A. Sharma, M.U. Trivedi, B. Tripathi, J. P. Tiwari, G. Gupta, M. Kumar, M.K. Pandey, *New J. Chem.* 41 (2017) 5836–5845.
- [500] H.-Y. Chen, J. Golder, S.-C. Yeh, C.-W. Lin, C.-T. Chen, C.-T. Chen, *RSC Adv.* 5 (2015) 3381–3385.
- [501] L. Chen, L. Huang, D. Yang, S. Ma, X. Zhou, J. Zhang, G. Tu, C. Li, *J. Mater. Chem. A* 2 (2014) 2657.
- [502] Y.-F. Lin, Y. Shu, S.R. Parkin, J.E. Anthony, G.G. Malliaras, *J. Mater. Chem.* 19 (2009) 3049.
- [503] Y. Shu, Y.-F. Lin, Z. Li, B. Purushothaman, R. Hallani, J.E. Kim, S.R. Parkin, G.G. Malliaras, J.E. Anthony, *Chem. Sci.* 2 (2011) 363–368.
- [504] V. Lami, D. Leibold, P. Fassl, Y.J. Hofstetter, D. Becker-Koch, P. Biegger, F. Paulus, P.E. Hopkinson, M. Adams, U.H.F. Bunz, S. Huettner, I. Howard, A.A. Bakulin, Y. Vaynzof, *Sol. RRL* 1 (2017) 1700053.
- [505] F. Liu, Z. Ding, J. Liu, L. Wang, *Chem. Commun.* 1 (2017) 12213–12216.
- [506] D. Liu, L. Yang, Y. Wu, X. Wang, Y. Zeng, G. Han, H. Yao, S. Li, S. Zhang, Y. Zhang, Y. Yi, C. He, W. Ma, J. Hou, *Chem. Mater.* (2018), doi:<http://dx.doi.org/10.1021/acs.chemmater.7b03142>.